UNIVERSITY OF SOUTHAMPTON

Faculty of Engineering, Science and Mathematics

School of Civil Engineering and the Environment

Performance of a propped retaining wall at the Channel Tunnel Rail Link, Ashford

Jo Clark

Thesis for the degree of Doctor of Philosophy

June 2006

UNIVERSITY OF SOUTHAMPTON

ABSTRACT

FACULTY OF ENGINEERING, SCIENCE AND MATHEMATICS

SCHOOL OF CIVIL ENGINEERING AND THE ENVIRONMENT

Doctor of Philosophy

PERFORMANCE OF A PROPPED RETAINING WALL AT THE CTRL, ASHFORD

Jo Clark

This thesis is based on the field monitoring of a propped bored pile retaining wall installed in an overconsolidated clay. Pile bending moments, prop loads, pore water pressures and lateral earth pressures were logged automatically at intervals of up to 5 minutes throughout construction (and for 4 years afterwards) and wall deflections were measured during construction, making this the most comprehensive instrumentation project of its kind.

The magnitude of the over-read associated with the use of spade cells (used to measure lateral earth and pore water pressures) in overconsolidated deposits was determined by comparing readings from a spade cell aligned to measure vertical stress with the estimated overburden acting on it as the overburden was excavated. This study adds significantly to the previous data as spade cells have not previously been used in the Atherfield Clay, and the performance of spade cells under a known changing load has not previously been measured in the field.

Analysis of the changes in lateral stress and pore water pressure during the wall installation process showed significant reductions in horizontal stress during wall installation, reducing the ratio of effective horizontal to effective vertical stress, K, from about 1 to nearly the active condition. Following wall installation there was no further change in horizontal stress over a period of about 10 months, during which time no further construction work took place.

Analysis of the data yielded good agreement between pile bending moments estimated from inclinometer and strain gauge measurements in the piles, and the onset of concrete cracking was identified. The components of strain measured in the reinforced concrete props due to shrinkage, creep and applied load were also identified, allowing prop loads to be estimated. A simple equilibrium calculation showed that these agree with the measured wall bending moments and total horizontal soil stresses, demonstrating the overall consistency of the data collected.

Simple equilibrium analysis of the behaviour of the wall during construction shows that the soil stresses measured are compatible with the measured structural loads. The long-term horizontal soil stresses, bending moments and RC prop loads show no increase over the 6 years since construction began.

TABLE OF CONTENTS

LIST OF FIGURES

LIST OF TABLES

PAPERS ARISING FROM THIS THESIS

Clark, J., Richards, D.J. and Powrie, W. (2004). Wall installation effects – preliminary findings from a field study at the CTRL, Ashford. *Proc. of the Skempton Memorial Conference*, London.

Richards, D.J., Clark, J., Powrie, W. and Heyman, G. (2005). An evaluation of total horizontal stress measurements using push-in pressure cells in an overconsolidated clay deposit. *Proc. Inst. Civ. Engrs. Geotech. Engng – accepted for publication.*

Clark, J. and Richards, D.J. (2005). Measurement of bending moments in concrete. *Proc. 16th Int. Conf. Soil Mech. Grnd Engng., Japan.*

Richards, D.J., Clark, J. and Powrie, W. Installation effects of a bored pile wall in overconsolidated clay. *Submitted to Geotechnique.*

ACKNOWLEDGEMENTS

First I must thank my supervisor David Richards for his valuable support and encouragement throughout the fieldwork, analysis and write-up periods of this work. I would also like to thank William Powrie and Chris Clayton for advising me and all three for being a fantastic combination of mentors.

The work described in this thesis was carried out with the support of the Engineering and Physical Sciences Research Council, (EPSRC), Rail Link Engineering, Union Railways and Skanska.

I would particularly like to thank, Howard Roscoe, Gary Holmes (who's invaluable support as a surrogate supervisor will not be forgotten), Fleur Loveridge, Hilary Shields, Adam Chodorowski, Alex Pendleton, Vernon Pilcher, David Twine and the site staff at Ashford Contract 430. I would like to thank Richard Wilson for collecting the bulk of the very high quality inclinometer readings.

I would like to thank the Geotechnical Group the many other members of the School of Civil and Environmental Engineering who have made my experience working at the University of Southampton so enjoyable. Of particular note are Harvey Skinner, Antonis Zervos, Michelle Theron, Martin Rust, Geoff Watson, Joel Smethurst and my office mates.

Thank you to my parents and brother for leaving me to it when I asked, for help with proof reading, for their constant support, and particularly for putting me up and feeding me, often at late notice, during the fieldwork period.

If it wasn't for Nellies heroes I would have completed this work much sooner, but would be a much poorer soul for it.

Thanks and love go to Jon for the support, for the encouragement during the despair, for sharing my excitement throughout the triumphs and for understanding what it is all for.

1 INTRODUCTION

1-1 *In situ* embedded retaining walls

In situ embedded retaining walls are formed by installing a structure in a pre-excavated cavity in the ground and removing the soil from one side of the structure to form a vertical retaining wall. The term *in situ* is used to indicate that the wall has been constructed on site from raw materials (fresh concrete and steel reinforcement). To provide stability, the bottom of the wall remains embedded in the soil and sometimes props are used, for example at the top of the wall, to provide extra support. These walls are typically used to form basements and cuttings in urban areas throughout the world, where space is restricted.

Traditionally, *in situ* embedded retaining walls have been designed using limit equilibrium techniques, which are known to provide sound design solutions for walls installed in sand and normally consolidated clays. More recently finite element techniques have been used during design and to back analyse existing walls. Back analyses of walls constructed in overconsolidated clays (which, due to their stress history, have a high horizontal to

vertical stress ratio compared to other natural soil deposits) have generally calculated much higher bending moments and prop loads than both those obtained using conventional limit equilibrium methods based on fully active pressures behind the wall and those observed directly in the field (e.g. Potts & Fourie, 1984 & 1985; Tedd *et al.*, 1984).

There are many uncertainties associated with the design of *in situ* embedded retaining walls in overconsolidated deposits, for example: the effect of their installation on the stress state of the surrounding soil; the equilibrium pore water pressures and their effect on the overall wall stability; and the long-term horizontal stress acting on the wall. These issues have been the subject of considerable research over the last few decades, including several projects which used instrumentation and/or *in situ* testing to investigate the behaviour of walls installed in overconsolidated clays (e.g. Garrett & Barnes, 1984; Tedd *et al.*, 1984; Symons & Tedd, 1989; Ng, 1992; Symons & Carder, 1993; Carswell *et al.*, 1993). In order to further investigate the long-term behaviour of retaining walls, attempts have been made to analyse walls already in service (Symons & Tedd, 1989; Carder & Symons, 1989; Symons & Carder, 1990).

Some of these field studies have investigated the effect of *in situ* embedded retaining wall installation on the stress state of the surrounding soil (e.g. Tedd *et al.*, 1984; Symons & Carder, 1993) as it is generally accepted that the effect of installing such a wall influences its subsequent behaviour in terms of loads and bending moments (Gunn *et al.*, 1993; Powrie & Kantartzi, 1996). Significant reductions in horizontal stress were observed in the field studies. In addition, wall installation may cause significant ground movements (which may be highly unacceptable) and its contribution to the recent stress history of the soil will affect the subsequent stress-strain response of the soil (Powrie *et al.*, 1998). Using finite element analysis, Powrie & Li (1991) used a simplified technique to model wall installation and calculated smaller wall bending moments than those obtained by Potts & Fourie (1984 & 1985), which were closer to those measured in the field. However, the process of wall installation in panels or piles is complex and three dimensional, so that the magnitude, extent and longevity of the stress reduction associated with *in situ* wall installation are all highly uncertain issues.

Many design standards are used for the design of *in situ* embedded retaining walls (including CIRIA 104 (Padfield and Mair, 1984); CIRIA C580 (Gaba *et al.*, 2003); Eurocode 7, (British Standards Institution, 1995) and BD42 (Department of Transport,

2000) and each contains differing advice on the method of analysis, use of factors of safety and selection of input parameters. The overall stability of these walls and conditions at collapse have been studied in depth (e.g. Burland *et al.*, 1981; Symons, 1983; Bolton & Powrie, 1987; 1988), however the number of standards in use illustrates clearly that there are still many uncertainties as to the best method for design.

A better understanding of the changes in stress that occur on installation of an *in situ* retaining wall, during excavation in front of the wall and in the long-term, could result in better estimates of prop loads, wall bending moments and ground settlements than were possible in the past, and lead to more economical designs. In this thesis the results from a field study carried out on a section of *in situ* embedded retaining wall which forms part of the Channel Tunnel Rail Link at Ashford, Kent, are presented and discussed. Strain gauges were used to measure permanent and temporary prop loads and wall bending moments, and push-in spade-shaped pressure cells were used to measure total horizontal stress and pore water pressure in the soil adjacent to the wall. Conclusions are drawn regarding the magnitude, pattern and longevity of horizontal stress changes due to wall installation and the overall stability of the wall. Data collection is ongoing, and data that describe the performance of the wall and the soil stresses existing 6 years after the retaining wall was installed and 4 years after construction was completed are included in this thesis. Observations are made on the long-term behaviour expected from consideration of the measurements taken in the 4 years since construction was completed.

1-2 Measurement of horizontal stress

A number of previous retaining wall fieldwork studies utilised push-in spade-shaped pressure cells (commonly known as spade cells), to measure horizontal soil stresses as they are relatively cheap, easy to install and give reasonably reproducible readings (Tedd & Charles, 1981). They were originally designed for use in normally consolidated clays but are now frequently used in stiff overconsolidated clays, although in such deposits it is known that they overestimate the magnitude of the soil stress due to the complex localised stresses created during installation (Tedd & Charles, 1983). Attempts have been made to predict the amount by which spade cells over-read in a particular material by relating the over-reading to soil strength (Tedd *et al.*, 1990; Ryley & Carder, 1995), but the data are rather scattered.

Due to the considerable uncertainty regarding the magnitude of the over-reading and the factors that may affect it, it is advisable to directly determine this over-reading wherever possible until more data are available. As part of the work for this thesis a study was carried out to evaluate the magnitude of the over-read given by a spade cell installed in Atherfield Clay – a stiff, overconsolidated clay – which exists at the site of the CTRL at Ashford. A spade cell was installed horizontally in the ground, aligned to measure vertical stress. The soil above the spade cell was excavated in stages over a period of several weeks, and at each stage the overburden was calculated and compared with the reading in the spade cell. Additionally, measurements of *in situ* horizontal stress obtained using the spade cells installed during the main instrumentation project have been compared with self-boring pressuremeter readings. In line with other recent research, the over-read due to the installation process has been expressed in terms of the undrained shear strength of the soil.

1-3 Channel Tunnel Rail Link

The Channel Tunnel Rail Link (CTRL) is the largest construction project in the UK and Britain's first new railway for over a century. It consists of 109 km of railway which starts at the Channel Tunnel entrance at Folkestone and ends at St. Pancras station in Central London (see Figure 1-1). It is being constructed in two sections: Section 1 consists of 74 km of track running from the Channel Tunnel to North Kent. Construction began in October 1998 and Section 1 opened in September 2003. There are two stations included in Section 1, at Ashford in mid-Kent and Ebbsfleet in North Kent, just south of the River Thames. Section 2 takes the CTRL under the River Thames and through London to St Pancras, with a station in North London at Stratford. Construction of Section 2 began in July 2001 and is due to be completed in early 2007.

A quarter of the total route is in tunnel, including 1·7 km of cut-and-cover tunnel and propped cutting in Ashford, which forms the approach to Ashford International Station from London.

1-4 Objectives

The objectives of this project are:

- To collect continuous field data, over the entire period of construction and into the long-term, from an instrumented section of a propped *in situ* embedded retaining wall in an overconsolidated clay.
- To investigate the changes in the horizontal stresses and pore water pressures in the soil during installation of the bored piles that form the retaining wall.
- To investigate the wall movements and the development of prop loads and bending moments associated with a retaining wall embedded in an overconsolidated clay, and to relate these data to the horizontal stresses and pore water pressures measured behind and in front of the monitored wall section.
- To analyse the observed performance.
- To investigate the performance of the spade-shaped pressure cells used in this study.

This thesis describes work carried out towards the realization of these objectives, as well as suggestions for future work.

1-5 Outline of report

Chapter 2 contains a review of retaining wall design, with references to previous instrumentation projects, model testing and studies that used finite element techniques to analyse the performance of retaining walls. This chapter also includes details of the use of spade cells to measure horizontal stresses in overconsolidated deposits.

In Chapter 3 the case study is described. This chapter includes details of the local geology, the geometry of the structure, the construction sequence and details of the instrumentation used to monitor the performance of the structure and the stress changes in the adjacent soil.

In Chapter 4 the structural monitoring is described in greater detail. The methods by which the data have been calibrated and evaluated are described. The wall bending moment, wall

deflection and prop load data at various significant stages during construction are presented.

In Chapter 5 the horizontal soil stress measurements are described in greater detail. The instrumentation used to measure horizontal soil stresses and pore water pressures is evaluated by means of a study in which the readings from a spade cell aligned to measure vertical stress were compared with the estimated overburden acting on it (calculated from bulk density measurements). The horizontal stress and pore water pressure data collected during wall installation and excavation of the cutting are presented and analysed.

In Chapter 6 the long-term data collected from the spade cells and the RC props up to November 2005, more than 4 years after construction was completed, are presented.

Chapter 7 contains conclusions arising from this research and recommendations for future work.

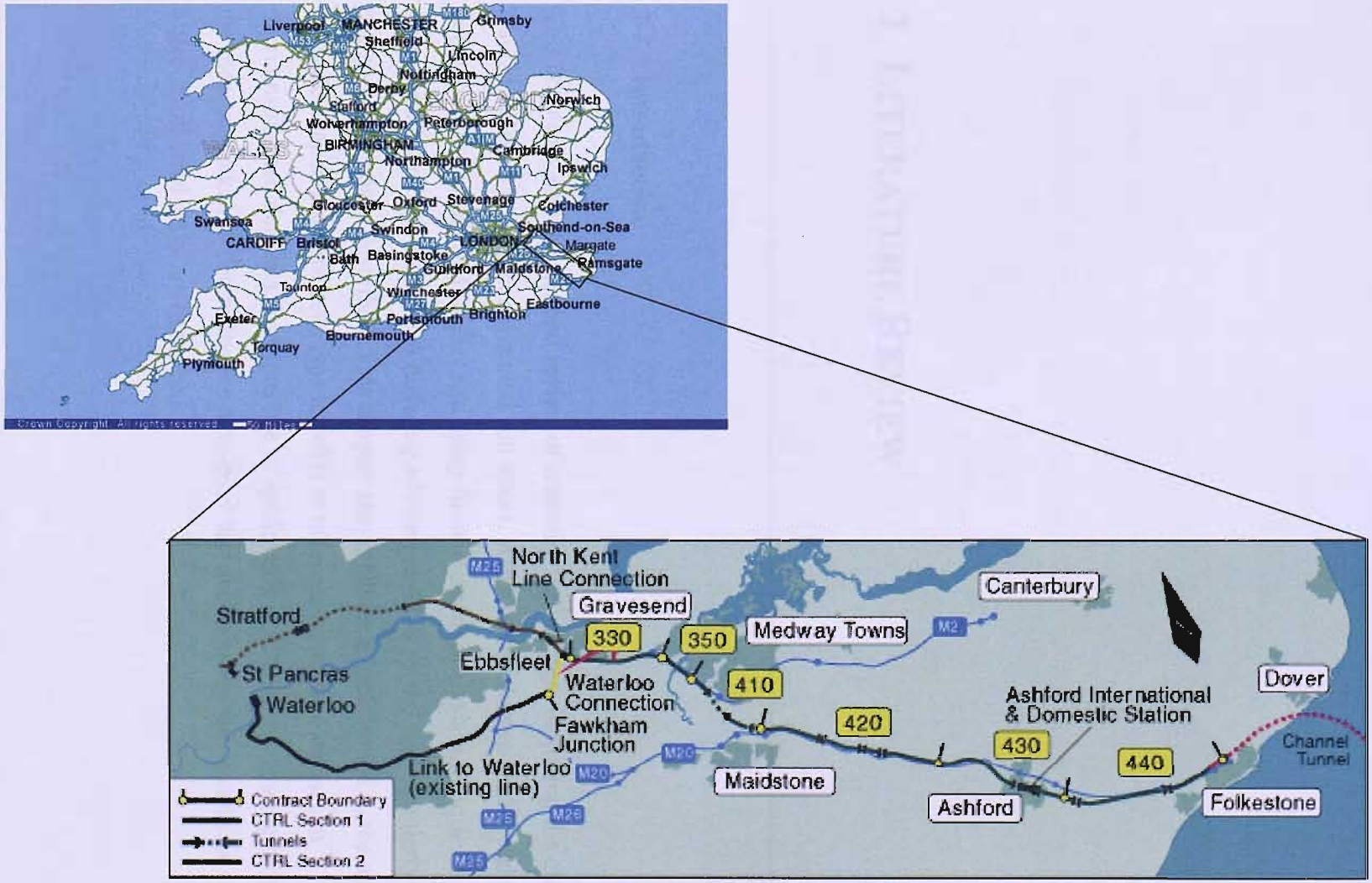

Figure 1-1: Map showing the route of the Channel Tunnel Rail Link

2 LITERATURE REVIEW

2-1 Introduction

This chapter contains a general review of retaining wall design, including the effects of wall installation on *in situ* horizontal soil stress. Work undertaken to study retaining wall behaviour in similar field studies and using finite element analysis techniques is summarised, and the sometimes differing advice provided by the most regularly used design guidelines is described. This chapter also includes a background to the use of push-in spade-shaped pressure cells (spade cells) to measure horizontal stresses in overconsolidated deposits. Previous use of spade cells in similar monitoring projects and the measures taken to determine the over-read that occurs when spade cells are used in overconsolidated clays are described.

2-2 Review of investigations into retaining wall behaviour

2-2-1 Background

There are essentially two design stages required for embedded retaining wall design:

1. determination of the depth of embedment required to prevent overall collapse of the soil/structure as a whole and

2. design of the wall member and ancillary elements such that they are strong enough to support the consequential forces and bending moments induced in service.

A limit equilibrium analysis is usually used to calculate the depth of embedment of the wall, and a factor of safety is applied to one or more of the variables involved to ensure against global collapse. The structural elements are then designed to carry the bending moments and loads which are expected as a result of the geometry determined by the limit equilibrium analysis. Separate consideration is given to the requirements for the working condition and the ultimate failure state, as deformations occurring under the ultimate state may be well beyond those that are acceptable under working conditions.

The following sections contain a brief outline of retaining wall design in which the various components of design and the choices that must be made are discussed.

2-2-2 Limiting conditions

Most modern codes of practice use limit state design principles, where limits are set, e.g. a maximum soil loading or a maximum wall deflection, and the corresponding structural forces are found by assuming the structure is on the verge of exceeding these criteria. As previously mentioned stability and displacement are considered separately; stability is considered to be the primary aim (the ultimate limit state, ULS) and displacements are usually only considered as a secondary serviceability issue (serviceability limit state, SLS). However, displacements can often become a ULS, for example, if the displacements cause ground movements that affect nearby structures or services, or if they cause unsightly conditions for the structure. In such cases the serviceability requirements often dictate the construction method utilised, e.g. the construction sequence, the propping methods and the type of wall. The serviceability requirements are different for each

project, and therefore the designer must have a full understanding of the overall project and surrounding factors before the serviceability criteria can be defined.

The principle of analysing retaining wall behaviour by determining the forces present when the structure is on the verge of collapse began with Coulomb (1776), who developed an upper bound solution for retaining wall analysis by assuming a planar wedge failure mechanism (Figure 2-1) and derived the limiting force as a function of depth behind the wall. Coulomb's solution produces sufficiently accurate results despite the inaccurate assumption that the wedge has a plane failure surface. More recent work in which the lower part of the sliding wedge was assumed to have a curved boundary, as is observed in model tests, produced equations that were considered overly complicated for practical use (Terzaghi, 1943).

Rankine (1857) developed a lower bound solution by assuming that the earth pressures acting on the wall held it at the limit of equilibrium. He derived limiting active and passive earth pressure coefficients (K_a and K_p respectively), given by the ratio of effective horizontal stress[1], σ'_h, to effective vertical stress, σ'_v (Equation 2-1) and determined the orientation of the surfaces of sliding. (The 'at rest' or *in situ* earth pressure coefficient is denoted by K_o.) The active state occurs when the rate of increase of horizontal earth pressure is slower than for the vertical earth pressure (in absolute terms), in this case behind a retaining wall, and the passive state occurs where the rate of increase of horizontal earth pressure is faster than for the vertical earth pressure, e.g. in front of a retaining wall. Coulomb and Rankine's solutions are identical for a smooth wall with a horizontal surface to the retained soil and a linear lateral pressure distribution.

$$K = \frac{\sigma'_h}{\sigma'_v} \qquad \textbf{Equation 2-1}$$

Coulomb's method underestimates the active pressure and overestimates the passive pressure, and hence may tend to an unsafe solution. Because Rankine's method relies on static equilibrium it cannot take account of wall friction, unlike the Coulomb method, and therefore overestimates the active pressure and underestimates the passive pressure, producing an inherently safe (although unnecessarily costly) embedment depth. To account for this, earth pressure coefficients have been developed which can be applied to

[1] where effective stress is given by $\sigma' = \sigma - u$, where σ is the total stress and u is the pore water pressure

K to take wall friction into consideration (British Standards Institution, 1995; Gaba *et al.*, 2003).

Idealized stress distributions used in limit equilibrium analyses are shown in Figures 2-2 and 2-3. The fixed earth support method assumes that fixity develops close to the wall toe so there is no lateral movement at this point. The free earth support method assumes that the wall toe is free to move laterally. Unpropped embedded retaining walls rely entirely on an adequate depth of embedment for their stability and so the fixed earth support method must be used. Retaining walls propped at the crest tend to fail by rotation about the prop level, so the free earth support method is usually used. It has been suggested that the fixed earth support method can be used for analysis of propped walls: this is discussed in Section 2-2-4.

2-2-3 Development of active and passive pressures

The limiting earth pressure coefficients for the active and passive states, K_a and K_p respectively, are given in Equations 2-2 and 2-3, where ϕ' is the soil strength or angle of friction and is given in degrees.[2] (These equations are derived from consideration of the Mohr circle of stress for a soil element on the verge of failure; see for example Powrie, 2004).

$$K_a = \frac{1-\sin\phi'}{1+\sin\phi'} \qquad \textbf{Equation 2-2}$$

$$K_p = \frac{1+\sin\phi'}{1-\sin\phi'} \qquad \textbf{Equation 2-3}$$

In order for active and passive pressures to be mobilized it is necessary for deformation or displacement of the wall to take place. The amount of displacement necessary depends on the type of soil and its overconsolidation ratio.[3]

Soils such as sands and normally consolidated clays are close to their active limit at the *in situ* state, i.e. the horizontal earth pressures are comparatively low ($K_o < 0{\cdot}7$). In such

---

[2] Tan ϕ is analogous to the coefficient of friction, μ, in the equation: $F = \mu N$ where F is a force pushing against a normal force, N.

[3] The overconsolidation ratio is given by: $OCR = \sigma'_{v\,(max.\ previous)} / \sigma'_{v\,(current)}$.

materials only a small movement of the structure is required to achieve full active conditions behind the wall, but relatively large movements, which may be unacceptable under working conditions, are required to achieve full passive conditions in front of the wall. This was shown in large-scale model tests (Terzaghi, 1934) in which a wall was rotated into and away from a bed of sand; the results are shown in Figure 2-4.

Overconsolidated clays ($K_o > 1$) have high horizontal earth pressures and are therefore often closer to the passive limit of the soil, so only small movements of the structure are needed to achieve passive conditions in front of the wall, but large, potentially unacceptable movements are necessary to achieve active conditions behind the wall. Potts & Fourie (1985) used finite element analysis to show that for an overconsolidated clay with $K_o = 2$, a similar amount of movement is required to reach passive and active conditions (see Figure 2-5). However bending moments measured in the field (Tedd *et al.*, 1984) and in centrifuge model tests (Bolton and Powrie, 1988) have not shown this to be true in practice. In addition, Simpson (1992) argues that this study should be treated with caution because it was carried out using a linear elastic soil model until it reached its maximum shear strength, therefore not allowing for large stiffness at small strains (as discussed by Burland *et al.*, 1979).

Powrie *et al.* (1998) undertook triaxial tests on samples of overconsolidated kaolin to investigate the total stress paths undertaken by elements of soil in front of and behind a retaining wall during wall installation and excavation in front of the wall. They found that the process of wall installation has a considerable influence in reducing the horizontal stresses and therefore predicted that during excavation in front of a retaining wall, only small movements of the wall are required to bring the earth pressure distribution close to its active limit.

The factors that affect the extent to which passive or active pressures can be achieved are still not well understood, particularly in the case of overconsolidated clay. In addition, the distribution of stress on a retaining wall varies significantly from the idealised stress distributions in Figures 2-2 and 2-3, as discussed in the following section.

2-2-4 Distribution of earth pressures

There has been considerable debate concerning the distribution of earth pressures on retaining walls, both under working conditions and at collapse. Work by Terzaghi (1943,

1954), Tschebotarioff (1951) and Rowe (1952, 1955 & 1956), studied the distribution of pressure on retaining walls and the effect of wall flexibility on the bending moments and prop/anchor loads.

As previously mentioned, some authors (e.g. Terzaghi, 1943) recommend the use of the fixed earth support method for the design of propped walls, because the increased fixity at the wall toe affects the distribution of pressure on the wall by raising the point of application of the passive pressure, thereby decreasing the flexibility of the pile and hence also the maximum bending moment. Terzaghi (1943) also suggested that for a flexible retaining wall (particularly referring to steel sheet piles anchored near the top) and assuming fixed earth support, there can be a further redistribution of earth pressure in certain soils which causes an increase in pressure at the top of the wall around the position of the restraint, and a decrease in pressure in the middle of the wall (see Figure 2-6). This pressure distribution is a form of arching and is maintained solely by shear stresses. Terzaghi stated that the bending moment calculated using the pressure distribution indicated by the curved line in Figure 2-6(a) is less than half that calculated using the linear pressure distribution.

Rowe (1952) undertook model tests with walls of varying flexibility in dense and loose sand ($K_o < 0{\cdot}5$) and compared the measured bending moments with those calculated from a limit equilibrium calculation assuming free earth support and triangular pressure distributions in front of and behind the wall. He showed that for the most flexible walls the observed bending moments were much lower than the calculated values, and that as the flexibility of the wall decreased the bending moment increased to that calculated by the limit equilibrium analysis. This occurs because for a flexible wall the deflection at excavation level is much larger than at toe level, and consequently more passive pressure is mobilized at the top of the zone of soil in front of the wall than for a stiffer wall where e the deflection at excavation level and the toe are similar (Figure 2-7). Rowe (1952) noted that this effect also occurred with a rise in soil density (and hence soil stiffness).

Rowe (1952) studied the effect of a small anchor yield on the horizontal earth pressure behind a retaining wall. He showed that an anchor yield of 0·1% of the wall height led to a breakdown in the arching that produces Terzaghi's pressure distribution and a return to the triangular Coulomb pressure distribution. He concluded (and Terzaghi (1954) agreed) that it was not justified to rely on the reductions indicated by the redistribution of pressure.

The debate on the use of the fixed earth support method for the analysis of propped or anchored retaining walls has continued. Decreasing the flexibility of the pile decreases its movement and therefore the ability of the soil to reach its active and passive limits. The relatively old retaining wall design standard CIRIA 104 (Padfield and Mair, 1984 – discussed in Section 2-3) recommends against use of the fixed earth support method for the design of propped walls embedded in clays, stating that it is not appropriate because of the long-term deformation characteristic of the soil. However, the most recently published guidance on embedded retaining wall design, CIRIA C580 (Gaba *et al.*, 2003), states that since modern support systems are somewhat stiffer it is now more likely that such a pressure distribution could exist.

Since the development of active (and passive) pressures depends on the degree of wall movement, there is some doubt that these pressures can be realised in overconsolidated deposits with a stiff wall and propping system as little movement is likely to occur. The work described above is, to some extent, of limited application to walls embedded in overconsolidated deposits because it was based on the assumption that active conditions would be met. In addition, the limit equilibrium methods used to calculate forces in cantilever and singly propped walls can not be used for statically indeterminate multi-propped walls; these must be designed using iterative computer aided techniques which give consideration to soil-structure interaction.

Potts & Fourie (1985) used finite element methods to investigate the influence of K_o on bending moments and prop loads. They first carried out an analysis with a similar geometry and soil profile to Rowe's, which produced results which were in good agreement. They then ran further analyses using the same geometry but with a K_o of 2, and found that increasing K_o produced very high bending moments, greater than the limit equilibrium value. They also found that the bending moments increased further as the stiffness of the wall increased. Potts & Bond (1994) also used finite element analysis to demonstrate that the bending moment and prop loads increase as wall stiffness and K_o increase, and that for $K_o > 0{\cdot}5$ the maximum bending moment and prop load are greater than the values given by a limit equilibrium analysis. However, this study did not take into consideration the effect of wall installation on horizontal earth pressures around a retaining wall, which is discussed in the next section.

Richards & Powrie (1998) used finite element techniques to show that the construction sequence can have an effect on ground movements behind the retaining wall during

excavation. They found that top down construction with early installation of a permanent prop at the top of the wall, a temporary prop at the excavation mid-height and use of a permanent prop at formation causes minimum ground movements behind the wall. This may affect the amount of stress relief behind the wall and therefore the soil's ability to achieve active pressures.

2-2-5 Change in horizontal earth pressure due to wall installation effects

The installation of a bored pile wall (or a diaphragm wall) in overconsolidated clay causes stress changes in the ground by the following process. On boring, the horizontal stress (σ_h) near the hole is reduced. If no support is used, σ_h at the edge of the borehole is reduced to zero and in the short-term the borehole is held open by shear stresses in the soil. If the soil is soft the hole may collapse quickly, so either a casing or bentonite slurry is used as support until the concrete is poured into place. In this case, σ_h at the edge of the borehole reduces to the value of the pressure exerted by either the casing or the bentonite slurry. When concrete is poured, σ_h at the edge of the borehole will increase to the hydrostatic pressure exerted by the wet concrete. During the curing process the heat of hydration causes the concrete to expand, exerting an increased pressure on the edge of the borehole. The concrete then cools, causing shrinkage, and a further pressure change can occur as the soil may swell due to the changes in pore water pressure.

It is well known that the stress state in the soil surrounding an *in situ* retaining wall is affected by the process of wall installation (Gunn *et al.*, 1993; Symons & Carder, 1993; Gourvenec & Powrie, 1999) and that the stress state of the adjacent soil following wall installation may have a significant effect on the behaviour as calculated in a numerical analysis (Potts & Fourie, 1984; Fourie & Potts, 1989; Powrie & Li, 1991). Wall installation will affect the recent stress history of the soil and hence its subsequent stress-strain response (Atkinson *et al.*, 1990; Powrie *et al.*, 1998), and in soft soils may cause significant ground movements in its own right (Stroud & Sweeney, 1977; Powrie & Kantartzi, 1996).

Powrie (1985) discussed the change in horizontal pressure that might occur on construction of a diaphragm-type retaining wall, and showed that a soil with $K_o = 2$ could experience a reduction in horizontal stress that reduced K_o to just over 1. As previously discussed in Section 2-2-3, Powrie *et al.* (1998) found that wall installation had a significant influence on the horizontal soil stress, and that the recent stress history applied

by the excavation and concreting processes "move the stress state of the soil outside the influence of its geological and pre-installation stress history." Furthermore Simpson and Powrie (2001) noted that if the shear stresses that maintain a difference in the far-field and near field horizontal stresses break down K will tend to no more than unity after construction.

Tedd *et al.* (1984) reported results from instrumentation installed to monitor the behaviour of a secant pile retaining wall during wall installation and excavation in front of the wall at the Bell Common Tunnel on the M25. They found that ground movements during installation of the retaining wall accounted for about 30% of the total movements that occurred during the cut-and-cover tunnel construction, which indicates that stress relief took place in the ground over this period. They also measured significant reductions in horizontal earth pressure as a result of wall installation, although it was difficult to establish the magnitude of these reductions due to difficulties arising from the construction process.

During the field monitoring of other retaining walls in London Clay, Symons & Carder (1993) measured changes in effective horizontal stress due to wall construction of 10% for a bored pile wall (comprising 1·5 m diameter, 24 m long piles installed in London Clay) and 20% for a diaphragm wall. Measurements of water pressure during excavation and concreting showed that after an initial reduction, followed by an increase to levels sometimes above pre-excavation levels, pore water pressures levelled out to values similar to those measured prior to construction. This has also been observed in centrifuge model tests of diaphragm wall installation processes (Powrie & Kantartzi, 1996).

Numerical analyses of *in situ* walls in which the effects of wall installation are neglected generally give much higher bending moments and prop loads than both those obtained using conventional limit equilibrium methods based on fully active pressures behind the wall and those observed directly in the field (e.g. Potts & Fourie, 1984 and 1985; Tedd *et al.*, 1984). Modelling wall installation by simply reducing the pre-excavation horizontal stress across the entire mesh (Powrie & Li, 1991; Richards and Powrie, 1994) may reduce the calculated wall bending moments. However, the process of wall installation in panels or piles is three-dimensional and the magnitude, extent and longevity of the stress reduction associated with *in situ* wall installation are all highly uncertain. Reducing the horizontal earth pressure coefficient across the entire width of the finite element mesh is at best a highly simplified approximation.

Using a plane strain analysis to model the process of wall installation leads to over-predictions of the magnitude of soil displacements and the degree and extent of horizontal stress relief (Gunn & Clayton, 1992; De Moor, 1994; Ng *et al.*, 1995). Therefore some authors have tried to model wall installation in three-dimensions. Ng (1992) modelled vertical and horizontal sections of a retaining wall in plane strain in order to investigate the three-dimensional nature of wall installation effects. He found that horizontal arching plays an important role in restricting ground movements, and that if this effect is ignored ground movements will be over-predicted. He also noted that in clays with very high stiffness at small strains, much stress relief can occur with only a small movement. Using three-dimensional finite element analysis techniques Gourvenic & Powrie (1999) showed that the installation of a diaphragm wall panel affects the horizontal earth pressures on adjacent panels. They also found that soil movements increase markedly for diaphragm panel shape ratios (the vertical dimension (depth) to the dimension in the direction along the wall (width)) of less than 3, i.e. soil arching is best achieved with a deep, narrow panel (the extreme of which is a pile) rather that a short, wide one.

A better understanding of the changes in stress that occur during installation of a retaining wall could result in more realistic estimates of prop loads, wall bending moments and ground movements than have been possible in the past. In this section the data collected during wall installation are described and discussed, and conclusions are made regarding the magnitude, pattern and longevity of horizontal stress changes due to the installation of walls of this type.

2-2-6 Behaviour of embedded walls in the longer term

There is some concern that the high horizontal stresses in an overconsolidated deposit may become re-established in the long-term, despite the reductions that occur during retaining wall installation and subsequent excavation in front of the wall. This is thought to occur because the shear stresses maintaining the difference in the far field and near field horizontal stresses may break down. As pointed out by Simpson and Powrie (2001) it seems unlikely, particularly in the design lifetime of the wall, that if the horizontal shear stresses break down then the vertical shear stresses necessary to produce a K_0 of more than 1 will not exist either. Therefore the long-term value of K can be no more than 1.

In order to determine the long-term stress state of the soil around a retaining wall, and hence the longevity of the reduction in stress due to wall installation, studies have been

undertaken on walls that have been in service for a number of years. Analysis of the long-term behaviour of the Bell Common Tunnel (Symons & Tedd, 1989) showed insignificant changes in earth pressure behind the wall and small decreases in earth pressure in front of the wall in the four years after construction. Very small changes in pore water pressure were measured on both sides of the wall.

Symons & Carder (1990) describe data obtained at two retaining wall sites: a cantilever wall and a wall propped just below the carriageway, several years after construction was completed. Measurements of total pressure and pore water pressure were taken in order to determine whether equilibrium conditions had been reached. For the cantilever wall they had, but for the propped wall pore water pressures were still gradually changing. Measurements taken 150 m and 1·5 m from the cantilever wall showed that significant stress relief had occurred due to construction/installation. However, for the propped wall, measurements taken at 16 m and 1·5 m from the wall suggested no stress relief had occurred in this case.

2-3 General overview of retaining wall design standards

A number of standards and guidelines regarding the design of embedded retaining walls are in general use, and they sometimes provide conflicting advice on matters such as: general approach to design, choice of soil parameters, choice of safety factors, estimation of long-term pore water pressures, determination of wall bending moments and the magnitude and distribution of horizontal earth pressure. Some of the guidance documents currently used include:

- **BS 8002**, the British Standards Code of Practice for earth retaining structures (British Standards Institution, 1994/2001);
- **CIRIA 104** (the Construction Industry Research and Information Association Report 104): Design of retaining walls embedded in stiff clay (Padfield & Mair, 1984);
- **British Steel Piling Handbook** (1997);
- The Highways Agency Design Manual for Roads and Bridges – Volume 2, Section 1, Part 2 - **BD 42** Design of embedded retaining walls and bridge abutments (Department of Transport, 2000);

- **Eurocode 7**. Geotechnical design, Part 1: General rules. (British Standards Institution, 2004);
- **CIRIA C580**, Embedded retaining walls: guidance for more economic design (Gaba *et al.* 2003). This supersedes CIRIA 104.

CIRIA 104 has proved to be an extremely influential report which is used by 91% of design engineers (Gaba, 2002), usually in conjunction with one or more of the other more recently released design guidelines. It was written strictly for the design of singly propped or cantilever walls embedded in stiff overconsolidated clay, but its principles have been applied to a wide range of wall types, including multi-propped embedded walls and non-embedded walls. It provides design guidance for permanent and temporary walls. As part of the development work for Eurocode 7, designers from countries across Europe were asked to design a retaining wall according to their country's normal design guidelines for a specific project. The UK design, based on CIRIA 104, produced a longer wall than most of the others, leading to questions regarding the severity of the recommended values for the factor of safety on soil strength (F_s – described later in Section 2-3-2) in CIRIA 104.

BS 8002 is the second most popular guideline after CIRIA 104, being used by 70% of design engineers. It was originally only applicable to retaining structures with a retained height of up to 8 m, but its latest amendment (2001) has increased this to 15 m. Some elements of the design specification in BS 8002 are thought to be rather onerous, particularly the unplanned excavation and surcharge requirements. These are being revised for a forthcoming version.

The Eurocodes are a set of standards which cover both structural and geotechnical design requirements, where Eurocode 7 is the geotechnical constituent. The codes have been written with the aim of allowing the design process to proceed fluidly from geotechnical to structural design without difficulty or confusion. The Eurocodes were written to be a consistent, internationally agreed set of codes for use throughout Europe and the rest of the World, so that legal disputes over choices made in design can be avoided.

The British Steel Piling Handbook was primarily written for the design of permanent and temporary sheet pile walls.

BD 42 covers the design of earth retaining structures where the "main stability is provided by a significant length of wall stem embedded in the ground" and adopts limit state

principles. It states how to "use ... BS 8002 and CIRIA 104 in a way which is compatible with ... BS 5400 (British Standard for steel, concrete and composite bridges, 2000)."

CIRIA C580 has been compiled with the intention of forming a comprehensive state-of-the-art replacement for CIRIA 104, reducing the need for cross-referencing between different design guidelines. It covers the design of temporary and permanent cantilever, anchored, single and multi-propped walls which are embedded in stiff clay, and other fine and coarse grained soils. Walls embedded in soft clay and rock are considered outside the scope of the report.

2-3-1 Choice of soil parameters

Soil parameters for a particular site are determined from a combination of: previous experience and publications; direct measurement of parameters from samples collected during site investigation (usually expensive and therefore of limited number) and indirect measurement of more easily and cheaply collected data for which correlations with the required parameters have been suggested. The most commonly required parameters are the undrained shear strength, c_u, the effective angle of friction, ϕ' and the effective cohesion, c'. Determination of these parameters is a difficult process where the cost/output relationship between the various sample and data collection techniques available must be carefully balanced.

A designer should have a good understanding of the correlations between data collected from difference sources, the factors that influence the values and the uncertainties and risk associated with the often limited data. They can then use their 'engineering judgement' to select suitable parameters. The more recent design guidelines have attempted to advise on this process and to make the designer think in terms of the probability of the parameter having a certain value or range of values.

In CIRIA 104 two alternative design approaches are put forward; the designer can either use 'moderately conservative' or 'worst credible' soil parameters (load and geometry are also selected on these bases), with less conservative safety factors being applied for the latter approach. 'Moderately conservative' is described as being a conservative best estimate, and 'worst credible' is "the worst which a designer could realistically believe might occur... a value which is very unlikely to be exceeded". BD 42 requires the

consideration of moderately conservative and worst credible parameters in conjunction with CIRIA 104.

BS 8002 requires consideration of the 'representative peak', which is generally considered to be analogous with the moderately conservative and the critical state strength parameters. The more onerous parameters are selected (after the relevant safety factors have been applied) and only one design calculation is undertaken. Eurocode 7 uses 'characteristic' values for the geotechnical parameters, which are described as "a cautious estimate of the value affecting the occurrence of the limit state".

The language varies, but in essence the emphasis is for a designer to use their experience to balance low risk with economy.

2-3-2 Application of safety factors

Once the soil parameters have been given design values, a factor of safety, F, is applied to one or more of the parameters in the ULS equation so that an adequate margin of safety is supplied within the embedment depth. There are several different approaches to applying this factor of safety: a factor on passive pressure, a factor on net pressure, a factor on embedment depth and/or a factor on soil strength. Full details of how these different safety factors compare with one another for different soil strengths are given by Burland *et al.* (1981) – a summary is given below. They go on to suggest a revised definition of the factor of safety for passive failure, F_r.

The factor on passive pressure method, F_p, (used in CP 2) employs a factor on K_p which is commonly taken to be 2. This is based on the findings of Terzaghi (1934), as described in Section 2-2-3, that (in sand) more wall movement is required to mobilize full passive pressures than active pressures. Since overconsolidated clay is very likely to reach its passive limit in front of the wall, it would be uneconomic to apply a factor of safety on passive pressure in such a deposit.

The net pressure method, described in the British Steel Piling Handbook, uses the net horizontal pressure distribution for walls propped at the crest. The depth of embedment is chosen by equating the moment about the prop of the net pressure in front of the wall with the moment of net pressure behind the wall factored by F_{np} (normally 2). Burland *et al.* (1981) showed that using this method a value of $F_{np} = 2$ leads to a factor of safety on shear strength of generally less than 1·1 for both drained and undrained conditions. CIRIA 104

expressly advises against the use of the net pressure method. Simpson and Powrie (2001) state that the net pressure method is fundamentally unsound and potentially dangerous.

As indicated by the name, the factor on the depth of embedment, F_d, requires the calculated wall depth to be increased (e.g. by a factor of 10%). CIRIA 104 advises that if this method is used then because it is empirically based it should be checked against one of the other design methods.

The use of a factor on soil strength, F_s, is consistent with the way in which factors of safety are applied in structural design. A factor is applied to the main soil parameters: tan ϕ'; the undrained shear strength, c_u; and the effective cohesion, c'; and in effect increases the active pressure and reduces the passive pressure assumed in design. CIRIA 104 provides values for F_s. This method is thought to be the most appropriate approach to design (Simpson & Powrie, 2000) and is the method recommended in CIRIA C580. (CIRIA 104 additionally requires that an unplanned excavation is applied in front of the wall, which should be the lesser of 10% of the retained height of the wall or 0·5 m, and that a minimum surcharge of 10 kPa must be applied to the surface of the retained soil. This produces a rather onerous loading condition that leads to uneconomical designs.)

BS 8002 focuses on serviceability requirements and in turn uses mobilization factors, M, which are essentially analogous to F_s, but are designed to restrict displacements for the serviceability limit state. The revised method devised by Burland *et al.* (1981) gives results consistent with F_s, and so appears to give no real advantage over the use of F_s in design.

Eurocode 7 uses limit state principles and partial factors with a design approach which is expressed as:

The Effects of Actions must be Resisted.

In terms of a retaining wall, for example, the 'actions' are the loads on the back of the wall; the 'resistance' is the resistance provided by the ground in front of the wall and the wall interface friction, etc.; and the 'effect' is the bending moment induced in the wall and the prop loads. Eurocode 7 includes three design approaches which allow for partial factors to be applied to different combinations of the Actions, Effects and/or Resistances. It is expected that Design Approach 1 (DA1) will be recommended for use in Britain. In DA1 partial factors are generally applied to the primary variables, i.e. the ground strength,

however for piles and anchors the Resistances, e.g. bearing capacity, are factored. Eurocode 7 also includes factors that allow for pile design from sensible interpretation of load tests.

2-3-3 Calculation of design bending moments

There are two main methods in common practise for calculating the bending moment in a wall in Britain. In the first, recommended in CIRIA 104, the wall length is calculated without using safety factors, i.e. the wall embedment depth is found using a limit equilibrium calculation with unfactored variables. The bending moment derived using this depth of embedment is then multiplied by a safety factor of 1·4 or 1·5 for ULS design of the wall section. In the second method, the wall length derived from using the factored parameters for the stability calculation is used to calculate the bending moment, which is then directly used for the ULS design. The second method often gives a higher bending moment than the first, meaning that if the wall was ever called upon to use its full embedment depth, its strength would not be sufficient to allow it, and it would fail in bending. This inconsistency of length and strength means the walls are either longer than they need to be, or not strong enough (Simpson & Powrie, 2000).

CIRIA C580 and Eurocode 7 use the same method for calculation of the SLS bending moment as CIRIA 104, but Soil Structure Interaction (SSI) analyses may be used to calculate the pressure on the retaining wall and therefore the redistribution of earth pressures due to arching, etc. can be taken into account, in contrast to other methods that use simple linear earth pressure distributions. In addition, CIRIA C580 requires that the wall reinforcement must not be curtailed at the point of zero bending moment, but should be extended to the bottom of the pile. Then, instead of applying a factor of safety to this bending moment for the ULS design, the designer must use the greater of: the value obtained from the most onerous soil parameters expected; a factor of 1·35 times the SLS values and the values calculated in consideration of a progressive collapse.

2-3-4 Advice on wall installation effects

The most widely used guidelines for the design of embedded retaining walls (CIRIA 104, BS 8002 and Eurocode 7) all agree that installation of a wall affects the stress state in the soil and that these effects should be considered during design, although they do not give

specific guidance about what type of stress changes may occur. CIRIA 104 notes that the installation of a diaphragm wall *may reduce* the horizontal stress in the soil from its original value. BS 8002 does not give any specific guidance on the stress change that might occur due to the installation process, it only mentions that the ratio of horizontal to vertical stress for the soil at rest should not be used as it is affected by the installation process.

CIRIA C580 goes further, giving guideline values for the reduction in the *in situ* horizontal earth pressure coefficient due to wall installation of 10% for bored pile walls and 20% for diaphragm walls installed in overconsolidated clays. These values are based on the work by Symons & Carder (1993) described earlier. It is clear that without further measurements of these stress changes in the field, considerable uncertainties remain and economy of design may not be fully achieved. CIRIA C580 also recommends that for linear elastic soil-structure interaction analyses a lateral earth pressure coefficient of 1 "is likely to give reasonably realistic bending moments and prop loads". This suggestion in part relies on the fact that in such analyses the stiffness under unloading is generally underestimated.

2-4 Use of spade cells to measure horizontal stress in overconsolidated clay

2-4-1 Background

Spade cells are increasingly used to measure horizontal soil stresses as they are relatively cheap, easy to install and give reasonably reproducible readings. However, pushing a spade cell into the ground generates high local stresses due to the displacement of the soil as the cell is advanced. These stresses reduce over time as the excess pore water pressures generated during the undrained loading dissipate (Tedd *et al.*, 1990). In natural and placed soft clays, readings stabilize within a few days and there is considerable evidence to show that realistic values of total stress can then be measured (Massarsch (1975); Massarsch *et al.* (1975); Tavenas *et al.* (1975); Penman & Charles (1981)). The use of spade cells in stiff clay was initially questioned, as it was thought that even if they could be pushed into stiff clay, the soil disturbance might be so great that the stresses would be vastly over-estimated (Tedd and Charles, 1981).

Tedd & Charles (1981) showed that it was possible to push spade cells into stiff London Clay deposits, but that a period of up to one month was needed for excess pore water pressures to dissipate. They reported that spade cells gave far more reproducible results than self-boring pressuremeter tests, but that the recorded stress following dissipation of excess pore water pressure was significantly greater than the true *in situ* value.

Tedd & Charles (1983) compared readings from spade cells installed to measure vertical stress in stiff clay with the overburden acting on them calculated from the bulk density of the soil, and concluded that the amount by which a spade cell will over-read is dependent on the soil stiffness. Owing to the difficulties in determining the appropriate soil stiffness, a correlation between the spade cell over-read and the undrained shear strength (c_u) of the soil was proposed. This was considered reasonable as the undrained shear strength of a stiff clay is related to its stiffness, and it is a commonly determined soil parameter and therefore widely available. A simple empirical correction of 0·5 c_u was suggested, although Tedd & Charles noted that where possible a direct site specific determination of the spade cell over-reading in stiff clay, for example by comparison with self-boring pressuremeter tests or calculation of overburden on a vertically aligned cell, is advisable.

In an experiment similar to that carried out by Tedd & Charles (1983), Ryley & Carder (1995) pushed several pressure cells horizontally into London Clay to measure the vertical soil stress at different depths, and compared the readings with the calculated overburden. They found that a correction of 0·8 c_u gave a closer fit for the cells in firm clay ($40\ kN/m^2 < c_u < 75\ kN/m^2$) and stiff clay ($75\ kN/m^2 < c_u < 150\ kN/m^2$). In very stiff clays ($c_u > 150\ kN/m^2$), the cell overestimated the stress by more than 1·0 c_u. They concluded that for very stiff clays, the correction factor might be as high as 2·0 c_u, and that the degree of over-read might be affected by local changes in the soil structure such as high clay content and plasticity. At the Bell Common Tunnel, Tedd *et al.* (1984) used a correction factor of 0·5 c_u for London Clay, which gave a close correlation with self-boring pressuremeter results, but a correction of 0·3 c_u gave better agreement with the self-boring pressuremeter results in the Claygate Beds. The results from some previous studies into the spade cell over-reading are plotted in Figure 2-8.

2-5 Conclusion

In this chapter the components of retaining wall design and the choices that must be made by the designer have been discussed, including the distribution of pressure on the wall, the expected effect of wall installation and the long-term behaviour of the wall. Work undertaken towards the further understanding of the importance and impact of these issues has been detailed. The design advice given by the most widely used guidelines has been discussed. It is evident that more information is required to further understand the pressure distribution on the wall, wall installation effects and the general wall stability in terms of the factor of safety.

A better understanding of the changes in stress that occur on installation of a retaining wall could result in better estimates of prop loads, wall bending moments and ground settlements than are currently possible and consequently lead to more economical designs.

The results of previous studies into the over-reading seen by spade cells installed in overconsolidated clays are rather scattered and show that a direct determination of the over-reading at any particular site is desirable.

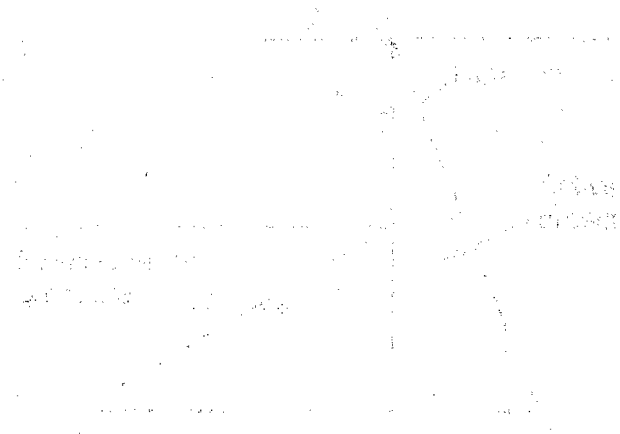

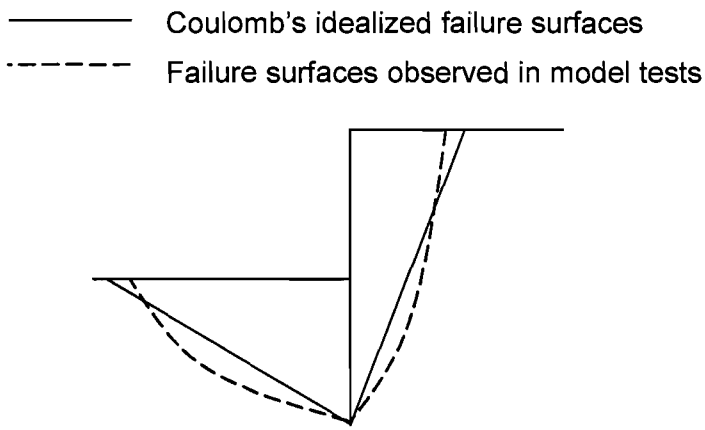

Figure 2-1: Failure surfaces arising from Coulomb's idealized earth pressure distribution

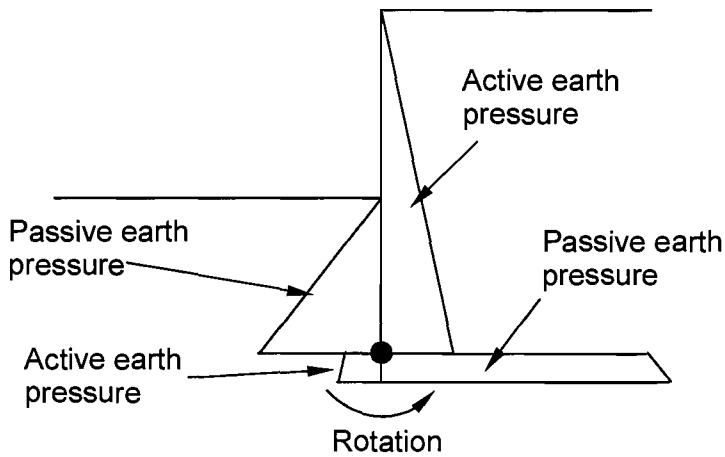

Figure 2-2: Fixed earth support

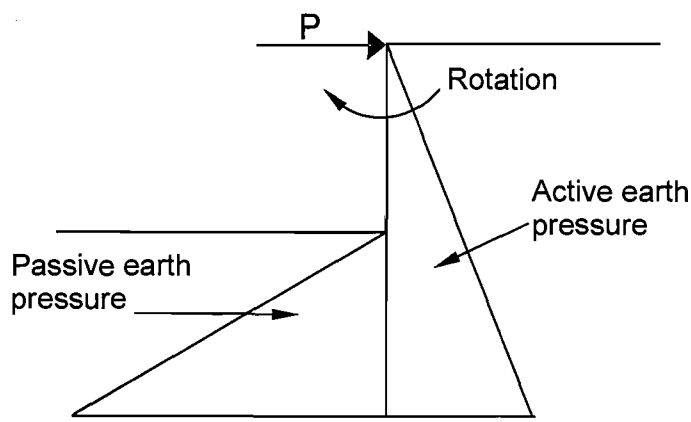

Figure 2-3: Free earth support

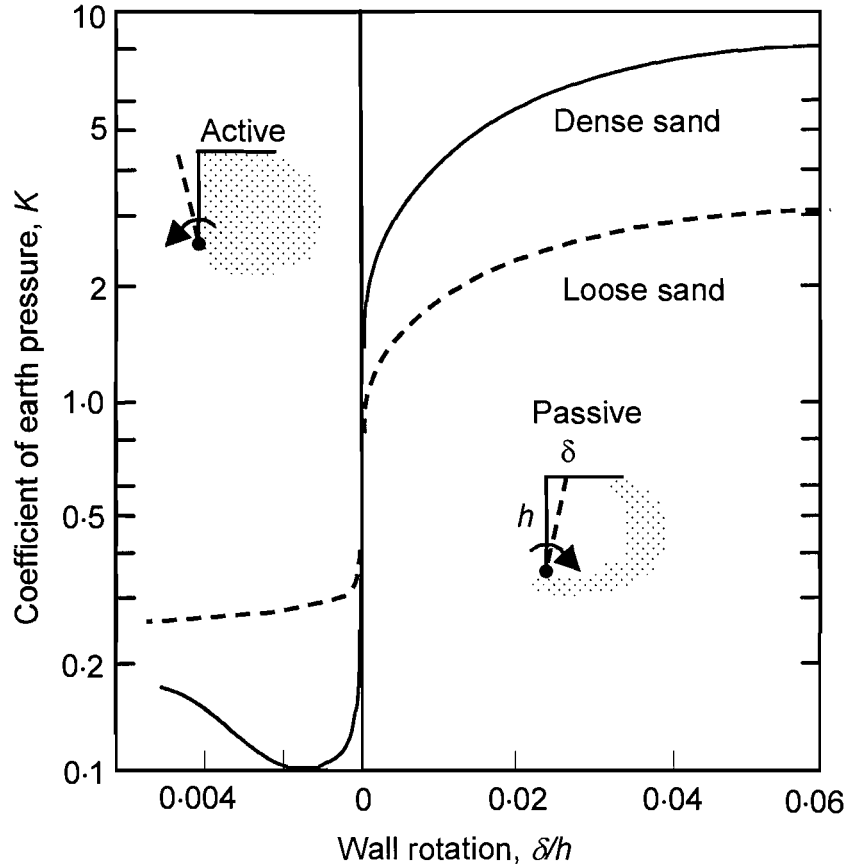

Figure 2-4: Relationship between earth pressure and wall rotation measured by Terzaghi for normally consolidated sand (different scales for active and passive pressure) (modified by Simpson, 1992)

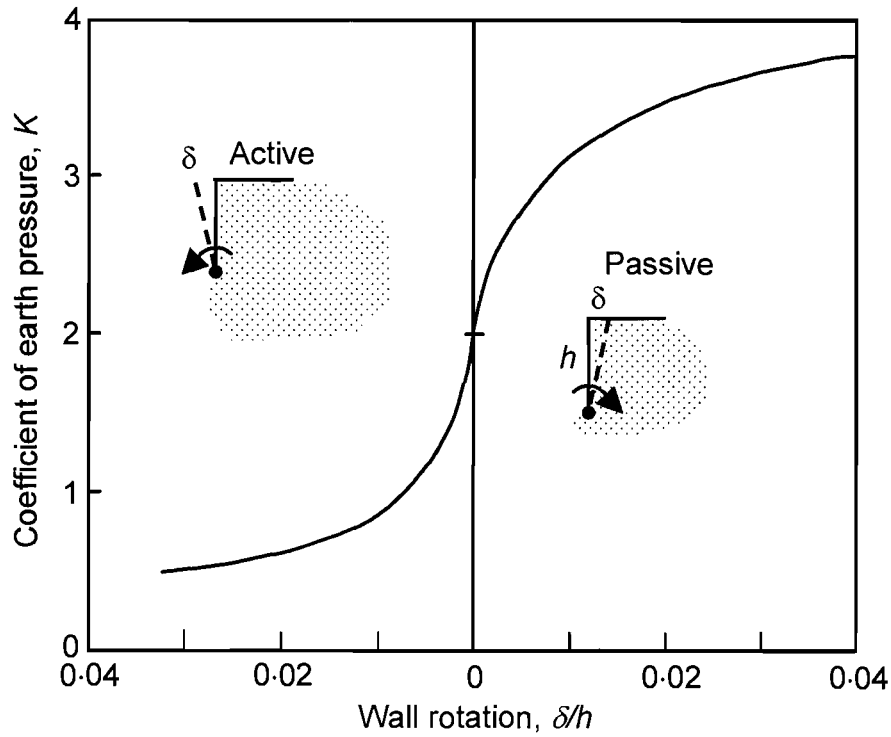

Figure 2-5: Relationship between earth pressure and wall rotation computed by Potts and Fourie (1986) for overconsolidated clay

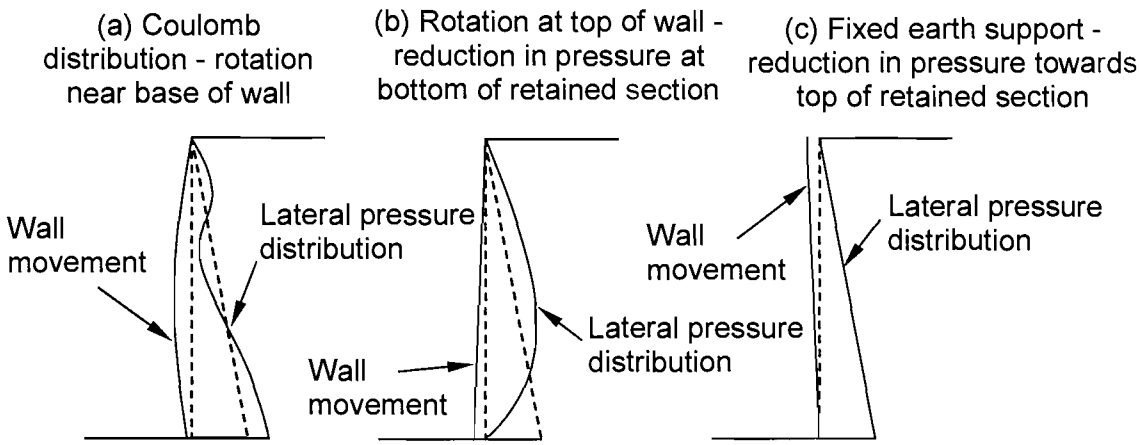

Figure 2-6: Influence of movement type on pressure distribution

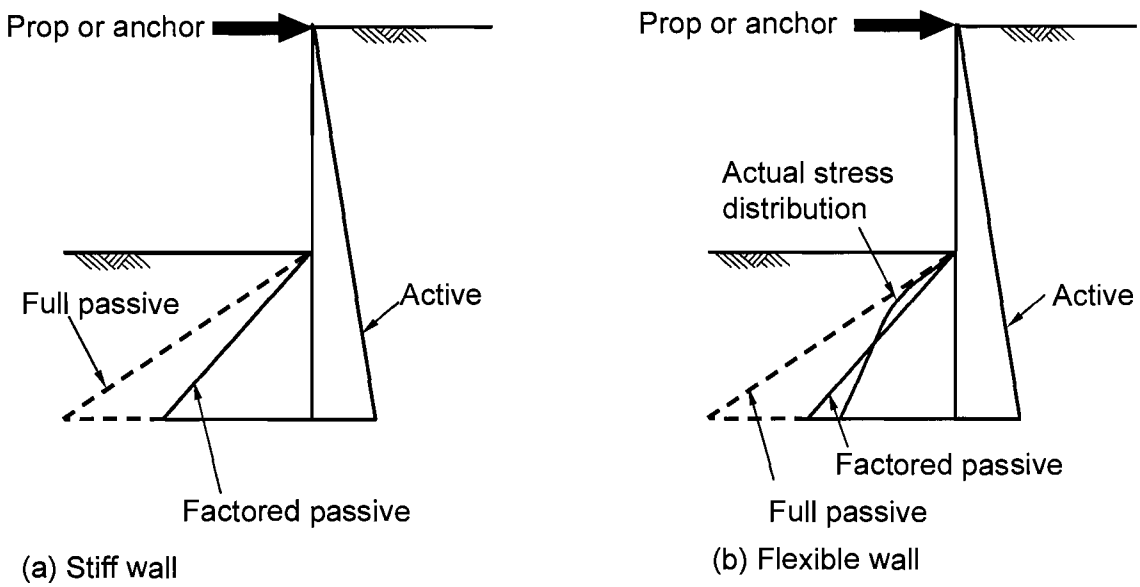

Figure 2-7: Stress distributions behind and in front of (a) stiff and (b) flexible embedded walls (after Rowe, 1952)

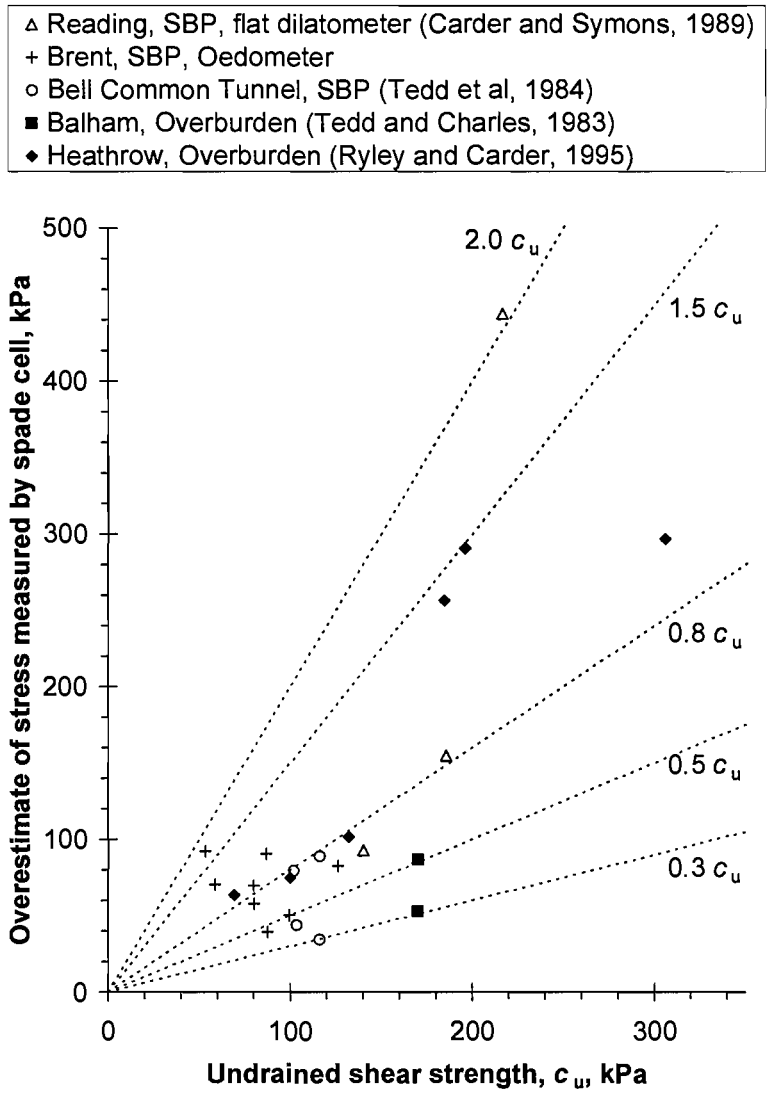

Figure 2-8: Over-reading v c_u. After Ryley and Carder, 1995.

3 CASE STUDY

3-1 Introduction

This chapter describes the geology of the field study site and details of the geometry and construction sequence of the monitored retaining wall. It includes details of the geotechnical design parameters obtained from the original site investigation for the soils at the field study site together with an outline of the instrumentation scheme implemented to measure loads within the structure and the stress changes within the ground adjacent to the retaining wall.

3-2 Geology

Two specific locations at the site are referred to in this thesis and the variation in the geology at these locations is detailed in this section. The locations are: a section of retaining wall that forms part of a propped cutting, which has been comprehensively instrumented as part of this project and is termed the 'instrumented section' and a drainage

sump next to the cut-and-cover tunnel, approximately 600 m to the north-west of the instrumented section, termed the 'nadir sump'. An assessment of the performance of the spade cells used in this study was undertaken at the nadir sump and is detailed in Chapter 5. The location of a self-boring pressuremeter (SBPM) test, referred to within this work because it exists in an area with similar geological boundaries to the instrumented section, is also noted (the relative positions of these locations are shown in Figure 3-1).

3-2-1 Geotechnical data and sample collection

Preliminary information regarding the nature of the geology at the CTRL site at Ashford and its geotechnical parameters was collected from: borehole records and laboratory tests obtained as part of the main CTRL site investigation (the locations of useful boreholes in the vicinity of the instrumented section and nadir sump are shown in Figure 3-1); the CTRL Central Ashford Geotechnical Design Basis Report (GDBR – Union Railways, 1997); the regional geology guide for the district (HMSO, 1978); the Geological Memoir (Smart *et al.*, 1966); the 1:50 000 British Geological Survey map for the area and from Humpage & Booth (2000).

A characterization of the geology at the instrumented section was carried out to gain a preliminary assessment of the nature and extent of the geological strata. Samples of material were taken from within the cutting during excavation. Block sampling techniques described by Heyman & Clayton (1999) were used to obtain undisturbed samples at the instrumented section at levels determined by the characterization. A series of steps were cut in the material with an excavation machine and blocks of approximately 0·3 × 0·3 × 0·3 m were then cut from the steps by hand. The blocks were wrapped in Clingfilm and foil to preserve the natural moisture content.

In order to obtain further high quality soil samples and to characterise the geological sequence, two wireline borehole cores were taken about 25 m from the instrumented section in July 2001 (labelled BH1 and BH2 in Figure 3-1). Photos of the wireline borehole equipment and logs of these boreholes are included in Appendix A. Samples taken from these cores and from the block samples were tested in the laboratory at the University of Southampton to determine the small strain stiffness behaviour of the clay (Xu, 2005).

At the nadir sump the geological profile was estimated from boreholes taken during the main site investigation and confirmed with observations made during excavation to form the cutting at the instrumented section. Samples were obtained during excavation of the nadir sump to provide additional bulk density data to compliment that reported in the main CTRL site investigation. The geological profile at the location of the SBPM test was obtained from adjacent borehole records (borehole reference PR3593, see Figure 3-1).

In Sections 3-2-3 and 3-2-4 descriptions of the reported and observed geology determined from these combined sources is described.

3-2-2 Site location and history

The monitoring is located in the south-east of England at Ashford, Kent. The topography of southern Kent, Sussex and part of Surrey is controlled by an anticline which can be seen on the early 19th century geological map shown in Figure 3-2 (Mantell, 1833). The stratum which overlies the Weald Clay, shown in Figure 3-2 as the Shanklin Sands, is now known as the Lower Greensand. The Channel Tunnel Rail Link (CTRL) at Ashford has been constructed along the side of the Weald of Kent valley on the basal layers of the Lower Greensand, just above its boundary with the Weald Clay, as shown in Figure 3-2. Construction of the CTRL included excavations which pass through the Lower Greensand into the Weald Clay. The Weald of Kent valley was created by the removal of the upper layers of material by denudation caused by the weakening of the material due to the folding process which produced the anticline. The removal of the upper strata results in the lower existing strata being overconsolidated, i.e. they were previously subjected to much higher vertical loading than they are at present. This process may have also caused a reduction in the effective horizontal stress in these deposits – this is discussed in more detail in Section 3-2-4.

Previous land use

The 1876 1:10560 map of Ashford shows that the site of the instrumented section was a (plant) nursery. A benchmark on this map indicates that the ground level close to the site of the instrumented wall was 40·8 m AOD (metres above ordnance datum). Before construction of the CTRL the ground level at the site was about 44 m AOD. Several metres of made ground have been placed at the site and were observed during excavation

and in nearby boreholes. The area was also used as allotments over the years and more recently has been the site of several warehouses.

3-2-3 Reported geology

Table 3-1 details the geological succession of the relevant deposits, and their approximate ages.

Period and Epoch	Succession	Age (Millions of years)	Stratotype	Thickness, m
Early Cretaceous	Lower Greensand	~112	Hythe Beds	25-90
		124	Atherfield Clay	6-28
	Wealden Formation	135	Weald Clay	up to 120 in mid Kent region

Table 3-1: Geological succession

The Weald Clay is generally a freshwater deposit, although the upper region is believed to have been laid in brackish waters. It is generally a stiff to very stiff, brown to grey clay, and in places it is thinly bedded with silt.

The overlying Lower Greensand was deposited in marine conditions. The basal layer of the Lower Greensand is the Atherfield Clay, a deposit generally up to 15 m thick in the Ashford region. The boundary between the Weald Clay and Atherfield Clay is sharply defined by an undulose erosion surface which represents a slight unconformity, however the bottom metre of the lower Atherfield Clay is sometimes confused for the top of the Weald Clay. This band of clay differs distinctly from the underlying Weald Clay and often contains a number of large oysters (Aetostreon or Exogyra) in the lowest 0·5 m, forming a useful marker horizon (Roberts, 2003). The boundary is also often stained light brown.

The Atherfield Clay is a stiff to very stiff, closely fissured fairly fossiliferous clay and consists of two distinct materials. The lower Atherfield Clay includes reddish brown or chocolaty-brown clay. The upper layer (upper Atherfield Clay) is closely to extremely closely bedded, greyish blue to brown, sandy and about 8 m thick. Humpage and Booth (2000) reported that the Atherfield Clay weathers to a brown mottled orange and red silty clay.

The GDBR notes that the Atherfield Clay has an "occasionally brecciated[1] structure" within its high plasticity zone. The boundary between the brecciated and non-brecciated clay is difficult to determine and for the purposes of design was taken to be the high-intermediate plasticity boundary. The GDBR also notes that there has been movement of the Atherfield Clay: a shear zone was found in a borehole about 750 m from the instrumented section, and cross-sections drawn through boreholes (using the high-intermediate plasticity boundary in the Atherfield Clay as a marker) show evidence of dislocation in the area of the instrumented section.

The Hythe Beds overlying the Atherfield Clay outcrop over much of the CTRL Ashford site and are approximately 1·5 m thick at the instrumented section. In general the Hythe Beds consist of alternating layers of Ragstone, a hard, greyish blue glauconitic sandy limestone and Hassock, a grey to brownish grey glauconitic, argillaceous, calcareous sand or soft sandstone. The junction between Hythe Beds and the Atherfield Clay is not distinct and as a result the top of the Atherfield Clay is sandy and glauconitic (HMSO, 1978). The Hythe Beds are generally recorded as having a basal clayey sandy layer. Springs issue at the junction of the Hythe Beds and the Atherfield Clay, hence at the Atherfield Clay outcrop the land is commonly wet and boggy and it is not possible to get an impression of the *in situ* state of the clay from its outcrops. In addition, the springs cause instability and there have been movements of large blocks of limestone and sand, which have slipped on the Atherfield Clay. The construction of the CTRL has provided an opportunity for the Atherfield and Weald Clays to be viewed in greater detail than has previously been possible.

From a study which included the Hythe Beds outcrop in the Weald of Kent near Sevenoaks, Skempton & Weeks (1976) noted that the boundary between the Hythe Beds and Atherfield Clay was difficult to determine, and that there is "probably a consistent error in plotting the base of the Hythe Beds".

---

[1] Breccia: Geol. A composite rock consisting of angular fragments of stone, etc., cemented together by some matrix, such as lime: sometimes opposed to conglomerate, in which the fragments are rounded and waterworn. (source: Oxford English Dictionary)

3-2-4 Observed geology

Weald Clay

The upper Weald Clay contains many silt laminations and occasional bands of siltstone, about 100-200 mm thick, were recorded (see Appendix A). In some cases the silt laminations were a few millimetres thick and there was proportionally more silt than clay in the recovered core. These laminations generally dipped at approximately 20°.

Figure 3-3 shows the Weald Clay exposed by excavation at another part of the CTRL. Layers in the Weald Clay can be clearly seen and are similar to those observed in the wireline borehole core taken at the instrumented section.

Atherfield Clay

The erosion surface reported to exist between the Atherfield and Weald Clay was observed in the cores taken close to the instrumented section (see Appendix A). The surface was stained brown and about 2 mm of crumbly organic material existed between the Atherfield and Weald clays.

The lower Atherfield Clay was chocolate-brown and very stiff. It is delineated by a distinctive 400-500 mm thick band of light brown material at the top, which was observed in the nadir sump (Figure 3-4).

In the upper Atherfield Clay zones of thin silt partings, which become more frequent towards the bottom of the stratum, were recorded. At the top of the upper Atherfield Clay stratum the material consists of peds[2] surrounded by a softer matrix. This is evidence of the brecciation described in the GDBR (see Section 3-2-3). It also indicates weathering (grade III – described as "stiffer, less weathered lumps of clay (lithorelics) in a matrix of disturbed, softer clay" by Chandler, 2000). The size of the peds reduces with depth and the soil becomes more consistent. Figure 3-5 shows a block sample of the upper Atherfield Clay prior to removal. On cutting the material very hard peds up to 100 mm wide, which can be seen in Figure 3-5, fell away. These peds are very hard and impossible to cut by hand with field instruments and the action of attempting to cut the soil caused significant disturbance and damage to the samples. The peds are surrounded by softer crumbly

[2] Ped: an individual natural soil aggregate (*U.S. Department of Agriculture Yearbook,* 1958).

material, to which some smearing caused by the cutting process is evident in Figure 3-5. This observation is consistent with the description of the Atherfield Clay near Ashford given by Smart *et al.* (1966) as a, "grey clay that crumbles into cubical lumps". These lumps are caused by the opening up of fissures on unloading of the soil – a process likely to provide drainage paths, thereby allowing easier movement of water than the measured *in situ* permeability of the material might indicate.

Hythe Beds

The Hythe Beds was approximately 1·5 m thick at the instrumented section and consists of stiff to very stiff yellow/grey mottled sandy clay (apart from the colour, it is very similar in appearance to the top of the upper Atherfield Clay). At the transition between the yellow/grey mottled material and the grey material there are peds of grey material within a yellow matrix. Samples of the Hythe Beds taken during excavation were observed to consist of firm to stiff mottled light brown and light grey sandy clay with pottery tile, rotten wood fragments and large dark brown rootlets (Figure 3-6). Block sampling within the Hythe Beds was found to be relatively straight forward, as the clay cut easily due to the presence of fine sand, and the samples remained intact.

For the purposes of this work the boundary between the Hythe Beds and the Atherfield Clay has been taken to exist where the colour of the clay changes from mottled yellow/grey to grey, which coincides with a small increase in the plasticity index (due to a reduction in the quantity of sand in the deposit). On this basis the upper Atherfield Clay layer is 8·75 m thick at the instrumented section, which is generally consistent with measurements from boreholes across the site.

Above the Hythe Beds is about 2 m of made ground, which is firm mottled dark brown/grey organic sandy clay with pottery tile, rootlets and rotten wood fragments. Figures 3-7 and 3-8 show the dark brown made ground, the yellow/light grey Hythe Beds and the dark grey upper Atherfield Clay during excavation of the cutting.

General

There is evidence to suggest that there has been historic movement of the upper regions of the Atherfield and possibly the Weald Clay in the area of the instrumented section. Figure 3-9 shows a shear plane observed in the excavation for the cutting 50 m to the west of the instrumented section. The shear plane dips at 45° to the south-southwest with a strike of

approximately 070° (east-northeast). Other shear planes have been observed within the Atherfield Clay and Weald Clays formations. Figure 3-10 shows a sketch of a discontinuity (possibly a shear plane) observed in the base of the excavation for the cutting at the instrumented section before blinding was laid for the base slab (see Sections 3-4 and 3-5 for details of the construction and instrumentation layout). There was an apparent error of approximately 1·5 m in the logging of the two wireline boreholes taken 25 m behind the north wall at the instrumented section. The observed shear plane suggests that rather than this being an actual error, this discrepancy may be due to disturbance/faulting between the two borehole locations.

3-3 Geotechnical properties

3-3-1 Plasticity

Due to the variable silt content of the Weald Clay its plasticity index ranges between 10-30%. The upper Atherfield Clay is generally of relatively high plasticity, with a plasticity index of approximately 50%. The lower Atherfield Clay has a plasticity index of 20-30%.

Profiles of the soil found from the wireline boreholes taken 25 m from the instrumented section, including liquid limit, plastic limit and moisture content data, are shown in Figure 3-11. The moisture content is at or close to the plastic limit and there is a clear change in plasticity from intermediate to low plasticity within the upper Atherfield Clay stratum, about 2·3 m above the level of the boundary with the underlying lower Atherfield Clay. This is explained by the increase in silt zones in the lower part of the upper Atherfield Clay stratum.

A comparison of the geology at the instrumented section, the nadir sump and the location of the pressuremeter test is shown in Figure 3-12. At the nadir sump the ground level was reduced by approximately 8·2 m before construction.

3-3-2 Bulk density

Bulk density measurements from the main CTRL site investigation and samples obtained during excavation of the nadir sump are shown (plotted in m AOD) in Figure 3-13.

3-3-3 Soil strength

The moderately conservative (see Section 2-3-1) value for the effective angle of soil friction, ϕ', recommended in the GDBR for the Weald Clay is 23° with the effective cohesion, c', equal to 0. Further interpretation of the presented data indicates a ϕ' of 24° with $c' = 0$ may give a more appropriate 'average' value.

The moderately conservative ϕ' value recommended in the GDBR for the intermediate plasticity Atherfield Clay is 21° with $c' = 4$ kPa. However, further interpretation of the presented data indicates a value of 24° with $c' = 0$ may be a more appropriate 'average' value. In addition, triaxial tests carried out at the University of Southampton by Xu (2005) on samples of the lower Atherfield Clay collected from the rotary drilled cores (described in Section 3-2-1) indicated a ϕ' for the lower Atherfield Clay of 26° with $c' = 10$ kPa (Figure 3-14).

For the high plasticity Atherfield Clay the GDBR generally recommends a moderately conservative ϕ' value of 24° with $c' = 10$ kPa for the non-brecciated and 29° with $c' = 0$ for the brecciated region in the central Ashford area. However, the report notes that the fissuring observed in the Atherfield Clay in the localised area of the instrumented section is indicative of land movements (described in Sections 3-2-3 and 3-2-4) and therefore a value relating to the remoulded state of the clay was used for design: $\phi'_{crit} = 18°$. This value was later increased to 20° on reinterpretation of the data (Union Railways Ltd, 1997 B).

In the GDBR the value taken for the Hythe Beds as the moderately conservative soil strength, ϕ', was 30° and $c' = 0$. The limestone and soft sandstone that the Hythe Beds generally consist of (see Section 3-2-3) would be responsible for much of this strength, but were not present at the instrumented section: the lowest part of the Hythe Beds consists only of sandy clay.

These soil strength parameters are summarised in Table 3-2.

		Effective angle of soil friction, ϕ' (moderately conservative), °	Effective cohesion, c', kPa
Weald Clay		23	0
lower Atherfield Clay and intermediate plasticity upper Atherfield Clay	GDBR	21	4
		24	0
	Xu (2005)	26	10
high plasticity upper Atherfield Clay	non-brecciated	24	10
	brecciated	29	0
	remoulded	18/20	0
Hythe Beds		30	0

Table 3-2: Soil parameters of the Atherfield Clay and Weald Clay

Figure 3-15 shows the undrained shear strength (c_u) as a function of depth, determined from unconsolidated undrained triaxial tests on 100 mm samples and estimated from standard penetration test (SPT) results. The SPT blowcount N multiplied by 4·5 (Stroud, 1974) correlates closely with the laboratory data for the Atherfield Clay, but gives values generally in excess of the laboratory tests for the Weald Clay. This is consistent with known sampling effects and in particular the disturbance to the microstructure, fabric and mean effective stress caused by thick walled tube sampling in stiff clays (e.g. Hight & Leroueil, 2003). In the Ashford site's Geotechnical Design Basis Report (Union Railways Ltd, 1997) a value of 4·5 was used to factor the SPT data for the Atherfield clay and 3·5 was used for the Weald Clay. The best-fit line to all the data in the Atherfield Clay is indicated, and is given by Equation 3-1. Figure 3-16 shows the undrained shear strength found from the SBPM test PR3593 (for the location see Figure 3-1). The SBPM data indicate slightly higher undrained shear strengths compared with the laboratory tests and SPTs.

$$c_u \text{ (kPa)} = 22 + 7\,z \text{ (z in m below ground level)} \qquad \textbf{Equation 3-1}$$

3-3-4 In situ horizontal stress

Figure 3-17 shows the *in situ* horizontal stress interpreted from the SBPM test. These data imply an *in situ* earth pressure coefficient of approximately 1 (although they are measurements of total rather than effective stress). This is rather less than would be expected on the basis of the one-dimensional stress history of the deposit. Movement of

the soil by faulting or a landslide (described in Section 3-2-4) may reduce the *in situ* horizontal earth pressure coefficient, K_o, to below that which might otherwise be expected for a stiff overconsolidated clay on the basis of its stress history.

As previously mentioned, the geological folding that created the anticline shown in Figure 3-2 may also have had the effect of releasing horizontal stress as the soil stretched and weakened. The London Clay (a much younger deposit than the Atherfield and Weald clays), also seen on the section shown in Figure 3-2, was folded inwards by this process which may have contributed to its relatively high *in situ* horizontal stress.

3-3-5 Permeability and Groundwater

Data from variable head permeability tests taken during the main site investigation are shown in Figure 3-18. Due to the paucity of the data no firm conclusions can be drawn, however, it appears that the Atherfield Clay has a very low permeability of about 1×10^{-8} m/s, the Hythe Beds have a slightly higher permeability of about 1×10^{-7} m/s and the Weald Clay has a variable permeability of between 4×10^{-9} m/s and 2×10^{-6} m/s (the variation is due to the silt laminations).

Roberts *et al.* (*in print*) state that reliable results from 5 tests in the Atherfield Clay and 20 in the Weald Clay carried out in the Central Ashford area gave an average permeability for the Atherfield Clay of 3×10^{-8} m/s (with a range of 2×10^{-9} m/s to 9×10^{-8} m/s) and 1×10^{-8} m/s for the Weald Clay (with a range of 1×10^{-9} m/s to 3×10^{-7} m/s). Roberts *et al.* state however that borehole permeability tests are known to be unreliable, often underestimating the true permeability by an order of magnitude or more. They go on to report the results of a pumping tests using ejector wells which indicated the permeability of the Weald Clay to be in the order of 1 to 2×10^{-6} m/s.

The GDBR indicates that the *in situ* groundwater in the area of the instrumentation is approximately 1 m below ground level. Extension of the best-fit line to the pore water pressure data in the strata above and including the upper Atherfield Clay (Figure 3-19) indicates the groundwater level to be at 42·7 m AOD (ground level is at 43·7 m AOD), concurring with the GDBR. The water pressure distribution in these strata is represented by Equation 3-2, where u is the pore water pressure and L is level in m AOD.

$$u = 8{\cdot}28 \times (42{\cdot}706 - L), \text{ for } L < 42{\cdot}706. \qquad \textbf{Equation 3-2}$$

This equation indicates under-drainage of the Atherfield Clay (if the equation represented a hydrostatic distribution of water pressure, the multiplier value 8·28 would be 9·81, the density of water). This is probably due to the horizontal silt laminations in the underlying Weald Clay acting as drainage paths, and the dewatering in a section of the CTRL approximately 100 m from the instrumented section was shown to have an influence on the groundwater regime up to 500 m away (Roberts *et al.*, *in print*). This dewatering occurred over the period of wall installation at the instrumented section.

The data collected at the dewatered section approximately 100 m away from the instrumented section indicates that the lower Atherfield and Weald clays have been subjected to a drawdown of 5 m. This is consistent with the lower pore water pressures measured in the lower Atherfield Clay. The water pressure profile produced by this drawdown is shown in Figure 3-19, and given in Equation 3-3. The dotted line indicates the likely water pressure profile in the lower Atherfield Clay.

$$u = 9{\cdot}81 \times (37{\cdot}709 - L), \text{ for } L < 37{\cdot}709. \qquad \textbf{Equation 3-3}$$

3-4 Description of site and geometry of structure at the instrumented section

The instrumented section of the Channel Tunnel Rail Link (CTRL) is approximately 350 m northwest of Ashford International Station in Kent (Figure 3-20). It consists of a propped contiguous bored pile retaining wall formed from 21 m long, 1·05 m diameter piles spaced at 1·35 m centres. The piles at the instrumented section were installed in November and December 1999. Figure 3-21 shows a cross-section of the instrumented section. The cutting width is approximately 12 m and the excavation depth 10 m. The walls are permanently supported at crest level by 1 m square reinforced concrete props spaced at 4·5 m centres and at formation level by a reinforced concrete base slab. A corbel was added to the retaining wall above the base slab at a later date to prevent slab uplift. Temporary tubular steel props were employed during excavation to support the walls until the base slab had been constructed.

In the Ashford area the CTRL follows a contour along a valley side, with the ground sloping down from the northeast to the southwest. The construction is therefore not symmetrical about the centreline of the excavation. Behind the south wall lies the London

to Dover main railway line and other local railway lines. The ground level behind the south wall was reduced by several extra metres during construction of the CTRL to enable construction of another railway line, as shown in Figure 3-22. Unfortunately access to the south wall was not available due to site constraints and so it was not possible to monitor its movement.

3-5 Construction sequence and installation of instrumentation

Approximately one month prior to installation of the contiguous piles, sixteen Soil Instruments vibrating-wire push-in pressure cells with integral vibrating-wire piezometers (spade cells) were installed adjacent to the line of the retaining wall. The spade cells measured the *in situ* total horizontal stresses and pore water pressures and the subsequent changes due to bored pile installation and further construction events. Figures 3-23 and 3-24 show the general arrangement of the spade cells in relation to the retaining wall. In determining the positions of the spade cells, careful consideration was given to the proximity of the individual bored piles allowing for pile installation tolerances (more relevant to the deeper instruments) and the localised effect of pile installation on the surrounding soil (Richards *et al.*, *accepted for publication*). The spade cells were installed at three different distances from the line of the wall, so that any variation in the influence of wall installation effects with distance from the wall could be determined. The array of instruments was spread out laterally along the wall owing to the need for a separate installation borehole for each spade cell. The spade cell cables were sheathed in brightly coloured sturdy plastic tubing near ground level behind the wall and to the depth of formation level in front of the wall, in order to protect the cables and to provide a visual marker during construction and excavation activities.

The dates of the main construction events are shown in Table 3-3, and details of the main construction events are outlined below. For the purposes of this thesis all graphs and data are referenced with respect to the number of days from the beginning of the project, with the day the first spade cell was installed, 8th October 1999, being Day 1. The last significant construction activity at the instrumented section occurred when the last instrumented temporary prop was removed on Day 595.

Stage	Name	Schematic	Day	Date
1	Spade Cell Installation	see Figures 3-23 and 3-24	1-13	8th-20th October 1999
2	Pile Installation	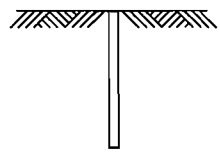	47-71	23rd November to 17th December 1999
3	Sand Drain Installation	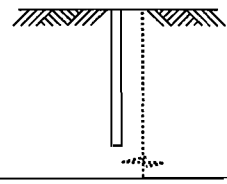	349-352	20th-23rd September 2000
4	Capping Beam Construction	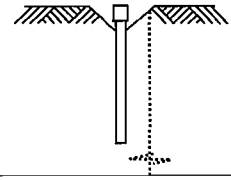	440-442	approximately 20-22nd December 2000
5	RC (reinforced concrete) Prop Construction	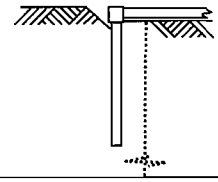	465 467	Props 1 & 2: 14th January 2001 Prop 3: 16th January 2001
6	Excavation Phase 1	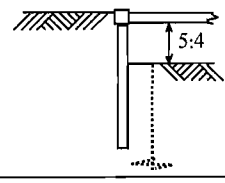	483-509	1st-27th February 2001 (no work 7th-21st Feb inclusive)
7	Temporary Prop Installation	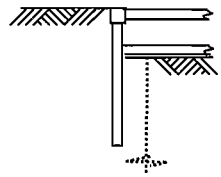	512 522	Prop 1: 2nd March 2001 Props 2 & 3: 12th March 2001
8	Excavation Phase 2	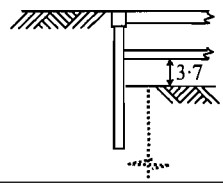	530-537	20th-27th March 2001
9	Base Slab Construction	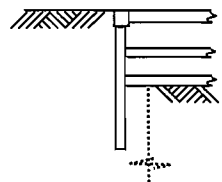	579	8th May 2001
10	Temporary Prop Removal	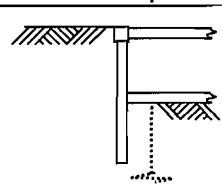	581 595	Prop 1: 10th May 2001 Props 2 & 3: 24th May 2001

Table 3-3: Dates of main construction events

An essential component of this project was the full-time presence of the researcher on site throughout the main construction period. This allowed the researcher to compile a detailed diary of the construction events (and any other activities which may have affected the soil stress or structural loads) and to link these changes with the collected measurements.

3-5-1 Pile installation

The lettering on the piles in Figure 3-23 indicates the sequence in which the piles were installed and is detailed in Table 3-4. Appendix B contains more detailed information regarding the pile installation period.

The pile installation process is shown in Figure 3-25 and illustrated in Figure 3-26, 3-27 and 3-28. In most cases, the uppermost 8 m of the pile bore was excavated on one working day following which a casing was inserted to support the sides (this process took between 20 and 80 minutes, with an average duration of 27 minutes). The remainder of the bore was excavated on the next working day without any further form of support, although on reaching the required depth bentonite slurry was introduced up to original ground level (this took between 20 and 50 minutes, with an average of 30 minutes). The reinforcement cage was then lowered into the borehole and concrete was tremied in from the base at the same rate that the bentonite was removed. (This process was implemented after observation of trial boreholes left open for several days showed that those in the Atherfield Clay would remain stable for at least 24 hours whereas deterioration occurred more quickly in Weald Clay; Roscoe and Twine, 2001). The exception to this installation sequence was a single pile in period D1 (see Figure 3-23 and Table 3-4) for which excavation and concreting were carried out within one afternoon, immediately after period D. It is also of note that certain piles were installed on a Friday (pm) and Monday (am), so following excavation to 8 m the hole was left cased and open over the weekend.

Installation period	Boring started		Casing depth reached, casing inserted	Boring restarted		Pile completed, bentonite added	Concreting started	Concreting ended
	Day	Time	Time	Day	Time	Time	Time	Time
A	47	1510-1550	1540-1620	48	1155-1255	1235-1330	1420-1550	1453-1638
B	49	1440-1720	1600-1740	50	0805-0916	0845-1001	0916-1225	1002-1311
C	53	1459-1625	1520-1646	54	0800-0934	0835-1000	0955-1227	1032-1315
D	55	1518	1542	56	0910	1000	1109	1150
D1	56	1220	1255	56	1255	1350	1626	1724
E	57	1150-1435	1218-1500	60	0906-1310	0941-1335	1112-1540	1156-1627
F	64	1040-1108	1130-1200	67	0810-0842	0842-0905	0950-1114	1036-1201
G	67	1715	1746	68	0848	0908	1058	1145
H	69	1631-1659	1657-1721	70	0810-0841	0840-0905	0933-1040	1006-1117
I	71	1135-1203	1200-1225	74	1120-1148	1146-1210	1430-1605	1545-1705

Table 3-4: Sequence of pile installation. Also see Figure 3-20

In each installation period, between 1 and 4 piles were installed. The times given represent the range including all piles within each period

An inclinometer tube was installed within pile Z (see Figure 3-23) to measure the deflected profile of the wall and to allow the bending moments to be estimated from the deformed wall profile. (An inclinometer tube was also installed in the pile nearest to spade cell 12 but the tube was damaged during construction and was unusable.) The inclinometer tubing extended 10 m into the natural ground below the toe of the pile thereby establishing a fixed point and eliminating the need to rely on surveying the top of the wall to determine its overall movement. Bending moments were also calculated from strains measured using vibrating-wire embedment gauges installed in piles X and Y (Figure 3-23). Pairs of gauges were situated at 1·5 m intervals down the piles (see Figures 3-29 and 3-30).

3-5-2 Sand drains

Sand drains were installed between the cutting walls to reduce the pore water pressures in front of the retaining wall during construction. The retaining wall design was based on the assumption that hydrostatic pore water pressures would exist on both sides of the wall: from ground level behind the wall and from the bottom of the excavation in front of the wall. However, there were concerns that the flow of water through the wall (or around the toe) could result in higher pore water pressures in front of the wall. This could reduce the passive effective stresses and therefore overstress the wall, or, depending on the permeability of the Atherfield Clay, cause pore water pressures to build up in the Weald Clay underneath the Atherfield Clay (due to the relatively high horizontal to vertical permeability of the Weald Clay) which may cause the 'plug' of Atherfield Clay above to be pushed upwards. The sand drains were therefore designed to relieve any pore water pressure build up in front of the wall and ensure that the hydrostatic pore water pressure profile assumed in design was achieved (Roscoe, 2005).

The 30 m deep sand drains were installed at 3 m ± 0·5 m centres in two lines, 3 m from each wall. The sand drains in the vicinity of the instrumented section were installed over a period of about 3 days. Each drain comprised a 150 mm diameter hole (bored without casing) filled with 10 mm gravel. The line of sand drains near to the north wall fell between most of the spade cells in front of the retaining wall, shown in Figure 3-23. A 0·5 m leeway in the position of the sand drains was used to ensure that spade cell 17 and its cable were not endangered by the sand drain installation. Figure 3-31 shows the sand drain nearest to spade cell 11 during excavation.

After excavation of the cutting to formation level a shallow channel (less than 200 mm deep) was excavated and filled with 10 mm gravel to link the sand drains under the base slab. Drain holes were installed in the base slab so that water could drain through it, thereby preventing the build up of pore water pressure under the base slab.

Data for the period immediately following sand drain installation is limited as construction activities had commenced within the instrumented wall section and during this period some of the gauge wires were broken; these activities included construction of a large slab behind the wall and excavation around the wall for the capping beam construction (see Section 3-5-7). Total horizontal stress and pore water pressure data collected prior to construction of the capping beam are shown in Figure 3-32 (total stress measurements are corrected by 0·35 c_u to allow for spade cell installation effects: see Chapter 5). The figure shows that installation of these drains appears to have had little effect on pore water pressures and total stresses in the short-term.

3-5-3 Removal of pile tops

A month after installation of the sand drains (Days 382 to 384) the soil on either side of the piles was excavated to a depth of approximately 2 m (Figure 3-33) in order that the piles could be broken down to competent concrete, the pile tops removed and the capping beam constructed. The pile tops were removed using the 'Elliot' method. This involves drilling holes through the pile at the pile cut-off point and inducing a crack across the pile section. Removal of the concrete pile top is aided by a foam covering on the reinforcement bars above the cut-off point which restricts bonding between the reinforcement and the concrete (Figure 3-34). The pile tops in the vicinity of the instrumentation were removed in the days around Day 413 (23rd November 2000) (see Figure 3-35).

During removal of the pile tops it was necessary to release the vibrating-wire strain gauge cables from the concrete. The cables were installed in a duct attached to the pile reinforcement and extending down to the level of the pile cut-off (about 1 m) before the pile concrete was poured, so that when the concrete was 'cut-off' the cables were carefully drawn through this ducting so that they exited the pile at the cut-off level. The pile gauge cables were then run through ducting within the blinding for the capping beam, along with the cables from the spade cells installed in front of the wall.

3-5-4 Capping beam

The capping beam had the dimensions shown in Figure 3-36 and can be seen in Figure 3-37. Around the time that the capping beam was constructed the ground level between the tunnel walls was reduced by up to 1 m in preparation for the construction of the reinforced concrete props. A 2 m high wall was built on the capping beam approximately 45 days after Temporary Prop Removal.

3-5-5 Reinforced concrete props

The reinforced concrete (RC) props were constructed on blinding approximately 75-100 mm thick. Plastic liner was used to separate the blinding form the poured concrete. Blackjack was pained onto the capping beam at the locations of the forthcoming RC props, as shown in Figure 3-38. There was no steel connection between the capping beam and the RC prop. Shuttering was then erected, the pre-fabricated steel cage installed and the concrete poured. During excavation under the props the blinding was removed.

Vibrating-wire embedment strain gauges were installed in three of the RC props to measure axial loads. The locations of the monitored props in the instrumented section are shown in Figures 3-39 and 3-40. Each RC prop was fitted with four gauges, 2 m from the northern end. The prop load is calculated from the average of the outputs of the four gauges at each cross-section to eliminate the effects of bending. In addition, bending was measured in prop P2 using two further sets of 4 gauges located at 4 m and approximately 6 m (at the centreline of the excavation) from the northern end. The gauges are situated at 0°, 90°, 180° and 270° on the cross-section of the prop and numbered as shown in Figure 3-29. The pre-instrumented reinforcement cage for RC prop P3 was erroneously placed in the position of RC prop 4: hence RC prop 3 is not instrumented.

3-5-6 Backfilling and material placement behind North wall capping beam

On Day 476 backfill was placed behind the capping beam on the north wall up to within 0·5-1·0 m of the western extent of the instrumentation. On Day 477 backfill was placed to within 0·5-1·0 m of the eastern extent of the instrumentation. Backfill was placed behind the capping beam at the instrumented section on Day 480 (Figure 3-41).

On Days 487 and 488 a large crane platform (1200 tonnes) was constructed behind the wall close to the instrumented section, using 400 tonnes of ballast. (The crane was used to lift a nearby footbridge into position.) Some time between Days 489 and 495 approximately 700-800 mm of hardcore was placed and compacted directly behind the wall over an area encompassing the whole length of the instrumented section to provide a stable platform for the long-reach excavator on its return.

3-5-7 Excavation

As illustrated in Table 3-3, there were two main excavation phases: Excavation Phase 1 reduced the ground level within the cutting to just below temporary prop level (36·759 m AOD) and Excavation Phase 2 reduced the ground to formation level (33·559 m AOD). Figure 3-42 shows an elevation of the instrumented section indicating the dates on which particular regions were excavated. The bulk of the material was removed with a long-reach excavator situated at ground level behind the wall (Figure 3-43). A more manoeuvrable mini-digger located within the cutting was used to remove any remaining material. In order to minimise instrument cable breakages the long-reach excavator operator avoided the soil around the cables within the excavation and the mini-digger was used to carefully remove this material at a later stage. A blinding layer was poured across the base of the excavation within a few days of reaching final formation level.

3-5-8 Temporary props

The temporary props were hollow steel sections with an external diameter of 1016 mm, a wall thickness of 22·2 mm and a Young's modulus, E, of 205 GN/m^2. The load from the wall was transferred to the temporary props by a concrete thrust block and waling beam arrangement, as indicated in Figure 3-21 and Figure 3-44.

The load in three temporary props was measured with 12 vibrating-wire surface-mounted strain gauges. Four gauges were fitted to each prop, 2 m from the northern end. The gauges are welded onto the prop (see Figure 3-45) at 45°, 135°, 225° and 315° on the prop cross-section and were covered with insulated metal housings to minimize damage from machinery and falling soil during excavation. The positions and numbering system are shown in Figure 3-29.

3-5-9 Base slab

The dimensions of the base slab are shown in Figure 3-46. The base slab was constructed in 11 m long segments. The instruments were installed such that they traversed the same section of wall as Slab A4 (shown in Figures 3-23, 3-39 and 3-42 – note that the intension was to monitor P3 instead of P4: see Section 3-5-5). The base slab to the west (A3) was poured on Day 571 and the slab to the east (A5) was poured on 590.

Eight vibrating-wire embedment strain gauges were attached between the reinforcement steel in pairs along the centreline of the base slab, at 2 m intervals, to measure load in the base slab. One gauge of each pair was at the top of the slab and the other at the bottom (Figures 3-29 and 3-47). These gauges were connected to the datalogger on Day 575, four days before the base slab was constructed, so that readings of strain and temperature could be taken before and throughout the concrete pour.

The base slab gauges were irrecoverably lost on Day 1278 (7th April 2003) when the tunnels were cleared out in preparation for installation of the over-head high-voltage transmission lines.

3-5-10 Installation of storm drain

Six months after the main construction activities had been completed a storm drain was installed approximately parallel to and behind the north wall on 9th November 2001 (see Figure 3-48). The storm drain was about 0.5 m diameter and the distance between its centreline and the edge of the wall was approximately 4 m. It was installed at an elevation of approximately 41m AOD.

3-6 Data collection and vibrating-wire instrument technology

Vibrating-wire instruments were used because they are relatively easy to install and can be monitored remotely and continuously using a datalogger. All of the instruments were wired to a CR10X Campbell Scientific datalogger with 2 vibrating-wire interfaces and 7 multiplexers (Figure 3-49). On collection the data was saved in both the datalogger and a storage module to minimise data loss during data downloading. A photovoltaic cell and inverter were connected to the datalogger battery to ensure continuous battery charging; hence the system was effectively self-maintaining. A remote data collection system was

set up to collect and process the data (Richards *et al.*, 2003). This enabled data to be automatically downloaded daily (via a modem) to several storage locations at the University of Southampton, the raw data readings to be converted to AGS-M format (CIRIA, 2002) and subsequently uploaded to a remote server where the data could be viewed via a website within 24 hours of their collection.

For operational reasons (for example to allow any cable breakages occurring during excavation and construction to be detected quickly) the datalogger was set up to take readings of all instruments every 5 minutes so that at any time on accessing the datalogger a reading obtained within the last 5 minutes could be viewed. Instrument readings were stored in the datalogger at intervals of between 5 minutes and 2 hours, depending on the level of activity on site.

All of the instrumentation used on site to monitor the structural loads, soil stresses and pore water pressures used vibrating-wire transducer technology. Vibrating-wire transducers contain a tensioned wire which is 'plucked' by a solenoid via a datalogger instruction and the resulting frequency of vibration of the wire, which is proportional to the strain in the gauge, is measured within the magnetic field of the solenoid (see Figure 3-50). As the length of the strain gauge (and therefore the wire within it) elongates or contracts (depending on the stress patterns in the member in which it is installed), the frequency at which the wire vibrates changes accordingly. The strain gauges also contain thermistors for temperature measurement.

To obtain a strain reading from a vibrating-wire transducer the datalogger sends an electric pulse which excites the solenoid within the instrument creating a magnetic field, causing the wire to vibrate. The minimum and maximum frequencies of the 'sweep' are specified by the user and depend on the type of gauge being used. The measured frequencies are sent to the strain gauge sequentially starting with the lowest frequency and finishing with the highest; this takes 150 ms. Although the wire vibrates at every frequency, the non-resonant frequencies die out quickly, leaving only the resonant frequency which remains for a relatively long time. After waiting for the non-resonant frequencies to die out (20 ms) the datalogger then measures the time taken for a user specified number of vibrations to occur. This is used to find a value for the average frequency of vibration. The datalogger then records the square of this frequency (expressed in units of kHz^2 – see Equation 3-4, where T is the period in milliseconds).

$$F^2 = \frac{1}{T^2}.$$ **Equation 3-4**

For this project the datalogger was set up to sweep between 800-1300 Hz and to obtain the average frequency reading over 80 cycles for the concrete embedded and surface mounted strain gauges and to sweep between 1600-30000 Hz and take readings over 100 cycles for the spade cells and piezometers. These figures were based on the instrument and datalogger manufacturers' advice.

At the reading interval specified in the datalogger (e.g. 5 minutes) readings are taken from all instruments in succession. When using a large number of instruments in any datalogging system it is important to ensure that the interval is long enough for all the instrument readings to be obtained successfully.

Some instruments experienced periods of downtime due to inevitable cable breakages caused by the machinery used during excavation. The full-time presence of the researcher on site, working closely with the contractor during the construction period, kept these losses and downtime to a minimum.

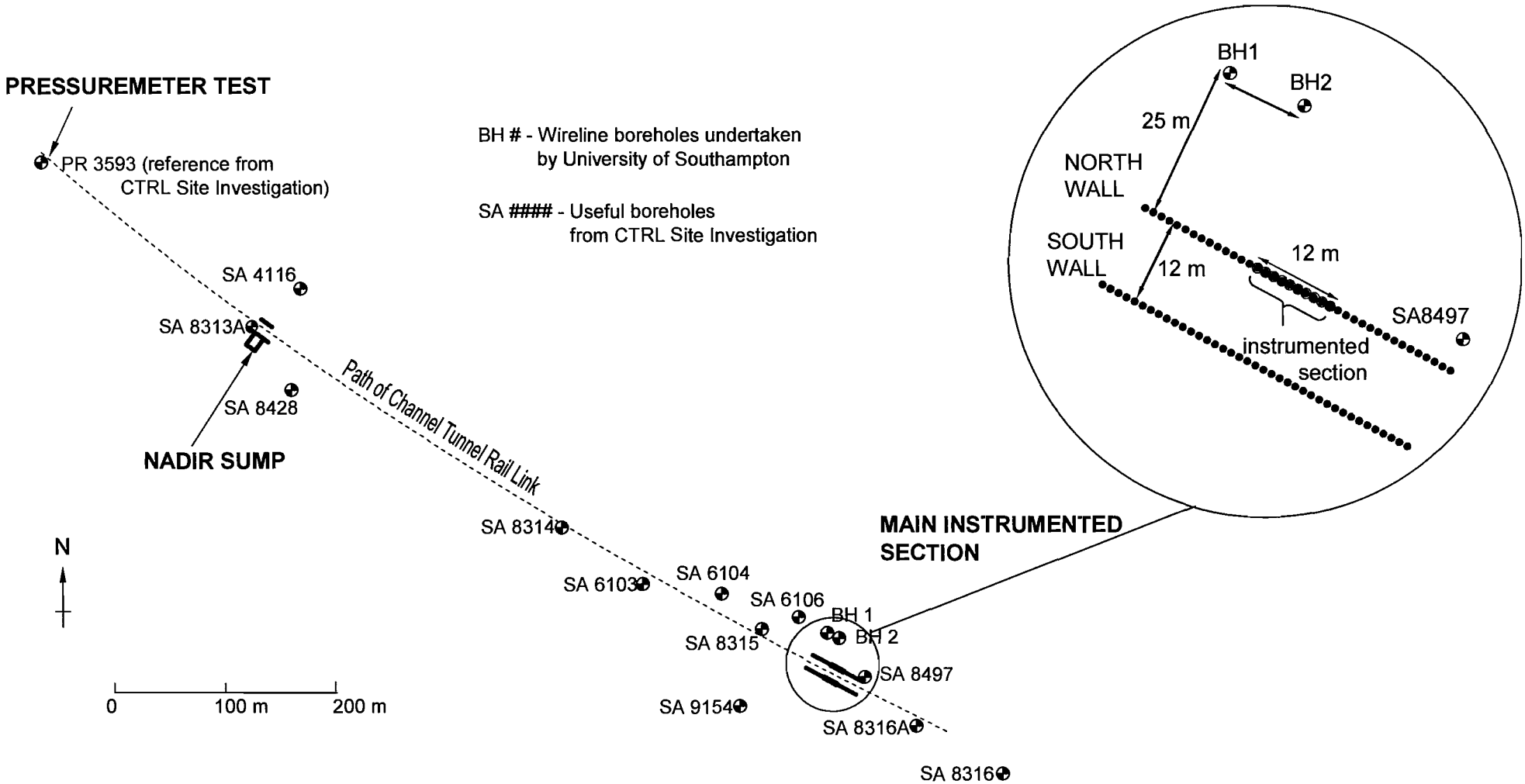

Figure 3-1: Plan showing the locations of the areas described in this work

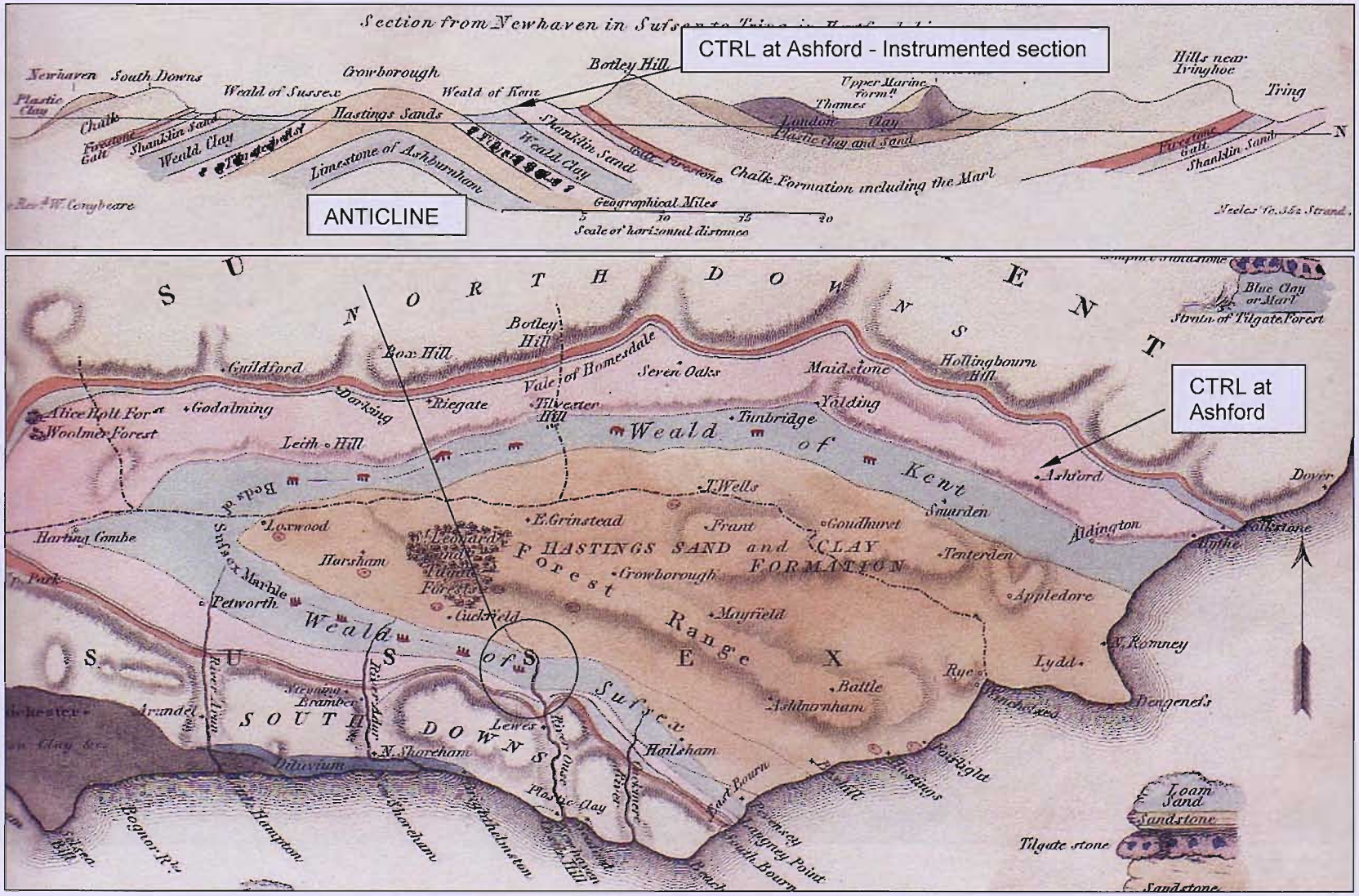

Figure 3-1: Geology of the Weald of Kent (Mantell, 1833)

Figure 3-3: Layering in the Weald Clay

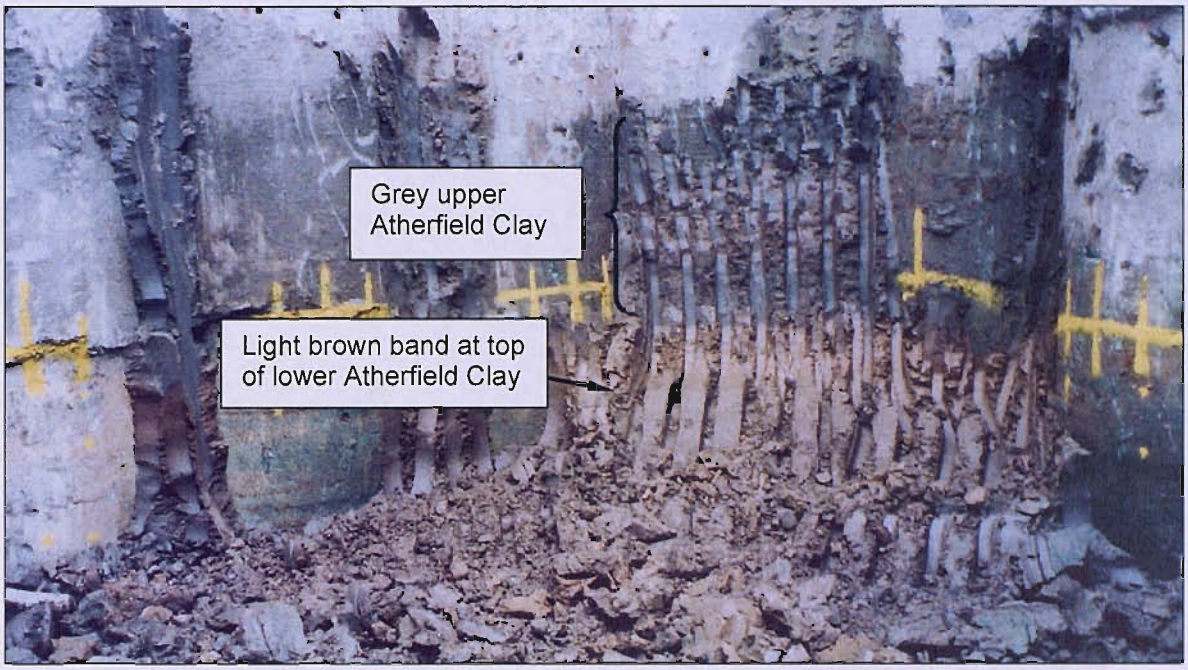

Figure 3-4: Light brown band defining the boundary between the upper and lower Atherfield Clay (observed in the nadir sump)

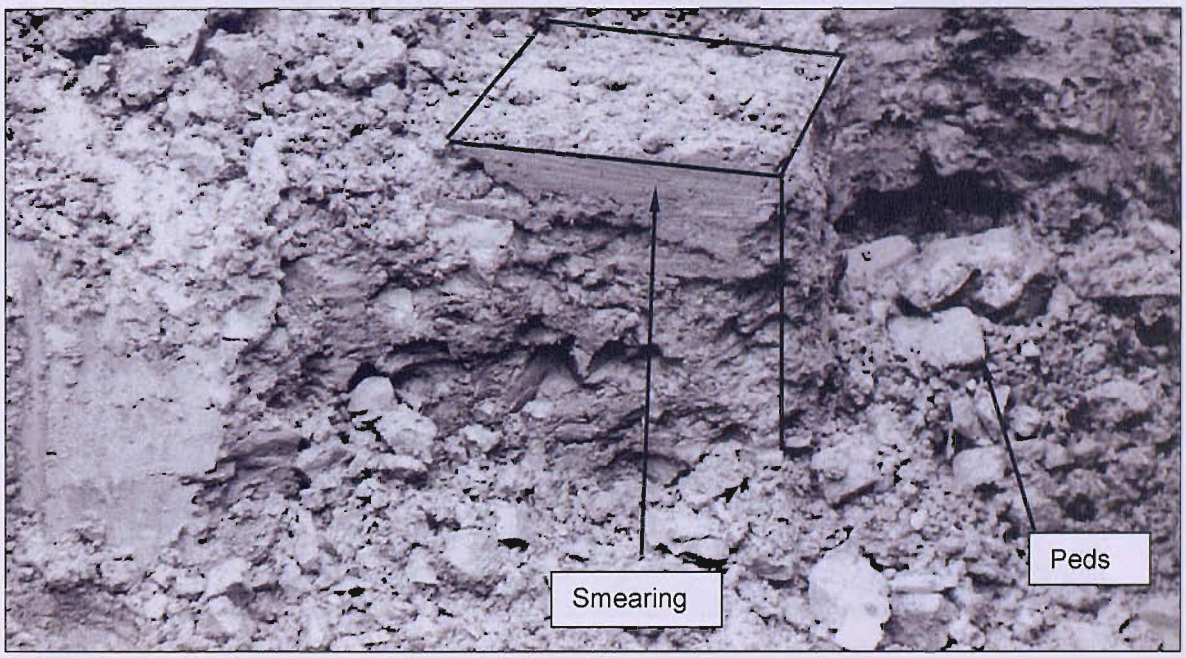

Figure 3-5: Showing the peds and softer matrix of the upper Atherfield Clay

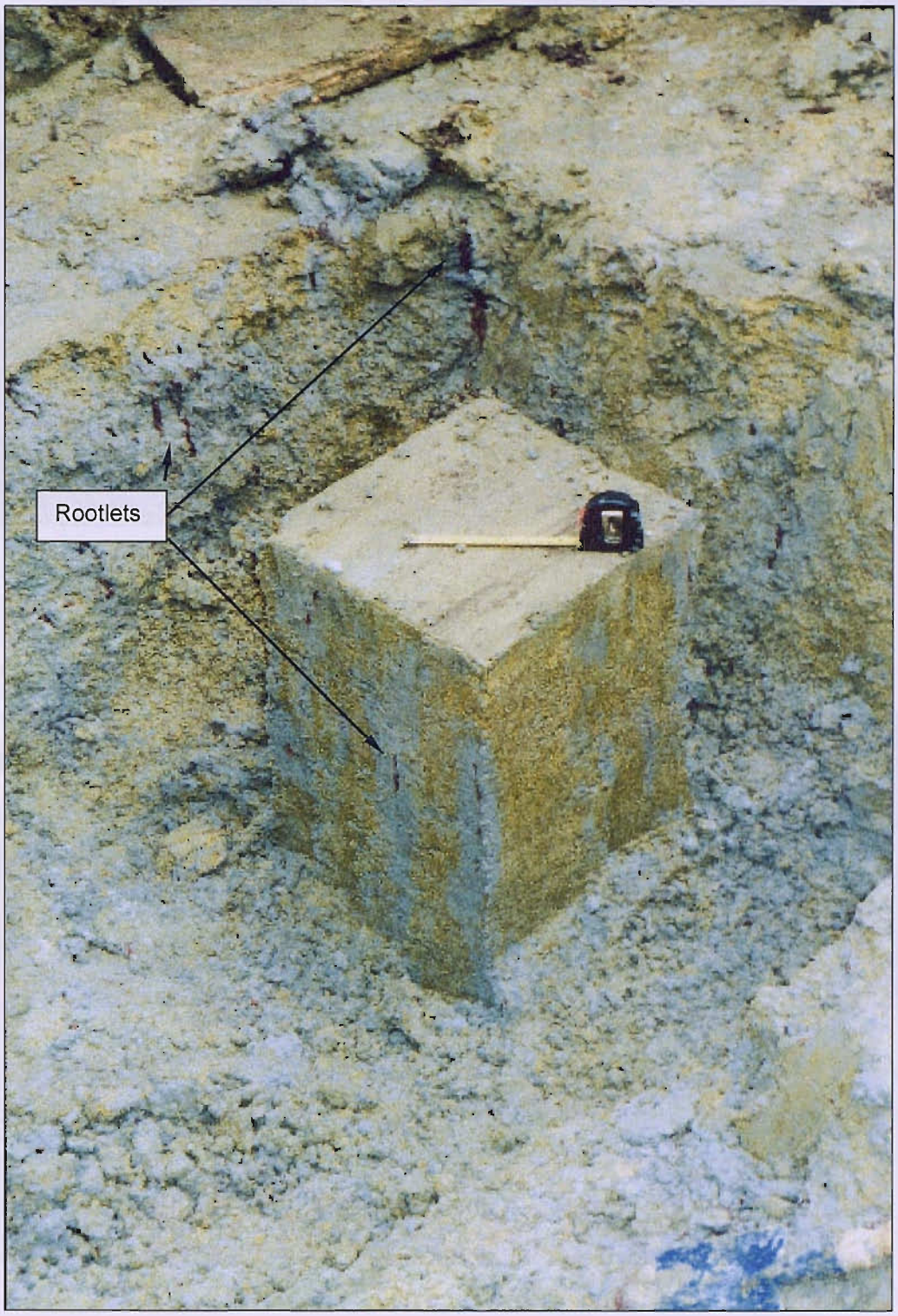

Figure 3-6: *In situ* block sample of the Hythe Beds showing yellow/grey mottling and dark brown root material

Figure 3-7: Looking into the cutting between RC props during excavation

Figure 3-8: Elevation of the excavation face

Figure 3-9: Shear plane in the upper Atherfield Clay, 50 metres from the instrumented section (courtesy of Mark Roberts, Geological Specialist for Skanska Technology Ltd.)

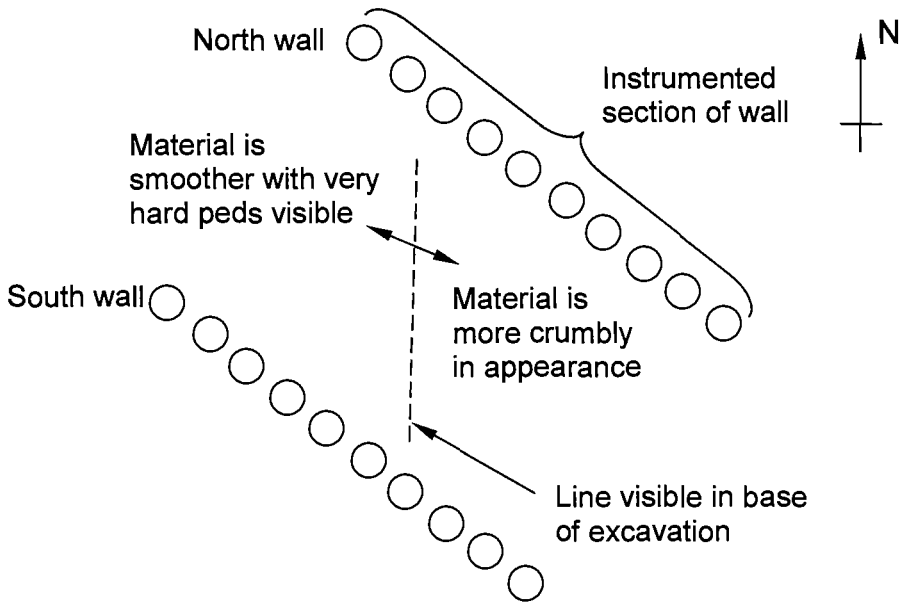

Figure 3-10: Sketch of discontinuity (possible shear plane) observed in the bottom of the excavation at the main instrumented section (plan view)

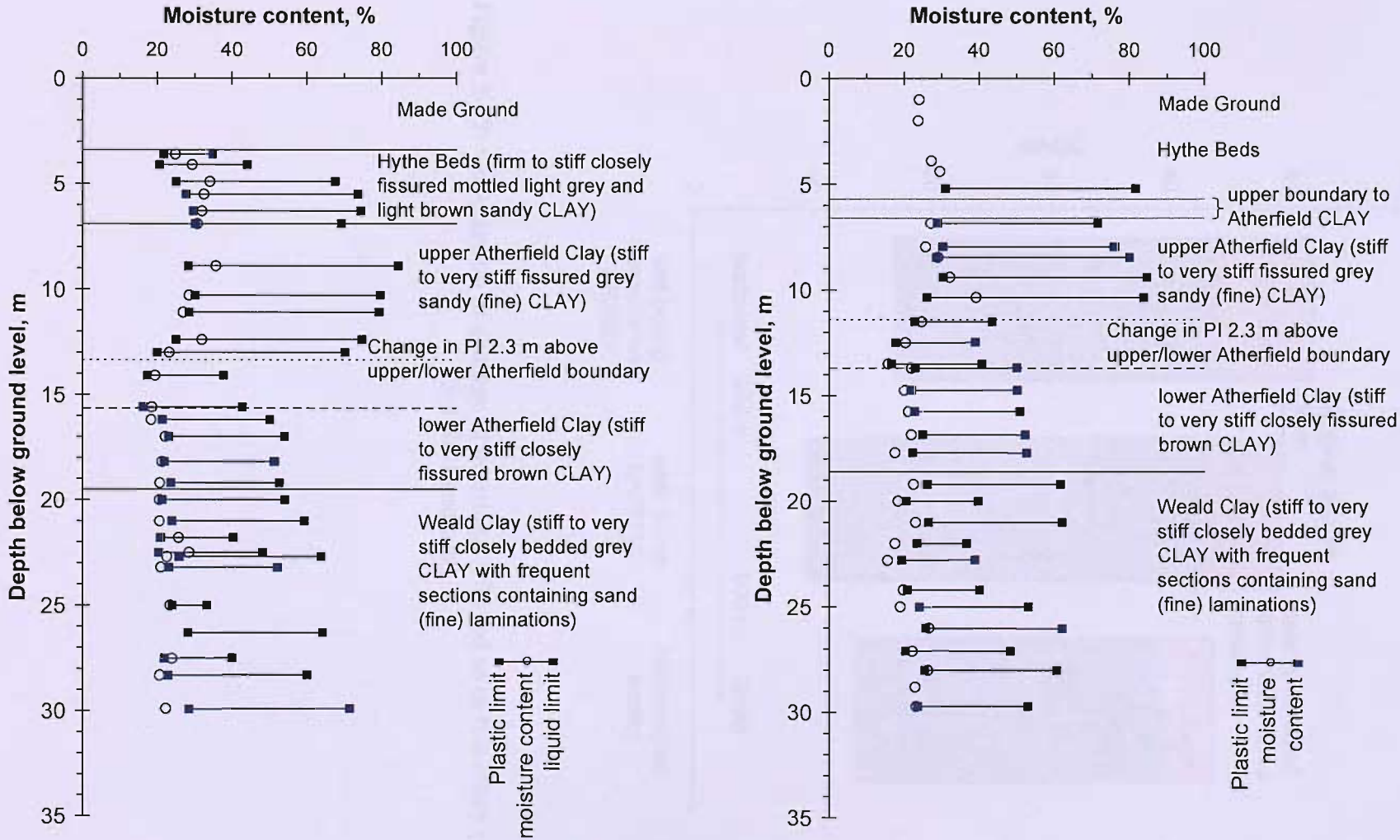

Figure 3-11: Geotechnical profiles including liquid and plastic limit data from wireline boreholes BH1 and BH2 (see Figure 3-1)

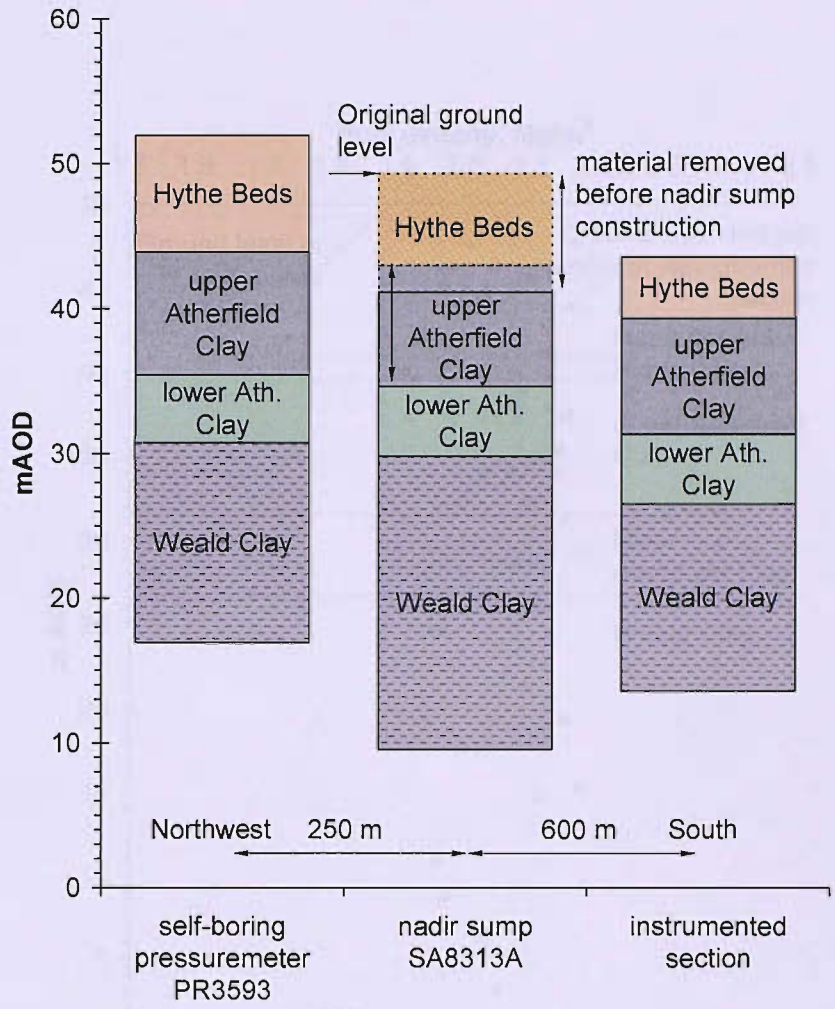

Figure 3-12: Comparison of geology at locations referred to in this study (see Figure 3-1 for locations)

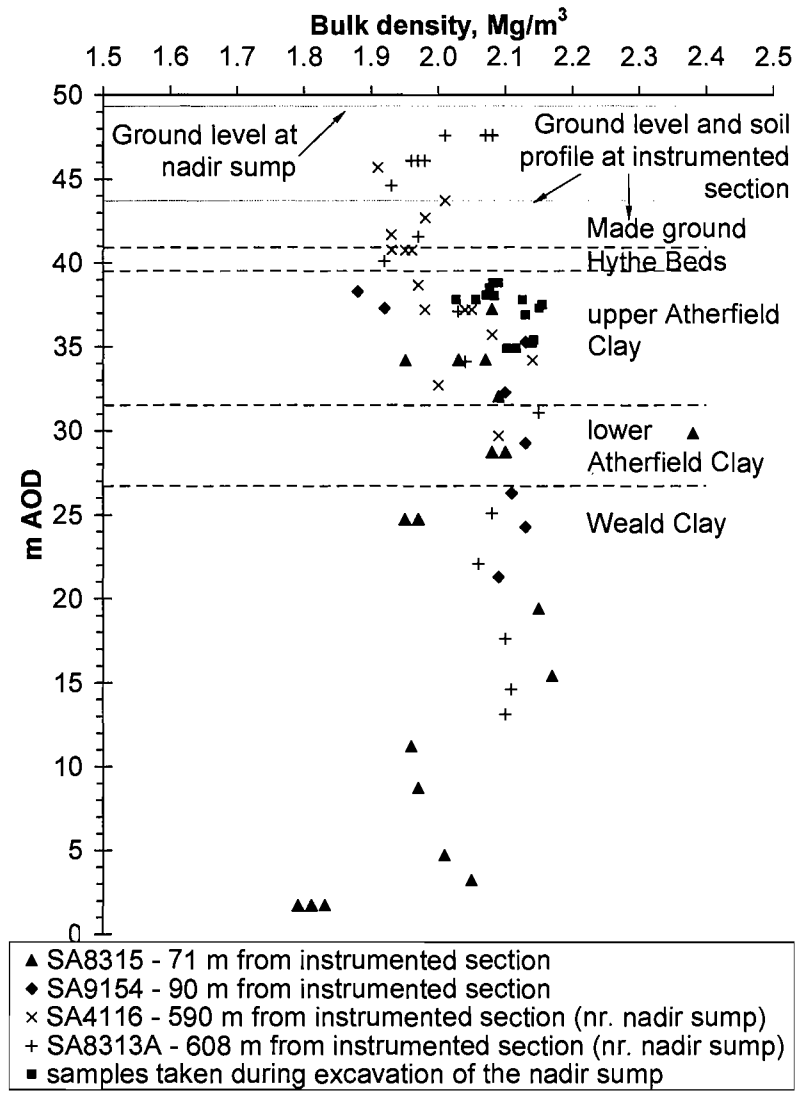

Figure 3-13: Bulk density with depth (see Figure 3-1 for relative borehole locations)

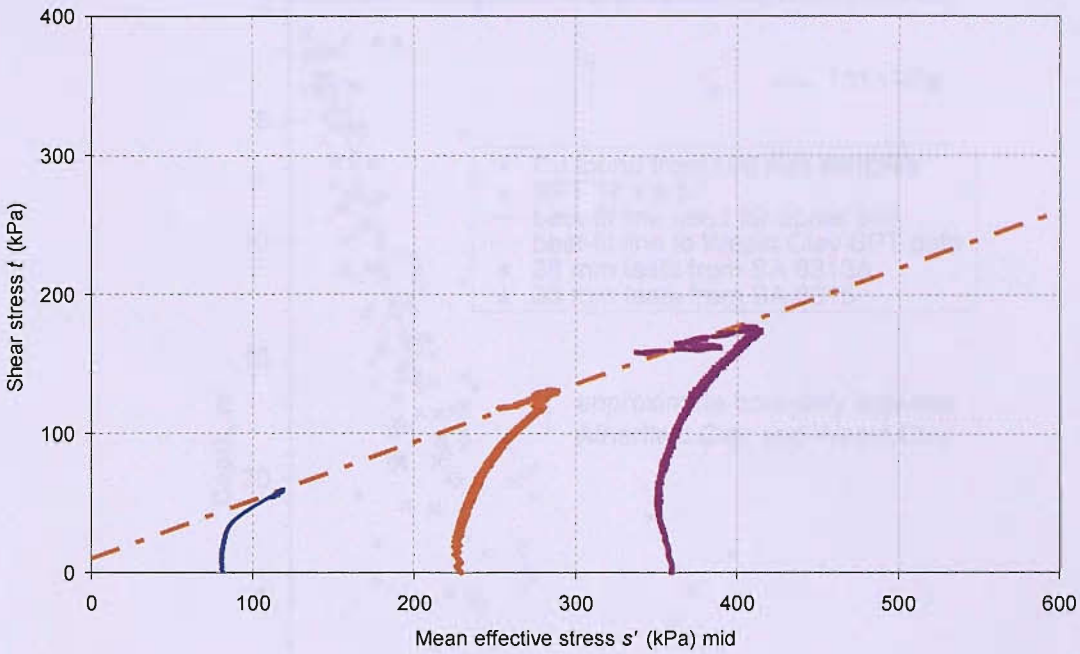

Figure 3-14: Effective stress paths of lower Atherfield Clay specimens during monotonic shearing (Xu, 2005)

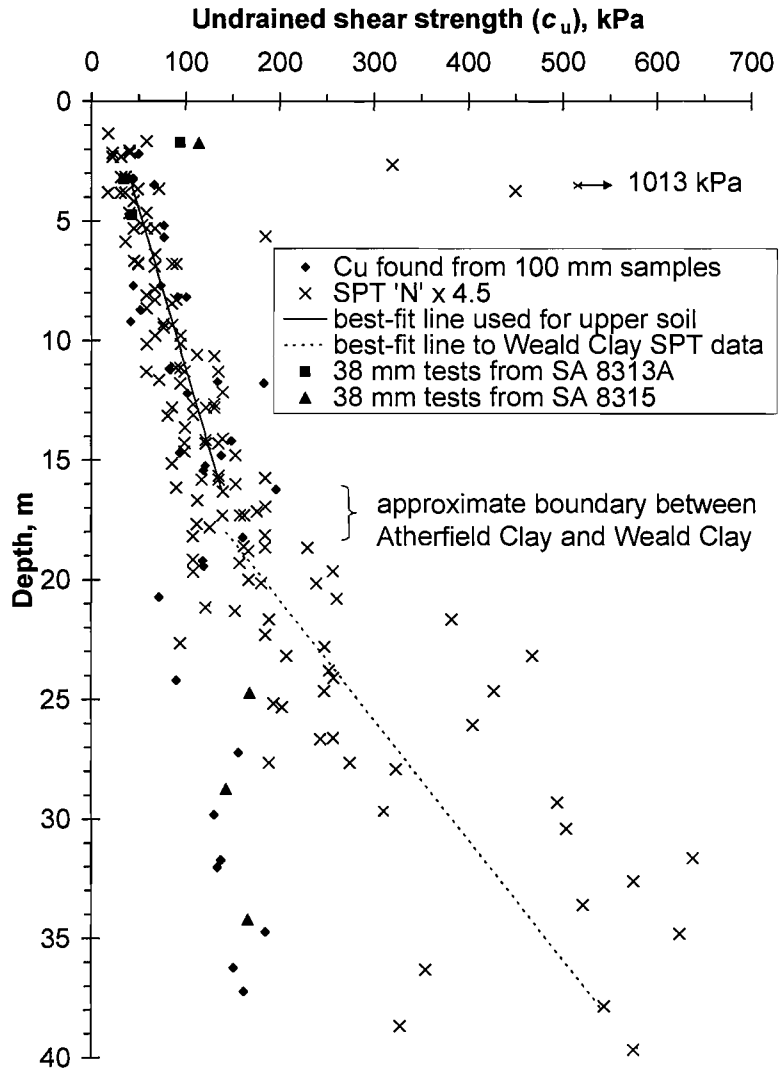

Figure 3-15: Undrained shear strength with depth found from 100 mm diameter laboratory samples and SPT results (38 mm test data are included for comparison)

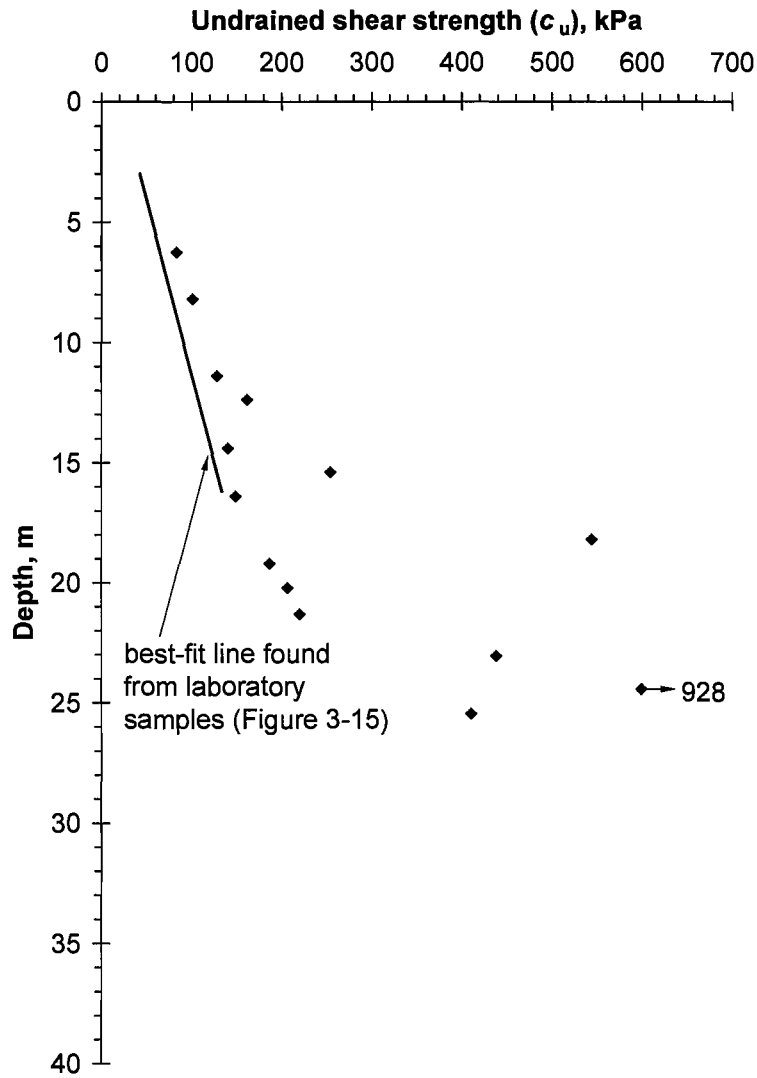

Figure 3-16: Undrained shear strength with depth measured with the self-boring pressuremeter

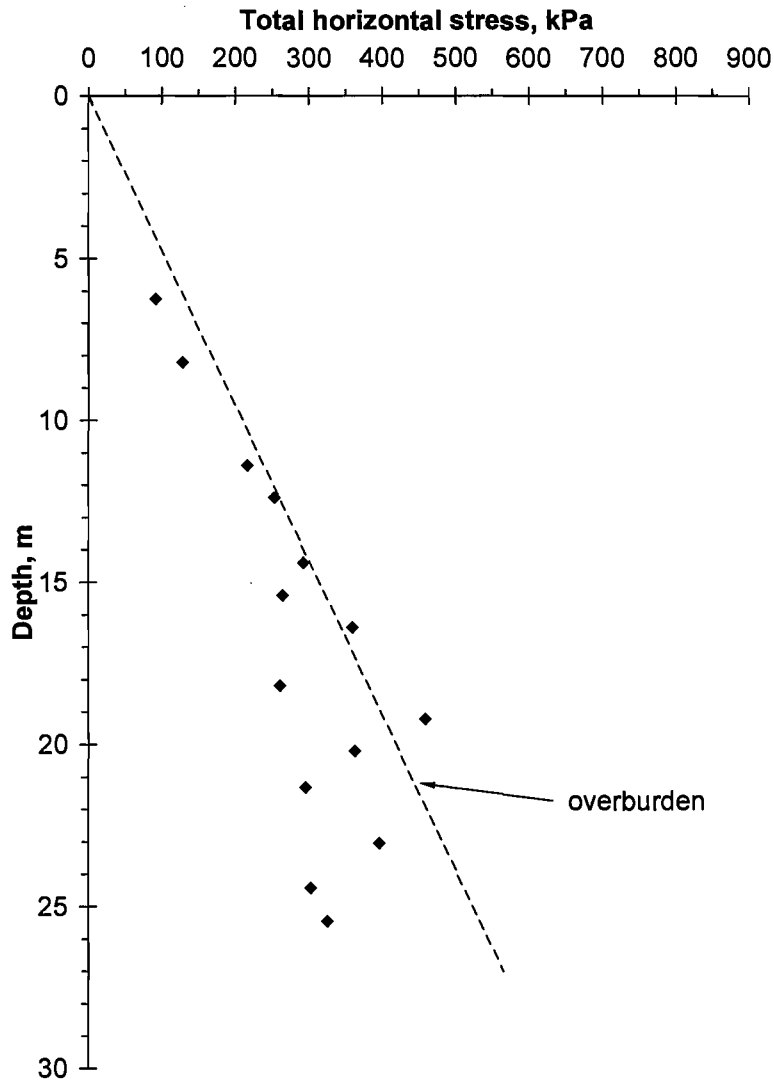

Figure 3-17: Total horizontal stress measured by self-boring pressuremeter

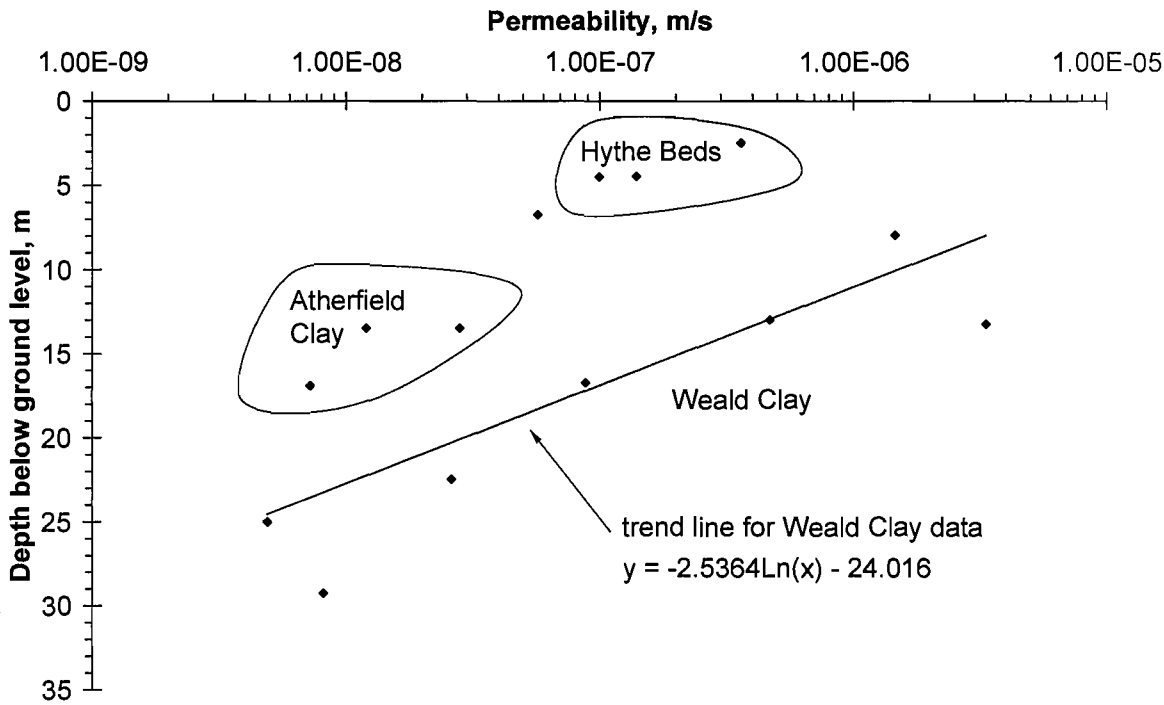

Figure 3-18: Permeability data

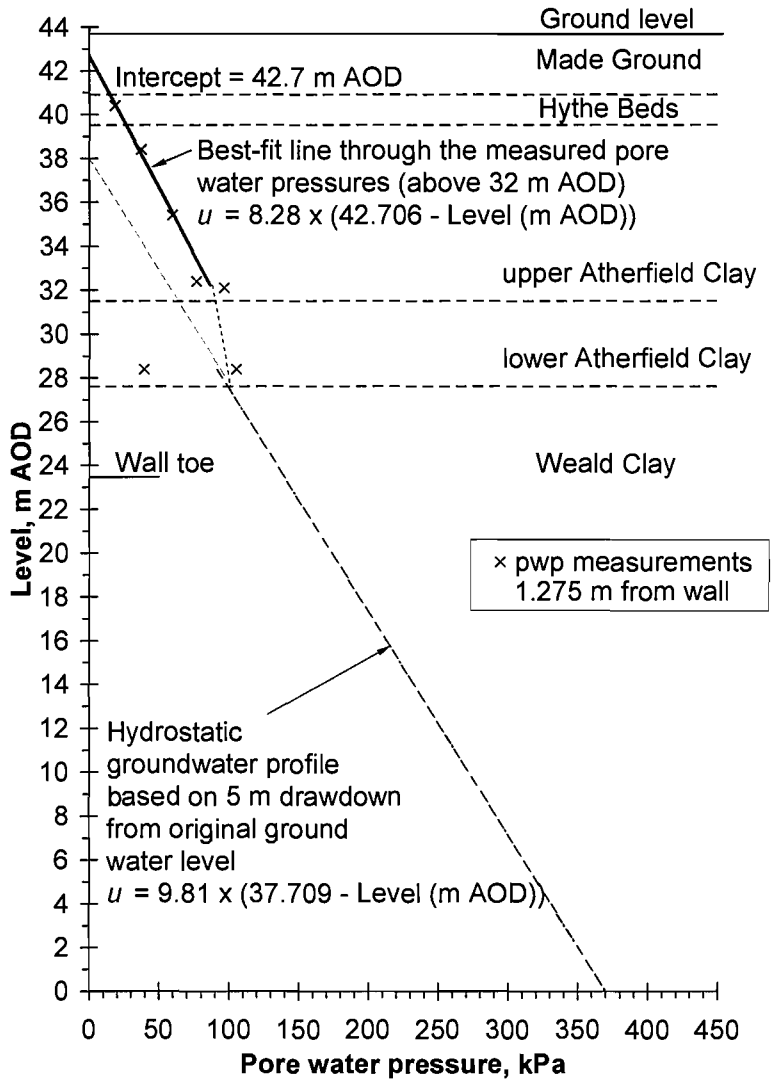

Figure 3-19: Pore water pressures: measurements and assumed profile

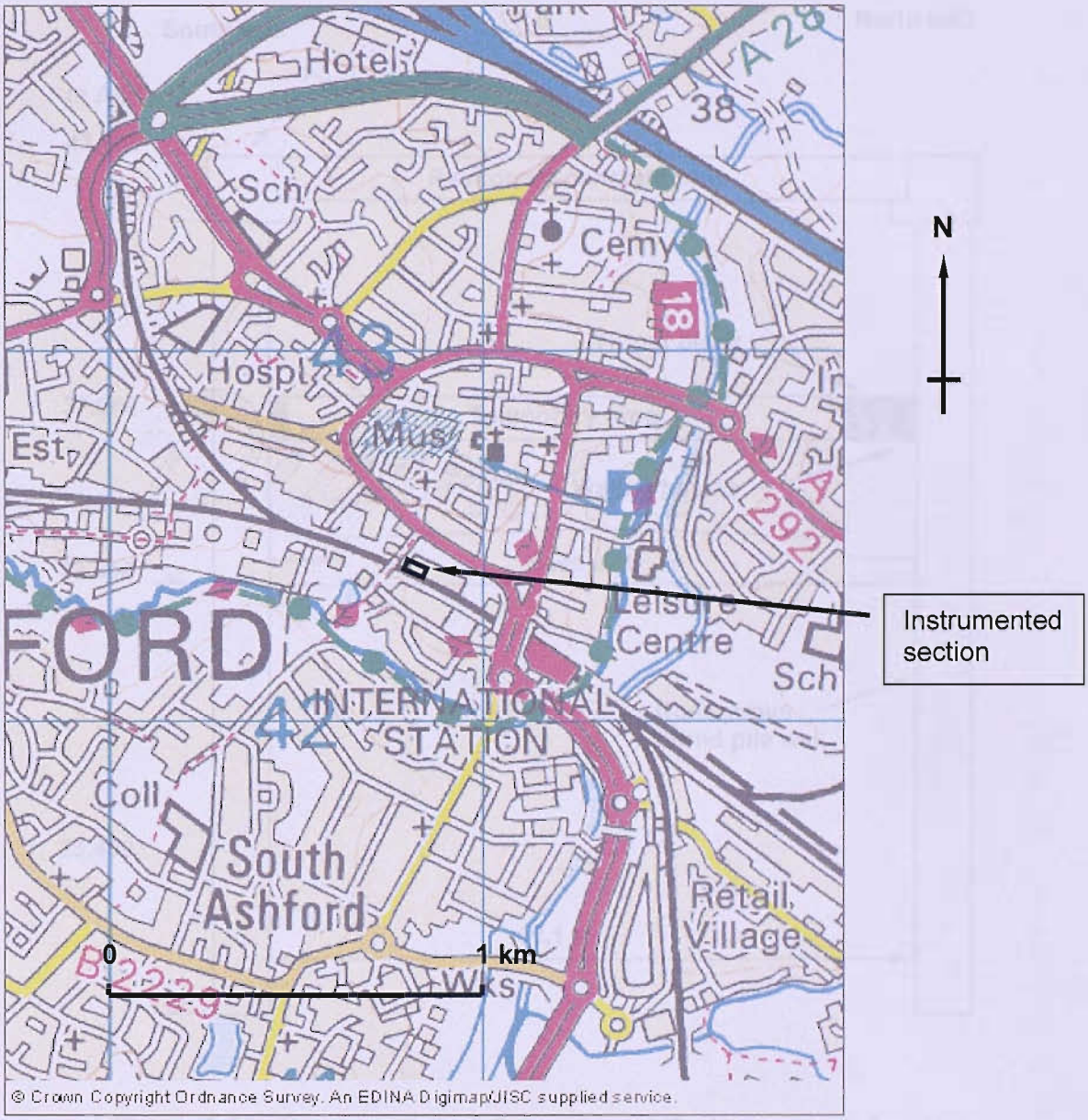

Figure 3-20: Map of central Ashford showing the location of the instrumented section (Grid reference: 60081424)

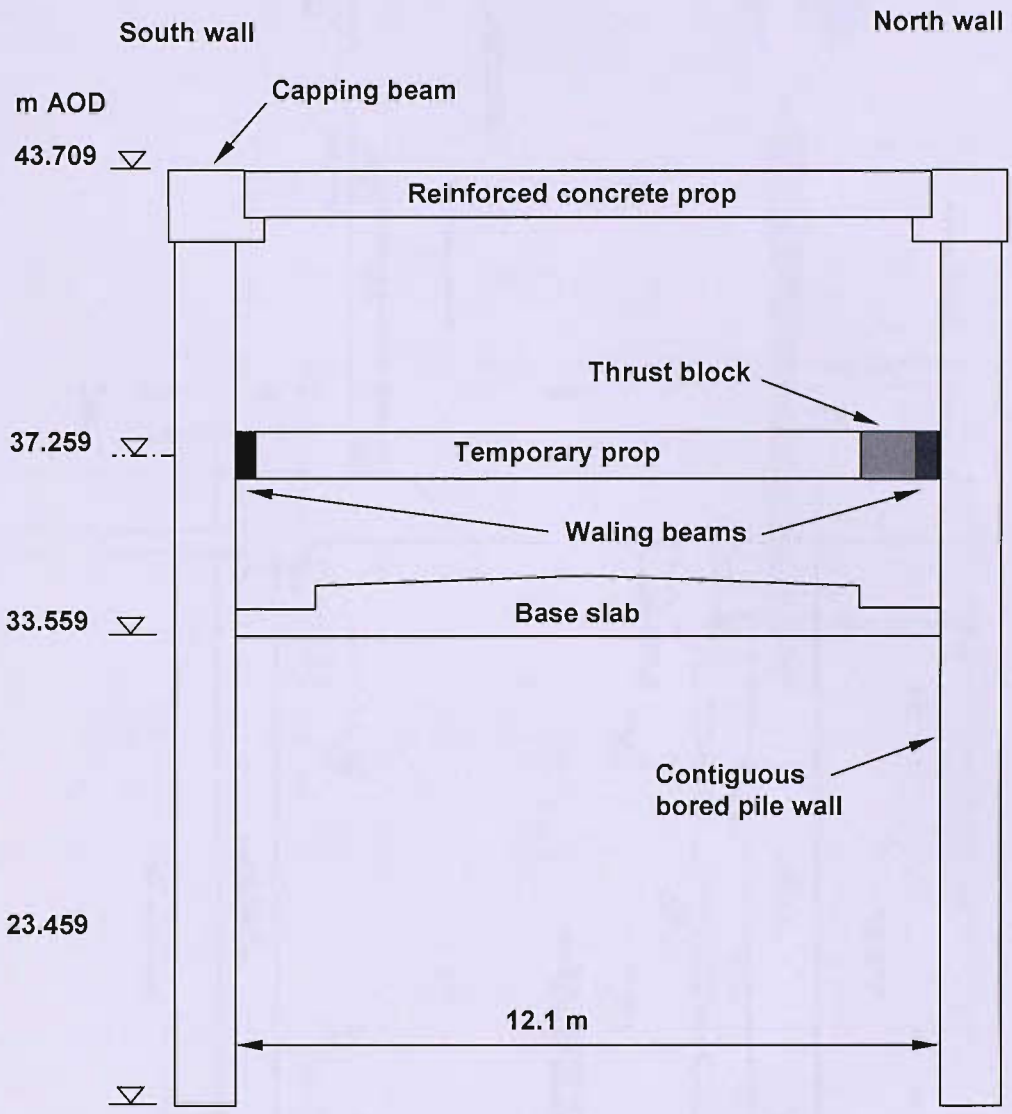

Figure 3-21: Cross-section of the cutting at the instrumented section

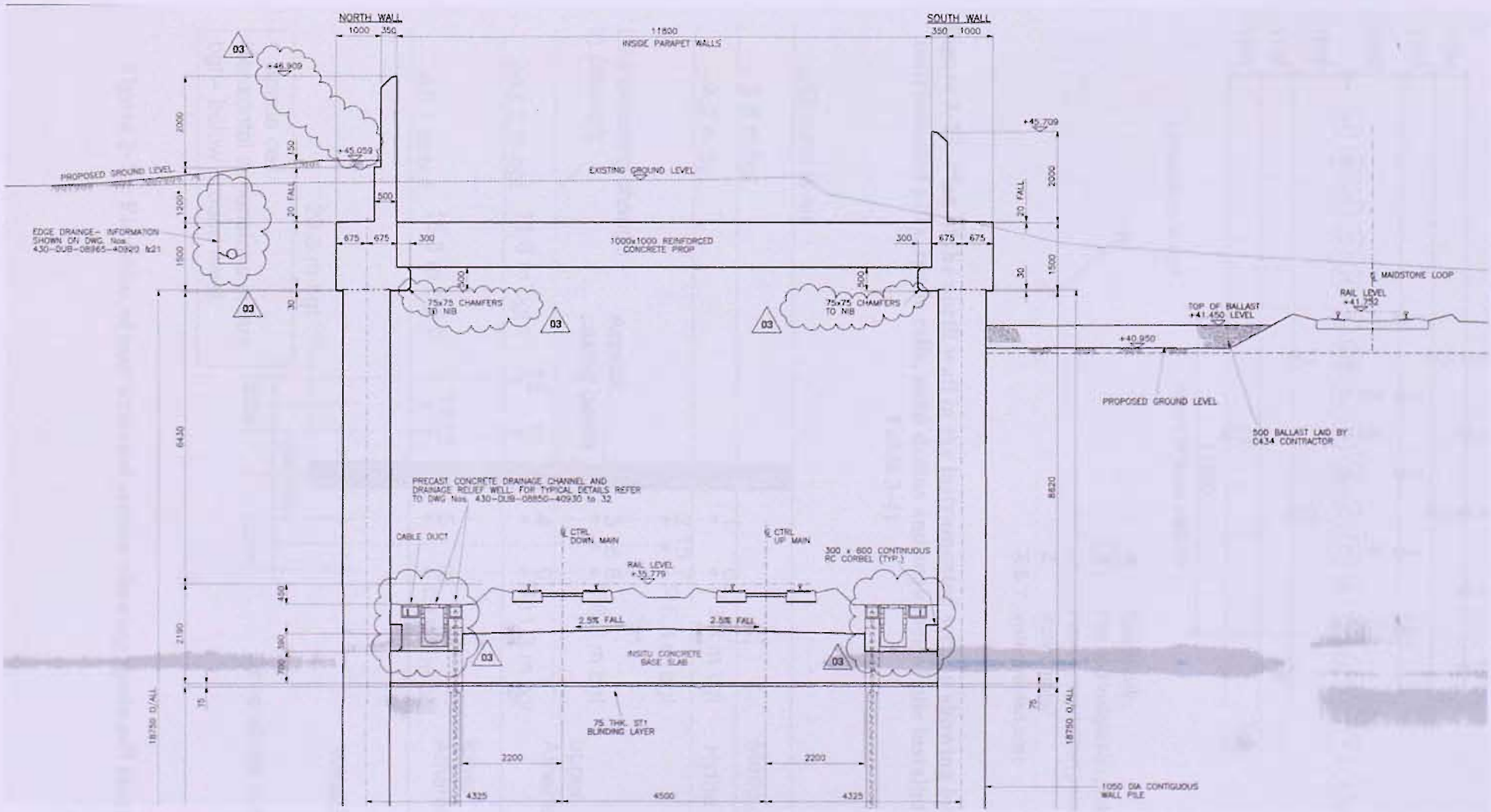

Figure 3-22: Elevation illustrating the ground profile around the structure

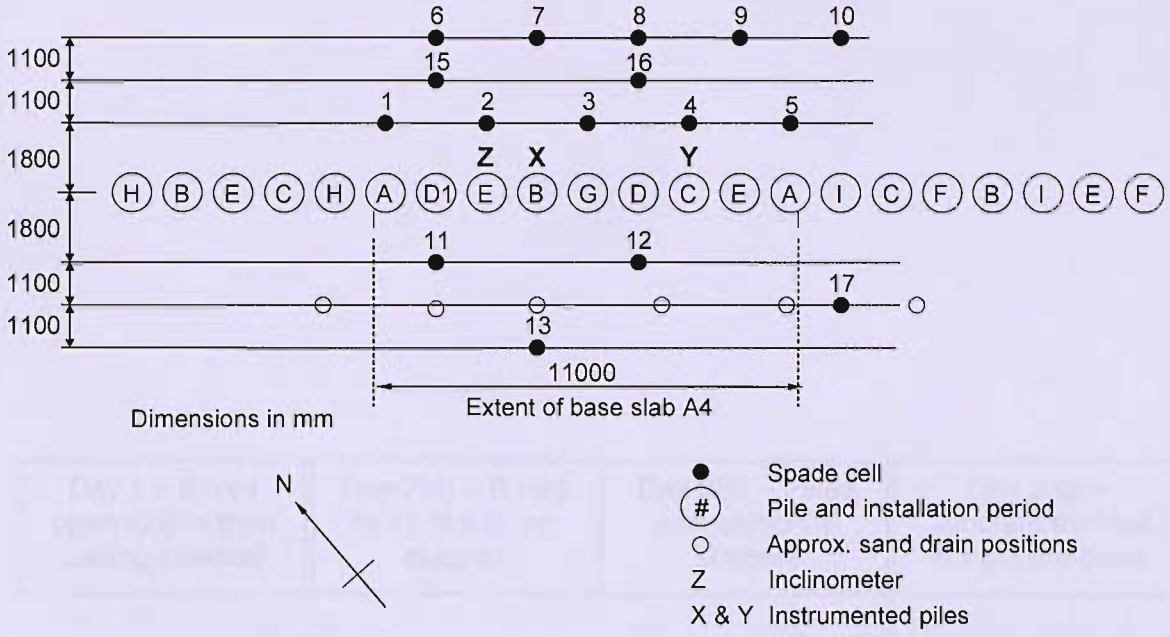

Figure 3-23: Plan of the north wall in the instrumented section showing locations of instrumented piles, spade cells, sand drains and sequence of pile installation (see Table 3-4)

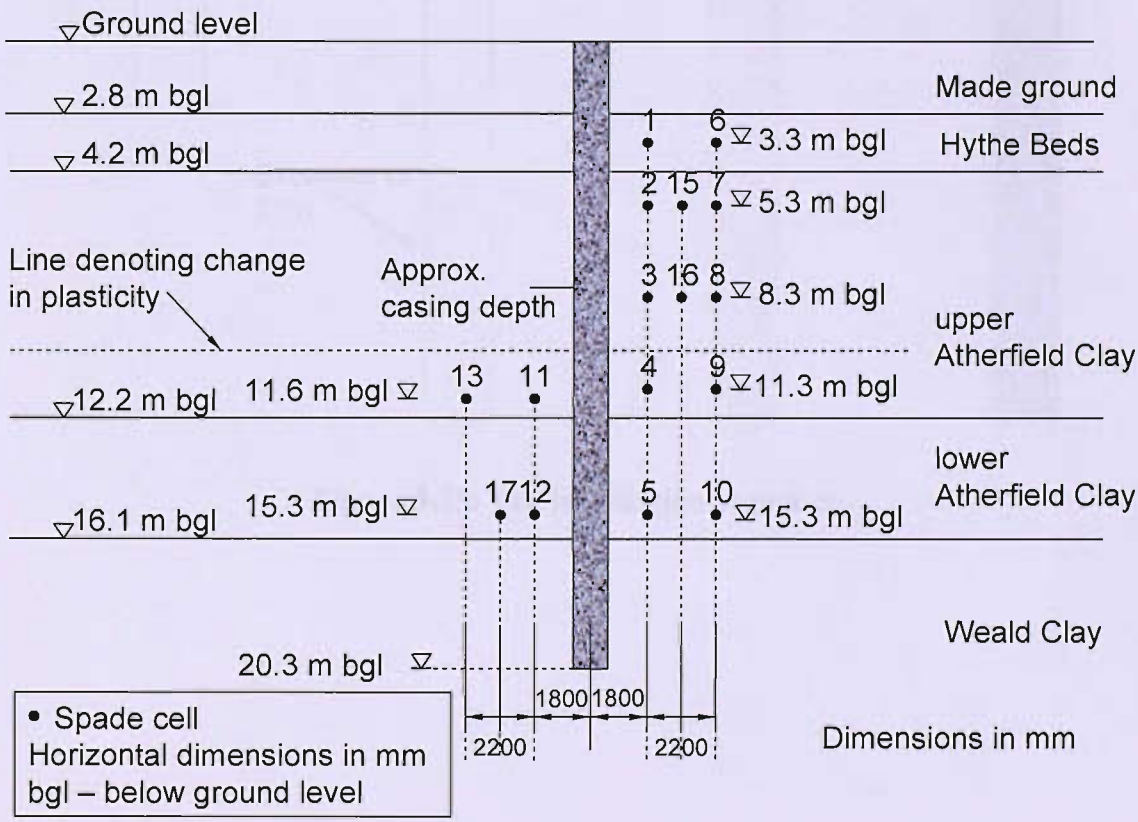

Figure 3-24: Elevation of instrumented section showing spade cell locations

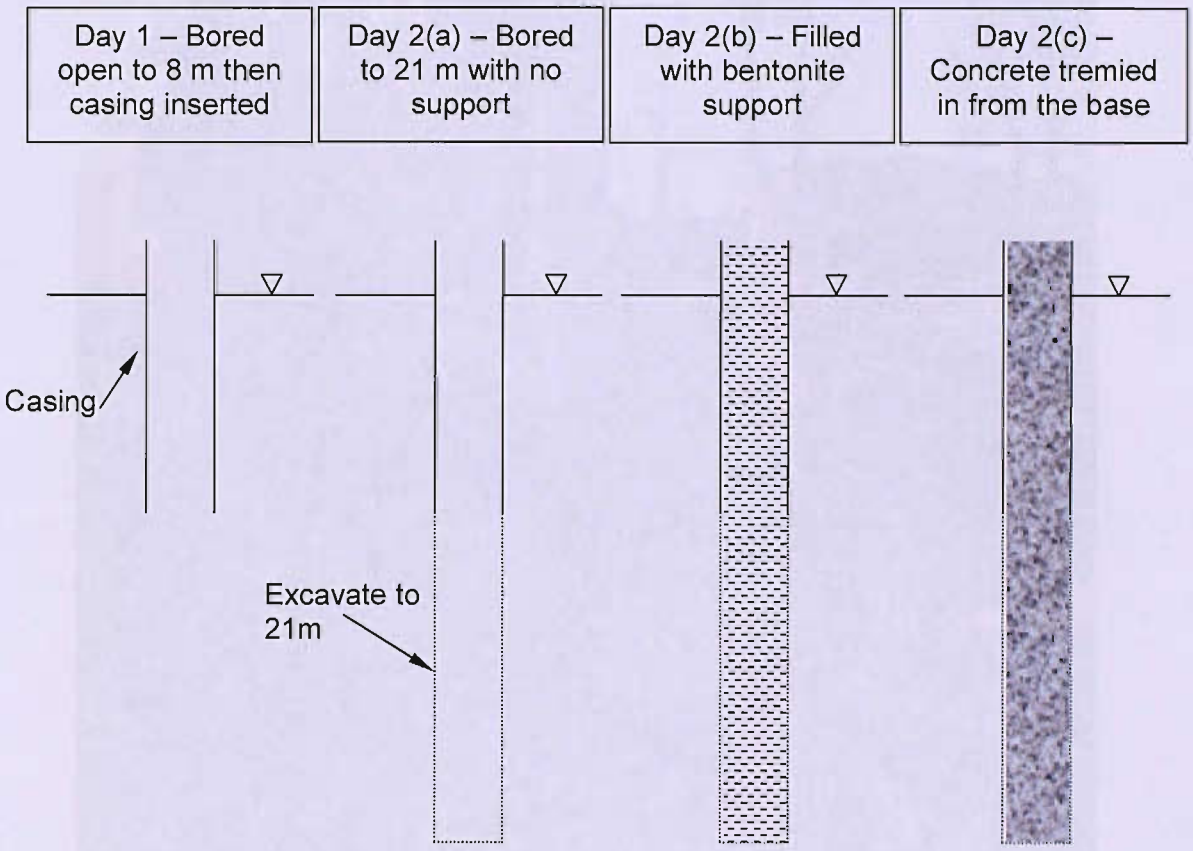

Figure 3-25: Pile installation sequence

Figure 3-26: Pile boring

Figure 3-27: Installation of casing

Figure 3-28: Installation of reinforcement cage

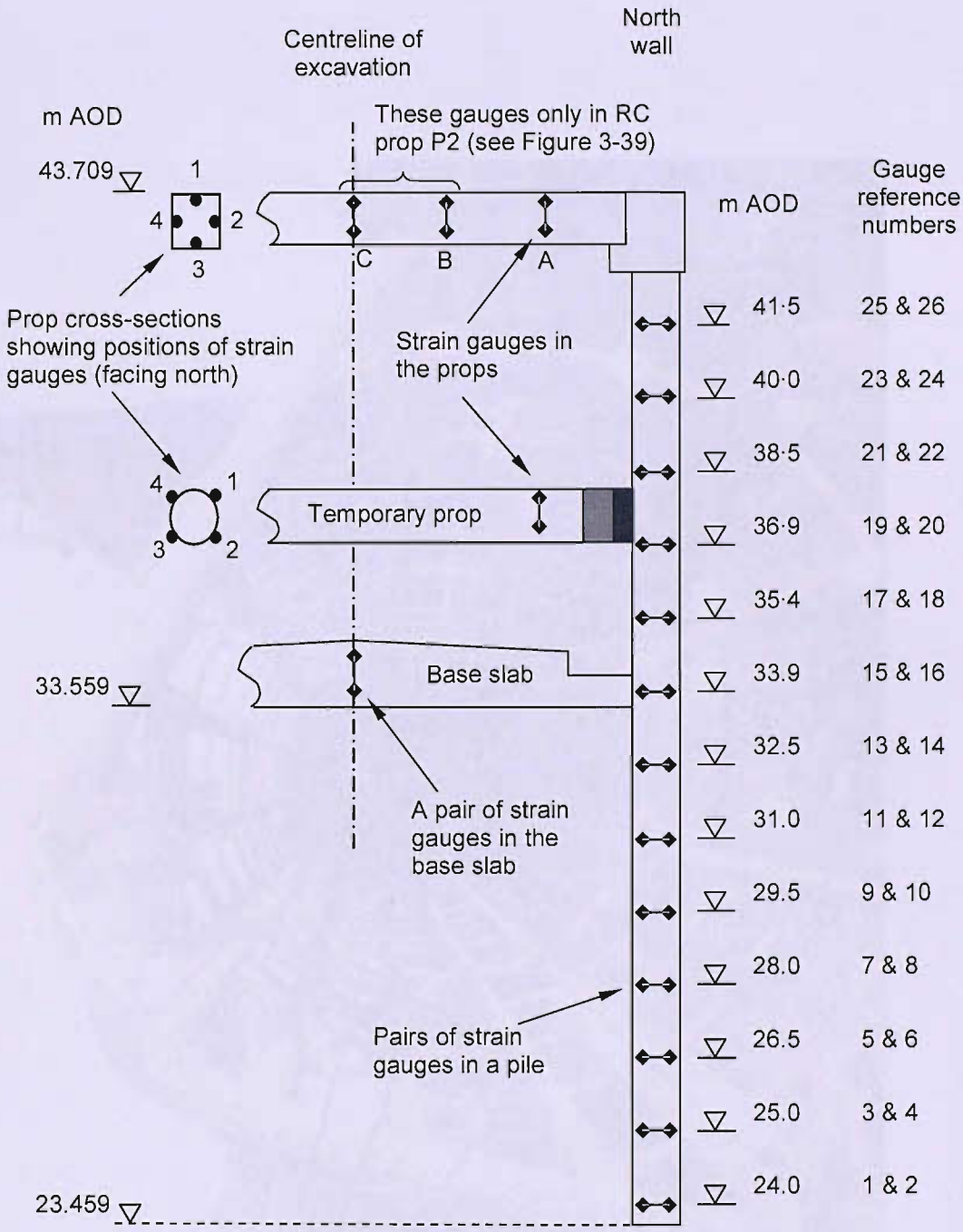

Figure 3-29: Elevation of instrumented section showing strain gauge arrangement

Figure 3-30: Strain gauges for measurement of pile bending moment

Figure 3-31: Photo showing sand drain and cable for spade cell 11 (taken on 13th February 2001 – Day 495)

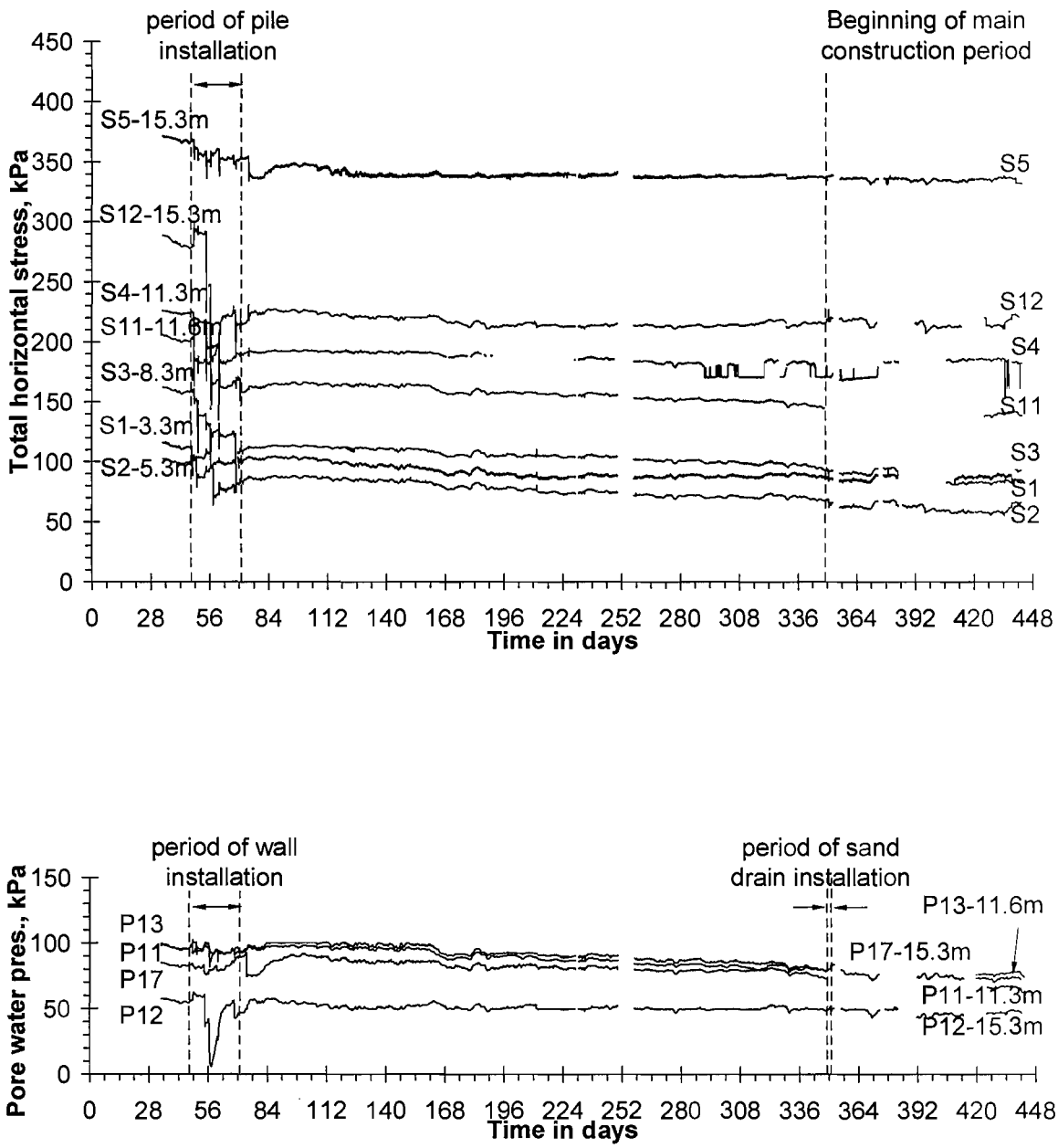

Figure 3-32: Changes in total horizontal stress and pore water pressure in front of the wall around the period of sand drain installation

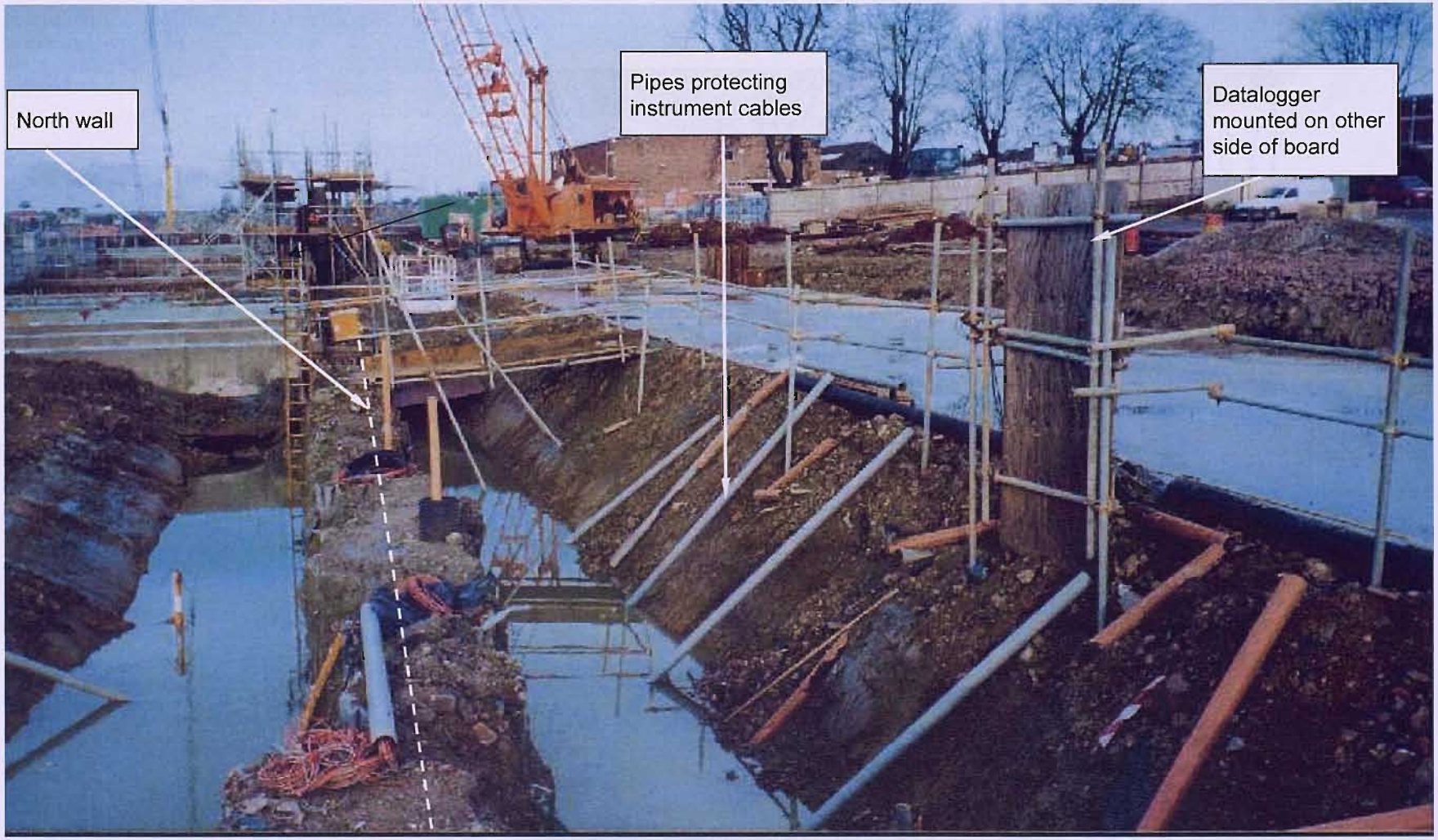

Figure 3-33: Excavation either side of the north wall before break down to level of capping beam (taken on 1st November 2000 – Day 391)

Figure 3-34: Pile top removal (south wall)
(taken on 31st August 2000 – Day 329)

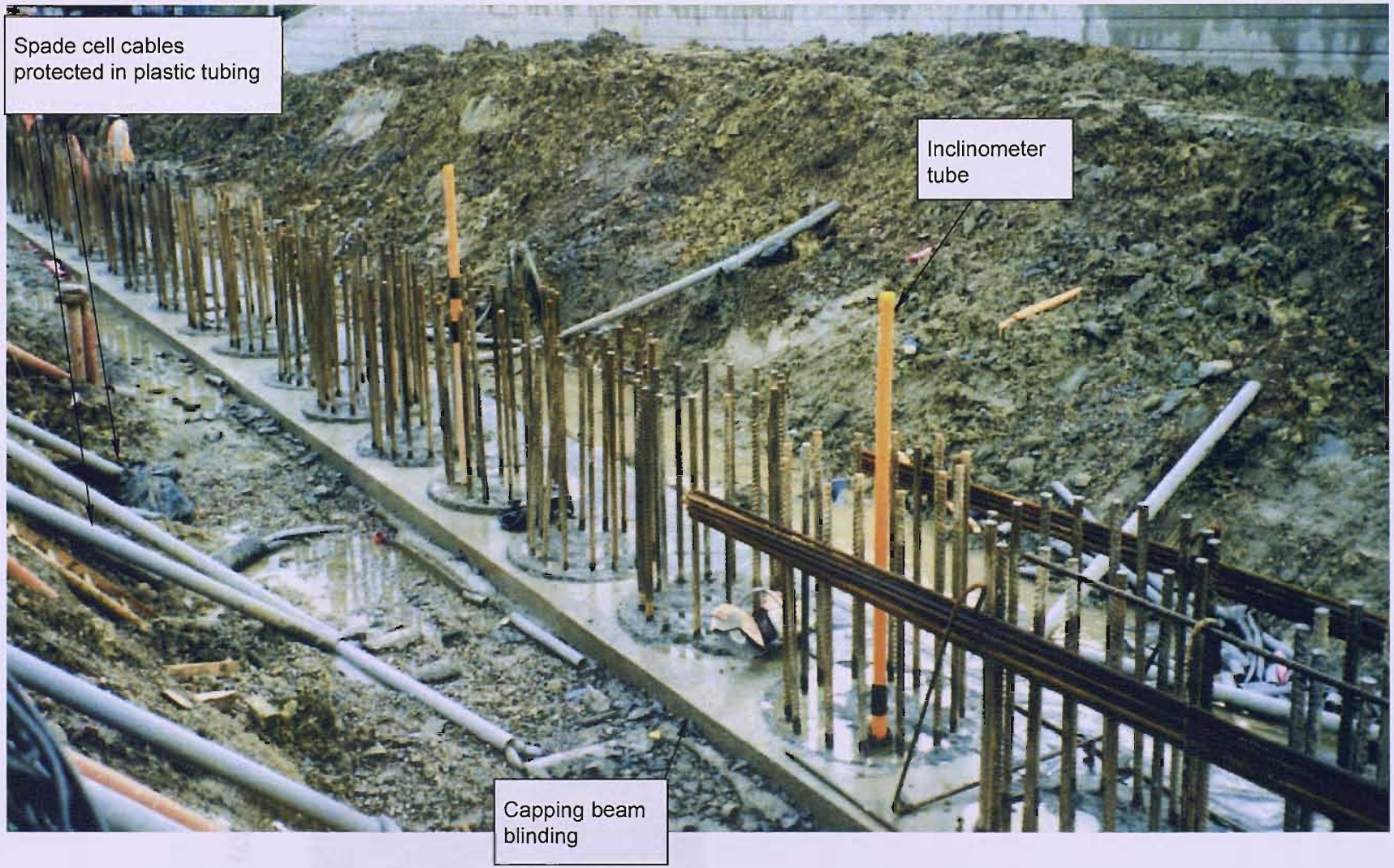

Figure 3-35: Wall before construction of capping beam (taken on 4th December 2000 – Day 424)

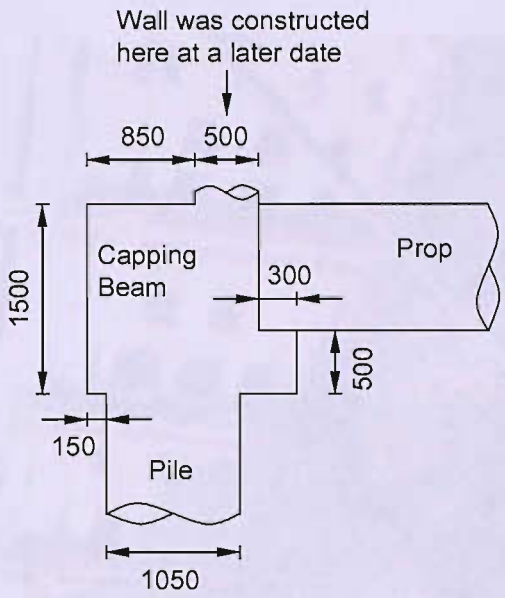

Figure 3-36: Dimensions of capping beam (in mm)

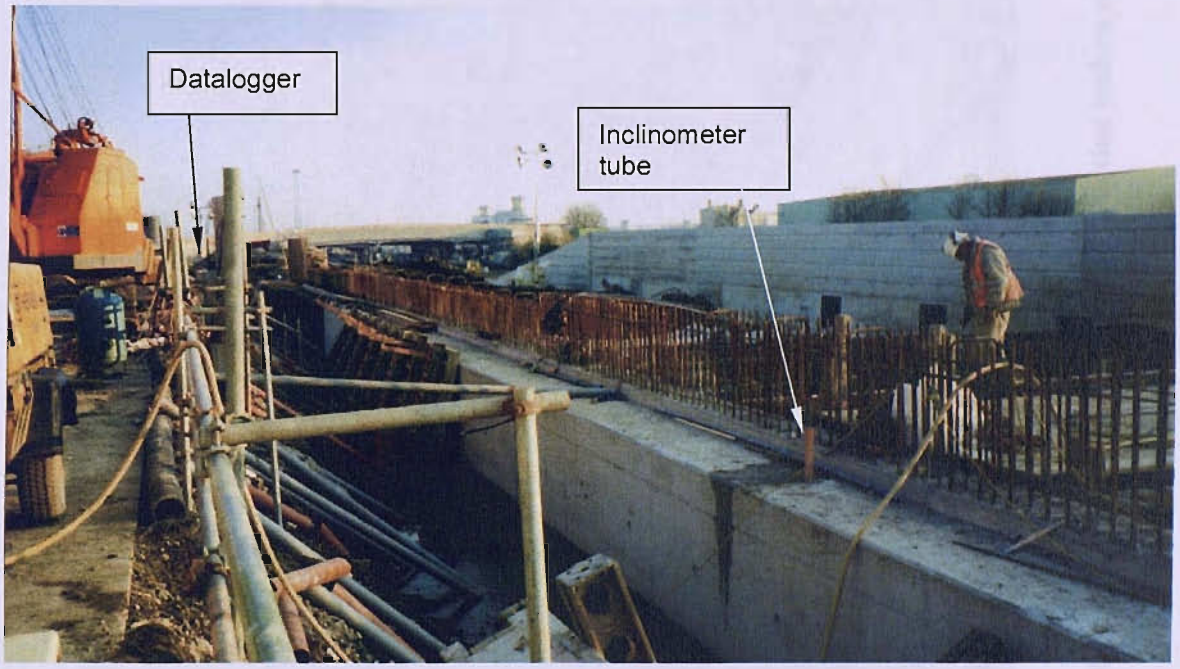

Figure 3-37: Capping beam (taken on 16th January 2001 – Day 467)

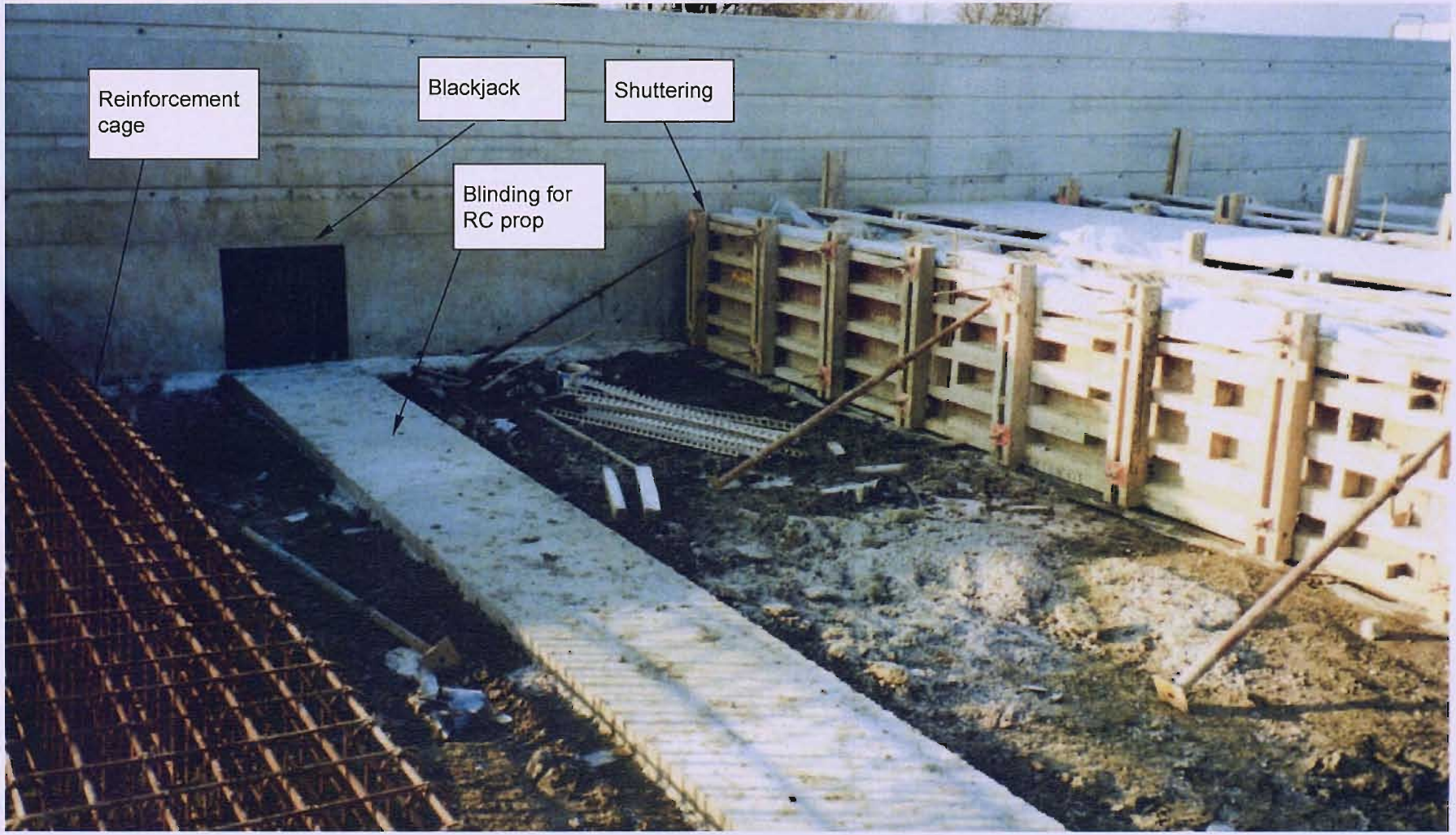

Figure 3-38: Preparation for RC prop construction (taken on 16th January 2001 – Day 467)

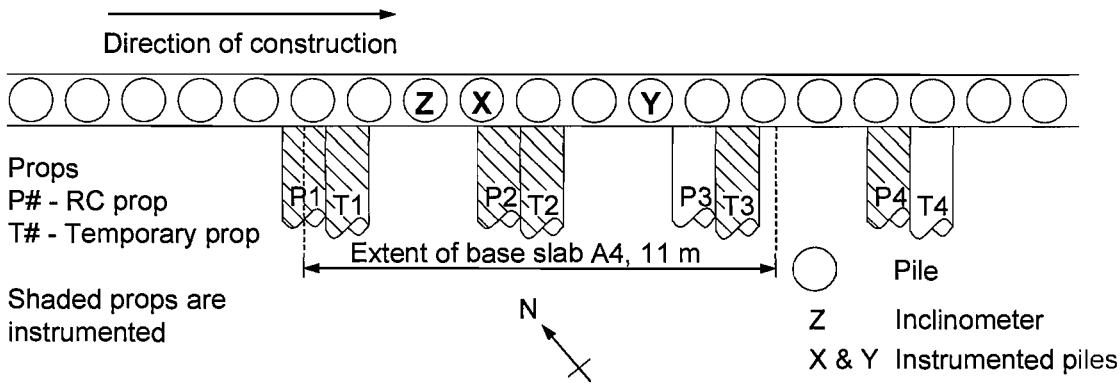

Figure 3-39: Location of the instrumented props in relation to the instrumented piles

Figure 3-40: Photo showing instrumented area before excavation (taken on 22nd January 2001 – Day 473)

Figure 3-41: Compacting backfill in the instrumented section (taken on 29th January 2001 – Day 480)

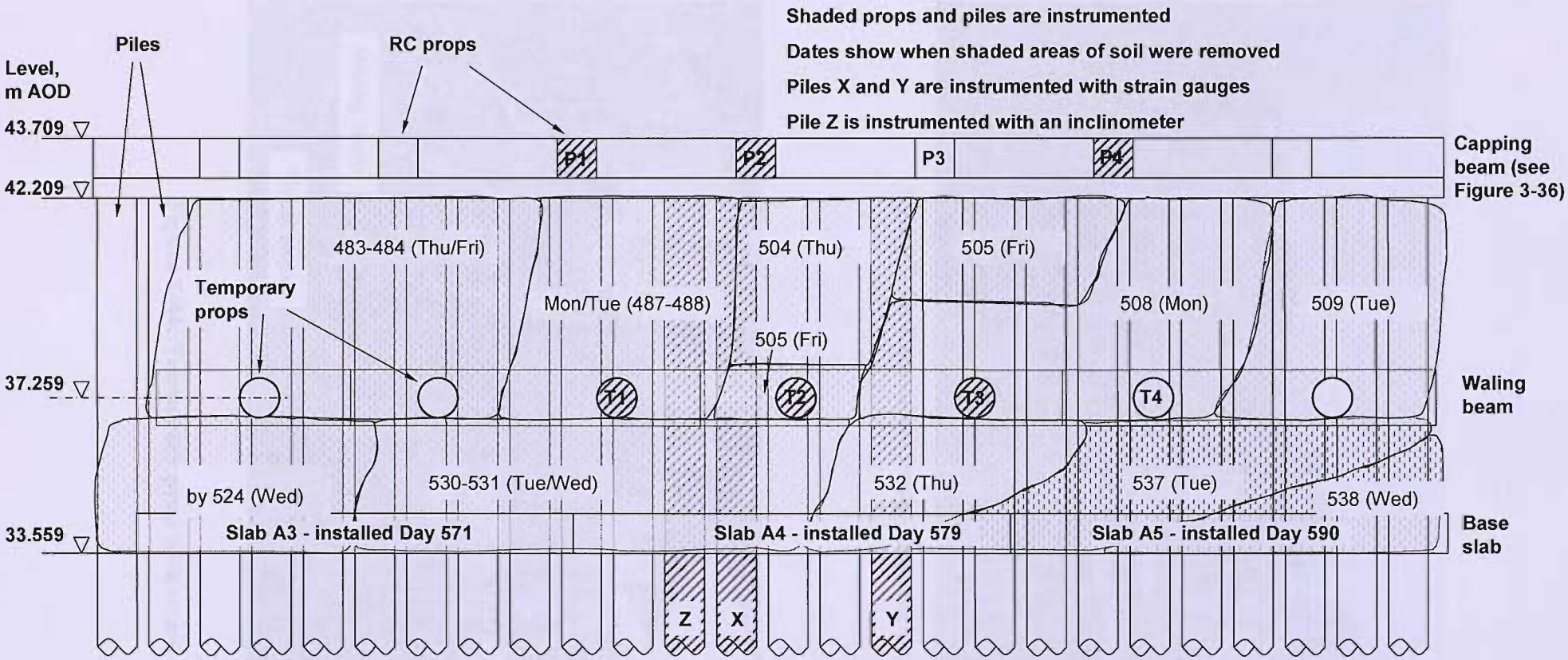

Figure 3-42: Elevation showing props and order of excavation. The shaded areas were excavated on the dates indicated, and the props and base slab were constructed on the dates indicated (excavation took place in 2001).

Figure 3-43: Excavation using long-reach excavator

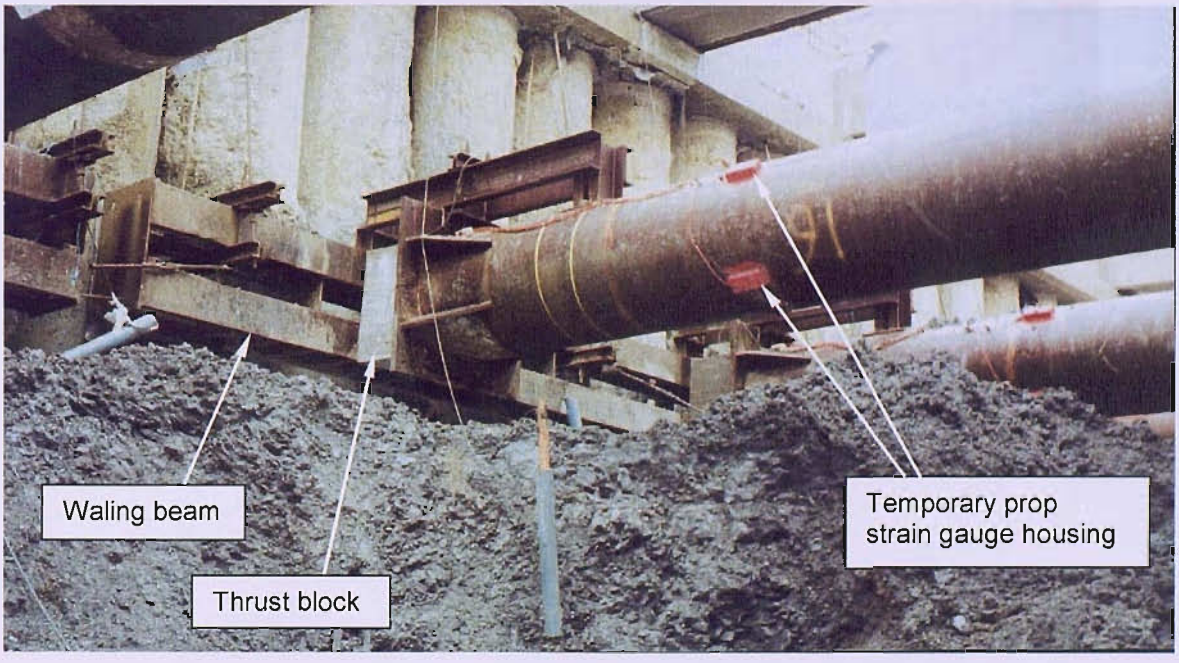

Figure 3-44: Temporary prop with strain gauges

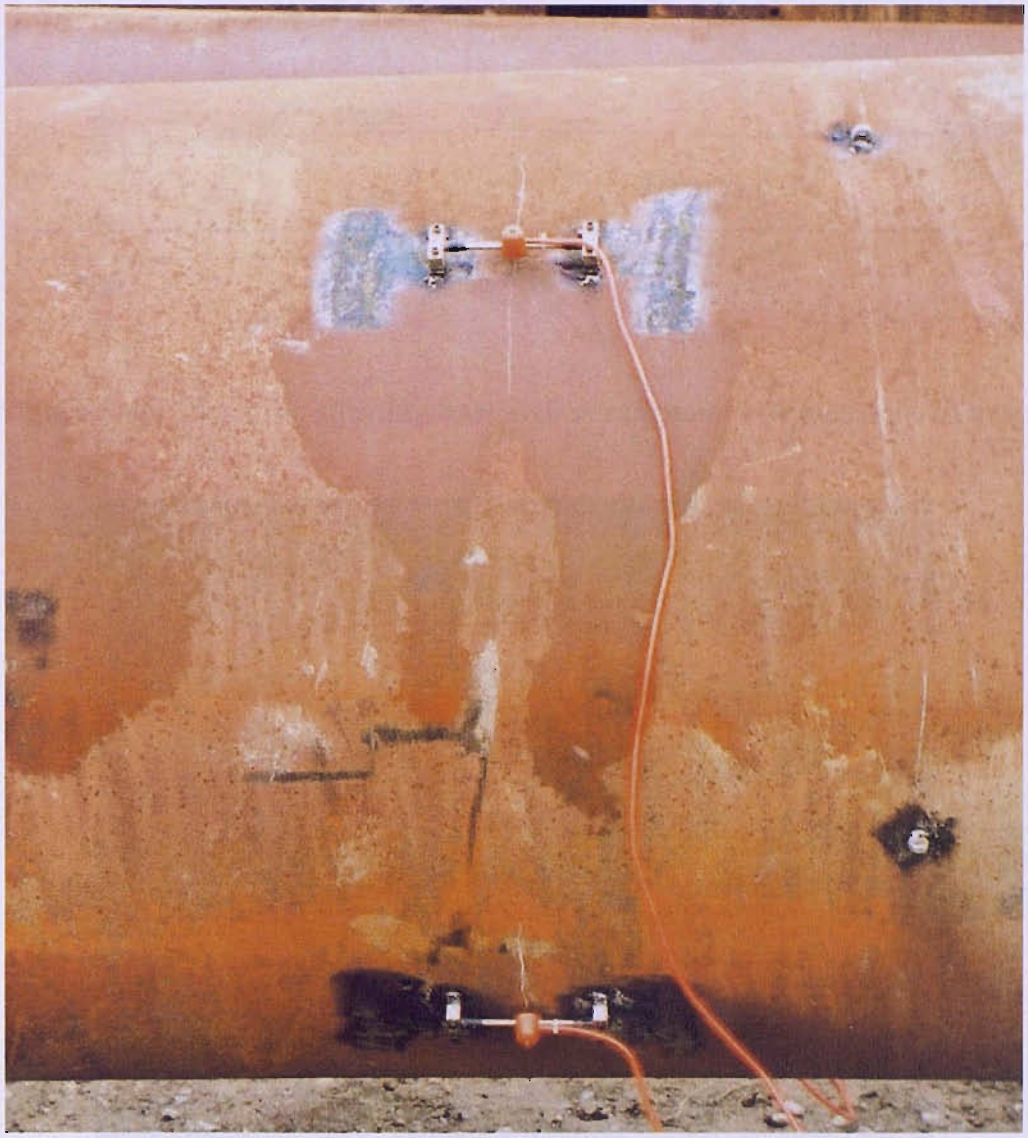

Figure 3-45: Temporary prop gauges welded onto prop

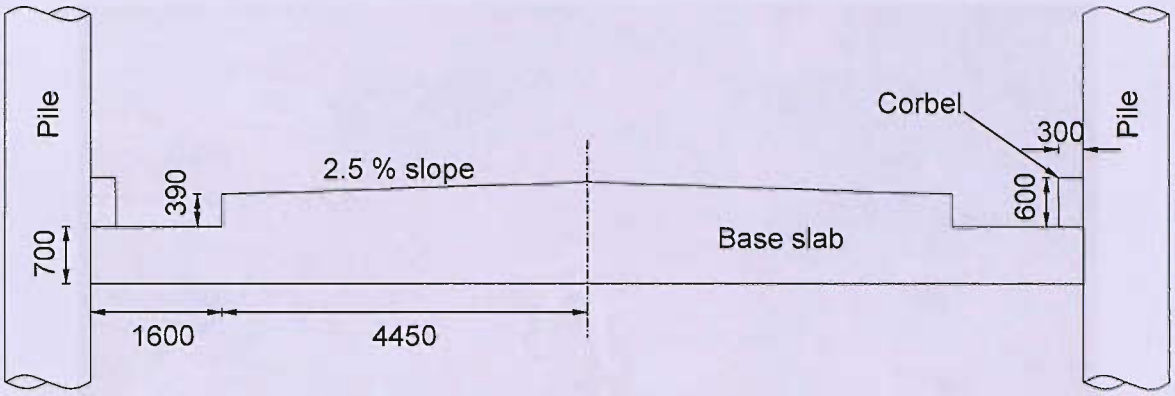

Figure 3-46: Elevation showing base slab arrangement (dimensions in mm)

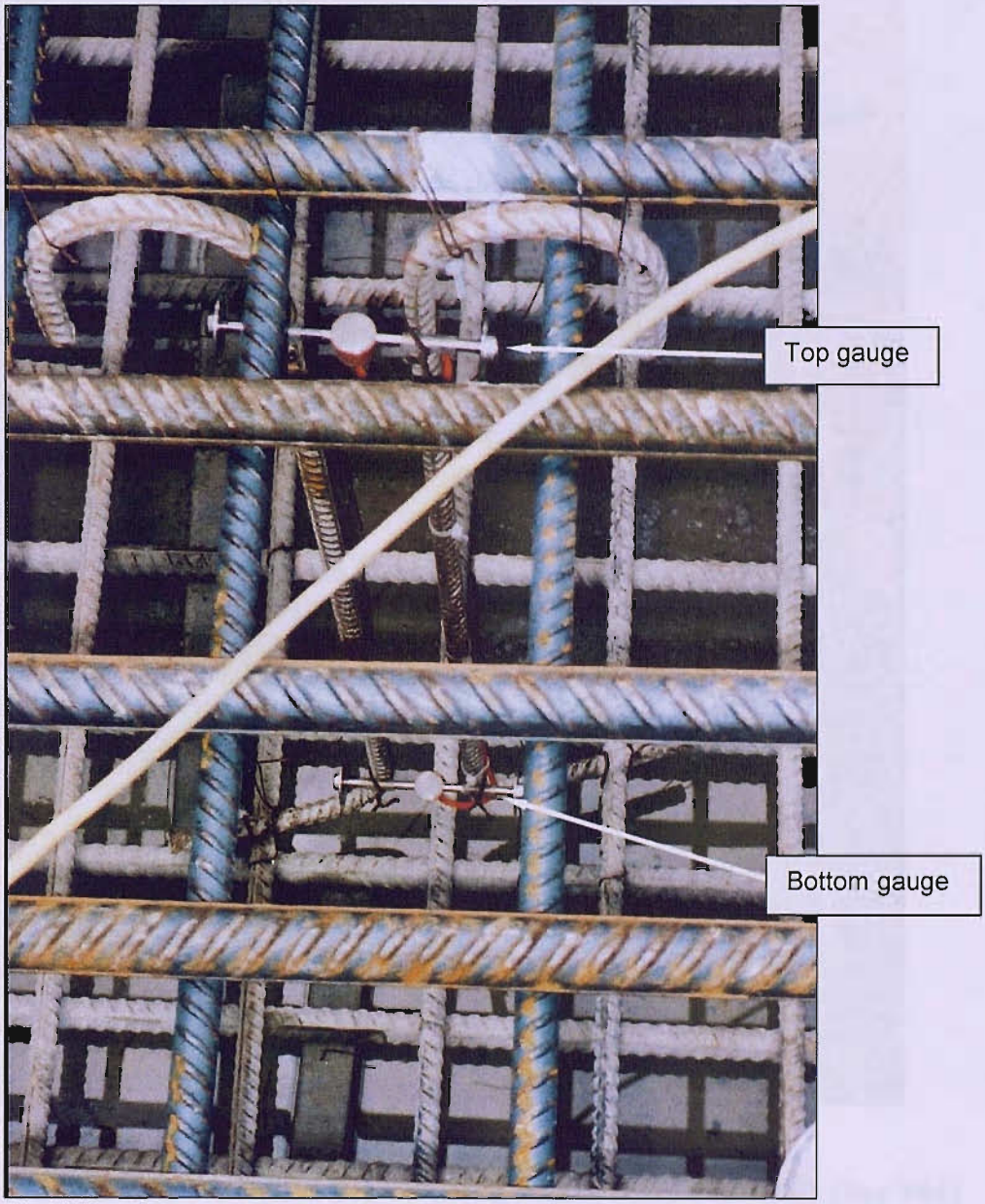

Figure 3-47: Strain gauges wired onto base slab reinforcement (photo was taken looking down through base slab)

Figure 3-48: Storm drain installed behind north wall in November 2001 (Day 864)

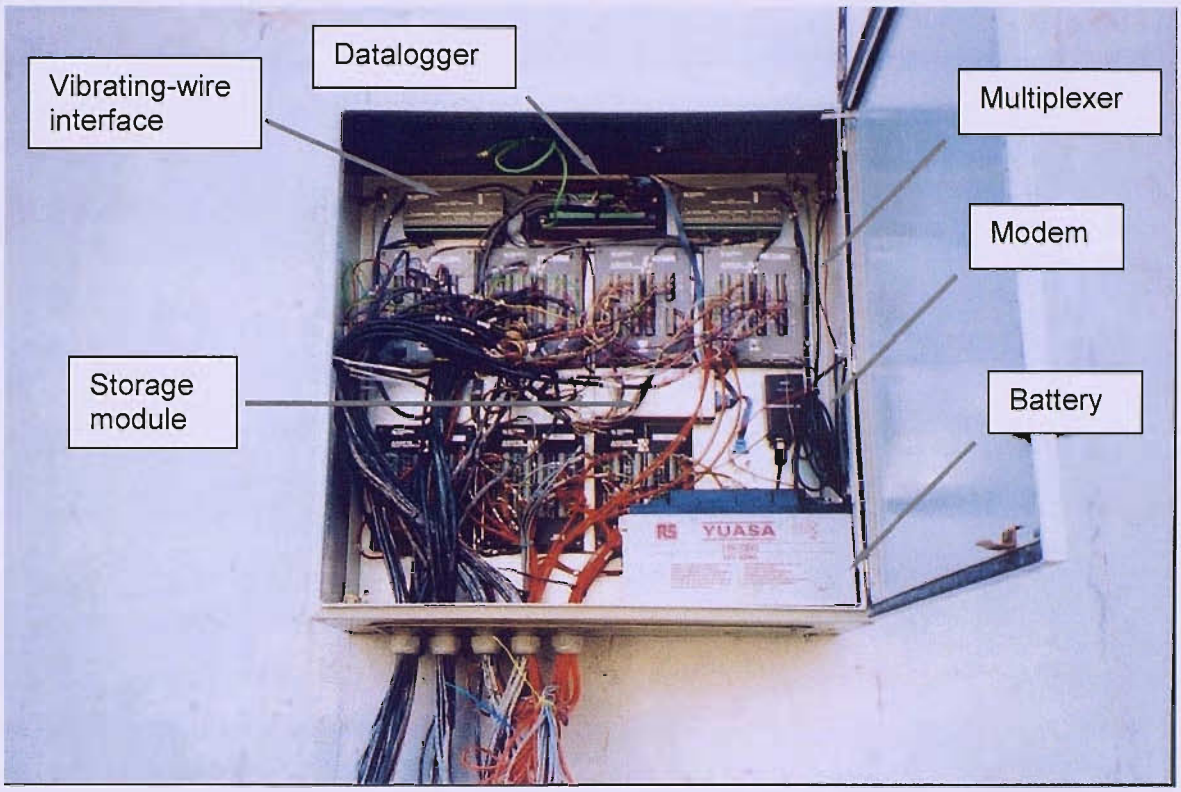

Figure 3-49: Datalogger set-up

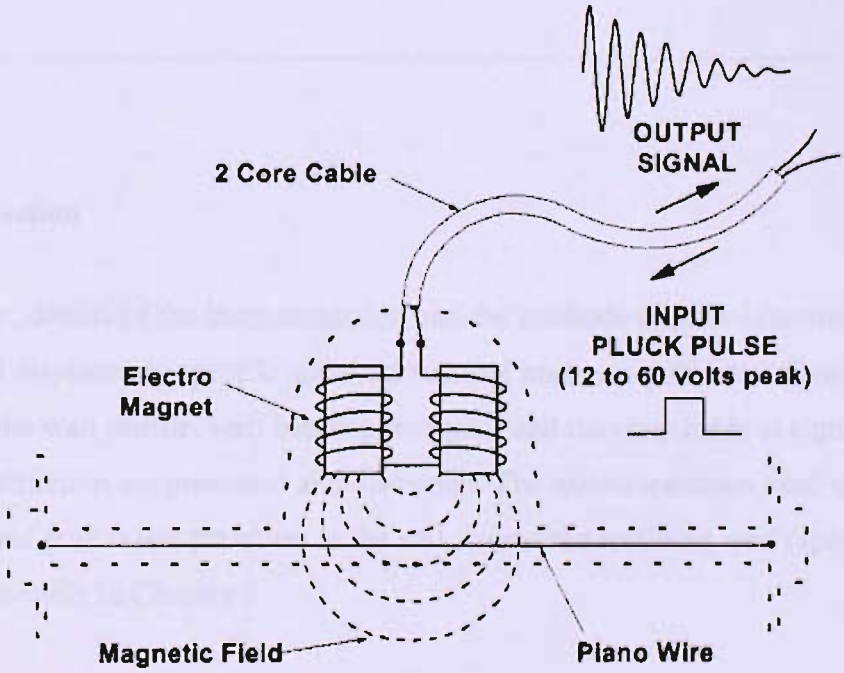

Figure 3-50: Vibrating-wire gauge (Gage Technique)

4 STRUCTURAL MONITORING

4-1 Introduction

In this chapter, details of the instrumentation and the methods used to determine the retaining wall displacement profile and the structural loads are presented. Data representing the wall profile, wall bending moments and the prop loads at significant stages of construction are presented and discussed. The instrumentation used to monitor soil stresses and pore water pressures in the soil around the retaining wall (spade cells) is described separately in Chapter 5.

4-2 Inclinometer

4-2-1 Description and Use

An inclinometer is a device for measuring inclination, or tilt. Inclinometers have been used in numerous construction projects over at least the past 30 years to monitor ground and structural movements, often as part of observational methods of construction (Peck, 1969), e.g. The World Trade Centre (Saxena, 1975); Limehouse Link (Glass & Powderham, 1994); Channel Tunnel Rail Link (Loveridge, 2000) and the Heathrow Airside Road Tunnel (Hitchcock, 2003).

To find the retaining wall's deflected profile an inclinometer probe (Figure 4-1) is manually lowered to the bottom of a tube installed within a pile. As the probe is pulled back up, readings of the tilt angle are taken (using accelerometers) at 0·5 m intervals in directions perpendicular and parallel to the wall. The inclinometer probe follows longitudinal grooves in the tube to ensure that it does not rotate as it moves upwards. Base readings are taken before the construction process being monitored begins (e.g. excavation) and subsequent readings reveal changes that occur due to construction activities.

To measure the absolute movement of the structure or ground mass being monitored, either the tube must be extended below the structural component into ground known to be stable (i.e. not affected by the construction process), or the top of the tube must be surveyed at each reading. At the instrumented section the inclinometer tube extends 10 m into the ground beneath the pile toe to ensure fixity so that the absolute movements of the wall can be determined. Further information regarding the use of inclinometers can be found in Dunnicliff (1993).

Mikkelsen (2003) describes the types of errors that may occur when using an inclinometer probe. In summary, these errors can be minimised by ensuring that:

- the same probe is used for all readings in a borehole;
- the same user takes the readings every time;
- the user is technically competent;
- the person who collects the data processes it; and
- the inclinometer probe is regularly calibrated.

These measures were taken by the monitoring team on the CTRL, who took inclinometer readings across the site at Ashford (the data were mainly used for implementing the Observational Method during construction).

In order to improve the accuracy of the inclinometer measurements two sets of data are collected for each profile: for the second set the inclinometer probe is rotated through 180°. The difference between individual pairs of readings at a given level is called the face error or *checksum*. This is equal to twice the zero offset, or *bias*. The face errors are displayed on the readout unit during data collection so that the user can check that these errors are approximately constant throughout the survey. If the face errors are constant there is no overall effect on the final inclinometer measurements. However, operator technique, instrument performance and casing conditions (such as variability at joints or dirt) can affect the face errors. For example, because the wheels on the inclinometer are angled (Figure 4-1: they are sprung to ensure that the inclinometer runs in the tube grooves), at tube joints the wheels may be resting on different sections of tubing and therefore larger face errors may occur. In this case, larger face errors will exist in all profile readings and can therefore be identified.

If the face errors are randomly inconsistent, analysis of the individual readings can reveal where the errors occur and the data can be altered accordingly. Figure 4-2 shows the face errors from an inclinometer profile taken on Day 581 (after Base Slab Construction and before Temporary Prop Removal). Some unusually large face errors are recorded at various locations in the inclinometer tube. Table 4-1 shows the Face A and Face B inclination readings at 41·593 m AOD and the calculated face errors for the data sets taken on Day 581. At this reading location only the Face A reading was inconsistent. Having identified the locations of these large face errors, comparison of the readings recorded at these locations with those taken on the preceding and following days allows the rogue readings to be identified and adjusted (amendments are shown in brackets).

Day	523	537	538	542	549
Face A	4·1	4·1	4·6 (4·1)	4·0	4·2
Face B	-2·4	-2·4	-2·5	-2·4	-2·3
Face error = (A+B)/2	0·85	0·85	1·05 (0·8)	0·80	0·95

Table 4-1: Example of inclinometer data analysis and correction using face errors: 41·593 m AOD

The original and amended profiles for readings taken on Day 581 are plotted in Figure 4-2. The other data points highlighted in this plot were similarly analyzed and altered. For this profile adjusting the data in this way 'moved' the top of the wall by 1·5 mm. This is about 8% of the overall movement at the top of the wall. All the inclinometer data were adjusted in this way.

A further check on the accuracy of the data can be made by studying the wall toe movement. Figure 4-3 shows the deflection of the wall toe with time (from the inclinometer measurements). Although the data are scattered, those recorded before the base slab was installed appear to show a general movement of the wall toe into the excavation. The equation of the best-fit line to the readings taken before Base Slab Construction is shown on the graph. (NB: The movement profile is not really linear as different construction activities would produce more movement than others, however since the total movement is so small (1·5 mm), the assumption of a linear movement profile is justified.) Figure 4-4 shows (a) the as read profiles of the entire inclinometer tube (adjusted for face errors as described above); (b) the corrected wall profiles assuming a fixed toe; and (c) the corrected wall profiles assuming the toe moves according to the equation found in Figure 4-3, for a small selection of the data taken during Excavation Phase 1. Figure 4-4 shows that the adjustment described above produces much more consistent data which is more easily viewed and analysed. The scale on which the deflection data are plotted covers a small range of deflections, showing that in general these errors are very small.

Less frequent inclinometer readings were taken after Base Slab Construction so it is more difficult to infer the wall toe movement after this time. Figure 4-3 suggests that after Base Slab Construction the wall returned to its original position and then slowly over the following year moved back out into the excavation by a similar magnitude as during excavation. This movement might seem reasonable; however Figure 4-5, which shows inclinometer measurements taken within the entire inclinometer tube (i.e. including those taken in the ground below the pile toe) following Base Slab Construction, shows that the whole tube below the wall toe appears to be moving. This is highly unlikely because movement of the wall toe would only be expected to cause movement of a metre or so of the tube beneath. Therefore after this time the wall toe has assumed to have been stationary.

Figure 4-6 shows all wall profile data found from the inclinometer data (adjusted for errors as described above). Figure 4-6(d) shows the inclinometer profiles taken after Base Slab Construction over this period corrected for zero movement of the toe. The profiles show the top of the wall gradually moving into the excavation with time, with the exception of the data taken in June and July where the wall moves very little. This behaviour would be expected during and following Temporary Prop Removal. Therefore, the assumption that the toe has remained in the same position as it was at the end of construction appears to be valid. The inclinometer measurements show that the wall toe is in a similar position on Days 585 (just after Base Slab Construction) and 718 (over 4 months later).

The large deflections measured at the top of the wall are likely to be due to the unsymmetrical geometry of the structure. The readings indicate that the structure has swayed towards the south wall, where the ground level is lower than that behind the north wall (Figure 3-22). This movement is described in more detail in Section 4-5-5.

The data taken below the toe of the pile can be used to determine the random errors associated with the particular instrument and survey point. The maximum reading taken over this section of inclinometer tube is 1·7 mm, indicating a maximum random error of 1·7 mm per 10 m of inclinometer tubing.

Figure 4-7 shows the movement of the top of the wall with time. It shows gradual movement into the excavation until Base Slab Construction after which the movement reduces significantly. (It must be noted that this data is however based on the readings that have been corrected for zero toe movement after Base Slab Construction. Therefore at a minimum, the graph shows that there is little relative movement of the top of the wall to its toe).

4-2-2 Calculation of bending moments from inclinometer data

Bending moments are frequently calculated from the bending strains measured using vibrating-wire strain gauges embedded in concrete retaining walls (e.g. Tedd *et al.*, 1984) and piles (e.g. pile stabilized slopes: Smethurst, 2003). In order to estimate pile bending moments from inclinometer readings, it is necessary to differentiate twice an equation representing the deflected profile of the pile (measured with the inclinometer). To find an equation for the wall's deflected profile, a curve (such as a polynomial) must be fitted to the deflection data.

Ooi & Ramsey (2003) compared twelve methods for calculating bending moments from inclinometer data including piecewise fitting of quadratic and cubic curves, and global polynomial curve fitting. They noted that if using global polynomial curve fitting, the lowest possible degree of polynomial that will "adequately" describe the data should ideally be used. This will allow the main changes in wall shape to be modelled without including small local errors in the inclinometer data. In general Ooi & Ramsey concluded that piecewise fitting of cubic curves to windows of five points yielded "middle" values of curvature and that when maximum curvature values found using this method were compared to strain gauge data collected from laterally loaded piles the values were in good agreement. For inclinometer data collected at the CTRL site global polynomial fitting has been found to give good correlation with bending moments calculated from strain gauge readings.

The second derivative of the equation representing the deflected wall profile yields an expression for its curvature, κ, of the wall, where $\kappa = 1/R_c$ and R_c is the radius of curvature of the pile. The bending moment, M, is calculated from the product of the curvature and the flexural rigidity of the pile, EI (Equation 4-1), where E is Young's modulus and I is the second moment of area. For a circular cross-section with constant stiffness the second moment of area is given by Equation 4-2, where r is the radius of the pile. The stiffness of steel is approximately eight times that of concrete, therefore the flexural rigidity must be calculated to include the effect of the steel in a reinforced section (see Section 4-3-3).

$$M = \frac{EI}{R_c}. \qquad \textbf{Equation 4-1}$$

$$I = \frac{\pi r^4}{4}. \qquad \textbf{Equation 4-2}$$

The pile concrete had 20 mm granite aggregate and a characteristic strength of 40 N/mm^2. The mean 56 day cube strength of 61 cubes taken from the piles cast in the period the piles in the instrumented section were cast was 73·0 N/mm^2. It should be noted that this is higher than might be expected, however it does refer to the 56 day cube strength (it is more common practice to quote the 28 day strength for concrete).

The bending moment is defined as positive when the excavated side of the wall is in tension.

It is important to carefully consider the degree of polynomial used to fit to the profile data. A polynomial with a similar number of inflections as the shape of the profile should be chosen, otherwise the bending moment plot produced will have too few/too many inflections and indicate an inaccurate bending moment profile. A 5^{th} order polynomial is most suitable for representing the deflected shape of a wall which has a linear horizontal pressure distribution acting on it (the pressure distribution is given by the 4^{th} derivative of the chosen polynomial). In reality the pressure distribution is unlikely to be perfectly linear, and therefore both 5^{th} and 6^{th} order polynomial equations were fitted to the deflected wall profile (determined by the inclinometer readings) before and after two construction stages at which cracking appears to have occurred (described later). The correlation coefficients for the curves were all greater than 0·997, which superficially[1] indicates a high level of accuracy for the curve fit. Comparisons between the bending moments calculated from the inclinometer and strain gauge measurements are made in Section 4-4-5.

Factors that affect the stiffness of the pile and in turn affect the suitability of the curve fitting include:

- changes in cross-sectional area of the element;
- changes in reinforcement stiffness; and
- concrete cracking.

These factors affect the continuity of the pile element and hence the mathematical accuracy of the curve fit. It may be better to fit several curves to sections of the pile with continuous properties. The reinforcement in the piles in the instrumented section reduced from 50 mm to 40 mm diameter bars about 6 m above the pile toe (described in Section 4-3-3). In addition, there was a bulge in the piles just below the level of the casing, (described in Section 4-4-4). In this case however a better curve fit and bending moment distribution was given by the curves fitted to the entire pile.

Cracking reduces the pile's cross-sectional area; therefore the value of I must be modified to take account of this or the calculated bending moments will tend to be overestimated. Further comments on fitting curves to inclinometer data are made in Section 4-4-5.

---

[1] It is important to note that the correlation coefficient can be misleading: the higher the order of polynomial fitted to the data, the higher the correlation coefficient, but this does not necessarily mean the curve fit will give the best equation for the bending moment profile for the reasons already explained.

4-3 Vibrating-wire gauges

4-3-1 Use

Precautions that must be taken when using vibrating-wire gauges include the avoidance of magnetic fields and magnetic particles. Since the railway was opened there has been no obvious influence from passing trains on the data. It is also important to ensure that the elasticity of the gauge approximates to the elasticity of the concrete for the period over which the measurements are to be taken (British Standards Institution, 1986).

4-3-2 Method for calculation of prop loads from strain gauge measurements

In order to calculate prop loads and bending moments from strain gauges the strain in the wire (and therefore the prop or pile), ε, is calculated from Equation 4-3 (where F_1 is the datum frequency of the wire equivalent to zero strain in the prop, F_2 is a subsequent reading and GF is the gauge or calibration factor, equal to $3{\cdot}025 \times 10^{-3}$ for the gauges used in this project). The prop load, P, can then be found from Equation 4-4 (where A is the cross-sectional area of the prop and E is the stiffness of concrete (for the RC props) or steel (for the temporary props). The stiffness of steel has been taken as 205 MPa and a value of 25 MPa has been used for the stiffness of concrete (Mosley and Bungey, 1976). This is a conservative value and the actual value may be higher (the concrete cube strength data collected for the pile concrete is relatively high, however once load is applied creep has a significant effect, effectively reducing the concrete stiffness). The calculated prop loads and bending moments might therefore be underestimated.

$$\varepsilon = \left(F_1^2 - F_2^2\right) \times GF \,. \qquad \textbf{Equation 4-3}$$

$$P = \varepsilon \, E \, A \,. \qquad \textbf{Equation 4-4}$$

Surface-mounted strain gauges are commonly used to measure temporary prop loads (e.g. Richards *et al.*, 1999; Batten & Powrie, 2000; Loveridge, 2000) as part of construction monitoring (for example using the observational method: see Section 4-2). Many of the issues concerning their use have been discussed by Batten *et al.* (1999), including temperature and end effects and the influence of the instrument's location on the prop.

4-3-3 Method for calculation of bending moments from strain gauges

Bending moments in concrete retaining walls are calculated from strain measurements obtained using embedment strain gauges placed in pairs at intervals up the concrete section, with one at the front and one at the back of the wall at the same elevation (see Figure 3-29). For an uncracked section of wall, the bending moment in the wall, M, is calculated from the longitudinal bending strains ε_1 and ε_2 measured by the strain gauges at the back and front of the wall respectively using Equation 4-5, (derived from Equations 4-1 and 4-6) where y is the distance from the gauge to the neutral axis.

$$M = \frac{EI(\varepsilon_1 - \varepsilon_2)}{2y}. \qquad \textbf{Equation 4-5}$$

$$R_c = \frac{y}{\varepsilon}. \qquad \textbf{Equation 4-6}$$

In the concrete piles used at Ashford there are 16 longitudinal reinforcement bars making up 3·6% of the total cross-sectional area of the pile. The flexural rigidity (EI value) of the pile has therefore been calculated to take the effect of the steel into account (see Appendix C). The lower section of the pile (incorporating gauges 1-10: see Figure 3-29) has smaller reinforcement bars and therefore a lower flexural rigidity. The flexural rigidity of the two pile sections are given in Table 4-2.

		Flexural rigidity:	
	Gauges	**per pile, kNm^2**	**per m run of wall, kNm^2/m**
Top of pile	11-26	2015300	1492800
Bottom of pile	1-10	1826600	1353000

Table 4-2: Flexural rigidity of concrete piles

For a circular section the flexural rigidity is proportional to the square of the cross-sectional area, A. (Equation 4-7: given that $I = A\,k^2$, where k is the radius of gyration (for a circle $k^2 = ¼\,r^2$ and $A = \pi\,r^2$)). Therefore when the area decreases (for example when cracking occurs) the flexural rigidity of the pile decreases rapidly.

$$EI = \frac{EA^2}{4\pi}. \qquad \textbf{Equation 4-7}$$

Uncracked behaviour is usually assumed to exist in the calculation of bending moments from strain gauge data (Tedd *et al.*, 1984; Wood & Perrin, 1984; Hayward, 2000). However, it is important to determine whether cracking has occurred because if so and the value of the *EI* is not adjusted accordingly, bending moments may be significantly over-estimated from gauge measurements. Details of how to calculate the cracked flexural rigidity can be found in Branson (1977).

The cracking moment of the wall, M_{cr}, is the moment corresponding to the maximum tensile stress that the wall can accommodate (the modulus of rupture of concrete, f_r). The most commonly used relationship between the modulus of rupture and cracking moment is shown in Equation 4-8, where f_r is given by Equation 4-9 (American Concrete Institute, 1992), I_g is the gross second moment of area of the pile (0·059666 m^4) and y_t is the distance from the centroid to the edge of the section. In Equation 4-9, f_c' is the cylinder compressive strength of concrete, and is taken to be 0·8 f_{cu}, where f_{cu} is the 100 mm cube compressive strength (Eurocode 2, 1992). On the basis of the analysis of the results from over 12 000 tensile strength tests, Raphael (1984) proposed Equation 4-10 for the calculation of f_r.

$$M_{cr} = \frac{f_r I_g}{y_t}. \qquad \textbf{Equation 4-8}$$

$$f_r = 0 \cdot 623\sqrt{f_c'} \text{ (in MPa).} \qquad \textbf{Equation 4-9}$$

$$f_r = 2 \cdot 3 f_c'^{2/3} \text{ (in psi).} \qquad \textbf{Equation 4-10}$$

As stated in Section 4-2-2, cube tests of samples taken on site showed that the pile concrete has a cube compressive strength of 73 MPa, giving the values for M_{cr} listed in Table 4-3. For these calculations y_t was taken as half the diameter of the pile.

Equation f_r is calculated from	**M_{cr}, kNm**
Equation 4-9	541
Equation 4-10	749

Table 4-3: The cracking moment of the wall, M_{cr}, calculated by different methods

4-3-4 Correction for temperature effects

Structural elements expand and contract with temperature which causes changes in load which are not induced by excavation or other structural loading. Temporary props are particularly susceptible to changes in load due to temperature, as they are made of steel which has a high thermal conductivity and therefore they absorb a great deal of heat, particularly when in direct sunlight. The relationship between temperature induced load and temperature for temporary props is approximately linear (see Figure 4-8) and a correction between temperature and load can be made based on this relationship. However, it is important to remember that the readings represent actual loads in the props which must be considered in design, and that the fluctuation of load with temperature can be very large. During construction of the Canada Water underground station in London the axial load varied by up to 50% during summer due to temperature effects (Batten *et al.*, 1999). The temperature versus load correction is therefore only made so that a comparison can be made between design loads and loads calculated from back analysis of field measurements.

The temperature corrected load, N_T, is given by Equation 4-11, where N is the measured load, T_0 is the temperature of the gauge at installation (before any loading in the prop), T_N is the temperature at the time of reading N and m is the gradient of the load versus temperature relationship (for example m = 44·439 kN/°C in Figure 4-8).

$$N_T = N + (T_0 - T_N) \times m. \qquad \textbf{Equation 4-11}$$

4-4 Analysis of instrumentation data

4-4-1 Temporary prop data

The temporary prop loads uncorrected for temperature effects and the average temperature measured by all gauges are shown in Figure 4-9. Before excavation there is very little fluctuation in the readings because the gauge wire and body are composed of material having the same coefficient of expansion as the prop and therefore there is no overall change in tension in the wire as the prop and gauge expand and contract with temperature. During excavation the prop loads are significantly affected by changes in temperature as the ends of the props are restrained by the retaining walls.

The temporary prop loads corrected for temperature effects are shown in Figure 4-10. The temperature correction has significantly reduced the variation in the readings with temperature when load is recorded. However, before excavation, when there is no end restraint to the props, the correction distorts the data so that it appears load is being recorded. Hence, temperature correction is only appropriate when the props are restrained to some degree.

The base readings for the temporary prop data (and the temperature correction) were taken as the average of the readings from installation of the prop until the day before Excavation Phase 2 began, over which time the readings were reasonably stable (this was 7 days for T1 and 6 days for T2 and T3). One of the gauges on T1 (number 4) was broken during excavation. Thereafter the load at the position of gauge 4 was taken to equal that measured in gauge 3, as the loads had been similar up to this point, and the loads measured in gauges 3 and 4 of the other props are also similar.

4-4-2 Base slab data

Data from the base slab for the period from just before installation to approximately two years later are shown in Figure 4-11(a). Set 1 relates to the pair of gauges to the north-west of the instrumented section (closest to slab A3 which was constructed previously) and the pairs are then equally spaced along centreline of the slab A4. Data collection began before the concrete was poured so the fluctuation at the start of the graph (shown in detail in Figure 4-11(b)) relates to the gauges expanding and contracting at a different rate to the reinforcement to which they are attached. Zero readings for the strain calculation were the average of the readings taken over the 72 hour period prior to concreting.

A large increase in load is indicated after the concrete was poured. The majority of this is not load carried by the slab but a change in strain induced by the rise in temperature caused by hydration of the cement as the concrete cures. The temperature increased to just over 40 °C, causing expansion of the gauge which is resisted by the setting concrete. There is no similar decrease in load as the concrete cools which indicates that the gauge and the concrete are cooling and contracting at the same rate. (It will be shown later in Section 4-5-4 that the bending moments measured in the piles at the level of the base slab reduce at the time of Base Slab Construction.)

Figure 4-12 shows the typical relationship between temperature and 'load' indicted by the measured strain for a base slab gauge over the period of the concrete pour and after temperature stabilization. There is no obvious relationship between load and temperature for the period after temperature stabilization, and it is not possible to determine whether the compressive strain indicated by the gauge is due to thermal effects or load being taken up by the slab.

The temperature fluctuations experienced by the gauges in the base slab are small because the slab is in contact with the ground at the bottom of the excavation which is at a reasonably constant temperature (being generally out of direct sunlight).

Figure 4-13 shows the strain measured in the separate gauges for sets 1 to 4, where compressive strain is positive. The strain behaviour is different in all sets and it is difficult to distinguish a general pattern. Figure 4-13 shows that after ballast was placed on the base slab between Days 998-1028 (July 2002), the daily fluctuations in temperature recorded by the strain gauges became negligible.

4-4-3 Reinforced concrete prop data

When concrete cures it undergoes shrinkage due to the hydration process, and when load is applied it is also subject to creep[2]. Analysis of reinforced concrete (RC) prop strain data is therefore complicated because the strain measured is a combination of the strain due to shrinkage, strain due to the applied load and strain due to the effects of creep. To illustrate the possible magnitude of strain occurring due to creep effects, Neville (1970) states that a typical creep deformation after a year under load is three times the deformation under that load.

Concrete undergoes continual shrinkage as it ages, with the majority of this shrinkage occurring in the first 28 days after the concrete is poured. It is possible to estimate the amount of strain occurring due to shrinkage if measurements of strain are taken in the immediate aftermath of the RC prop concrete pour and before any load is applied to the prop. Any strain occurring during this period is due to shrinkage alone and therefore the relationship between shrinkage and time can easily be established. A curve fitted to even

[2] Creep is deformation occurring under, and induced by, a constant sustained stress (or applied load).

only a few weeks' of such data can provide a sound basis for estimating the strain due to shrinkage that has occurred after any time period, even after load is applied to the prop.

The shrinkage due to creep is more difficult to quantify. Creep occurs when the strain continues to increase after the application of load. This indicates that the stiffness, E_{conc}, is decreasing. It is possible to estimate the amount of creep that has occurred through analysis of the data collected in the long-term, when the applied load is considered to be relatively constant.

Calculation of strain due to shrinkage

The reinforced concrete prop strain data was not collected until 9 days after the last RC prop concrete was poured, and it was then only another 7 days before Excavation Phase 1 commenced. It is therefore difficult to determine from the strain gauge data the rate of shrinkage due to concrete curing and how much of the final shrinkage had occurred before load was applied to the props. The strains measured in the concrete props over the period of excavation (using for the zero strain reading the average of the readings taken over the 24 hours immediately before excavation under the props began) are shown in Figures 4-14, 4-15 and 4-16 for props P1, P4 and P2 respectively. It appears from these figures that the strain is increasing at a reasonably regular rate and the changes due to construction events are difficult to identify.

The strains plotted in Figures 4-14 to 4-16 are a combination of strain due to shrinkage and loading. To establish the effects of shrinkage it was proposed to cast a short section of 'prop' using the same concrete mix design and reinforcement detail, and to embed a number of vibrating-wire strain gauges in it. Owing to site constraints this was not possible, however it was possible to analyse strain data collected from RC props (with a similar concrete mix and dimensions) cast elsewhere on site to estimate the concrete shrinkage. These props were at chainage 89+205, approximately 700 m away from the instrumented section.

Ross (1937) proposed the hyperbolic equation for concrete shrinkage given in Equation 4-12, where $\varepsilon_{sh}(t)$ is the shrinkage at time t and a and b are constants found from experimental data, being the y-intercept and slope respectively of the linear relationship between t / $\varepsilon_{sh}(t)$ and time. This relationship was deduced for three instrumented props at chainage 89+205. Strains in these props were monitored (using identical vibrating-wire embedment gauges to those used at the instrumented section) throughout the concrete pour

and the period before excavation; a period of at least 28 days. It should be noted that at the instrumented section the RC prop concrete was poured in January when temperatures were 3-8 °C, while at chainage 89+205 the concrete was poured in July when daily temperatures ranged between 6-28 °C (measured by the thermistors in the RC prop vibrating-wire gauges). The rate of curing and shrinkage is likely to be affected by the ambient temperature at the time of the concrete pour and during curing, however the resultant total shrinkage is considered to be independent of temperature.

$$\varepsilon_{sh}(t) = \frac{t}{a + bt}. \qquad \textbf{Equation 4-12}$$

Figure 4-17 shows a graph of $t/\varepsilon_{sh}(t)$ against time for a typical strain response gauge at chainage 89+205. The values for a and b calculated for all the gauges at chainage 89+205 are presented in Table 4-4, together with the maximum strain due to shrinkage indicated by the data from each gauge using Equation 4-12.

Prop	gauge	a	b	$\lim_{t\to\infty} \frac{t}{a+bt} = \frac{1}{b}(microstrain)$
1 (Ch 89+205)	1	23170·8	4235·3	236·1
	2	21346·9	4756·33	210·2
	3	15583·5	5238·6	190·9
	4	28178·6	4626·79	216·1
2 (Ch 89+205)	1	26562·5	4676·08	213·9
	2	19539·1	4624·83	216·2
	3	18549·1	4685·94	213·4
	4	22791·9	4389·48	227·8
3 (Ch 89+205)	1	17151·9	4683·19	213·5
	2	17198·8	4474·94	223·5
	3	13626·8	5113·68	195·6
	4	15783·0	4551·24	219·7
			average	215 με

Table 4-4: Values of *a* and *b* calculated for all gauges at chainage 89+205 m

The strain predicted by Equation 4-12 is compared with the measured strains (for the same data plotted in Figure 4-17) in Figure 4-18. Using Equation 4-12, the strain measurements from the RC prop gauges at chainage 89+205 predict that 215 με of strain (with a range of

191-236 με) would have occurred in the long-term due to shrinkage, with 95% of this strain occurring within 85 days of the props being cast. At the instrumented section this was Day 552 (11th April 2001); 15 days after Excavation Phase 2 and 27 days before Base Slab Construction.

In Table 4-5 the following details are listed:

1. the length of time between construction and excavation directly underneath for the props in the instrumented section,

2. the amount of shrinkage strain that would have occurred during excavation under the props (calculated from the analysis on the props at chainage 89+205) and

3. the equivalent load that this strain would indicate if a correction was not made.

Prop	**P1**	**P2**	**P4**
Day constructed	465	465	467
Day Excavation Phase 1 began directly underneath prop (see Figure 3-42)	483	487	505
Number of days between prop construction and excavation directly underneath	18	22	38
Average strain at chainage 89+205 after this length of time, με	160	166	202
Load indicated by this strain, kN	3989	4149	5049
Amount of shrinkage strain occurring in prop after excavation began directly underneath, με	55	49	13
Equivalent load, kN	1379	1218	318

Table 4-5: amount of strain occurring due to shrinkage and equivalent load indicated by this strain for the props at the instrumented section

The calculations in Table 4-5 clearly indicate that if a correction is not made for concrete shrinkage in cases where load is applied soon after prop construction, prop loads may be significantly overestimated. Figure 4-19 shows the RC prop loads calculated using the strains in Figures 4-14 to 4-16 and Figure 4-20 shows the loads calculated by reducing the measured strains according to the analysis carried out on the readings from chainage 89+205. There are several points to make about these graphs regarding the shrinkage correction:

1. The correction for shrinkage reduces the prop load by approximately 800 kN by Day 552 (after which 95% of the shrinkage strain will have occurred).

2. The correction appears to have reduced the amount by which the readings increase during periods when load is (apparently) not being applied, however there are still periods where the load increases more than expected: during Excavation Phase 1 (particularly in P1 and P2); before Excavation Phase 2; and after the temporary props are removed.

Figure 4-21 shows the RC prop load data only up to the end of Excavation Phase 2. On this graph the periods during Excavation Phase 1 when material directly under the RC props was removed are indicated, and the corresponding increases in load are clear. Another point of note is that after T1 was installed, the RC prop loads appear to decrease when the temperature increases, and visa versa. This effect is particularly prominent at the positions indicated by 1 and 2. This may be because as the temporary props expand with an increase in temperature the walls are pushed into the soil and the load in the RC props is therefore reduced. It is also likely that because load is now being applied to the RC props, creep is beginning to have an effect.

Calculation of strain due to creep

Equations representing the change in stiffness with time (due to the effects of creep) for each prop have been estimated by assuming that the prop loads do not change after Day 607 (other than for seasonal and daily temperature variation). Day 607 was chosen because it is 28 days after the base slab was poured and after the temporary props were removed (on days 581 (T1), 595 (T2 and T3) and 600 (T4)), and therefore it is assumed there is no further change in load due to the preceding construction events. To remove the effect of seasonal and daily variations, the load in the props has been assumed to be the same as that recorded at 9 am on Day 607 as at the same time on the same day every year following, i.e. on Days 972, 1337, 1702 and 2067. The variation in temperature recorded at 9 am on these days by the thermistors in the gauges was only 3 °C.

The Young's modulus, E_{conc}, was found on each of these days using Equation 4-4, assuming that the initial stiffness was 25 MPa. Equations with the form given in Equation 4-13, where N is the number of days and A, B, and C are constants, were then found (using the least squares fitting method) to these data for each prop – see Figure 4-22. The calculated values of A, B and C which provide the best-fit curves to the prop stiffness/time

relationship are given in Table 4-6. (Exponential expressions have commonly been used to model creep behaviour in the past: see Neville, 1970.)

$$E_{conc} = Ae^{\frac{-N}{B}} + C . \qquad \textbf{Equation 4-13}$$

	P1	P2	P4
A	12·756	12·971	14·741
B	12·222	11·981	10·222
C	558·12	816·98	606·20

Table 4-6: Values of constants for best-fit line to stiffness/time relationship (to 5 significant figures)

These equations were then used to calculate the stiffness used in the calculation of the RC prop load from Day 607 onwards. As data collection is ongoing, in the future it will be possible to get a better estimate of the creep behaviour.

Because the correction for creep has only been applied to the measurements taken after Day 607, it only affects the long-term data, presented in Chapter 6. An adjustment for creep should really be made as soon as load is applied, and therefore the reported RC prop loads may be over-estimated (however the value of the initial Young's modulus is also an estimate – see Section 4-3-2). In the first year after Day 607, 39 με can be attributed to creep. This is equivalent to 974 kN of load, calculated using a Young's modulus of 25 MPa. It was 4 months (or a third of this time) between the time excavation began under the props (i.e. load began to be applied to the props) and Day 607. Although the strain due to creep occurs at its fastest rate when load is applied, the load was initially small. Therefore the creep occurring before the correction was made can be estimated to be a maximum of 500 kN.

Effect of changes in temperature

The temperature versus load data for a typical RC prop strain gauge during periods when no construction activities are taking place is shown in Figure 4-23. This figure shows that there is no clear relationship between prop load and temperature which can be used for correcting the daily and seasonal temperature induced fluctuation in load. However, the RC props are not affected by temperature to the same degree as the temporary props and are therefore more straightforward to analyse.

Further comments

There are a number of further comments that can be made regarding the reinforced concrete prop data.

1. The load measured in prop P4 is significantly lower than that measured in props P1 and P2. The reason for this is uncertain, but may be due to anomalies in the construction detailing such as a lack of fit at the prop wall interface.

2. The daily fluctuations in prop load in P4 are smaller than in props P1 and P2. This may be caused by variations in the concrete cover to the gauges, making them more thermally insulated. This might have occurred if either P4 is larger than the other props (which is unlikely but would also explain the smaller load recorded in this prop as a larger surface area would indicate a larger load) or the gauges are embedded further into the prop. Smaller strains would be expected to be measured in either of these cases, as the gauges are proportionally closer to the neutral axis of the prop.

3. A reduction in load was recorded in all 3 RC props on the removal of temporary prop T1, whereas an increase load in props P1 and P2 was recorded when props T2 and T3 were removed, and similarly an increase was recorded in prop P4 when prop T4 was removed. The base slab concrete reached its maximum strain and temperature on the same day as T1 was removed, resulting in the decrease in load measured by the other RC props, and masking the effect of the temporary prop removal.

4-4-4 Pile data

Theoretically, if the neutral axis is in the middle of a pile section and there is no axial load the bending strains at the front and back of the pile at any elevation will be equal and opposite. In reality, as well as the self-weight of the pile and the capping beam, axial load in the pile will be caused by wall friction on the front and back faces of the piled wall. Figure 4-24 shows the difference in strain measured between the front and back of the pile at each gauge pair elevation against time for piles X and Y (see Figure 3-29 for gauge elevations). Figure 4-24 shows that for most gauge pairs the difference in strain between the front and back of the pile is small. However, the values increase suddenly for gauge pairs 15&16 and 17&18 in pile X at the start of Excavation Phase 2, and for 21&22 in pile

Y after Temporary Prop Removal. Figure 4-25 shows the strain measurements for these individual gauges. Figure 4-25(a) shows that during the Excavation Phase 2 much larger strains are measured by gauges X16 and X18 (even numbered gauges are at the front of the pile) than by their partners, gauges X15 and X17 respectively. Figure 4-25(b) shows that during Temporary Prop Removal a larger strain is measured by gauge Y22 than Y21. These changes in strain are likely to be caused by to cracking in the piles. Figure 4-25(a) also shows that following cracking of the pile during Excavation Phase 2, the response to Temporary Prop Removal is much larger in the gauges at the front of the wall than the gauges at the back.

Pile deflections measured with the inclinometer in Pile Z around the time of Excavation Phase 2 and Temporary Prop Removal are shown in Figure 4-26. The elevations of gauges 15&16, 17&18 and 21&22 are indicated. The figure shows that the points at which the strains have increased to a greater degree at the front of the pile than the back of the pile correspond with the points where the maximum deflections over the period have been measured.

Table 4-7 lists the wall deflections and curvatures measured by the inclinometer for the gauges at which the largest values were recorded before and after the two construction activities that appeared to cause cracking (temporary prop removal and excavation phase 2). The changes in the values over these periods are included. The values relating to the positions at which cracks occurred have been highlighted. As expected, the data show that cracks occurred at positions where the largest changes in deflection and curvature occurred, and indicate that the change may be more important than the degree of deflection and curvature in initiating cracks. However, cracks do not appear to have formed at the position of gauges 13&14 during Excavation Phase 2 and at gauges 23&24 during Temporary Prop Removal, where the changes in curvature that occurred were at least as high as values at other locations where cracks did form. It is therefore likely that a combination of the changes in deflection and curvature affects the propensity for cracking.

As previously noted, the bending moment in the pile may be affected by local changes in the pile's cross-sectional area, which affects the flexural rigidity, *EI*, of the pile. Figure 4-27 shows a bulge in the pile just underneath the bottom of the casing used during installation, indicating that overbreak has occurred at this level during excavation for the piles, and the resulting cavity was consequently filled with concrete. This level corresponds approximately with the level of gauges 17&18 and 19&20, which indicate a

smaller bending moment than those calculated at the locations of gauges 15&16 and 21&22 in the stages before cracking occurred, shown in Figure 4-29 (see next section). This excess concrete was removed after construction was completed, some time between August and October 2001.

Gauges	**13&14**	**15&16**	**17&18**	**19&20**	**21&22**	**23&24**
Elevation, m AOD	32·5	34	35·5	37	38·5	40
δ, pre Exc. Phase 2 (Day 529)	7·5	8·7	9·7	10·3	10·6	10·8
δ, post Exc. Phase 2 (Day 540)	16·9	18·6	19·1	18·8	18·1	17·3
Change in δ	9·4	***9·9***	***9·4***	8·5	7·5	6·5
δ, pre TP Removal (Day 564)	18·3	20·2	20·7	20·4	19·5	18·6
δ, post TP Removal (Day 617)	21·7	24·3	25·9	26·5	26·1	25·1
Change in δ	3·4	4·1	5·2	6·1	***6·6***	6·5
κ, pre Exc. Phase 2	-0·065	-0·099	-0·125	-0·139	-0·139	-0·119
κ, post Exc. Phase 2	-0·306	-0·344	-0·348	-0·312	-0·232	-0·102
Change in κ	-0·241	***-0·245***	***-0·223***	-0·173	-0·093	0·017
κ, pre TP Removal	-0·3	-0·343	-0·353	-0·321	-0·24	-0·101
κ, post TP Removal	-0·289	-0·402	-0·459	-0·446	-0·366	-0·231
Change in κ	0·011	-0·059	-0·106	-0·125	***-0·126***	-0·13

Table 4-7: Changes in deflection, δ, (mm) (relative to the toe) and changes in curvature, κ, ($\times 10^3 m^{-1}$) (from the 5th order polynomial curve fit) over periods of pile cracking. Positions where cracks have occurred are highlighted.

Figure 4-28 shows strains measured in Pile Y (see Figure 3-29 for the gauge elevations) after excavation and before Base Slab Construction; (Days 542-571) therefore the ground was at the level of the bottom of the base slab, just below gauges 15&16. Over this period the average temperatures measured in the temporary props ranged from 1 to 21°C, with an average of 10°C. The figure shows that there is a linear relationship between temperature and strain for the gauges at the front of the pile (odd numbers). The temperatures in these gauges vary by 6 °C; this was 30% of the temperature variation measured by the temporary prop thermistors over the same period. This caused the strain to vary by approximately 30-40 με, which would indicate 66-89 kNm of bending moment. There is no clear relationship with temperature for the gauges at the back of the pile, although the temperature range experienced by these is much smaller due to the insulation provided by the concrete and soil. Below excavation level the gauges at the front and back of the pile are equally affected by temperature. Gauges 13&14 are affected slightly, gauges 11&12

even less so, and below this there is no relationship between strain and temperature. From this, ambient changes in temperature can be assumed to only affect gauges within 2·5 m of the excavation or ground level (excavation level minus the level of gauges 11&12).

4-4-5 Comparison between pile bending moments calculated from strain gauges and inclinometer

Figures 4-29 and Figure 4-30 show bending moments calculated from the strain gauge and inclinometer measurements at four instances; before and after Excavation Phase 2 (when cracking occurred in Pile X: Figure 4-29) and before and after Temporary Prop Removal (when cracking occurred in Pile Y: Figure 4-30). Data at points where cracking has been shown to have occurred (in Figure 4-24 and Figure 4-25) are highlighted on Figures 4-29(b) and 4-30(b). Bending moments calculated from the 5th and 6th order polynomial curve fits to the inclinometer data are shown. The upper and lower bounds for the cracking moments, M_{cr} (calculated in Section 4-3-3) are indicated on the figures. *EI* values are all based on uncracked concrete properties.

In Figure 4-29(a) and (b) there is close agreement between the bending moment data derived from the wall profile and the strain gauges. In Figure 4-29(a) the measured bending moments are all smaller than M_{cr}, and there is little difference between the bending moments calculated from the 5th and 6th order fits to the inclinometer data.

Figures 4-29(b) and 4-30(a) show that at some strain gauge locations the calculated bending moments have exceeded M_{cr}. The two highest of these are those where cracking has been observed. At the other locations the section may be cracked but not specifically at the strain gauge (the strain gauges are 140 mm long and at 1·5 m intervals). In general there is close agreement between bending moments calculated from inclinometer readings and strain gauge measurements for the middle section of the pile. However, at the pile toe and the pile head the curves bear away from the strain gauge measurements. This is obviously a mathematical problem with the curve fitting process, and is caused by attempting to fit a polynomial curve to a wall profile which contains straight sections (the bottom of the wall is straight below approximately 27·5 m AOD – this was observed by noting that the gradient of the pile is constant below 31·5 m AOD, and that the strain gauges measure zero bending moments below about 27·0 m AOD). Further analysis has shown that polynomials fitted only to the curved parts of the pile (i.e. leaving out the lowest few metres) produce very similar bending moment profiles but with the top and

bottom parts absent. It follows that the bending moments calculated for known straight sections of the pile can simply be ignored.

Figure 4-30(b) shows the bending moment profiles found after Base Slab Construction and Temporary Prop Removal. Again, at the pile toe and top the inclinometer derived bending moments bear away from the strain gauge measurements. In Figure 4-30(b), unlike Figure 4-30(a), the inclinometer derived bending moments are larger than those measured using the strain gauges around the position of the maximum bending moment.

4-5 Measured changes due to construction events

4-5-1 Temporary props

Figure 4-31 shows the individual temporary prop loads. It can be seen that approximately 800 kN of load was recorded in temporary props T1 and T3 as a result of Excavation Phase 2, and 1000 kN in T2. When the base slab in bay A3 (see Figure 3-42) was constructed the load in the nearest temporary prop to it, T1, reduced by approximately 200 kN over the following 3 days. This is because the base slab concrete applied a lateral load on the wall as a result of the weight of the wet concrete and the initial expansion of the concrete due to curing. The combined load and expansion of the slab forced the wall back into the soil for a short period, inducing a temporary decrease in the temporary prop loads (in the piles a reduction in bending moment is measured in the gauges around the level of the base slab when the base slab concrete is poured against them, see Section 4-5-4). After the initial expansion of wet concrete it contracts while cooling and setting, and therefore the load in the temporary props recovered to close to the original value over the following 5 days, until the next base slab, at the instrumented section, was poured. This caused the load in prop T1 to reduce by nearly 100 kN over the following 2 days, until it was removed.

Temporary props T2 and T3 exhibited no change in load due to the installation of base slab A3. Following construction of base slab A4, the base slab in the instrumented section (i.e. directly below props T2 and T3), a reduction of approximately 200 kN was recorded in both T2 and T3 over the following 2 days. Then only 2 days after casting slab A4, prop T1 was removed and the load in prop T2 rose rapidly by approximately 200 kN. The load in prop T2 continued to rise by approximately another 200 kN over the following 14 days,

until it was removed. There was no change in load in prop T2 when the next base slab, A5, was constructed.

After base slab A4 was poured the load in prop T3 increased slowly over the following 9 days, by a total of approximately 80 kN, until the next base slab, A5, was installed. At this point the load reduced by approximately 40 kN. The load in prop T3 was then reasonably steady over the following 5 days until it was removed along with prop T2.

It is important to note that the changes in loads and bending moments due to the removal of prop T1 are masked by the loads applied by the expansion and contraction of the base slab concrete poured only 2 days earlier. Therefore the removal of props T2 and T3 might be expected to have different consequences.

4-5-2 Base slab data

Although the temperatures indicated by the base slab gauges during the concrete pour were very similar, Figures 4-11 and 4-13 shows that the strain rates were different. The strain in set 1 rose much more quickly than the strains in set 4, and the strains in sets 2 and 3 rose at a very similar rate. Despite their different rates of strain during the concrete pour and curing, sets 1-3 indicated a similar 'load' by Day 586 and set 4 by Day 596. The difference in strain may be affected by the different frictional qualities of the boundaries to the base slab: the previous concrete slab acts as a boundary near set 1 and there is shuttering near set 4.

4-5-3 Reinforced concrete props

The changes in the reinforced concrete prop loads that occurred as a result of excavation directly under the individual instrumented props are listed in Table 4-8 (also see Figure 4-21). The loads measured at various construction stages are presented in Table 4-9.

	Change due to excavation under:		
	P1	P2	P4
P1	550	200	0
P2	400	500	0
P4	150	150	150

Table 4-8: Changes in RC prop load due to excavation directly under individual props

	Load after excavation	Load after Temporary Prop Removal	Load after construction was completed		
			1 year	2 years	3 years
P1	1600	2700	3800	4500	5200
P2	1800	3100	4200	4900	6600
P4	900	1900	2700	3300	3900

Table 4-9: Load at specific stages of construction

4-5-4 Pile bending moments measured with strain gauges

Figures 4-32 and 4-33 show bending moments measured in Pile Y against time for the gauges below and above the base slab respectively. For clarity only the data taken at 0900 each day is plotted to remove the fluctuations due to daily temperature changes. Figures 4-34 and 4-35 show similar data for Pile X.

Table 4-10 shows the different changes in bending moment that were experienced by different parts of the pile as a result of specific construction activities. The information in the table is representative of both piles, as they behaved similarly (although the magnitudes of some of the changes differ).

Analysis of the data shows that the largest changes in bending moments occurred during Excavation Phase 2, at the level of the base slab. This corresponds with the largest changes in deflection and curvature shown in Table 4-6. Reductions in bending moment were recorded during this construction event in the gauges near the top of the wall; this is because rotation occurs around the temporary prop, the point of maximum bending moves down the wall and therefore the top of the wall is under less stress (this rotation can be seen in Figure 4-6 (a) and (b)). Before Excavation Phase 2, the maximum bending moment was approximately at excavated ground level, i.e. about the location of the temporary prop

(gauges 21&22). After Excavation Phase 2, the point of maximum bending moment was approximately at formation (gauges 15&16). The reduction in bending moments at the top of the wall could also be partly due to redistribution of stresses in the wall resulting from the cracking induced at this stage of construction.

The expansion and contraction of the base slab during its construction and the effect this had on the wall induced a temporary decrease in the bending moments close to the level of the base slab. The gauges near the top of the wall were not affected, probably because of the presence of the temporary props, which restricted movement of the wall and therefore load redistribution above its position.

As the heat generated in the base slab during the curing process dissipated the concrete contracted, therefore the load being applied to the wall reduced and the bending moments near the level of the base slab increased, as shown in Figures 4-32, 4-33, 4-34 and 4-35. However, temporary prop T1 was removed only 2 days after the base slab was cast, and therefore the change in bending moment is a combination of the loads occurring due to the concrete setting and temporary prop removal. On removal of props T2 and T3, the bending moment near the level of the base slab decreased. Therefore it is reasonable to assume that the removal of temporary prop T1 would also initiate a decrease in bending moment near the level of the base slab, and if prop T1 had not been removed so soon following Base Slab Construction the increase in bending moment in the following days may have been substantially higher.

Temporary prop removal resulted in an increase in the bending moments in the top of the wall and a decrease in those near the level of the base slab. The inclinometer measurements in Figure 4-6 (d) show that the point of maximum deflection moved up the wall after temporary prop removal (the last temporary props, T2 and T3, were removed on Day 595).

Stage	Top section of wall	Middle section of wall	Bottom of wall	Max change	Notes:
Exc. Phase 1	11&12-25&26: increase	not applicable	1&2-9&10: decrease	Increase at 21&22	Approx. the same change recorded in 15&16-19&20 and 23&24 due to second part of Exc. Phase 1.
Exc. Phase 2	21&22-25&26: decrease	5&6-19&20: increase	1&2-3&4: no significant change	Increase at 15 &16	Trend of changes generally continues for about 2 days after Exc. Phase 2 has finished.
Base Slab Construction	21&22-25&26: no significant change	11&12-19&20: reduction	1&2-9&10: small increase/no significant change	Decrease at 15&16	
Removal of T1	23&24-25&26: small increases over period of 10 days/no significant change	13&14-21&22: slow increase over period of about 10 days	1&2-11&12: slow decrease over about 10 days. No significant change in 1&2 and 3&4	Increase at 15&16	
Removal of T2 and T3	19&20-25&26: increase (no change in 25&26 pile X)	17&18: no change; 15&16-9&10: decrease	1&2-7&8: no significant change	Increase at 21&22	

Table 4-10: Changes in bending moment for piles X and Y due to particular construction stages. Ranges are inclusive of gauge numbers quoted

4-5-5 Inclinometer data

The inclinometer readings illustrated in Figure 4-6 show that the wall moved consistently into the excavation as construction progressed and that the majority of the movement occurred during excavation phases 1 and 2. Further movement occurred at temporary prop removal. The readings indicate that after temporary prop removal the wall continued to move, with the top of the wall moving into the excavation by 4 mm over the following 11 months. However, Figure 4-7 shows that the movement was not in one direction and that few readings were taken over a relatively long period of time, so the accuracy of these measurements is questionable. It is possible that the wall movements may be affected by yearly temperature changes, however the paucity of the readings prevents a definitive conclusion.

As previously mentioned, the relatively high deflections measured at the top of the wall lead to the conclusion that the cutting has swayed due to the difference in ground level behind the north and south walls (see Figure 3-22). (N.B: A compression of 1 mm in the RC prop would produce 25 000 kN of load; therefore the movement could not be due to compressive loading.) Unfortunately it was not possible to monitor the south wall due to access restrictions and very little is known about the progress of the construction of the 'Maidstone loop', the line which was constructed behind the south wall, and the corresponding changes in ground level. However from photographic evidence (Figure 3-34 – taken 110 days before excavation activities began) the existing railway lines can be seen and preparations for construction are being made, therefore the ground level must have been reduced by this time.

In the early part of Excavation Phase 1 (Days 483-488: before work temporarily stopped) the wall appears to be well propped at the top with excavation causing the wall to bend in the middle. Figures 4-32, 4-33, 4-34 and 4-35 show that the bending moments induced at this time were small. Later during Excavation Phase 1, the changes in deflection measured at all points in the section of wall above temporary prop level were similar, indicating that the wall was rotating and that the RC prop was not providing significant restraint. Figures 4-33 and 4-35 show that bending moments did not increase in either pile until the end of Excavation Phase 1. The top of the wall moved approximately 7 mm during Excavation Phase 1 and a further 3 mm before the start of Excavation Phase 2.

Between Days 530 and 533, at the beginning of Excavation Phase 2, the top of the wall moved very little while lower down the wall the measured change in deflection was approximately 5 mm. Days 534/535 were a weekend, after which excavation appears to have produced similar changes in deflection in the top section of the wall, indicating little restraint in the prop. The readings taken during Temporary Prop Removal also show the whole top section of the wall moving.

4-6 Conclusions

At the CTRL site at Ashford, UK, wall deflection profiles have been found from inclinometer measurements, inclinometer measurements and strain gauges have been used to derive bending moments in a propped contiguous bored pile retaining wall, and strains gauge measurements have also been used to measure temporary and reinforced concrete prop loads. The following points can be made:

1. Use of vibrating-wire instruments and a datalogging system capable of taking readings at up to 5 minute intervals has allowed (effectively) continuous data to be collected on site at Ashford.

2. The implementation of rigorous procedures during data collection, thorough analysis and error checking has produced good wall displacement profiles from the inclinometer data.

3. It was not possible to infer load measurements from strain data collected in the base slab, because the strains caused by changes in load could not be distinguished from the strains caused by thermal effects arising from the concrete curing process.

4. The temporary prop data proved to be more straight-forward to analyse and was corrected for temperature effects so that the average prop loads occurring due to construction events could be determined.

5. Analysis of concrete shrinkage occurring in reinforced concrete props constructed elsewhere at the Channel Tunnel Rail Link site has allowed prop loads at the instrumented section to be estimated, despite the fact that excavation under the props occurred very soon after the concrete pour while considerable shrinkage was occurring.

6. Careful consideration of the mathematical restraints to curve fitting have allowed wall bending moment profiles to be determined from inclinometer readings, and these show good agreement with bending moment profiles found from vibrating-wire strain gauges. Identification of concreting cracking and an analysis of the effect this has had on the bending moment profiles calculated from the inclinometer measurements has explained the differences in bending moment plots found by the two different methods after cracking had occurred.

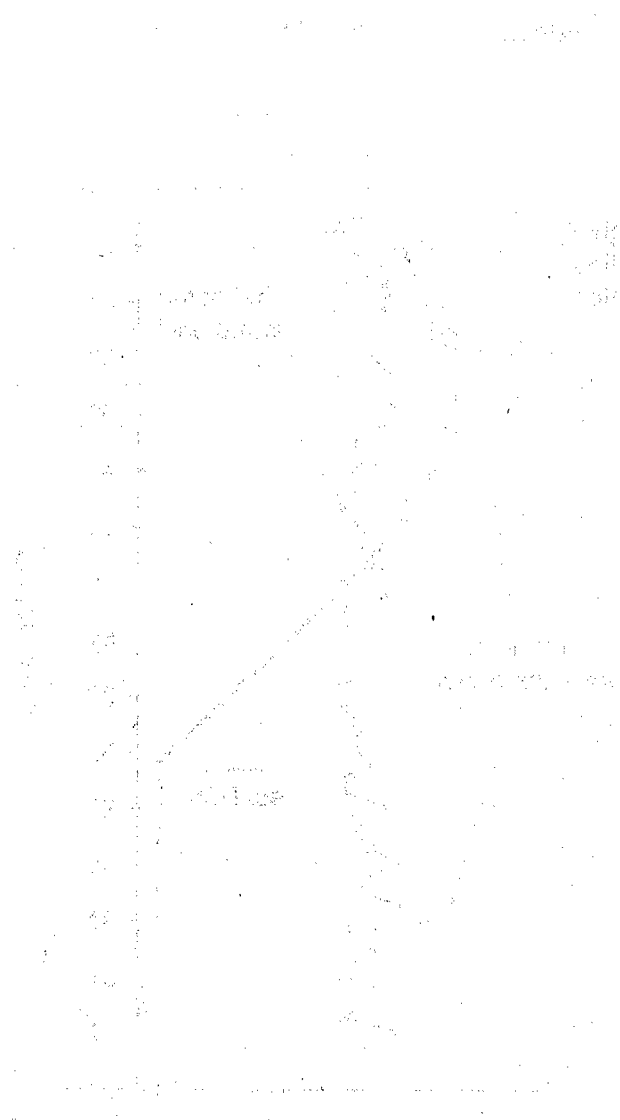

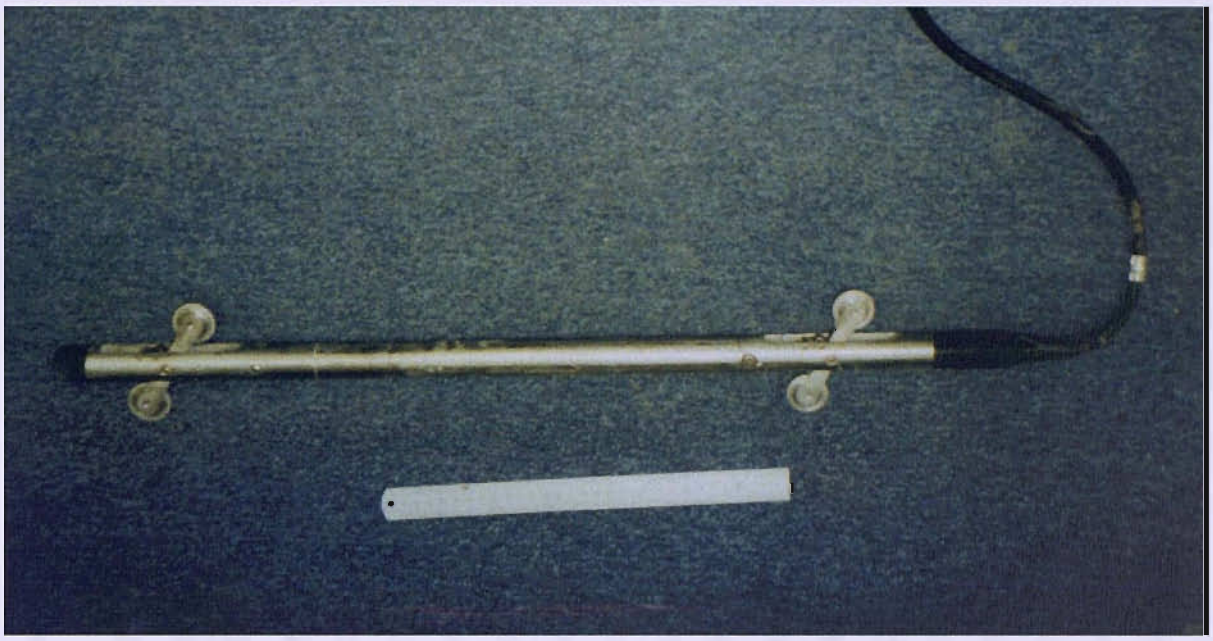

Figure 4-1: Inclinometer probe

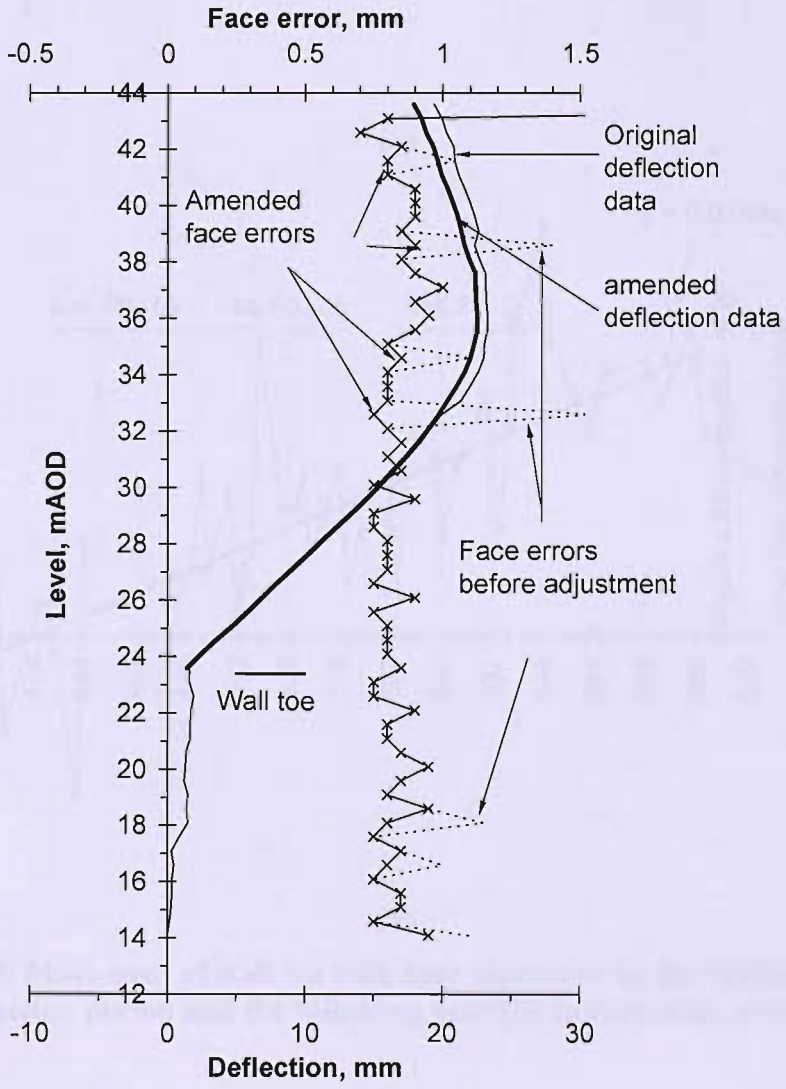

Figure 4-2: Analysis of inclinometer data face errors: Day 581

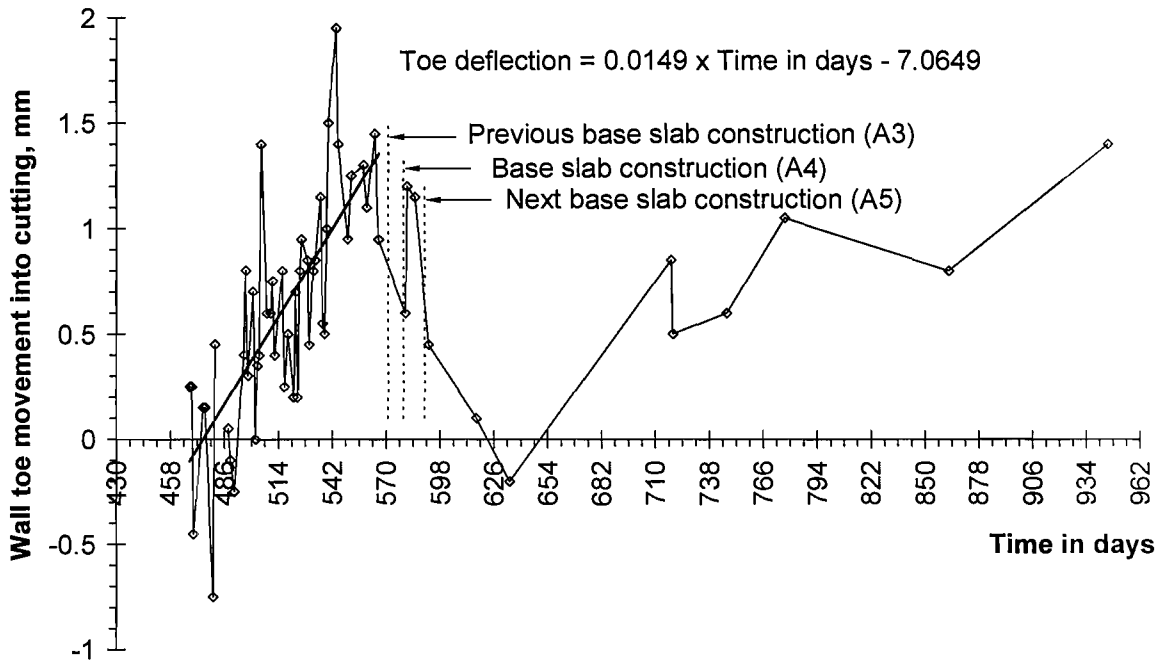

(a)

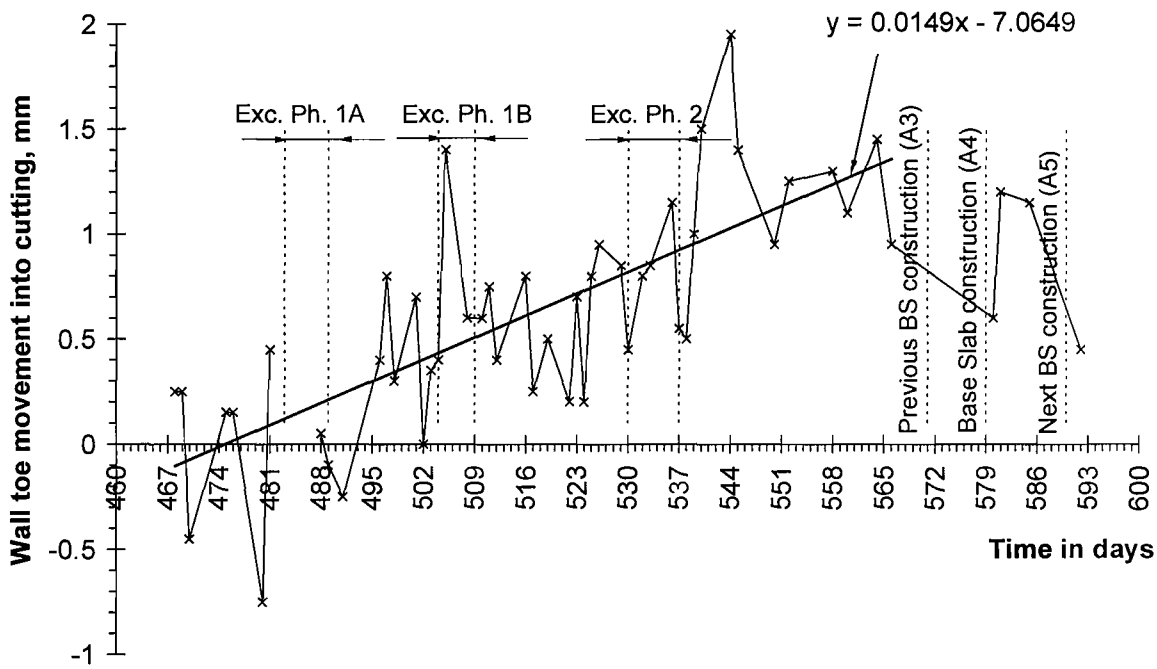

(b)

Figure 4-3: Movement of wall toe with time measured by the inclinometer (a) construction period and the following year (b) construction period only

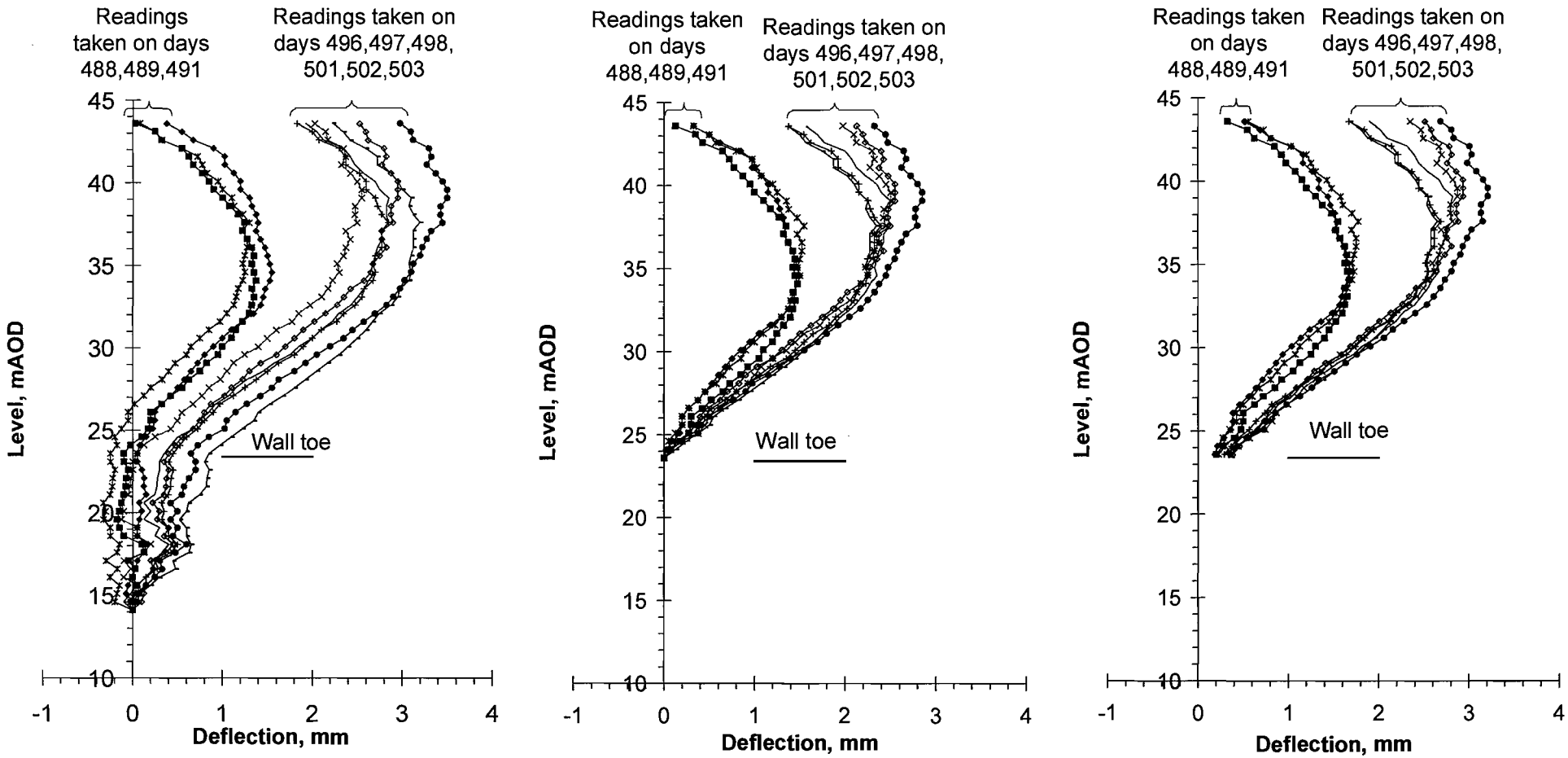

Figure 4-4: Correction of inclinometer data: (a) As read, (b) adjusted for zero movement at the toe and (c) adjusted for movement at toe indicated by equation given in Figure 4-3

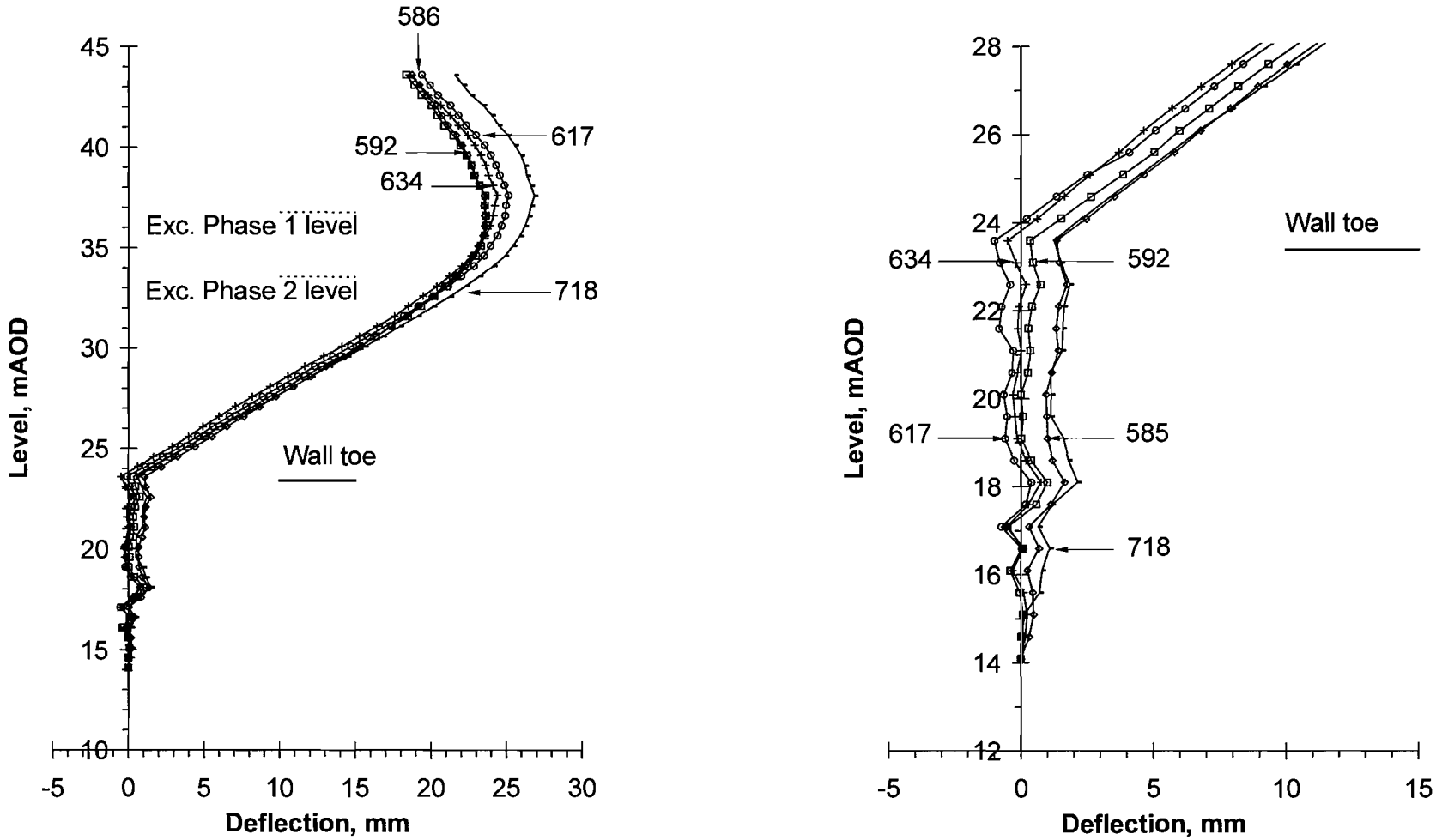

Figure 4-5: (a) Measured deflected profile of the wall and the bottom 10 m of tubing installed in the underlying soil. (b) Excerpt of (a) showing deflection of the bottom 10 m of inclinometer tubing

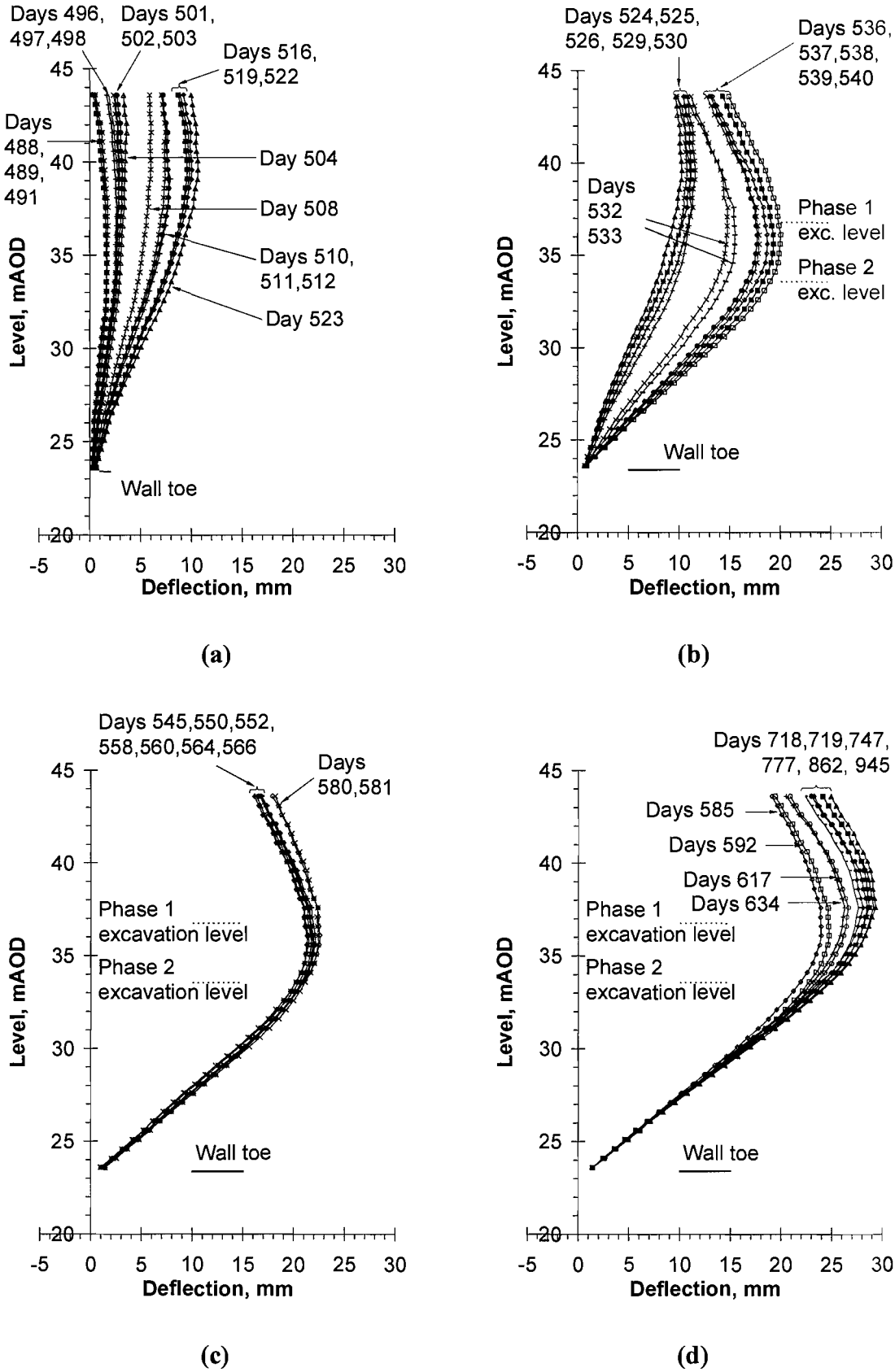

Figure 4-6: Error adjusted inclinometer measurements taken during construction (2001): (a) around Excavation Phase 1 (Days 483-488), (b) around Excavation Phase 2 (Days 530-537), (c) around Base Slab Construction (Day 579) and (d) after Base Slab Construction

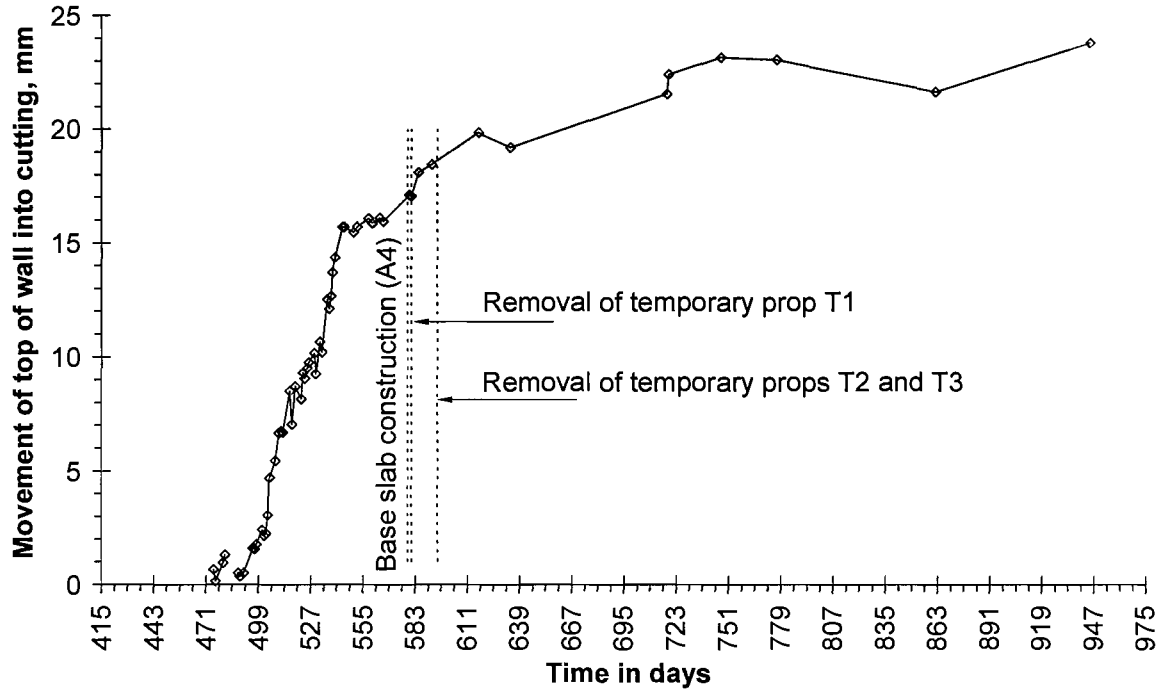

(a)

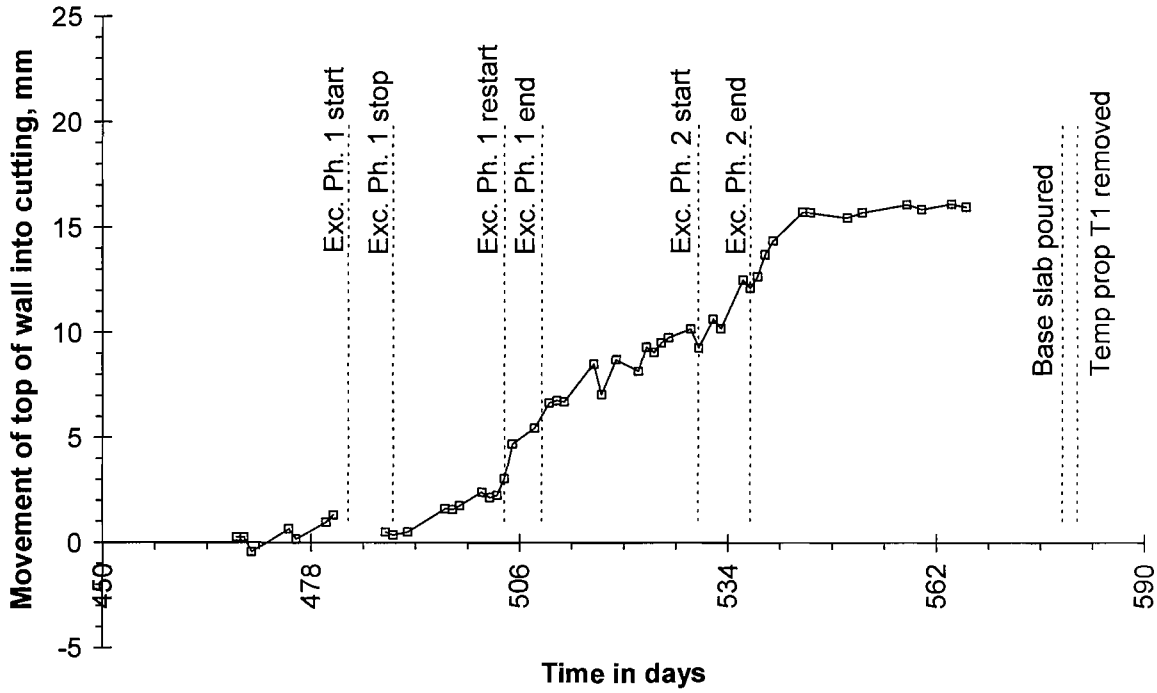

(b)

Figure 4-7: Movement of the top of the wall (a) all measurements (b) excerpt of (a) showing construction phases only

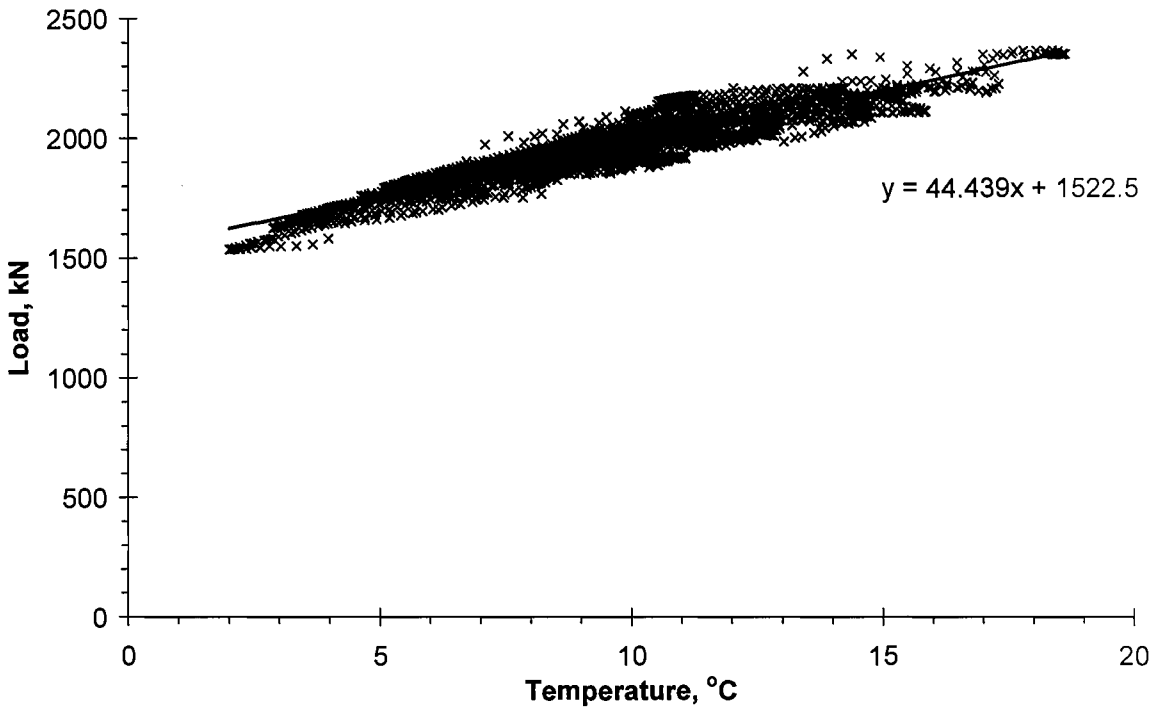

Figure 4-8: Typical relationship between load and temperature for temporary prop data taken over the 30 days between Excavation Phases 1 and 2, when no construction activities were taking place.

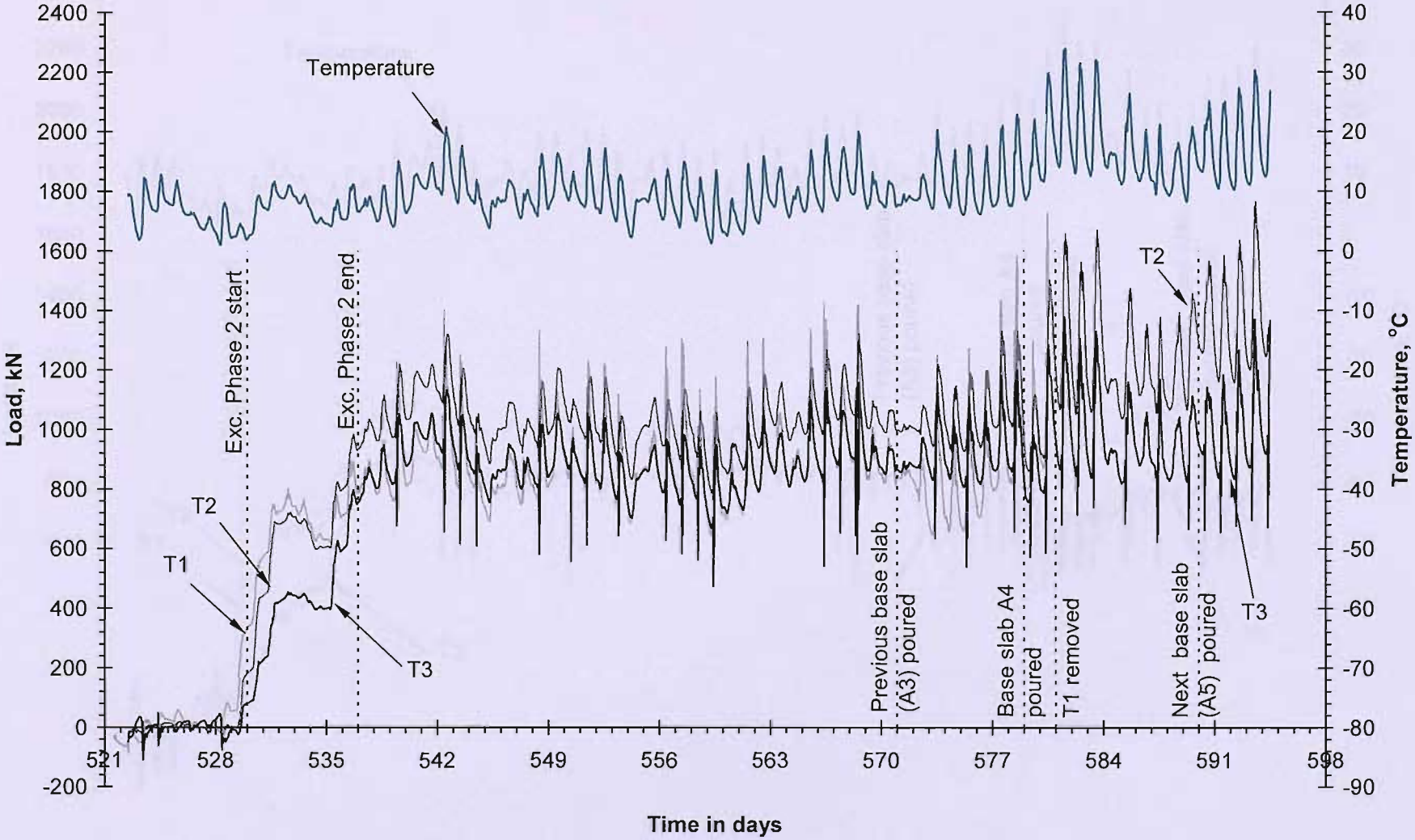

Figure 4-9: As measured temporary prop loads

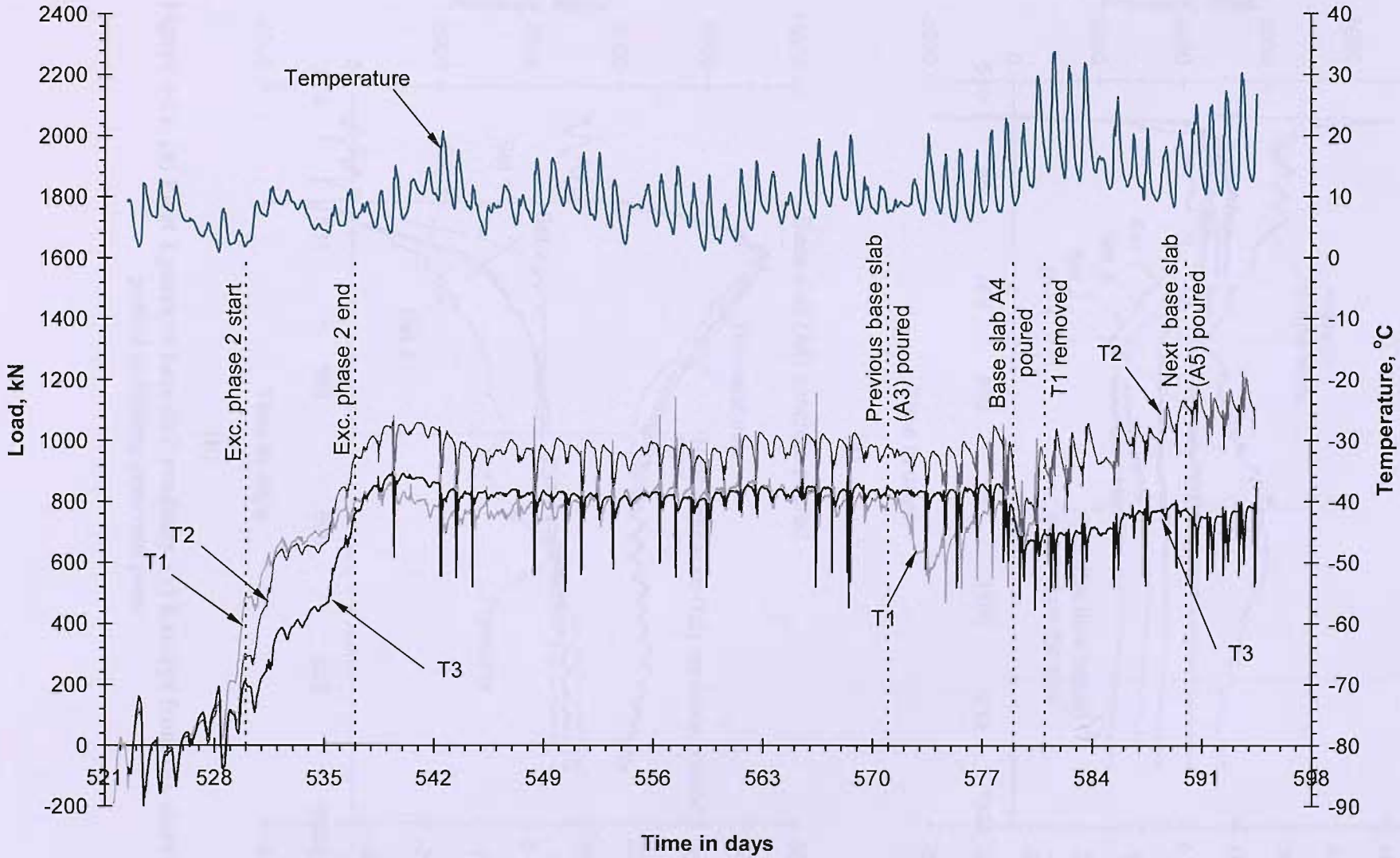

Figure 4-10: Temporary prop loads corrected for temperature effects

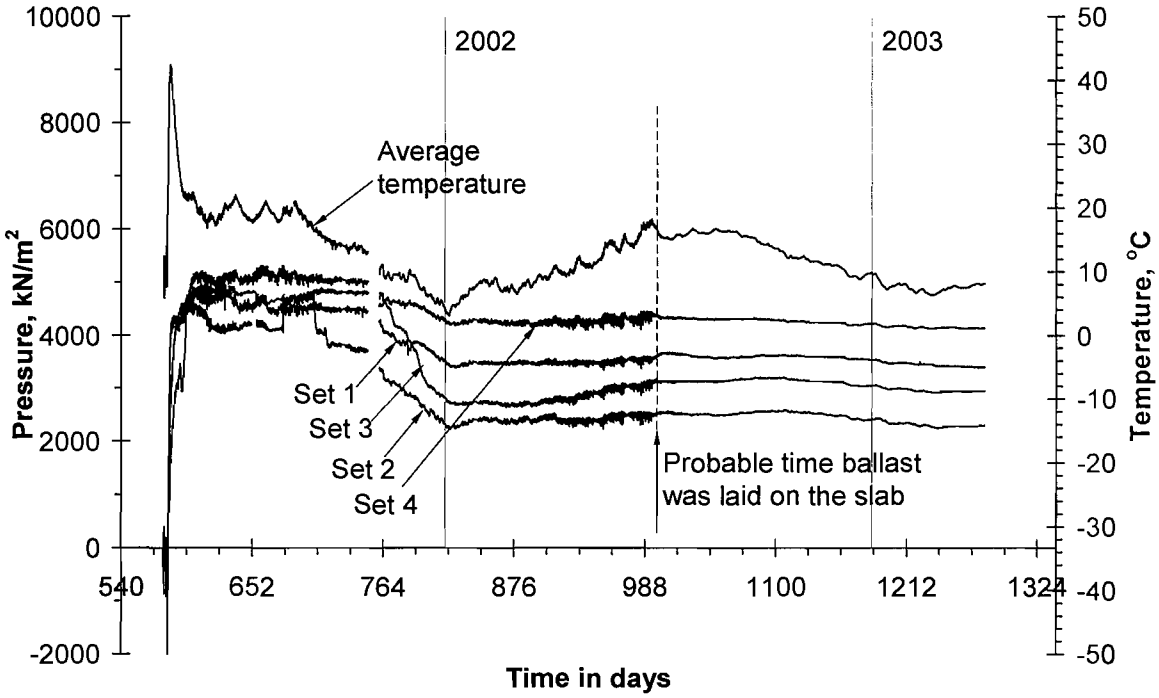

(a)

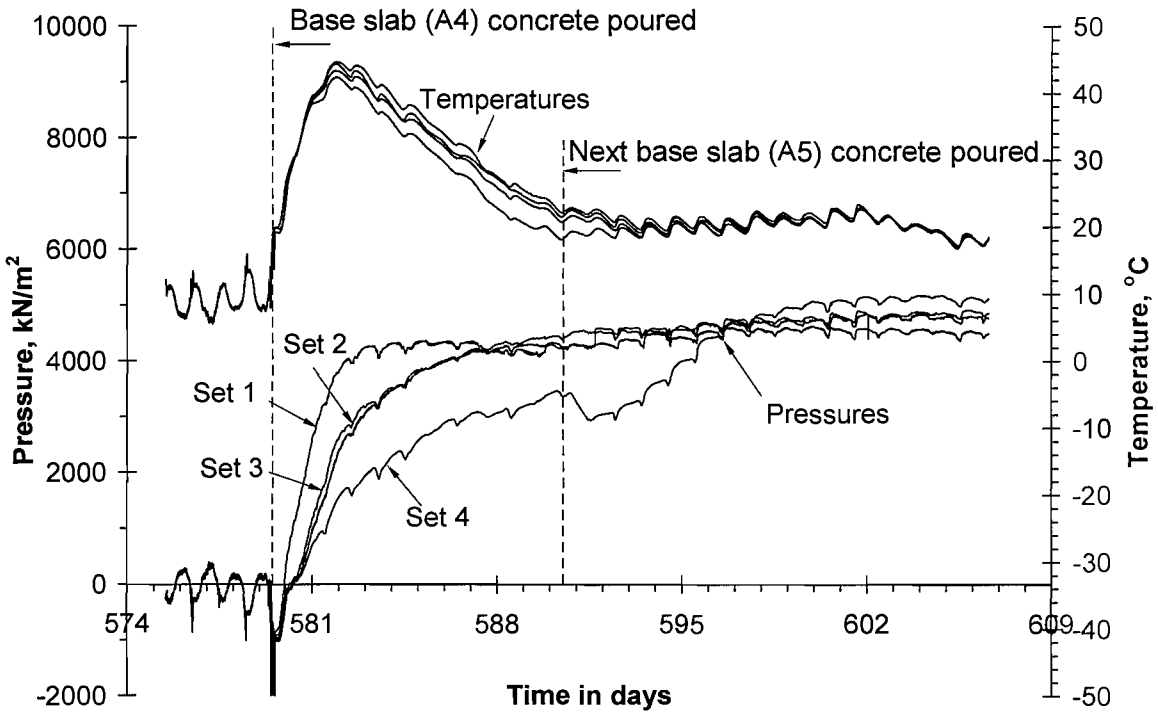

(b)

Figure 4-11: (a) First 2 years of base slab readings. (b) Excerpt from (a), showing period including concrete pour

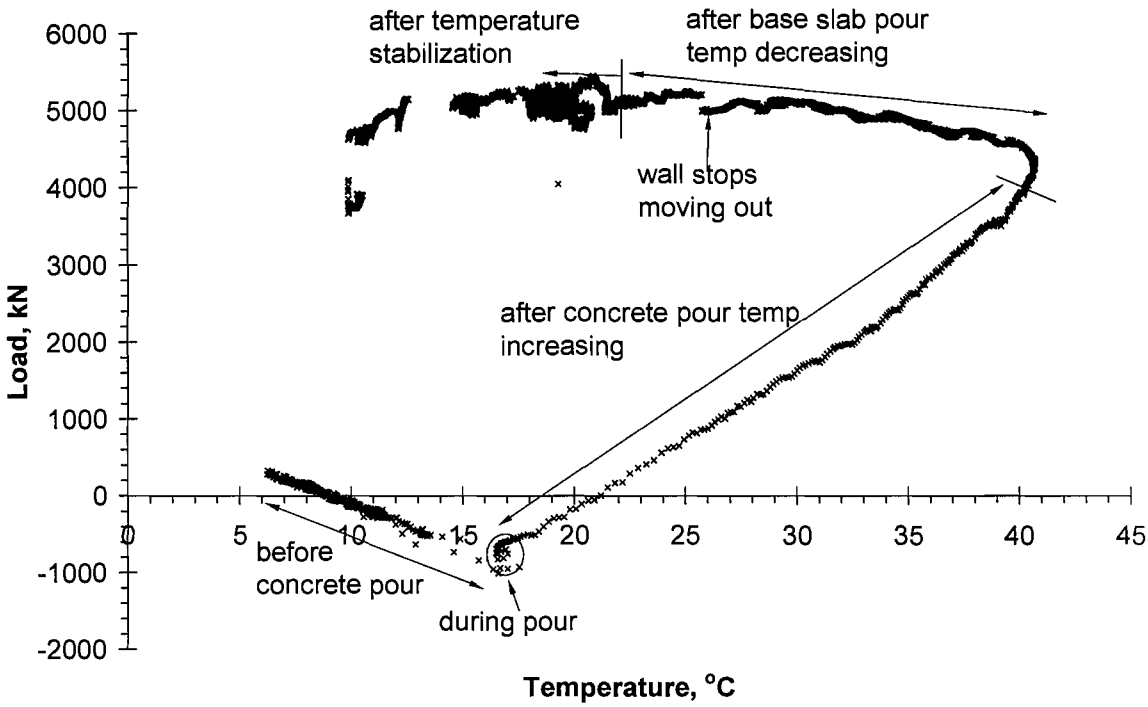

Figure 4-12: Temperature versus load for a typical base slab gauge from before concreting to after stabilization of concrete temperature

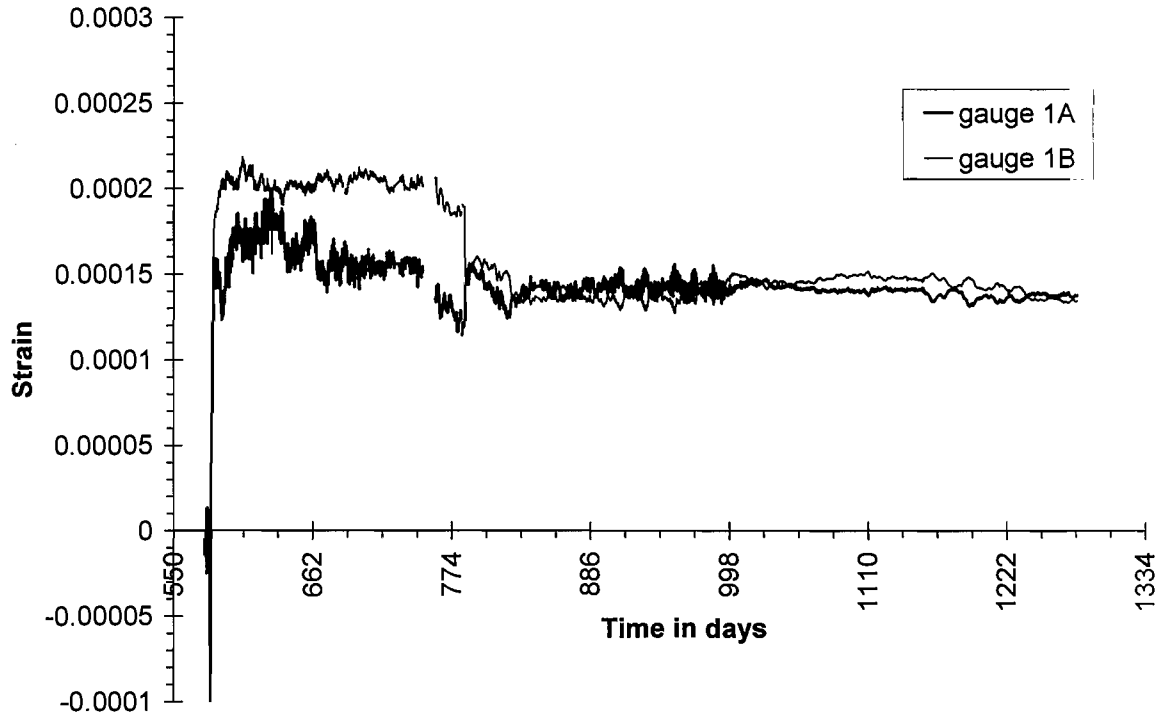
0.0003
0.00025
0.0002
0.00015
0.0001
0.00005
0
-0.00005
-0.0001
Strain
550
662
774
886
998
1110
1222
1334
Time in days
gauge 1A
gauge 1B

(a)

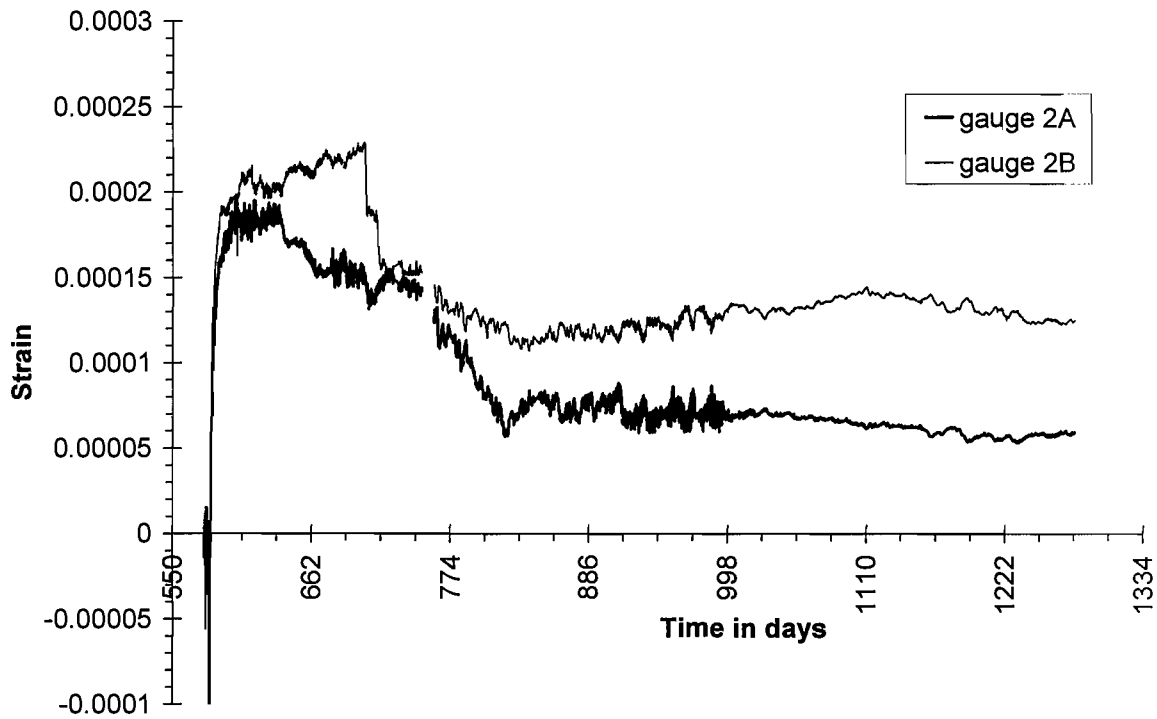
0.0003
0.00025
0.0002
0.00015
0.0001
0.00005
0
-0.00005
-0.0001
Strain
550
662
774
886
998
1110
1222
1334
Time in days
gauge 2A
gauge 2B

(b)

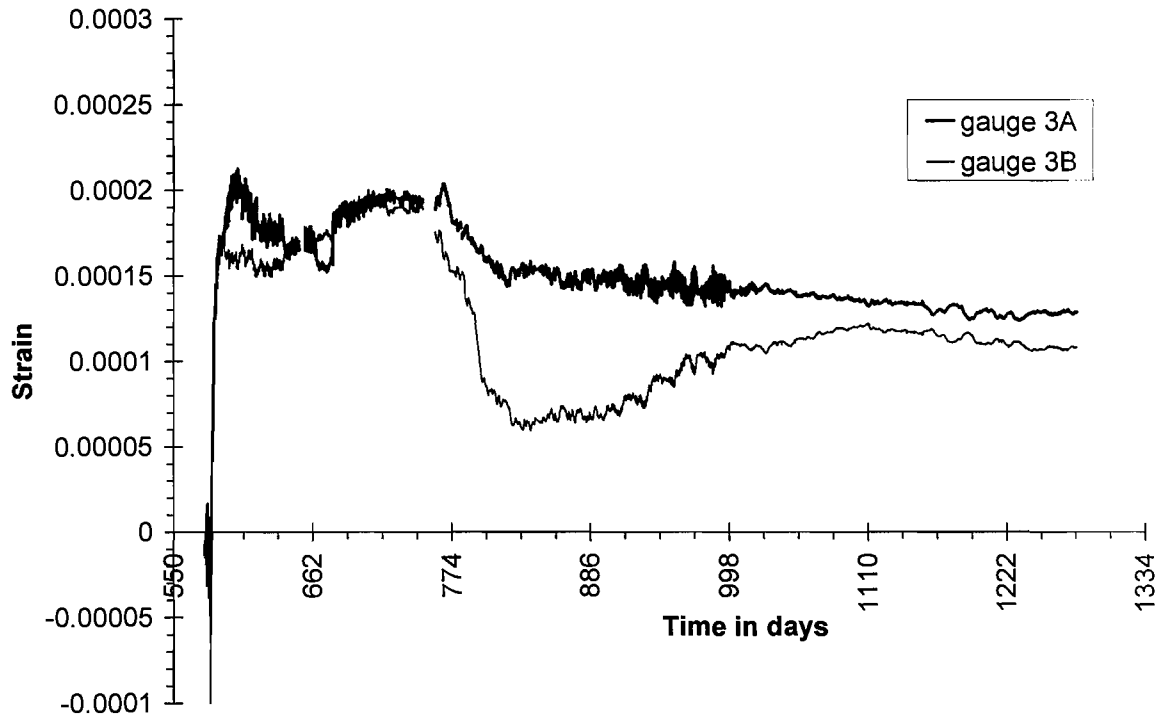

(c)

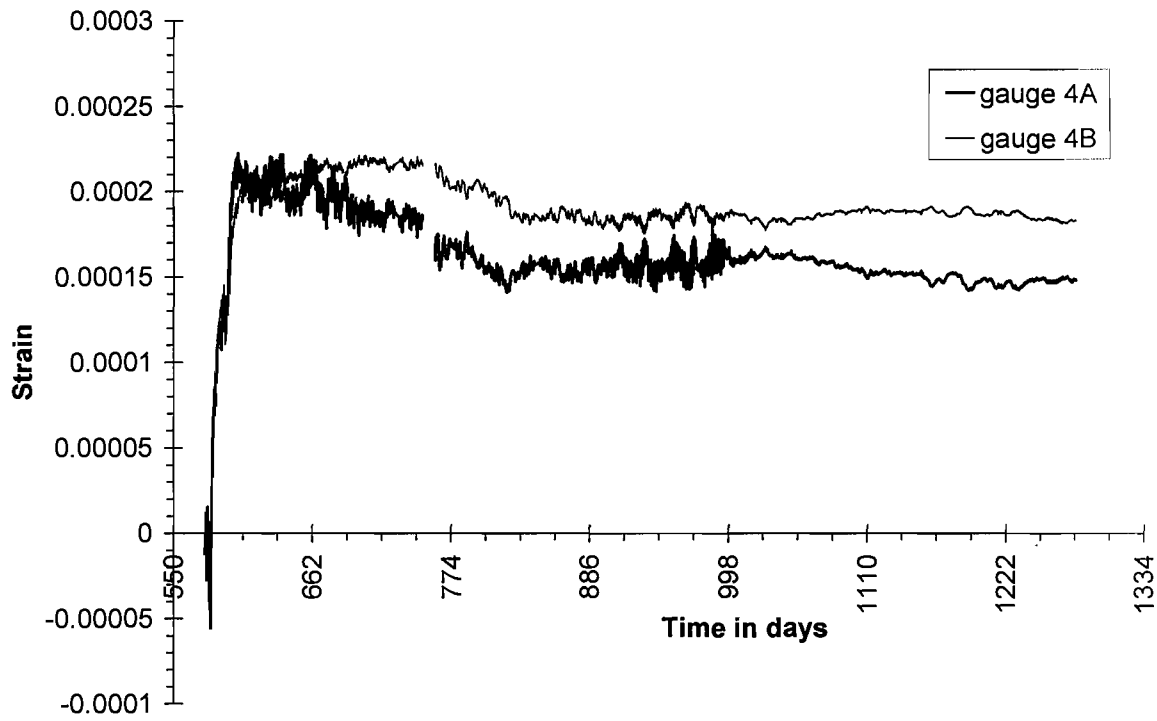

(d)

Figure 4-13: Strains measured in the base slab gauges: (a) set 1, (b) set 2, (c) set 3 and (d) set 4

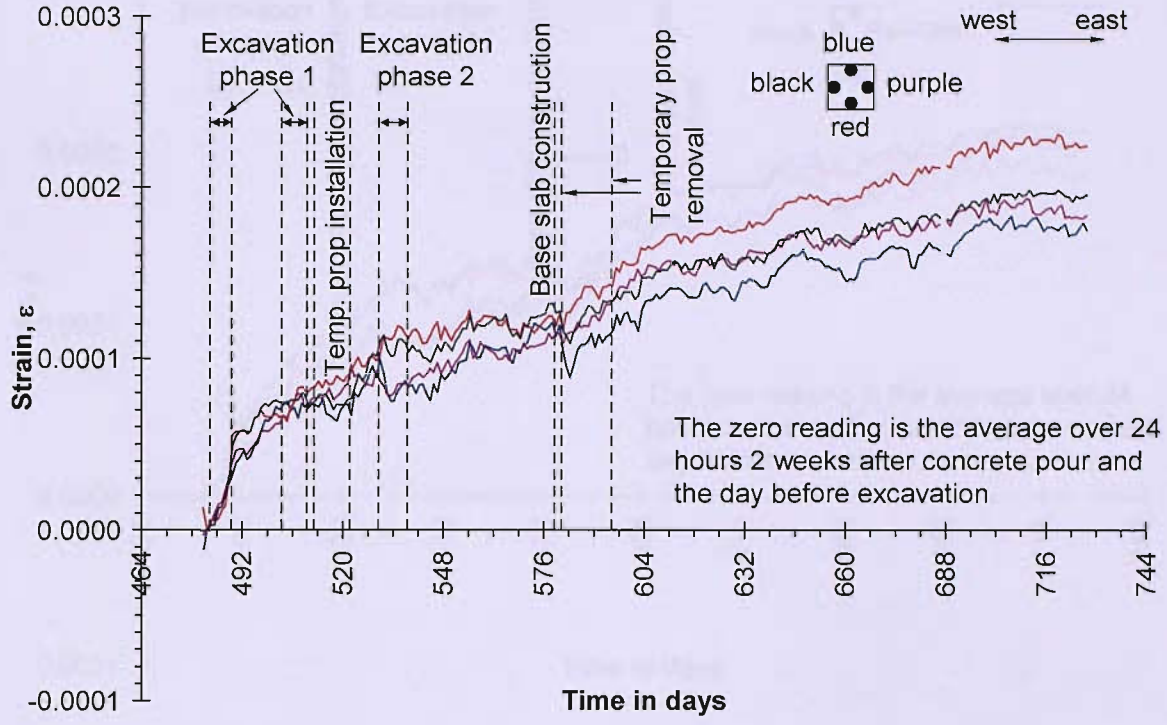

Figure 4-14: Strains measured in P1

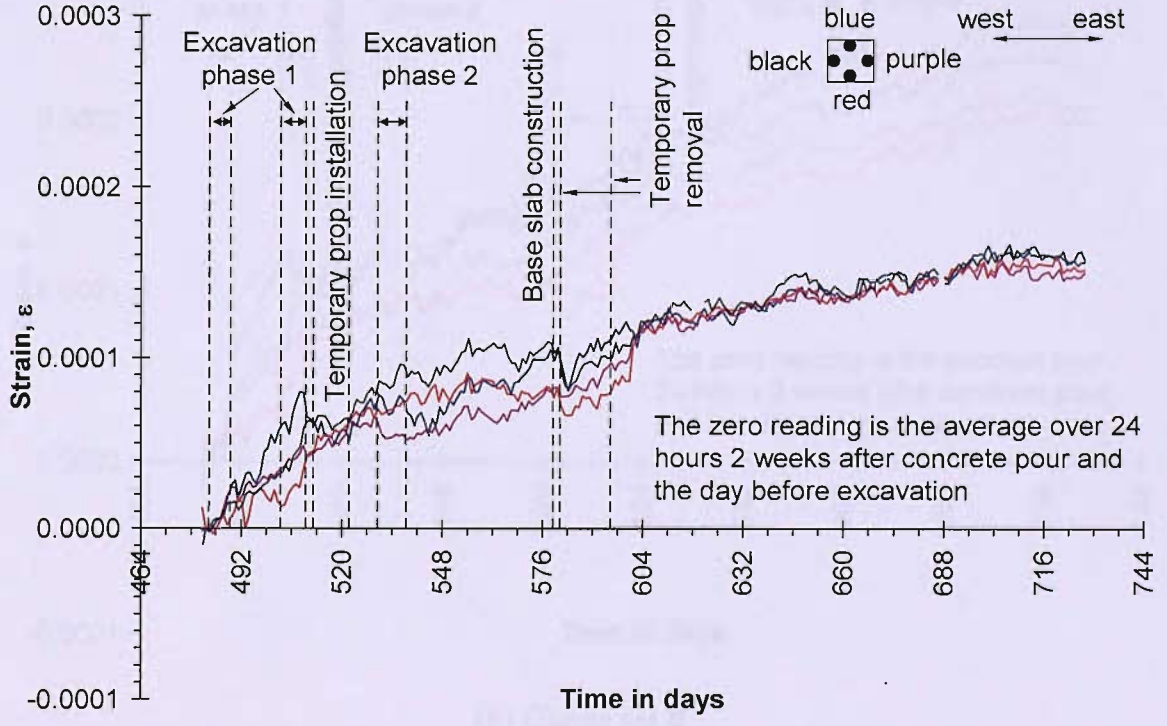

Figure 4-15: Strains measured in P4

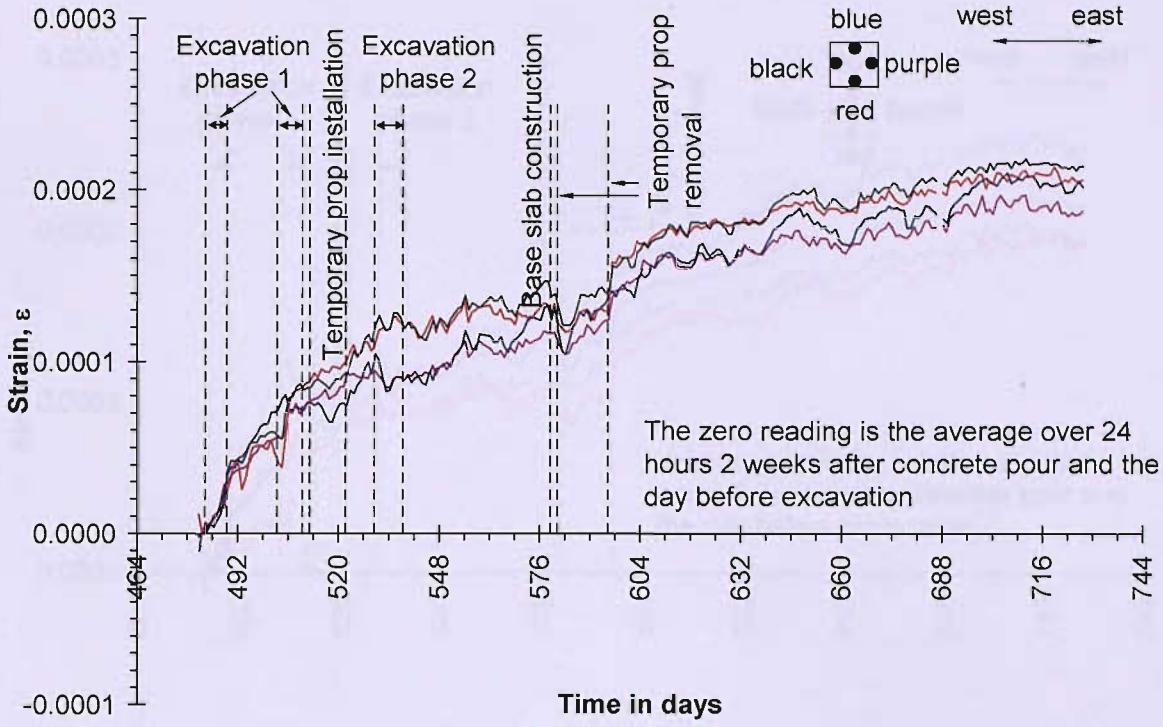

(a) Gauge set A

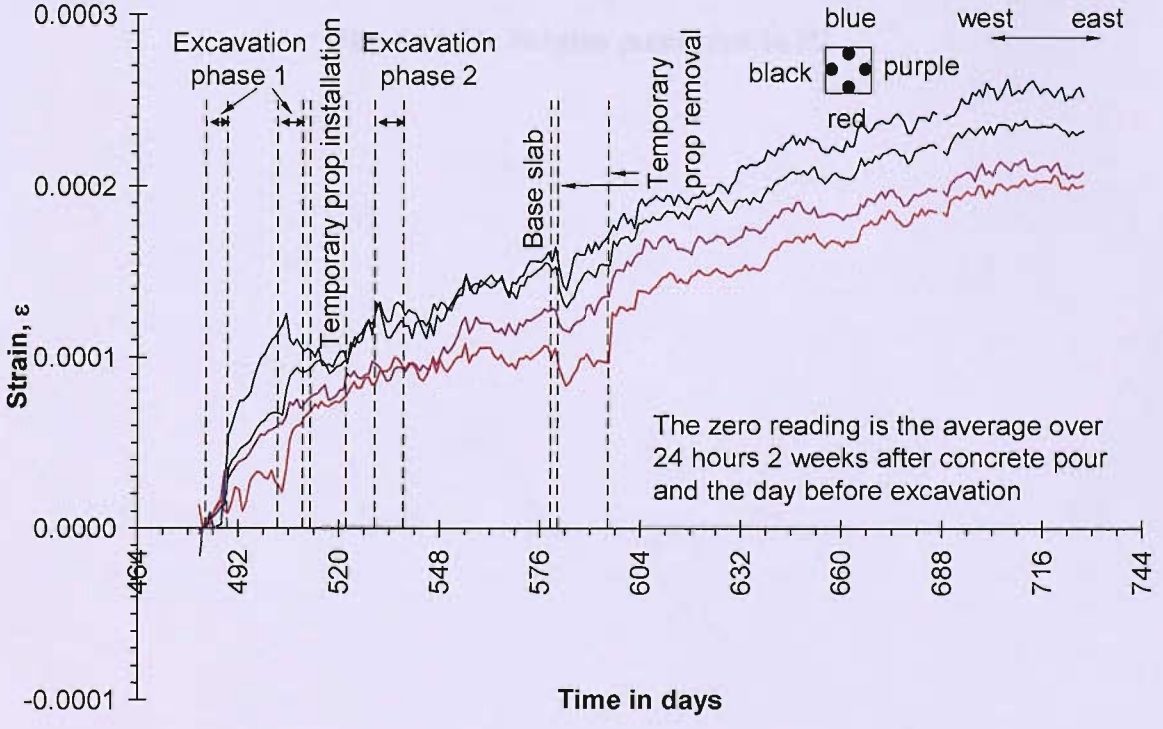

(b) Gauge set B

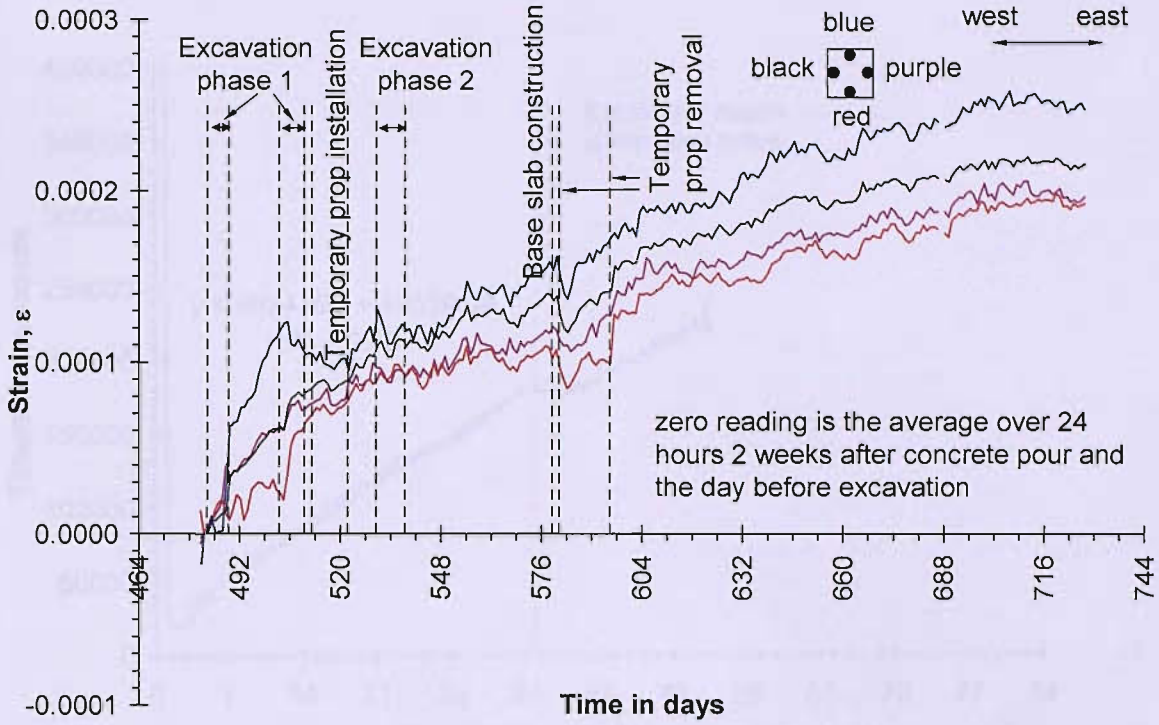

(c) Gauge set C

Figure 4-16: Strains measured in P2

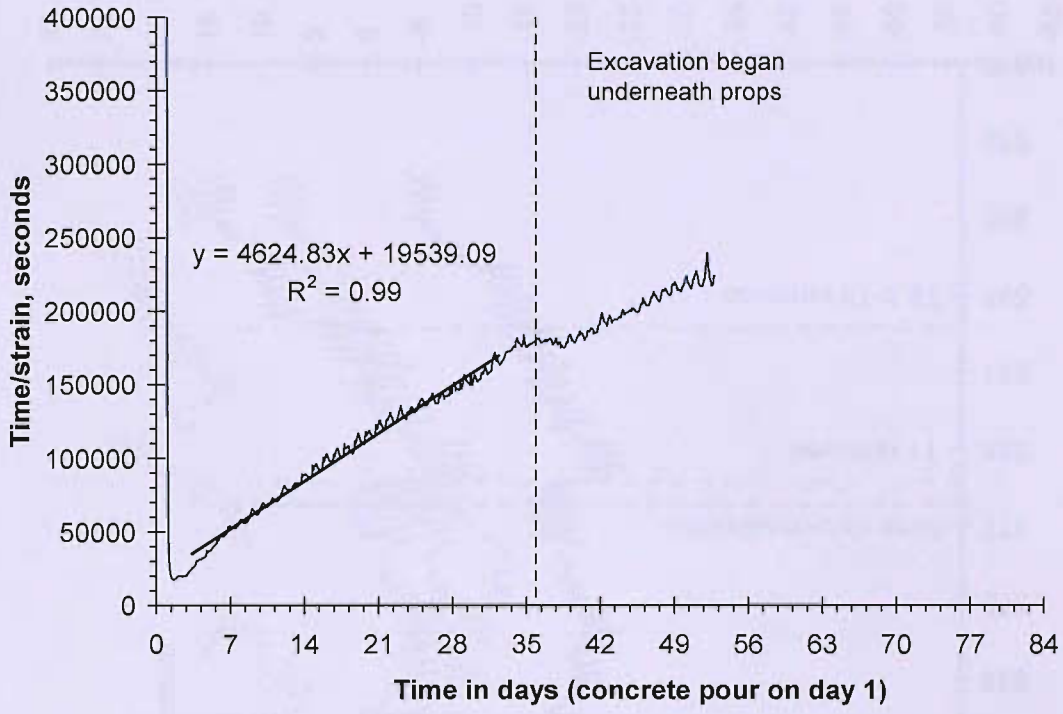

Figure 4-17: Time/strain versus time for an RC prop gauge at chainage 89+205

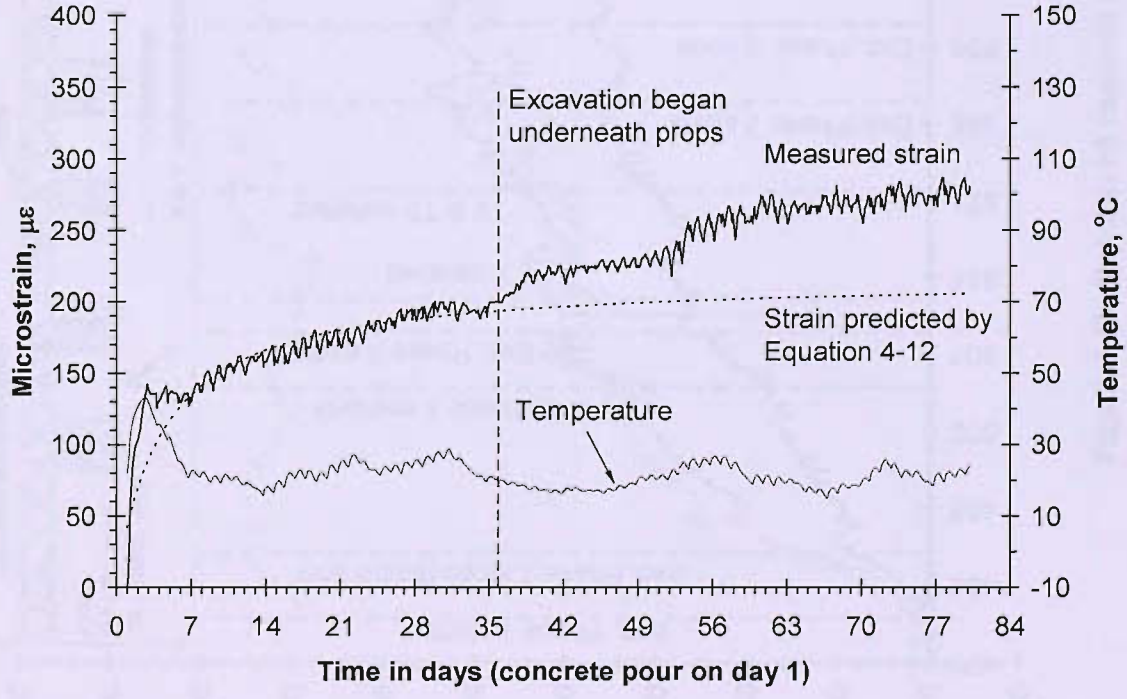

Figure 4-18: Measured and calculated strain against time for an RC prop gauge at chainage 89+205

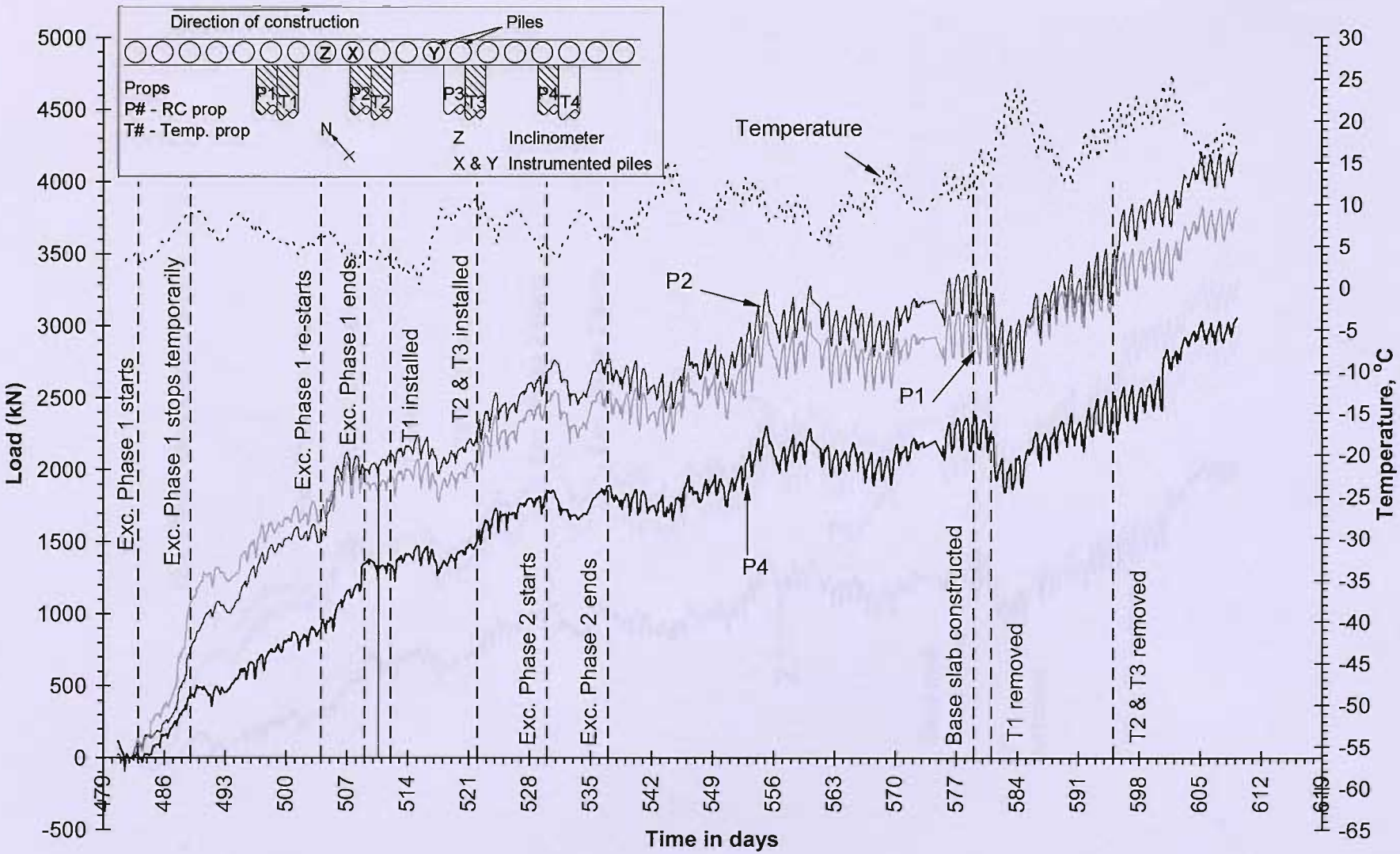

Figure 4-19: Reinforced concrete prop loads uncorrected for effects of shrinkage

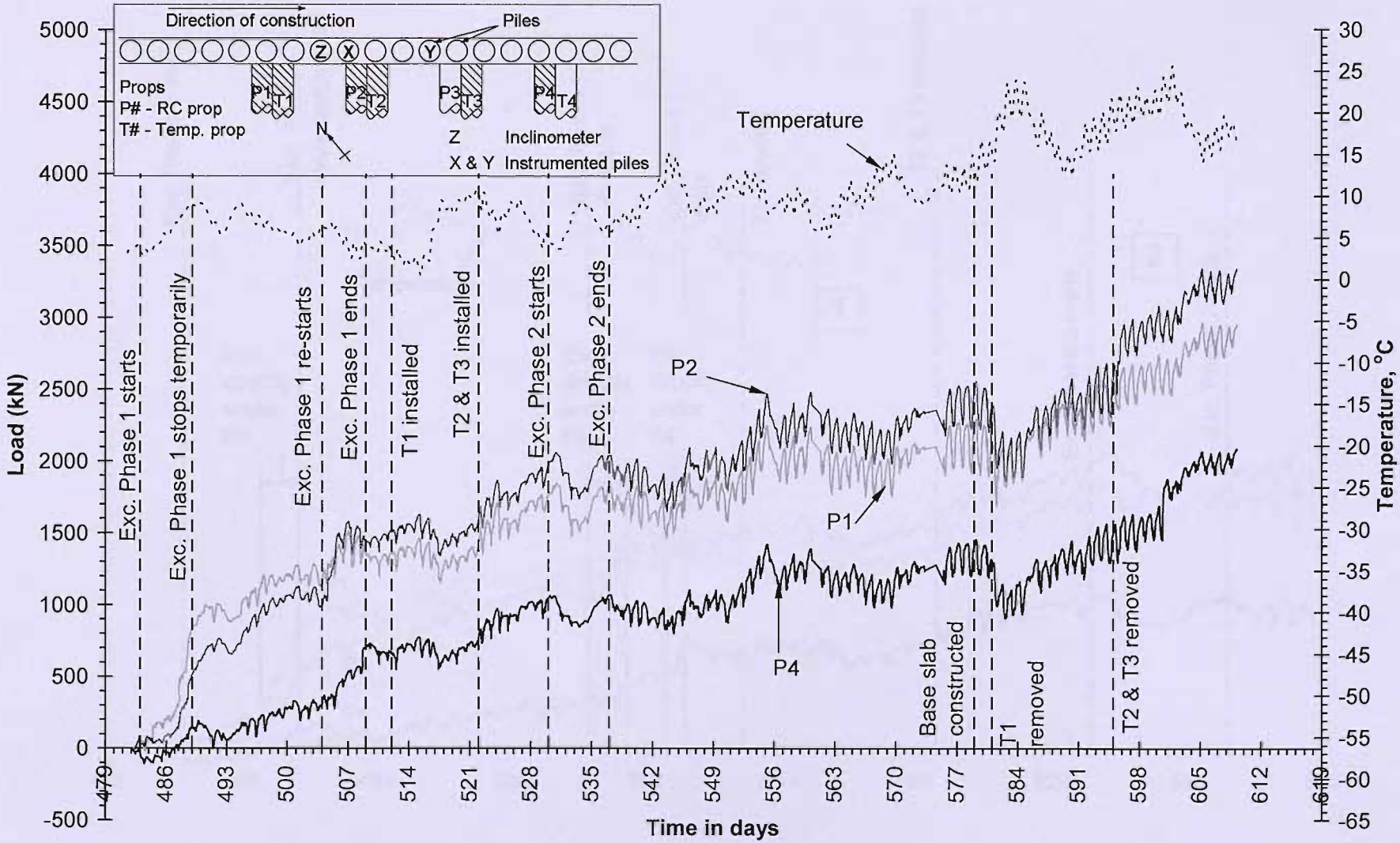

Figure 4-20: Reinforced concrete prop loads corrected for effects of shrinkage using Equation 4-12

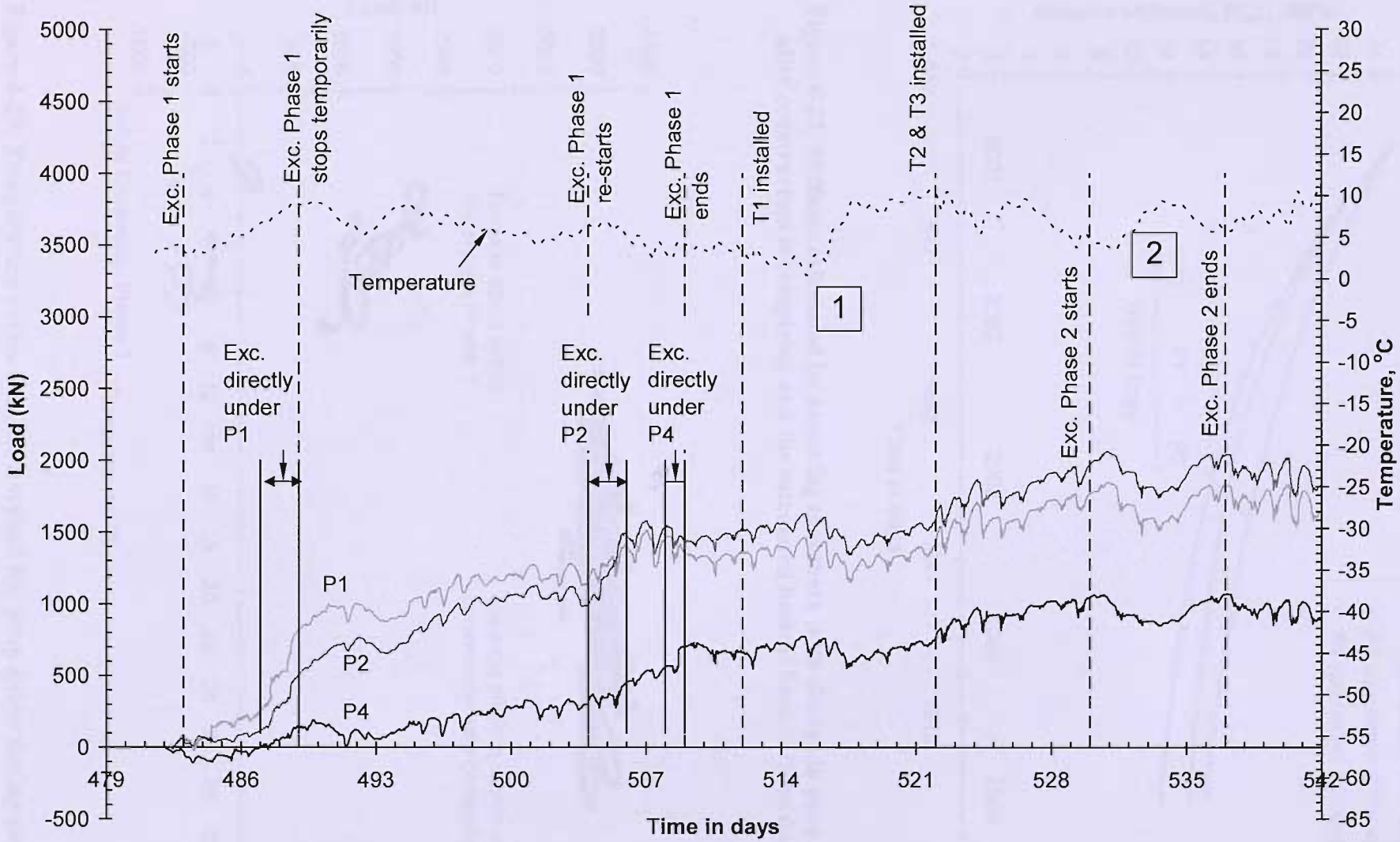

Figure 4-21: Close up of Figure 4-20 showing reinforced concrete prop loads up to just after Excavation Phase 2

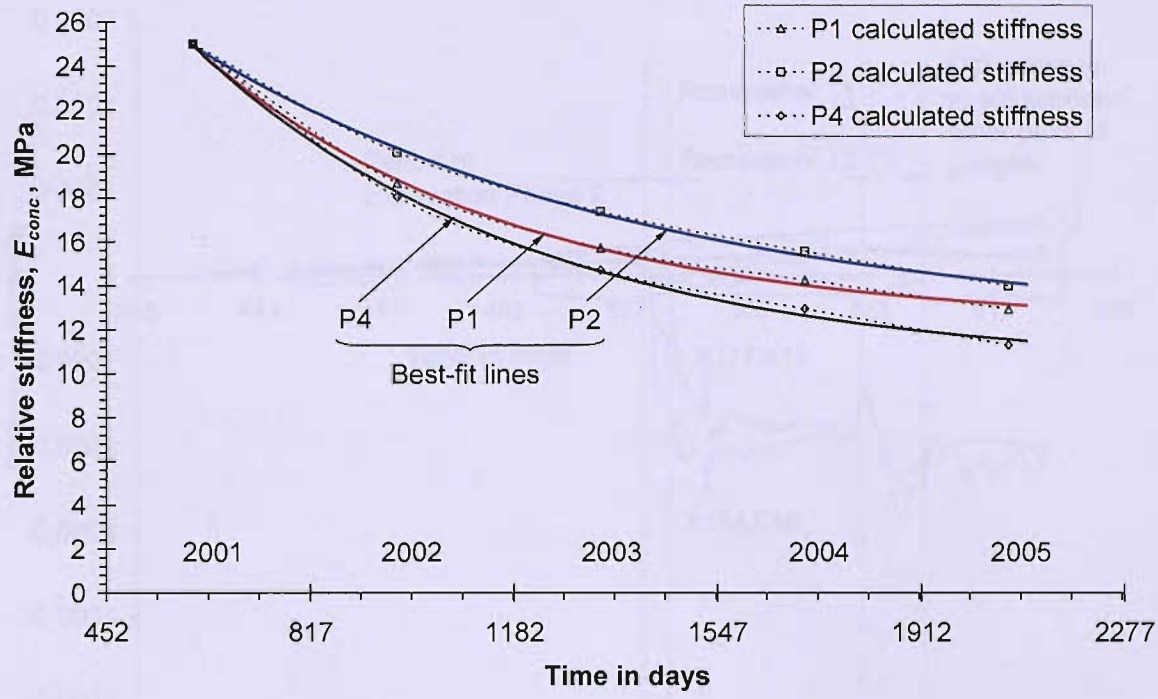

Figure 4-22: Stiffness calculated by assuming that there is no change in prop load after construction is completed and the calculated best-fit lines to these data

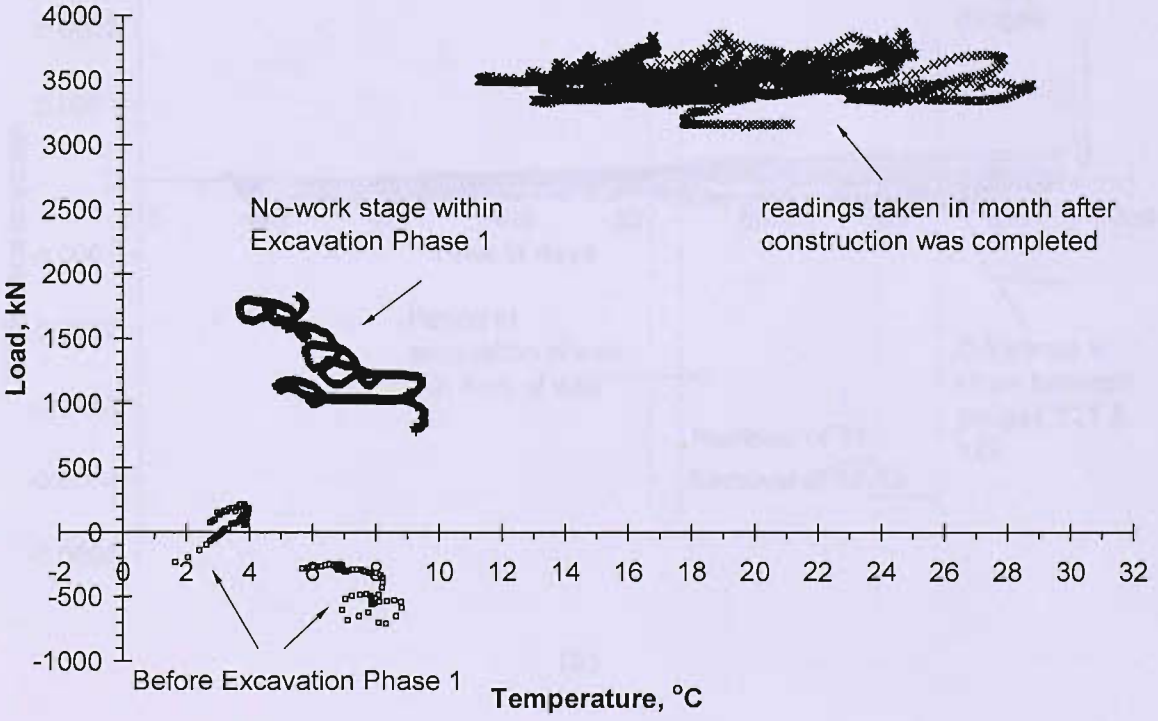

Figure 4-23: Temperature versus load for a typical RC prop gauge during periods when no construction activities are occurring

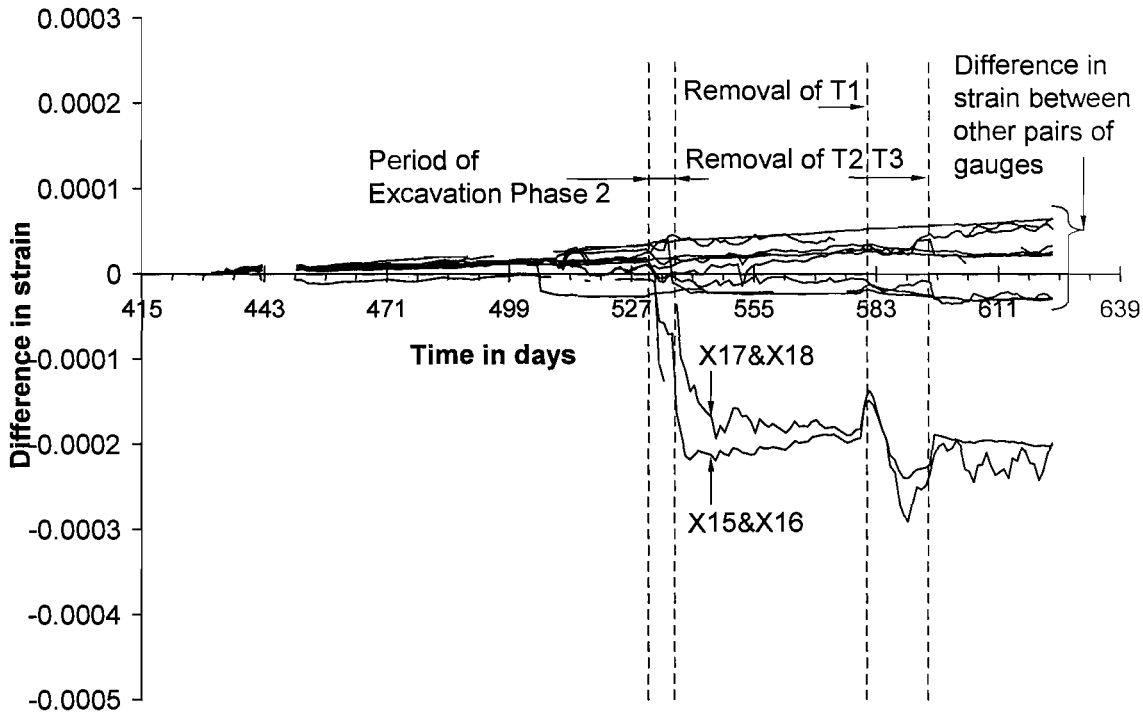

(a)

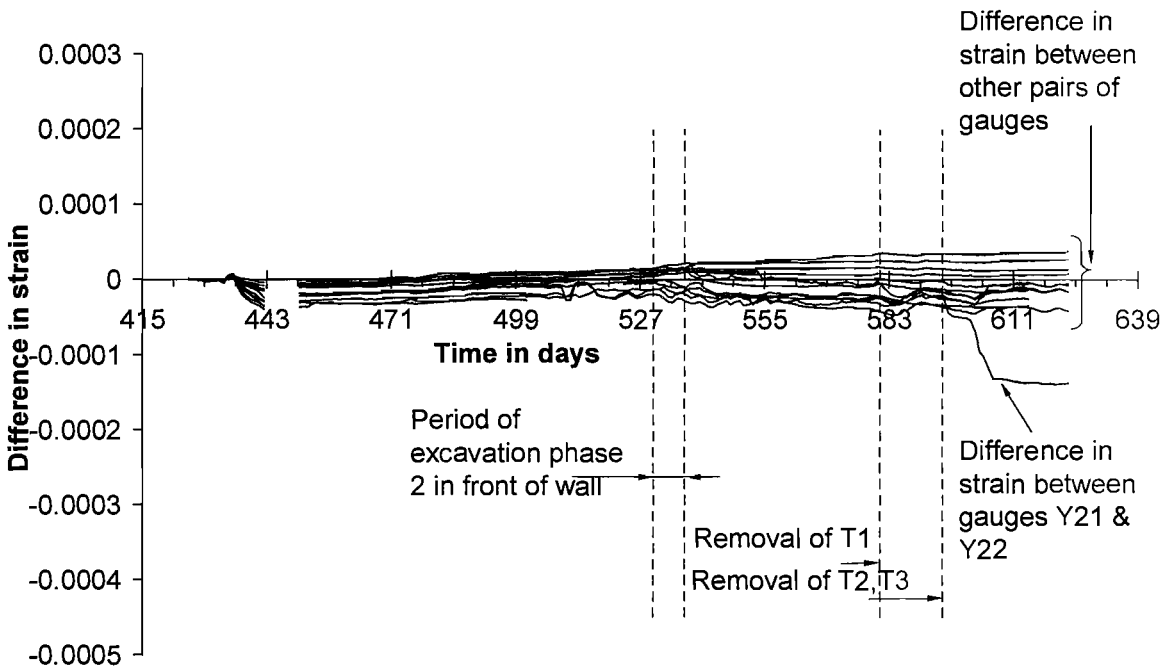

(b)

Figure 4-24: Difference in strain measured for the pairs of strain gauges in (a) pile X and (b) pile Y over the period of construction

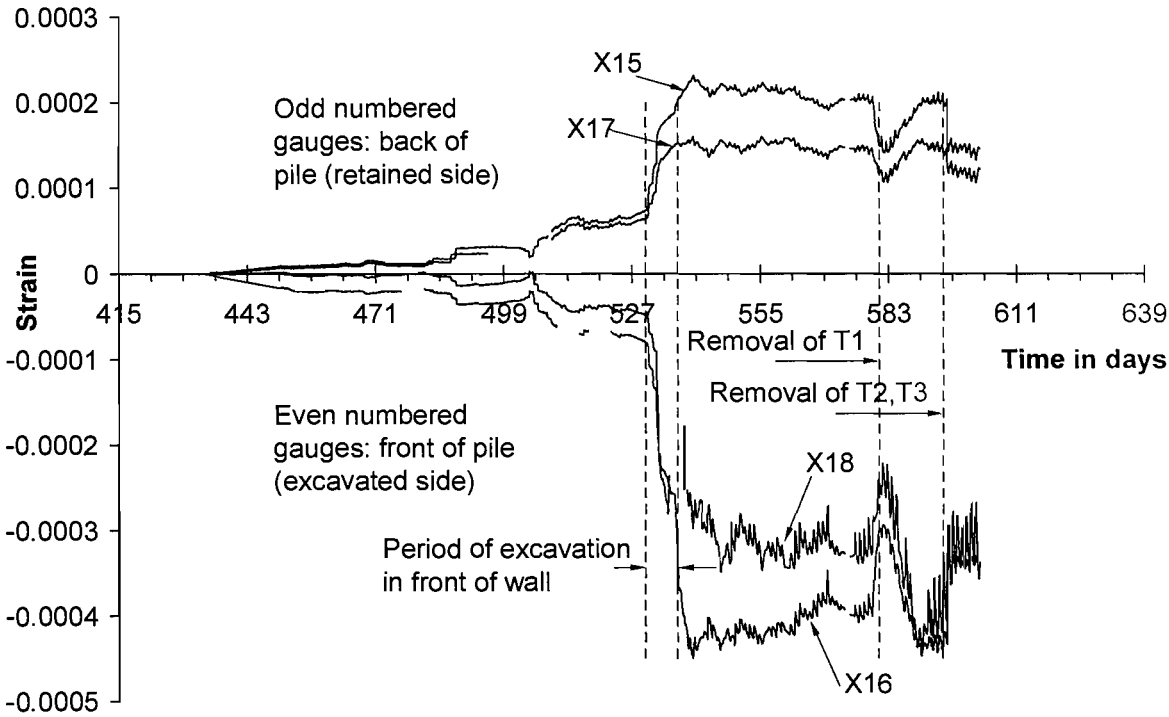

(a)

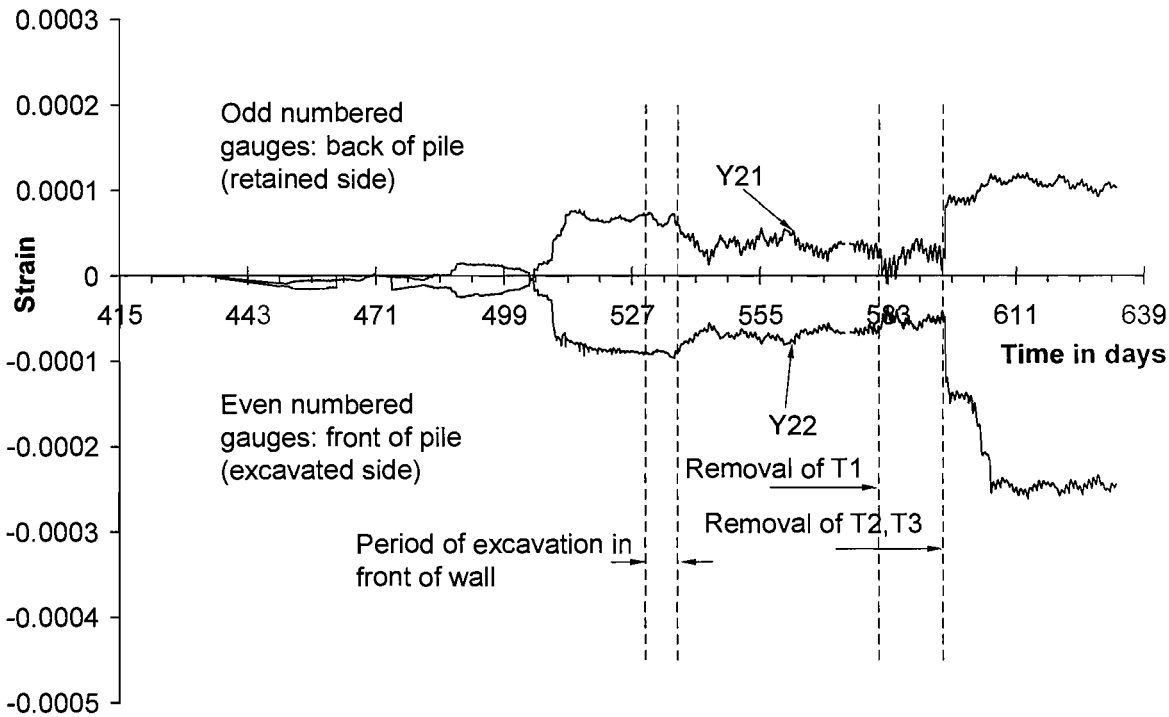

(b)

Figure 4-25: Strain measurements over period of construction for (a) gauges X15, X16, X17 and X18 and (b) gauges Y21 and Y22

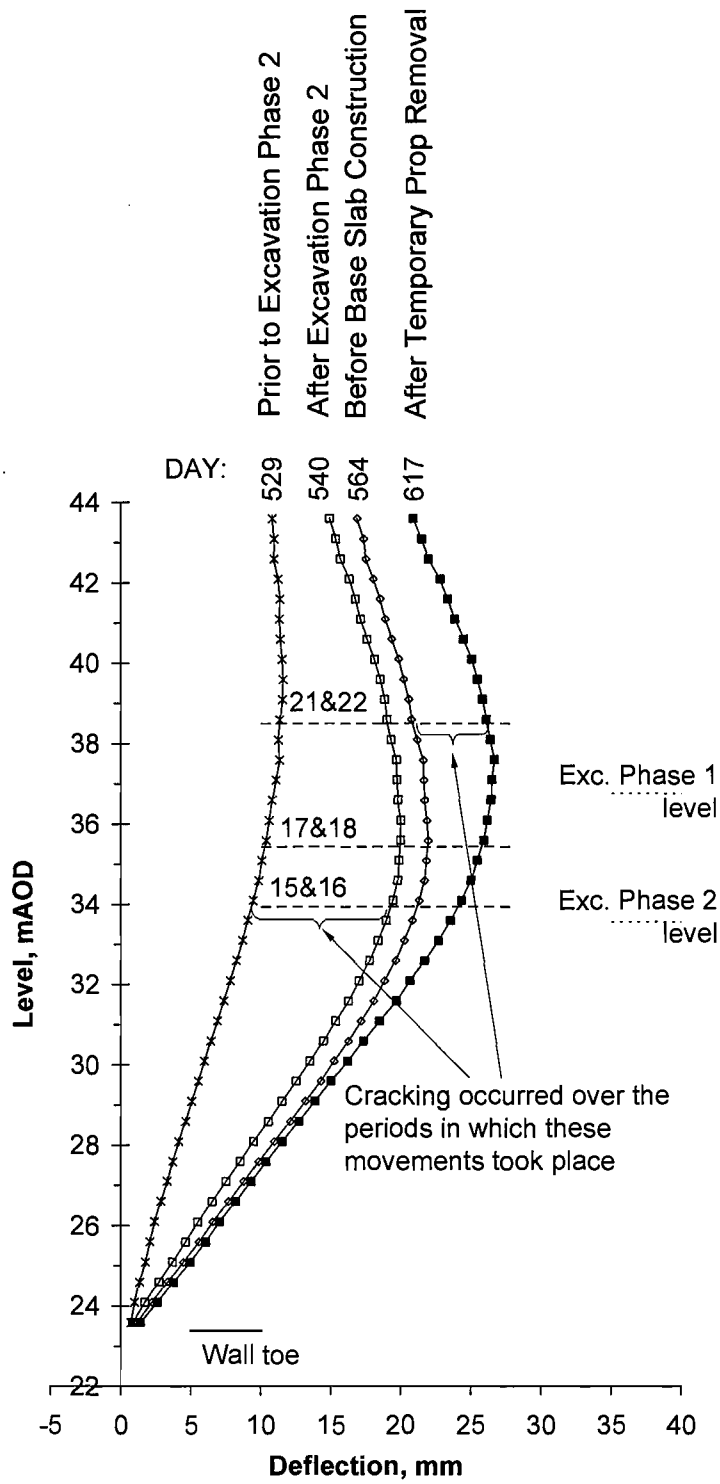

Figure 4-26: Deflections measured in pile Z with the inclinometer around the time of Excavation Phase 2 and Temporary Prop Removal. Readings taken in 2001.

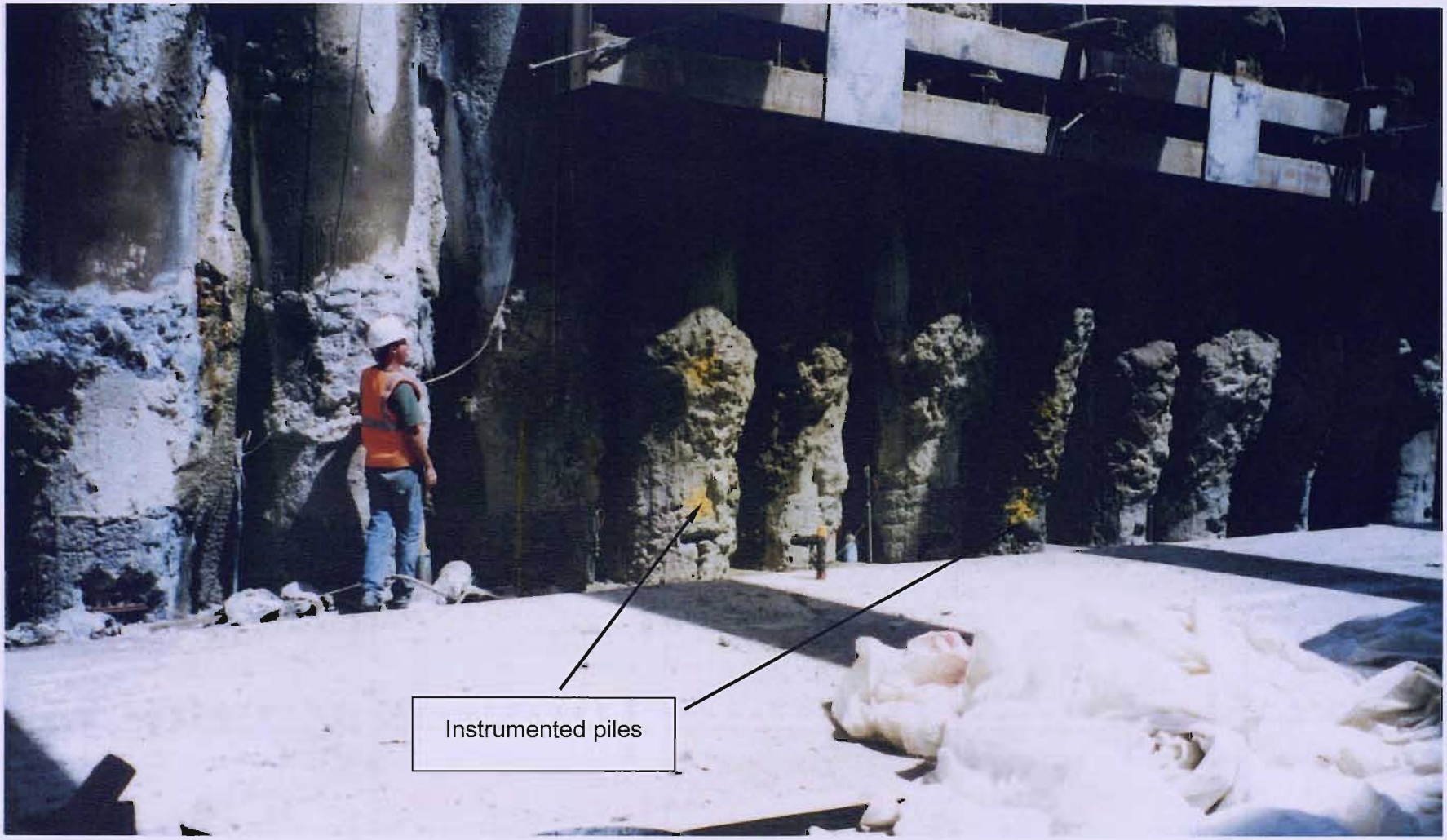

Figure 4-27: Photos showing bulge in concrete between the levels of the temporary prop and base slab. The concrete above the bulge was poured within the casing and is therefore very smooth.

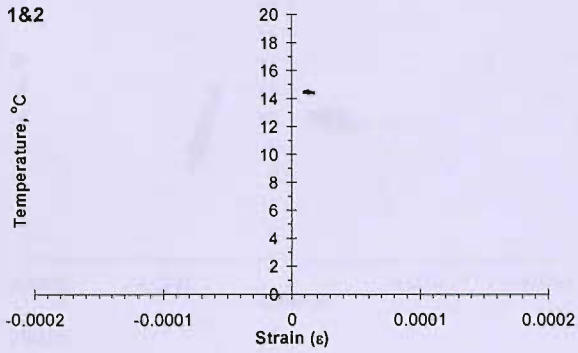
1&2
Temperature, °C
Strain (ε)
-0.0002
-0.0001
0
0.0001
0.0002
0
2
4
6
8
10
12
14
16
18
20

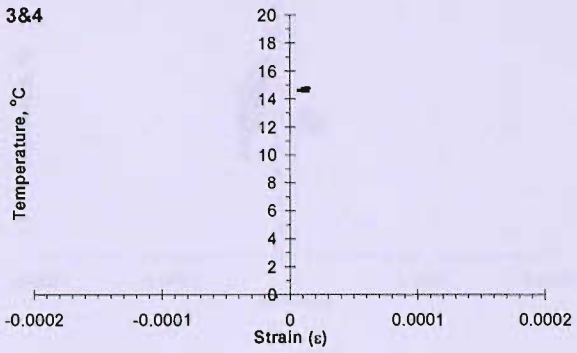
3&4
Temperature, °C
Strain (ε)
-0.0002
-0.0001
0
0.0001
0.0002
0
2
4
6
8
10
12
14
16
18
20

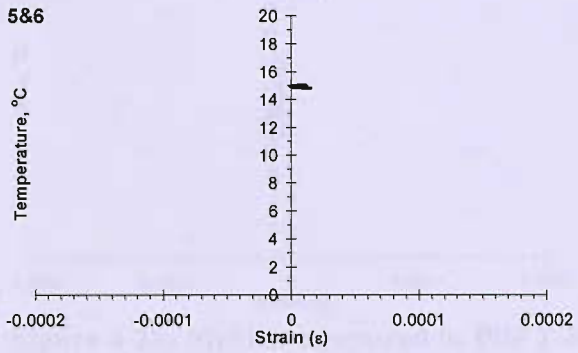
5&6
Temperature, °C
Strain (ε)
-0.0002
-0.0001
0
0.0001
0.0002
0
2
4
6
8
10
12
14
16
18
20

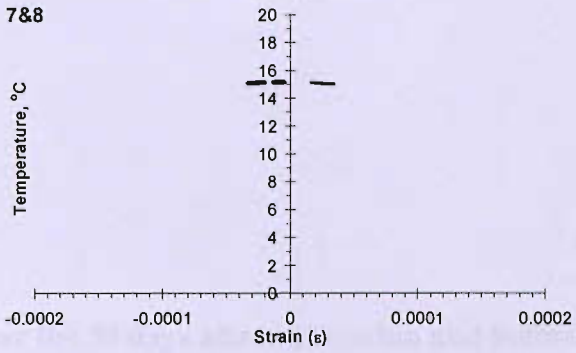
7&8
Temperature, °C
Strain (ε)
-0.0002
-0.0001
0
0.0001
0.0002
0
2
4
6
8
10
12
14
16
18
20

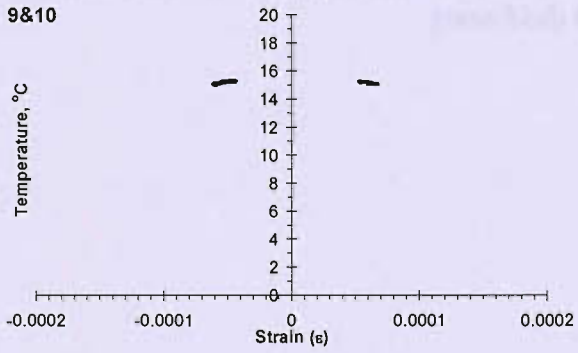
9&10
Temperature, °C
Strain (ε)
-0.0002
-0.0001
0
0.0001
0.0002
0
2
4
6
8
10
12
14
16
18
20

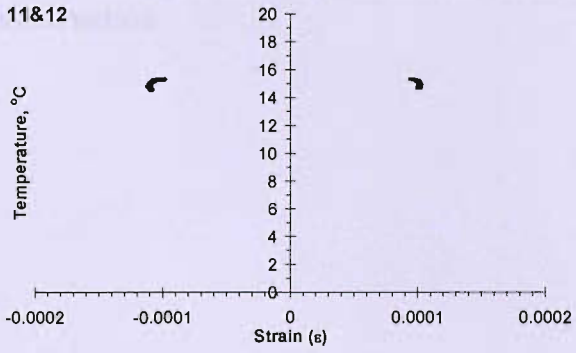
11&12
Temperature, °C
Strain (ε)
-0.0002
-0.0001
0
0.0001
0.0002
0
2
4
6
8
10
12
14
16
18
20

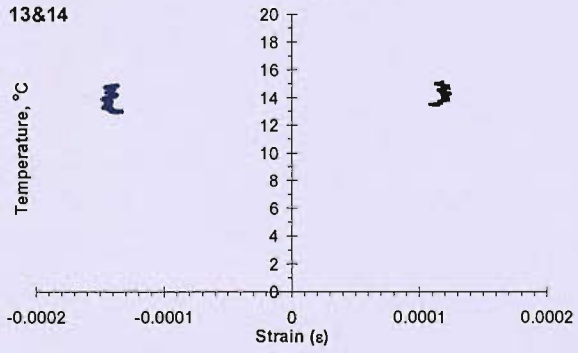
13&14
Temperature, °C
Strain (ε)
-0.0002
-0.0001
0
0.0001
0.0002
0
2
4
6
8
10
12
14
16
18
20

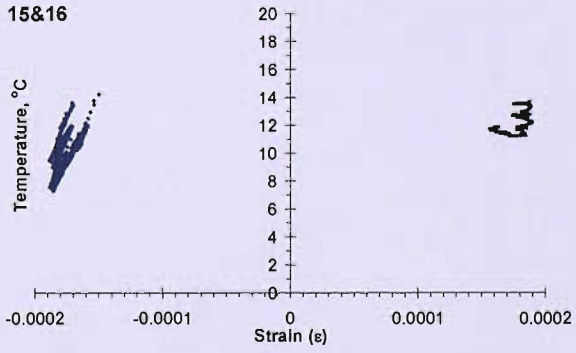
15&16
Temperature, °C
Strain (ε)
-0.0002
-0.0001
0
0.0001
0.0002
0
2
4
6
8
10
12
14
16
18
20

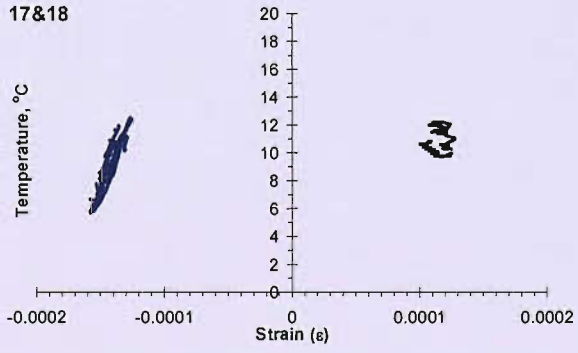
17&18
Temperature, °C
Strain (ε)
-0.0002
-0.0001
0
0.0001
0.0002
0
2
4
6
8
10
12
14
16
18
20

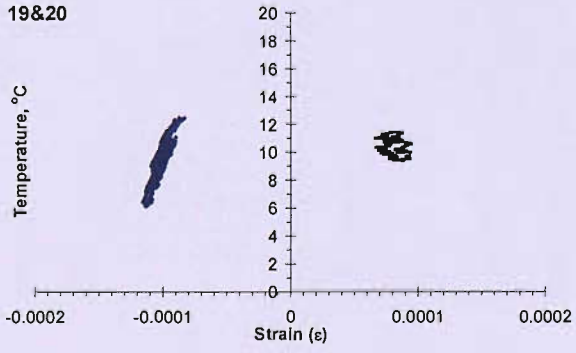
19&20
Temperature, °C
Strain (ε)
-0.0002
-0.0001
0
0.0001
0.0002
0
2
4
6
8
10
12
14
16
18
20

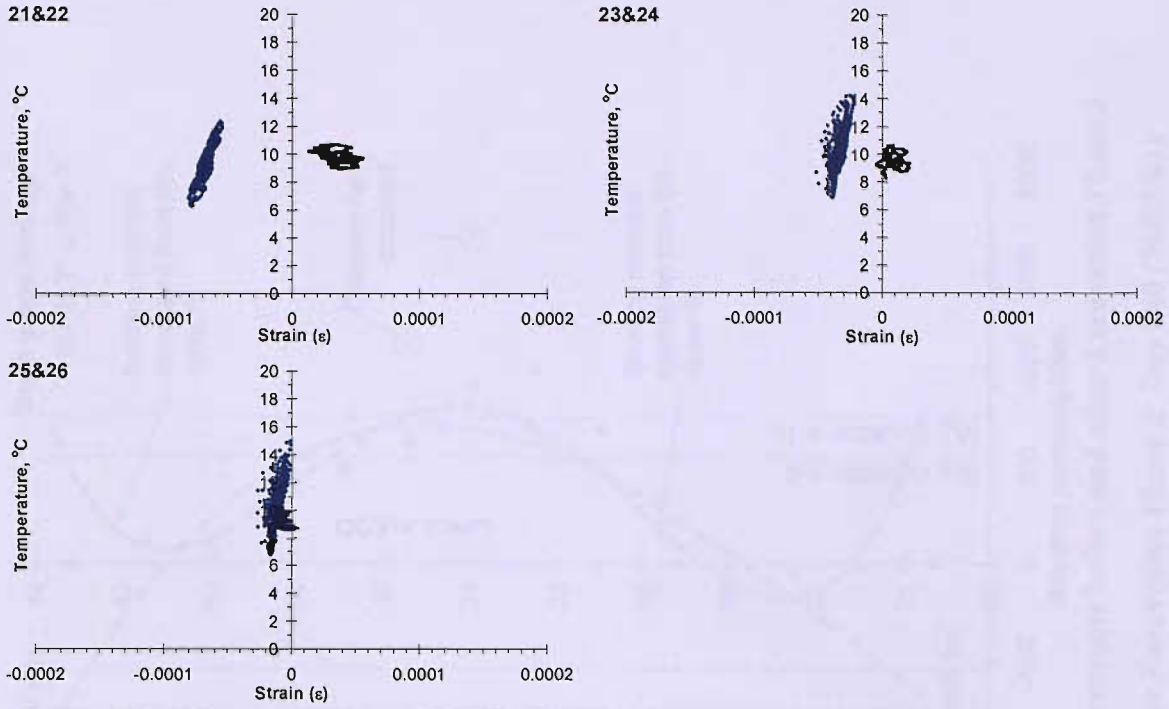

Figure 4-28: Strains measured in Pile Y over the 30 days after excavation and before Base Slab Construction

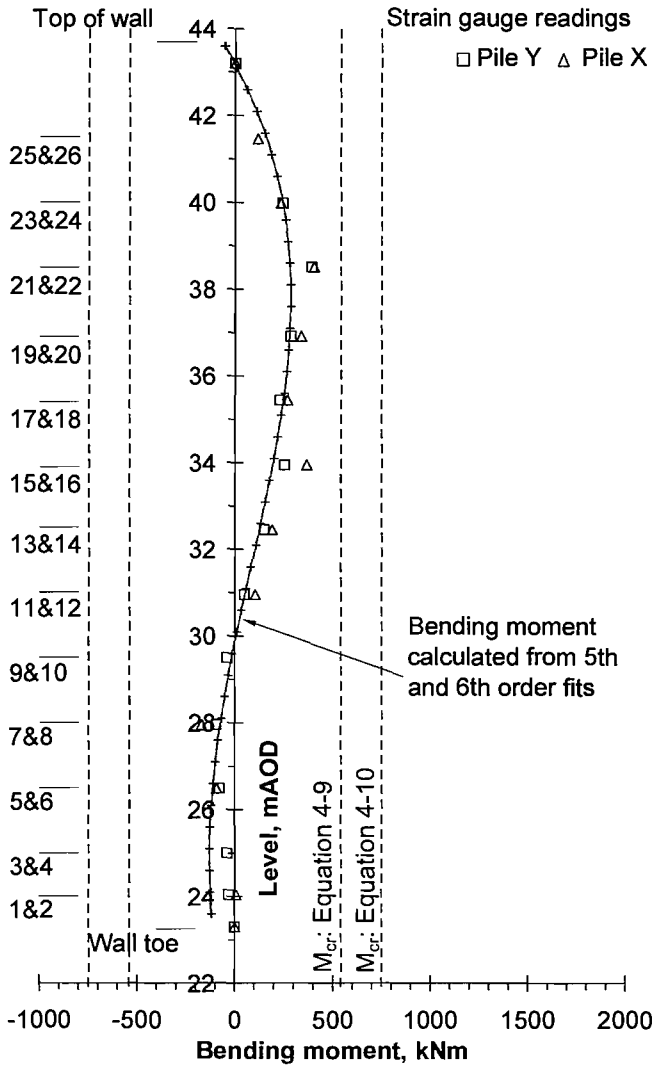

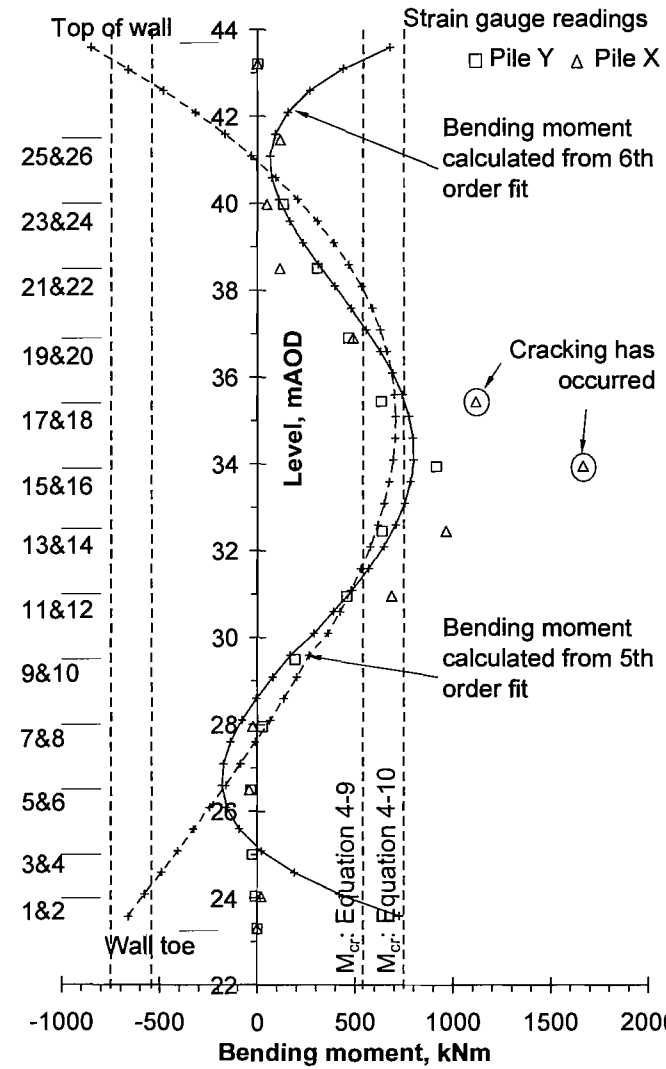

Figure 4-29: Bending moments calculated from inclinometer and strain gauge measurements before and after Excavation Phase 2

(a) Before Excavation Phase 2: Day 530 (20/03/01)

(b) After Excavation Phase 2: Day 540 (30/03/01)

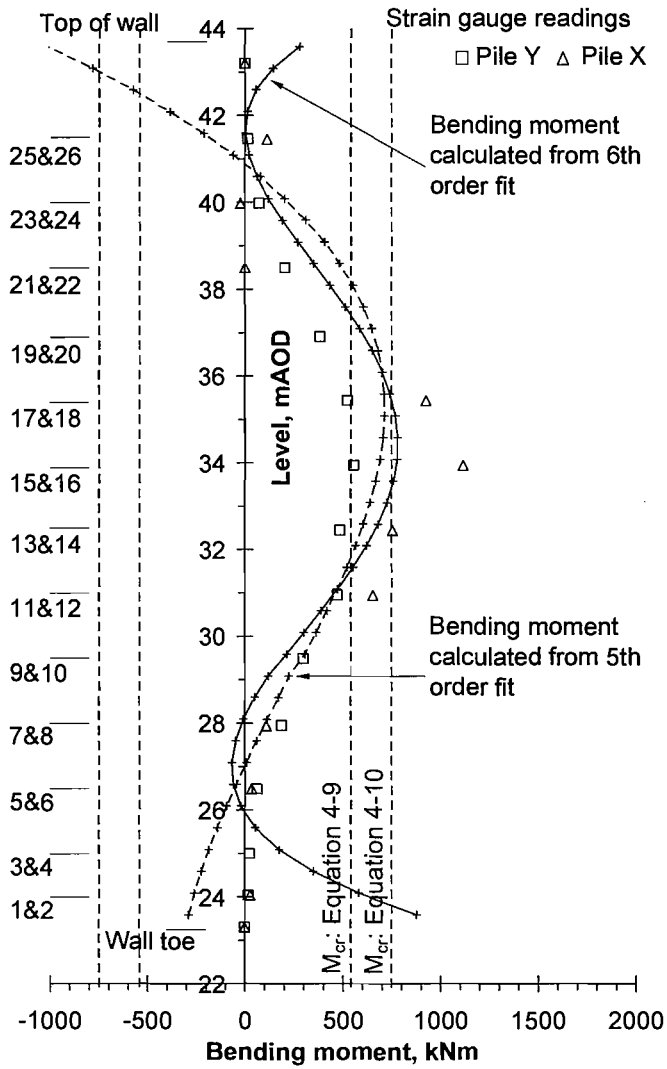

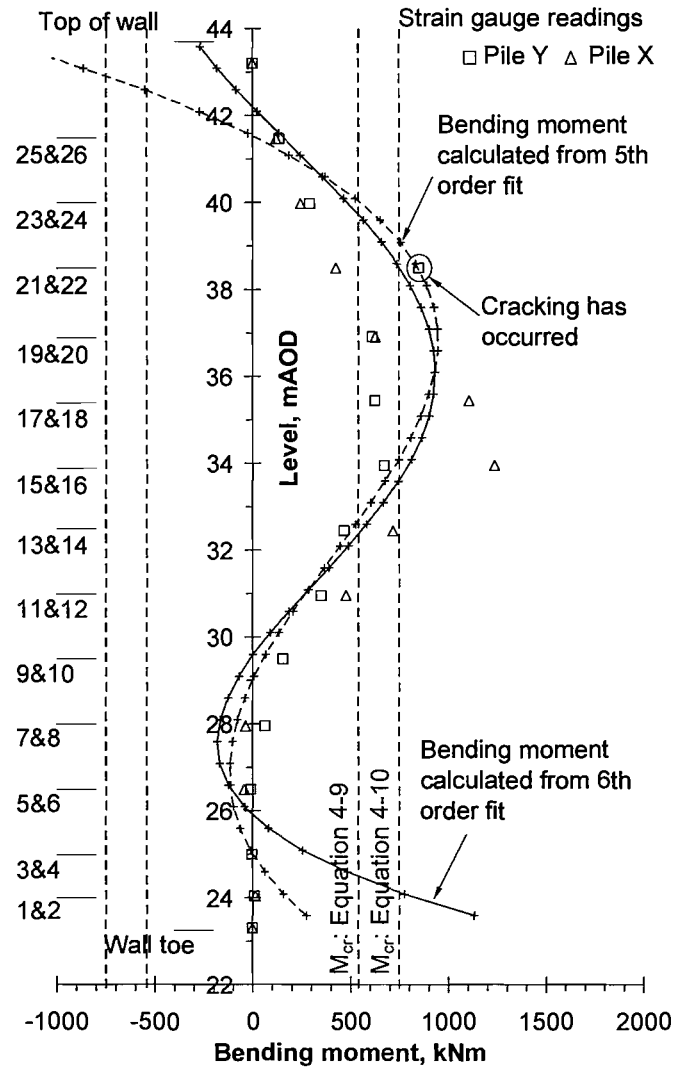

Figure 4-30: Bending moments calculated from inclinometer and strain gauge measurements before and after Temporary Prop Removal

(a) Before Temporary Prop Removal: Day 551 (10/04/01) **(b) After Temporary Prop Removal: Day 617 (15/06/01)**

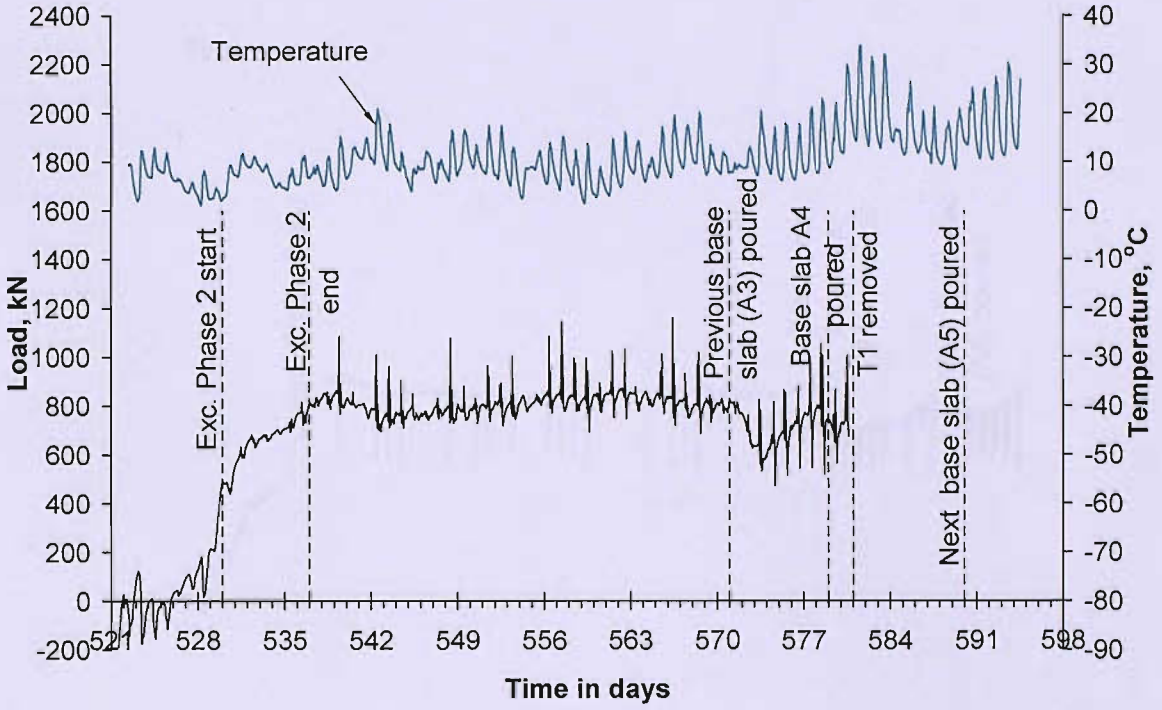
Temperature
Exc. Phase 2 start
Exc. Phase 2 end
Previous base slab (A3) poured
Base slab A4 poured
T1 removed
Next base slab (A5) poured
Load, kN
Temperature, °C
Time in days

(a) T1

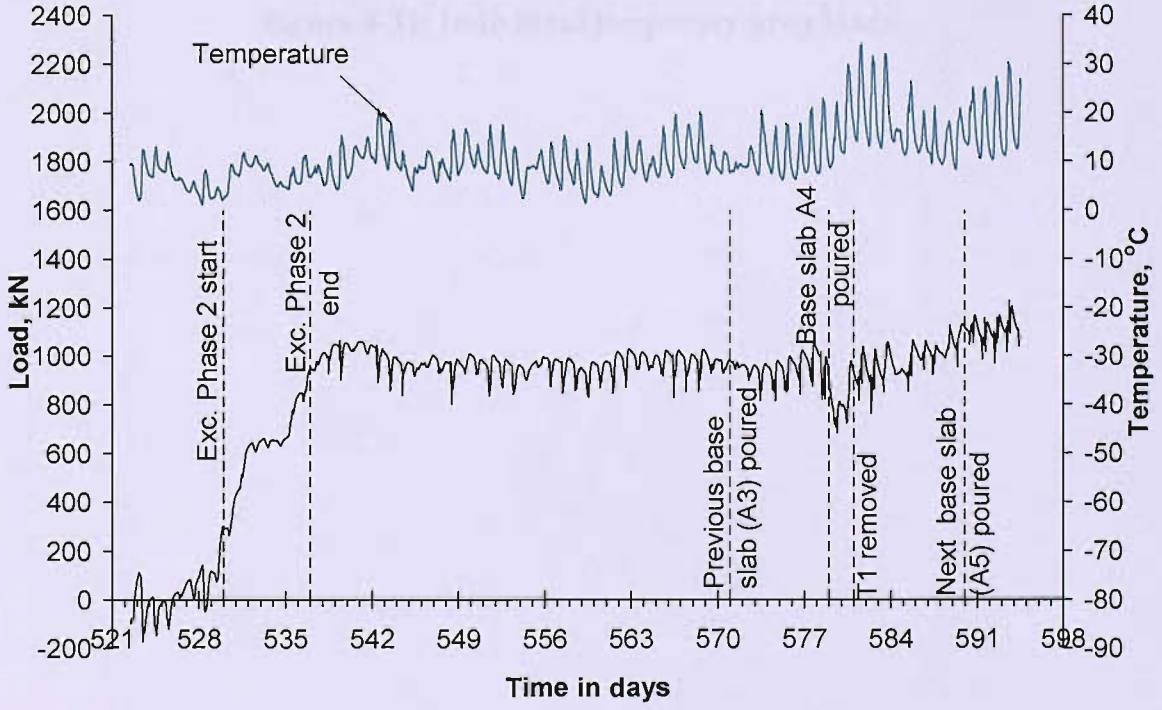
Temperature
Exc. Phase 2 start
Exc. Phase 2 end
Previous base slab (A3) poured
Base slab A4 poured
T1 removed
Next base slab (A5) poured
Load, kN
Temperature, °C
Time in days

(b) T2

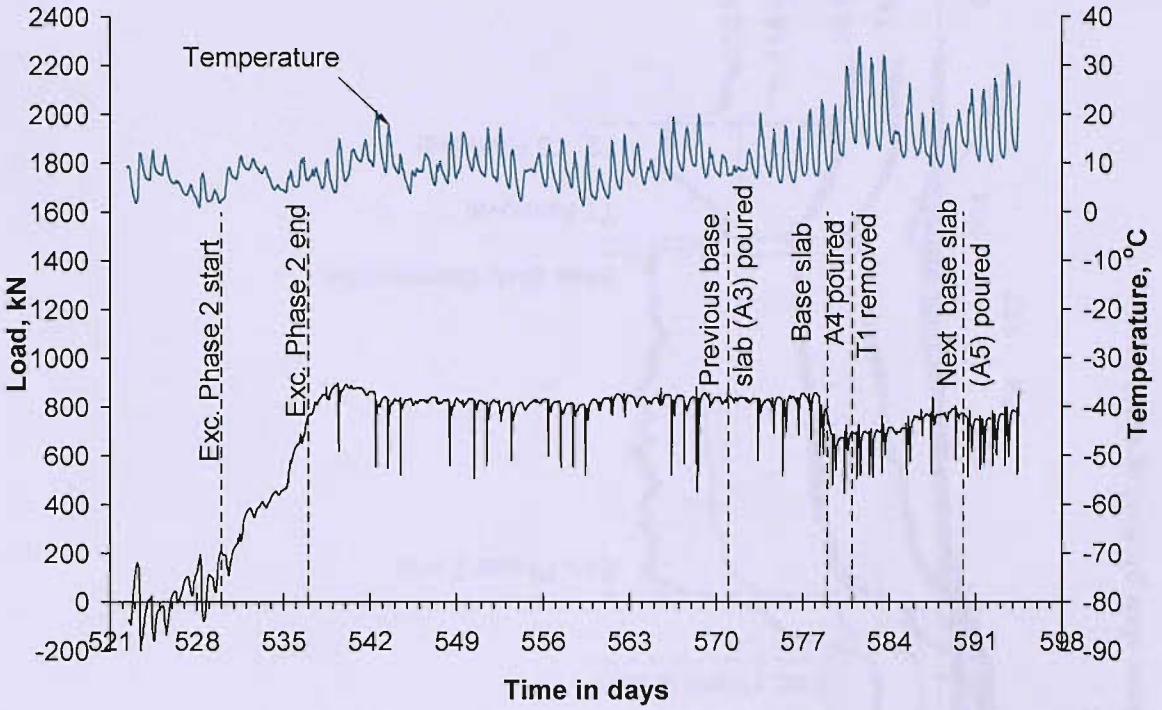

(c) T3

Figure 4-31: Individual temporary prop loads

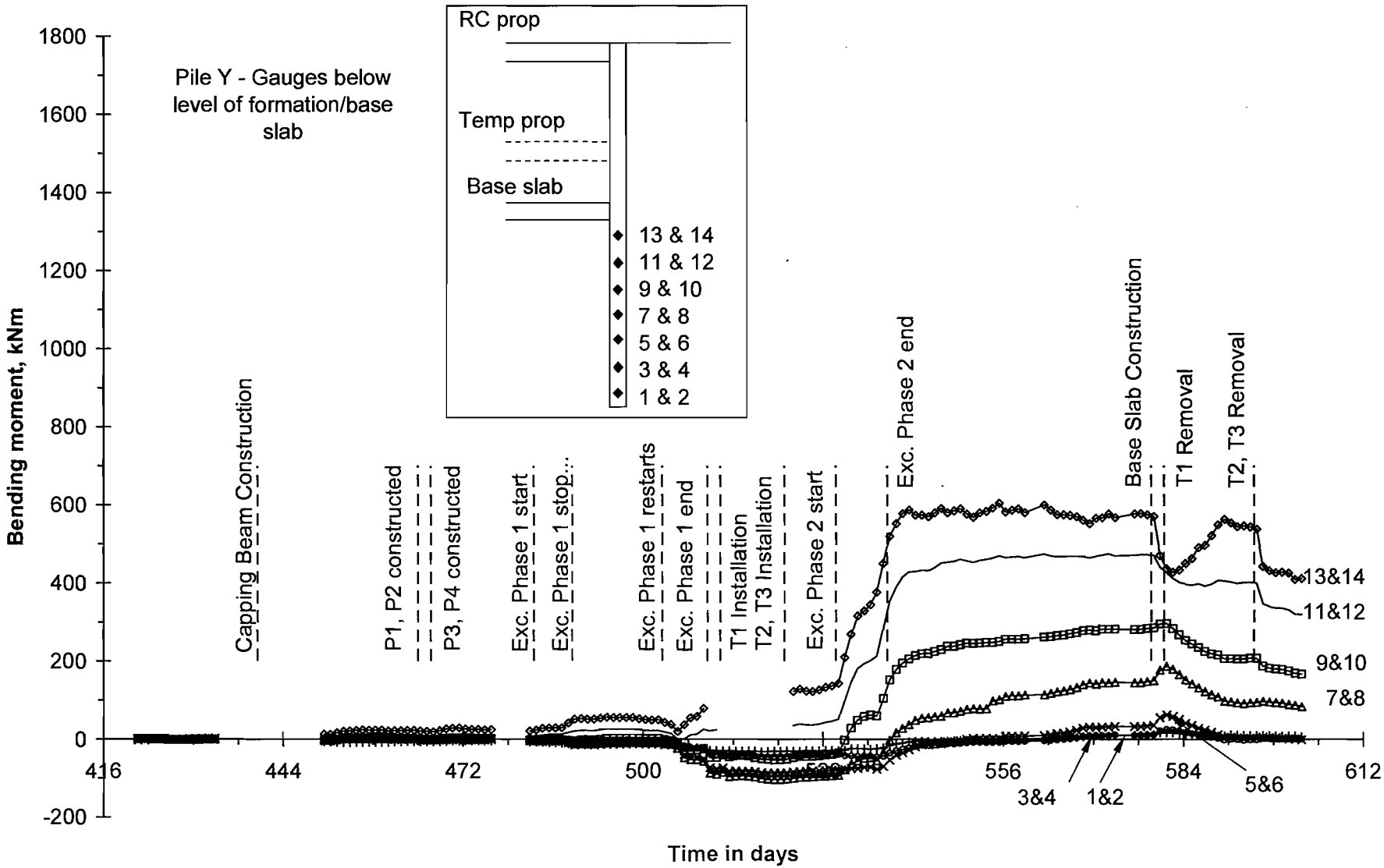

Figure 4-32: Pile Y bending moments below the base slab plotted against time

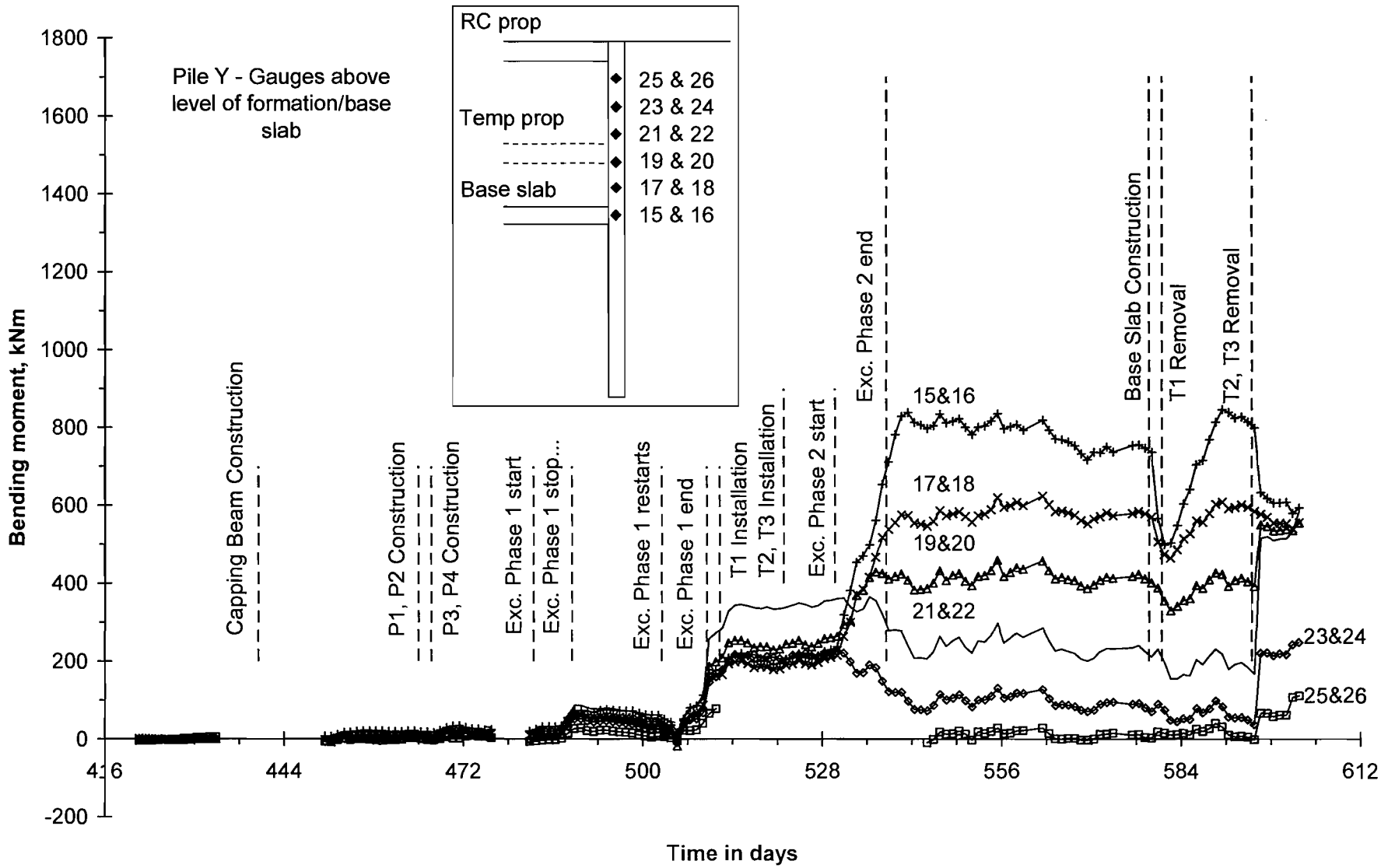

Figure 4-33: Pile Y bending moments above the base slab plotted against time

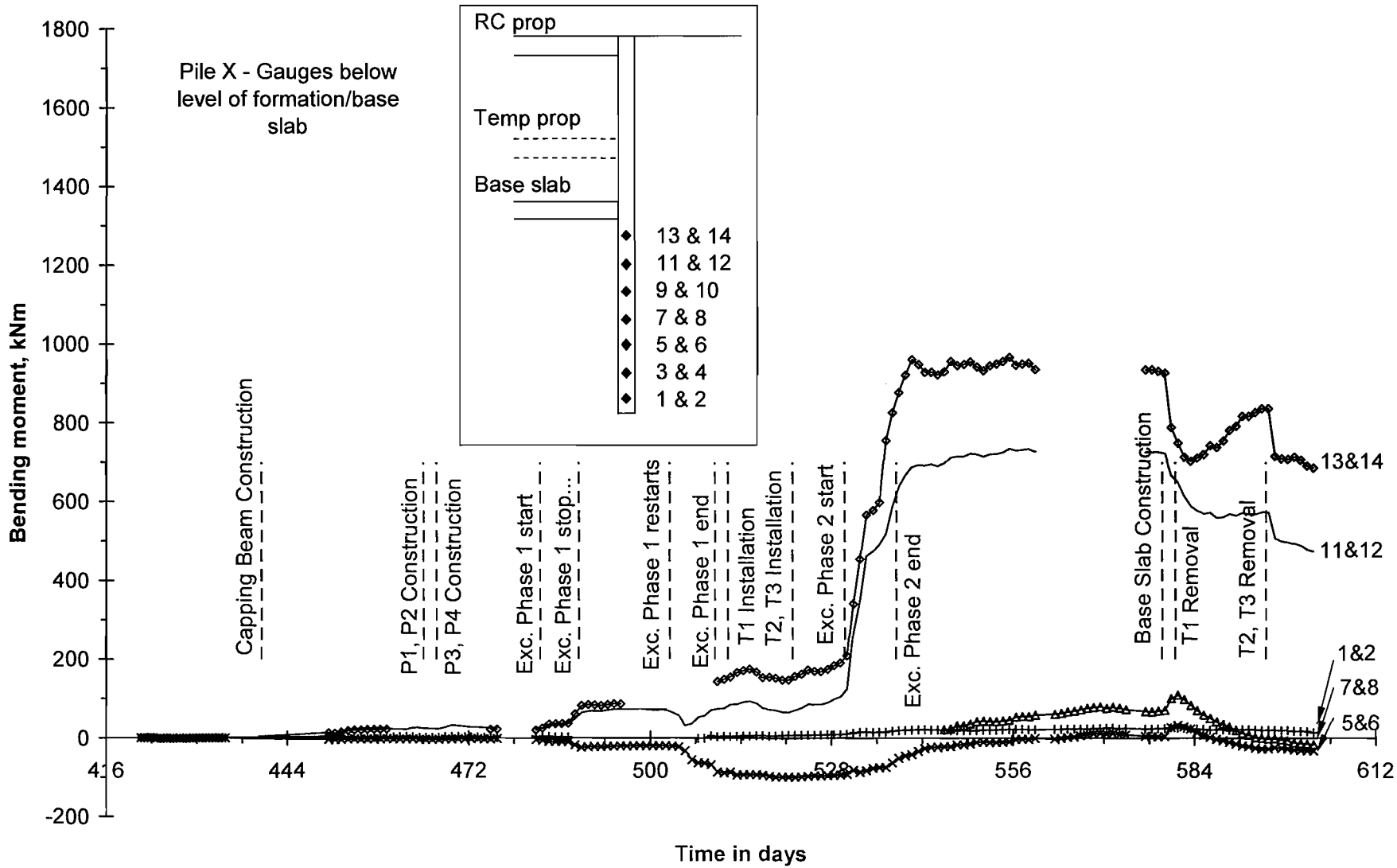

Figure 4-34: Pile X bending moments below the base slab plotted against time

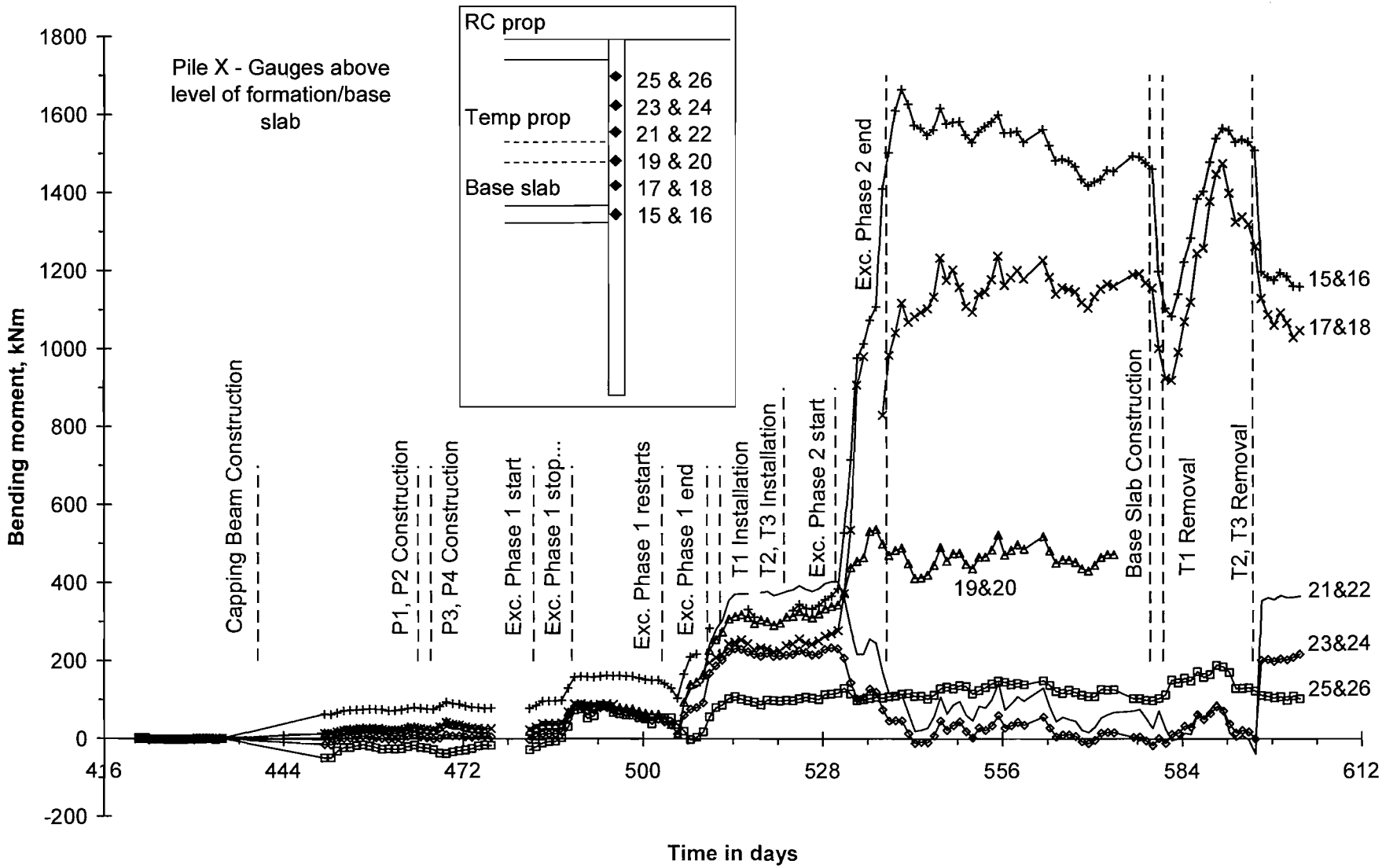

Figure 4-35: Pile X bending moments above the base slab plotted against time

5 HORIZONTAL SOIL STRESS MEASUREMENT

5-1 Introduction

In this chapter the instrumentation used to study changes in the total horizontal stress and pore water pressures around the retaining wall is described (push-in spade-shaped pressure cells (spade cells)). A study carried out to determine the over-reading given by a spade cell installed in overconsolidated clay is described in Section 5-4. This chapter also includes a study of the stress changes measured in the soil around the retaining wall during installation (Section 5-5) and data is presented which shows the changes in horizontal soil stress measured due to excavation and construction of the cutting (Section 5-6).

5-2 Spade cell description

The spade cells used in this study were manufactured by Soil Instruments Ltd and consisted of a pointed rectangular spade-shaped flat jack, approximately 7 mm thick and 100 mm wide, formed from two sheets of steel welded around the edge (Figure 5-1). The

narrow gap between the plates is filled with oil, and is connected to a vibrating-wire pressure transducer by a short length of steel tubing forming a closed hydraulic system. The spade cell body also houses an integral piezometer, in the form of a porous filter disc connected to a second vibrating-wire transducer. The use of vibrating-wire transducers allowed effectively continuous data to be obtained, as discussed in Section 4-6.

Tedd & Charles (1983) and Ryley & Carder (1995) used spade cells containing pneumatic rather than vibrating-wire transducers. The vibrating-wire spade cell used in this study was found to be unaffected by temperatures in the range expected to be exhibited in the ground on site (9-24 degrees Centigrade) when unconfined. Readings from vibrating-wire embedded strain gauges (incorporating temperature sensors) measuring strain in buried concrete piles showed that the readings only became sensitive to ambient temperature changes when the ground level was within 2·5 m of the cell (see Section 4-3-3).

5-3 Calibration

The spade cell used in the study to determine the spade cell over-reading was calibrated by Soil Instruments. Figure 5-2 shows the equipment used for spade cell calibration. For total stress measurement the spade cell is lowered into a compression chamber and readings from the pressure transducer are taken as the pressure in the chamber is increased. During this process plates are clamped over the ceramic disk (for pore water pressure measurement) to protect it, as it has a smaller measurement range than the total stress transducer.) To calibrate the pore water pressure transducer the clamp remains over the ceramic disk and water pressure is applied to the transducer at its outlet point on the transducer at the top of the spade cell. Again, transducer readings are taken as the pressure acting on the transducer is changed.

5-4 Evaluation of spade cell over-reading

5-4-1 Introduction

Due to the considerable uncertainty regarding the magnitude of the over-reading and the factors that may affect it (described in Section 2-4), a direct determination of the over-reading seen by spade cells installed in overconsolidated clays should be made wherever

possible until more data are available. The spade cell over-reading associated with the geology at Ashford was evaluated by means of a field study in which a cell was installed horizontally from the cut-and-cover excavation, aligned to measure the vertical stress, and its readings were compared with the overburden acting on it. The soil above the spade cell was excavated in stages over a period of several weeks, and at each stage the overburden was calculated and compared with the reading in the spade cell. Additionally, measurements of *in situ* horizontal earth pressure taken with the spade cells in the instrumented section have been compared with pressuremeter readings. In line with other recent research, the values of over-reading have been expressed in terms of the undrained shear strength of the soil.

5-4-2 Test procedure

The borehole into which the spade cell was installed was drilled horizontally and perpendicular to the wall using a continuous flight auger (see Figure 5-3), to a point approximately half a metre short of the centre of the nadir sump (see Figure 5-4). Owing to the stiffness and undrained shear strength of the clay it was not necessary to line the borehole. A jacking platform was then erected, tension bars installed into the piles on either side of the installation point, and a reaction beam connected to the bars to allow the spade cell to be pushed into position using a hydraulic jacking system. The installation barrel was connected to the spade cell which was then moved to the end of the borehole, so that zero readings could be taken. Considerable care was taken to ensure that the borehole was horizontal and that the active faces of the spade cell were horizontal aligned. To complete the installation, the borehole was backfilled and sealed using a cement grout. The installation barrel was left in place to protect the cables. The exact location and orientation of the spade cell were confirmed when it was uncovered during excavation (Figure 5-5).

Prior to installation of the spade cell the instrument was kept submerged in water to prevent the porous stone from de-saturating and so that it was close to ground temperature before installation. As an added precaution, a period of fifteen minutes was allowed to elapse between the transfer of the spade cell to the borehole and installation into the soil to allow the spade cell temperature to equilibrate fully with the surrounding soil; readings taken proved this to be the case.

The spade cell was pushed approximately 50 mm at each jack stroke during installation and at each stroke a reading of total vertical stress was obtained using a hand-held vibrating-wire readout meter. On completion, the transducers were connected to a datalogger and readings were taken every 15 minutes. Figure 5-6 shows the spade cell output during the installation phase and during excavation within the sump: the total stress readings gradually stabilized over a period of approximately 2 weeks prior to excavation.

During excavation careful surveying of the level of the material within the sump at the end of each day has enabled the overburden to be calculated. However, as excavation proceeded after the ring beam had been installed access to the base of the excavation was restricted due to the amount of machinery within the excavation. The excavation phases are listed in Table 5-1 and the volume of material removed at each excavation phase is shown schematically in Figure 5-7.

Stage	Description	Date	Day
1	Excavation of 3·8 m leaving steps cut in clay for access	Tues 26/06/01	628
2	Steps removed. Mini-digger lowered into excavation	Wed 27/06/01	629
3	Excavate another 2·65 m generally although only 1·4 m directly over spade cell	Thurs 28/06/01	630
4	Further excavation less than 1 m	Fri 29/06/01	631
5	Excavation and levelling to ring beam formation level	Mon 02/07/01	634
6	Ring beam and wall installation and time for concrete setting	July 2001	633-663
7	Excavation restarted. 1·7 m of material below the ring beam removed.	Wed 01/08/01	644
8	Uncovered spade cell	Mon 16:20 06/08/01	669

Table 5-1: Details of nadir sump excavation

5-4-3 Results and Discussion

Figure 5-6 shows that reductions in total stress were measured at every excavation stage and an increase in total stress resulted from installation of the ring beam. At the end of the test when there was no load on the spade cell the total stress readings returned to zero. The pore water pressure was approximately zero throughout the test period.

Figure 5-8 shows the measured total vertical stress just prior to excavation and at the end of each excavation stage plotted against the total vertical stress calculated from the depth of overburden acting on the spade cell (calculated using a bulk density of 21 kN/m^3: see Chapter 3). Any discrepancy between the initial steady spade cell reading and the *in situ* overburden stress must be due to the effect of inserting the cell. Figure 5-8 shows that the initial overburden is 180 kPa, giving an over-read of 49 kPa or 0·35 × c_u. As the overburden is removed, further discrepancies may arise as a result of the differential cell/soil stiffness (cell action factor effects), and/or the development of shear stresses between the soil and the walls of the nadir sump, acting so as to resist heave.

In addition to an over-read of the *in situ* stress due to the effects of insertion, it is well known that a pressure cell will generally either over-read or under-read changes in stress depending on whether the cell is stiffer or less stiff than the soil within which it is embedded. This was investigated by Peattie and Sparrow (1954) in terms of the relative cell to soil stiffness. They provide guidance on the design of pressure cells to measure soil pressures irrespective of the type or condition of the soil. Determination of the relative cell to soil stiffness is complicated by the fact that, even for a given stress history, stress state and load path, the stiffness of the soil may vary by several orders of magnitude as strain occurs.

The data shown in Figure 5-8 suggest an under-read of the reduction in vertical stress, which is consistent with a cell that is over-compliant (i.e. insufficiently stiff: Clayton & Bica, 1993) and/or the mobilization of shear stress on the nadir sump walls. Measurement of the change in thickness of the spade cell blade (by means of high resolution miniature linear variable displacement transducers (LVDTs)) during calibration in a fluid filled cell (Figure 5-9) indicated an effective cell stiffness (E) of 4·55 GPa. This is far in excess of the measured small strain soil stiffness of the lower Atherfield Clay of 270 MPa (Xu, 2002); thus over-compliance is not an issue, and the under-read of the reduction in vertical stress must have been due to the mobilization of shear stresses on the nadir sump walls. To confirm this, a plane strain undrained finite element analysis was carried out using the continuum finite element program CRISP (Britto and Gunn, 1987), across the narrow section of the nadir sump.

The analysis started with the walls already in place and a pre-excavation earth pressure coefficient of 1. Excavation was modelled by the gradual removal of elements to a depth of 6·7 m, corresponding to the level at which the intermediate concrete ring beam support was constructed. The mesh used in the analysis is shown in Figure 5-10 and comprised

1904 non-consolidating linear strain triangular elements. The base boundary was fixed in both the horizontal and vertical directions. The vertical mesh boundaries were fixed in the horizontal direction only. An elastic-perfectly plastic soil model with a Tresca (undrained shear strength) failure criterion in terms of total stresses, $\tau_{max} = c_u$ was used for each soil layer and the wall was modelled as a linear elastic material. An undrained soil stiffness (E_u) profile was derived from the measured undrained shear strength profile (Figure 3-15 and Equation 3-1) using $E_u = 1500\ c_u$. This is based on laboratory test data presented by Jardine *et al.* (1984) for a variety of clays including London Clay, at a characteristic shear strain of between 0·01% and 0·1% (Jardine *et al.*, 1986; Mair, 1993).

An effective soil stiffness (E') profile was derived from the measured undrained stiffness (E_u) profile using Equation 5-1, where Poisson's ratio (ν') = 0·35.

$$E' = \frac{1+\nu'}{1.5}.E_u . \qquad \textbf{Equation 5-1}$$

The effective soil stiffness profile given by Equation 5-2 was used to derive the effective bulk modulus of the soil (K').

$$K' = \frac{E'}{(3(1-2\nu'))}. \qquad \textbf{Equation 5-2}$$

Undrained conditions were imposed by specifying the bulk modulus of water (K_w) as 100 times the effective bulk modulus of the soil (K').

Figure 5-11 shows the calculated total vertical stress as a function of overburden at an integration point located at the same depth as the spade cell (approximately 8·5 m below original ground level). The aspect ratio of the sump box (its breath, b, to length, l, ratio = 0·72) is high, suggesting that further arching effects would be expected across the longer dimension of the box due to the shear stresses on the shorter walls. In very simple terms, multiplying the calculated over-read by 1·72 gives an upper estimate of the possible error due to arching between the sump walls.

The raw data from the finite element analysis were adjusted for comparison with the spade cell data by:

- Multiplying the initially calculated over-read by 1·72 to allow for shear stresses on the short sides of the sump as well, and

- Adding the over-read due to spade cell installation of 49 kPa.

Figure 5-11 shows that the adjusted finite element analysis results match closely the measured data. This tends to confirm that the discrepancy between the calculated and measured overburden may be accounted for by a combination of (a) spade cell over-read of 0·35 c_u due to installation effects, and (b) the mobilization of shear stresses at the walls of the nadir sump.

A simple equilibrium analysis of the mobilized soil/wall adhesion further supports this conclusion. For an excavation of dimensions $l \times b$ in a soil of average undrained shear strength $\overline{c_u}$ and unit weight γ, a mobilized soil/wall adhesion of $\alpha\,\overline{c_u}$ and a depth of soil remaining (above the spade cell location) of h, the downward force acting on the soil in addition to the weight is:

$$2\alpha\overline{c_u}h(l+b). \qquad \textbf{Equation 5-3}$$

This is equivalent to an average increase in vertical stress of:

$$\frac{2\alpha\overline{c_u}h(l+b)}{lb}. \qquad \textbf{Equation 5-4}$$

The undrained shear strength (c_u) varies with height above the spade cell location (h) at a rate of β kPa, and as previously stated in Section 3-6-3, the undrained shear strength at the position of the spade cell c_u = 140 kPa. Thus the average undrained shear strength $\overline{c_u}$ in the soil mass remaining above the spade cell is:

$$\overline{c_u} = 140 - \frac{\beta h}{2}. \qquad \textbf{Equation 5-5}$$

Substituting equation 5-5 into equation 5-4 provides an indication of the error (over-read) E_{rr} due to the mobilized shear stress on the sump wall perimeter as a function of the height of the remaining soil above the spade cell:

$$E_{rr} = \left(280\alpha h - \alpha\beta h^2\right)\frac{(l+b)}{lb}. \qquad \textbf{Equation 5-6}$$

Figure 5-12 shows the measured spade cell over-read and the calculated error (E_{rr}) for adhesion factors (α) between 0 and 0·4. It can be seen that the measured discrepancy could

be accounted for by the mobilization of approximately 30% of the undrained shear strength at the soil/wall interface as the overburden is removed.

Figure 5-13 shows the *in situ* total horizontal stresses measured at the instrumented section, both raw and corrected for installation effects by subtracting 0·35 c_u, and self-boring pressuremeter data obtained 250 m northwest of the nadir sump. The subtraction of 0·35 c_u to account for spade cell installation effects brings the spade cell data largely into line with the self-boring pressuremeter test results. Consequently all total horizontal stress measurements have been corrected by 0·35 c_u (unless otherwise stated).

5-5 Installation effects of a bored pile retaining wall in overconsolidated clay

5-5-1 Introduction

This section contains an analysis of the effects of wall installation on the soil surrounding the contiguous bored pile retaining wall.

5-5-2 Calibration and installation of spade cells

The spade cells in the instrumented section were calibrated and installed by the Transport Research Laboratory. Figure 5-14 shows the installation of one of these spade cells.

5-5-3 Stabilization of spade cells following insertion

Figure 5-15 shows the readings of total horizontal stress and pore water pressure during spade cell insertion and for a period of one month afterwards (readings from spade cell or piezometer number *n* are referred to as S*n* and P*n* respectively). The excess pore water pressures induced during spade cell insertion had dissipated and readings of total horizontal stress had stabilized prior to the installation of the bored pile wall.

5-5-4 In situ total horizontal stresses and pore water pressures

Figure 5-16 shows the corrected, stabilized readings of total horizontal stress and pore water pressure from all spade cells and piezometers, plotted against depth below original ground level. The initial *in situ* pore water pressures were slightly less than hydrostatic

beneath a water table 1·2 m below the original ground surface in the upper Atherfield Clay. In the lower part of the stratum the deviation of the pore water pressure from hydrostatic was more pronounced. This distribution of pore water pressure with depth is consistent with underdrainage of the Atherfield Clay into the underlying Weald Clay, within which an ejector well pore pressure control system was in operation about 100m from the instrumented section (see Section 3-3-5).

The variation of *in situ* total horizontal stress σ_{ho} with depth z (below ground level) was approximated by the linear function given in Equation 5-7.

$$\sigma_{ho}\ (\text{kPa}) = 0{\cdot}8 + 20{\cdot}6 \times z\ (z \text{ in m}). \qquad \textbf{Equation 5-7}$$

5-5-5 Effective stress profile

The profile of effective horizontal stress σ'_{ho} with depth (obtained by subtracting the measured pore pressure from the total horizontal stress at each location) is shown in Figure 5-17. The implied *in situ* earth pressure coefficient K_o ($=\sigma'_{ho}/\sigma'_{vo}$) is generally within the range 0·9 to 1·5 with an average of 1·1. This is rather less than would be expected on the basis of the one-dimensional stress history of the deposit (as discussed in Section 3-3-4).

5-5-6 Pore water pressure changes during and after wall installation

Figure 5-18 shows the variations in pore water pressure measured during the period of wall installation, together with the periods of installation of each pile group. Detailed interpretation of these data is complicated by the sequential nature of pile installation, together with the fact that the spade cells could not all be installed at one cross section but had to be spread along the length of the wall. However, the general response of each transducer comprises a reduction in pore water pressure on excavation followed by an overcompensating increase in pore water pressure on concreting. The pore water pressure then gradually falls to the original value over a relatively short period of time (in this case less than a day) as the concrete begins to set. This response is similar to that measured in the field by Symons & Carder (1993) and in centrifuge model tests by Powrie & Kantartzi, (1996). The magnitudes of the measured changes vary, but generally reduce with distance from the pile being installed. The changes in pore pressure were consistently most pronounced at piezometer P4. The reason for this is unknown.

Pile installation may be idealized as an expanding or contracting circular cylindrical cavity. Analysis following Gibson & Anderson (1961; reproduced in Powrie, 2004) shows that if it remains elastic, the soil surrounding the cavity deforms at constant volume and constant average total stress p (= $[\sigma_r + \sigma_\theta + \sigma_v]/3$). In an elastic medium, deformation at constant volume occurs at constant average effective stress p'; hence while p remains constant there should be no change in pore water pressure. However, a reduction or increase in cavity pressure (from the *in situ* condition) equal to the undrained shear strength of the soil, c_u, is sufficient to cause yield and hence potential changes in pore water pressure. In the present case, the *in situ* total horizontal stress (given by Equation 5-7, $\sigma_{ho} = 0{\cdot}8 + 20{\cdot}6\ z$) is greater than the undrained shear strength (given by Equation 3-1, $c_u = 22 + 7\ z$) for depths z greater than 1·6 m. Unloading the pile bore from an *in situ* total horizontal stress σ_{ho} to a cavity support pressure P (where $[\sigma_{ho} - P] \geq c_u$) will cause yield of the surrounding soil within a plastic radius r_p given by Equation 5-8, where R is the cavity radius.

$$r_p = R \times \exp\left[\frac{\sigma_{ho} - c_u - P}{2c_u}\right]. \qquad \textbf{Equation 5-8}$$

In the present case, taking the cavity support pressure $P = 0$, the cavity radius $R = 0{\cdot}525$ m and the profiles of *in situ* total horizontal stress and undrained shear strength with depth given by Equations 5-7 and 3-1 respectively, the width of the plastic zone ($r_p - R$) varies from zero at a depth of 1·6 m to 0·6 m at the bottom of the pile bore.

Even the closest pore water pressure transducers were outside the theoretical plastic zone, and might therefore have been expected to show no change in pore water pressure. However, it is well known that soil does not behave as an ideal elastic material. Also, the neglect in this simple analysis of both the potential for vertical load transfer to the soil below the pile toe and the effect of any piles already installed introduces further degrees of approximation. Nonetheless, the measured pore water changes are generally not large, and decrease rapidly with distance from the wall as the effects of the approximations become less significant.

For a wall constructed from diaphragm wall panels rather than individual piles, a greater pore water pressure response would be expected. Excavation in plane strain results in a reduction in average total stress p of half the reduction in horizontal pressure within the trench, in the soil close to the trench (Powrie & Kantartzi, 1996). If the soil is again

assumed to deform elastically with p' = constant in undrained conditions, the change in pore water pressure would be expected to be the same as the change in p, i.e. half the reduction in horizontal stress within the trench. Powrie & Kantartzi (1996) report centrifuge tests modelling diaphragm wall panel installation in which the measured changes in pore water pressure clearly reduced with reducing panel length. However, the difference in pore water pressure response between bored pile and diaphragm walls is not so clear from the field observations described, but not presented in any great detail, by Symons & Carder (1993).

Figure 5-19 shows the measured pore water pressures plotted against time for periods before, during and 10 months after wall installation. When viewed in this way, the fluctuations in pore water pressure due to pile excavation and concreting are little more than noise, and the data show clearly that the overall net effect of wall installation on the *in situ* pore water pressures was negligible. This is consistent with the observations of Symons & Carder (1993) and Powrie & Kantartzi (1996), and confirms that, in an overconsolidated clay, the overall effect of bored pile or diaphragm wall installation on the *in situ* pore water pressures may reasonably be neglected. In the 10 months following wall installation the pore water pressure slowly reduced at the positions of many of the spade cells. The pore water pressure began to fall in March (approximately Day 150), probably due to seasonal variations and/or construction dewatering being carried out about 500 m from the instrumented section.

5-5-7 Total horizontal stress changes due to wall installation

Figure 5-20 shows the total horizontal stresses measured during installation of the wall. As with the pore water pressures, interpretation is complicated by the sequential installation of the piles and the staggered pattern of the spade cells along the length of the wall. Nonetheless, the influence of pile construction on the individual traces (generally, a reduction in total horizontal stress on excavating at least the lower portion of the pile and an increase in total horizontal stress on concreting) is clear. Overall, pile installation resulted in a reduction in total horizontal stress to below the *in situ* value, the magnitude of the reduction generally decreasing with distance from and along the wall.

The changes in stress measured due to the installation of a single pile can be compared with values calculated using an elastic analysis, assuming as an upper limit that the change in stress at the pile bore is from the *in situ* stress to zero (as the pile was initially bored

with no support). The change in radial stress, $\Delta\sigma_r$, at a distance r from the centre of the pile, is related to the change in stress at the pile bore, $\Delta\sigma_{PB}$, and the radius R of the pile bore by Equation 5-9 (see for example Fjaer *et al.*, 1992).

$$\Delta\sigma_r = \frac{R^2}{r^2}\Delta\sigma_{PB} \text{ for } r > R \qquad \textbf{Equation 5-9}$$

The installation of any pile affects the stress state of the ground at the positions where further piles are to be installed. Assuming that at the depth under consideration pile installation results in a reduction in stress, then at the centres of piles yet to be installed, the stress in the direction perpendicular to the wall increases (due to arching) and the stress in the direction along the wall decreases. Calculation of the changes in stress seen by a spade cell due to the installation of piles after the first pile is therefore more complicated. A lower limit to the change in stress may be estimated by assuming that the *in situ* stress at the positions of the piles not yet installed is reduced (as happens to the stress in the direction along the wall). An upper limit may be estimated by assuming that the *in situ* stress increases (as happens to the stress in the direction perpendicular to the wall).

Consideration of the Mohr circle of stress shows that the change in horizontal stress acting on the plane of the spade cell, $\Delta\sigma_{SC}$, due to the installation of any pile is given by Equation 5-10, where θ is the angle between the normal to the wall and the line joining the pile to the spade cell (Figure 5-21) and $\Delta\sigma_r$ is the change in radial stress at the spade cell (as given by Equation 5-9).

$$\Delta\sigma_{SC} = \Delta\sigma_r \times \cos 2\theta \qquad \textbf{Equation 5-10}$$

Figure 5-22 shows the measured and calculated changes in stress, normalised with respect to the *in situ* stress plotted as a function of the distance along the wall (in pile spacings) between the spade cell and the nearest pile being installed in a particular pile installation period. Due to the complexity of the installation sequence, the following rules have been adopted:

1. Where two piles were installed simultaneously at an equal number of pile spacings from a spade cell, the change in stress measured at the spade cell attributed to the installation of a single pile was assumed to be half the total. For example two piles, each four pile spacings from spade cell 3, were installed during Period A, so half the measured total stress change has been attributed to each.

2. Where two piles were installed simultaneously at distances from a spade cell differing by one or two pile spacings, the change in stress has been halved and assigned to a pile at the average distance from a spade cell. For example piles were installed 2 and 3 pile spacings from spade cell 12 in Period E, so half the measured total stress change has been plotted as a change due to pile installation 2·5 pile spacings away.

3. Where in any installation period the difference in the distance between the spade cell and the nearest pile installed and the second nearest pile was more than two pile spacings, the entire change in stress has been assigned to the nearest pile. For example, the two piles installed in period A were two and six pile spacings from spade cell 2, so the change measured at spade cell 2 during period A has been plotted as a change due to a pile installation two pile spacings away.

The change in stress was calculated over the period from 2 hours before the pile installation process began to 2 hours after it finished. Figure 5-22 shows that the reduction in total horizontal stress measured on installation of the pile in line with a spade cell was approximately 0 to 20% of the *in situ* value 1·275 m from the edge of the wall, 3 to 9% 2·375 m from the edge of the wall and 1 to 5% 3·475 m from the edge of the wall.

Figure 5-22 shows that the measured reduction in stress due to pile installation is generally larger than that calculated using the simple elastic analysis – even assuming zero pressure (rather than the pressure of bentonite or wet concrete) in the pile bore and an *in situ* stress corresponding to the upper limit value resulting from the installation of previous piles. This could be a result of shrinkage of the concrete (possibly due to thermal effects) as it sets, and/or vertical arching and stress transfer below the bottom of the bore, which is not taken into account in the simple analysis. The underestimation of the measured reductions in horizontal stress is confirmed by Figure 5-23, which shows the calculated and average measured reductions in stress (expressed as a percentage of the *in situ* value), for piles directly opposite the spade cell (i.e. in Figure 5-21 a distance of zero pile spacings along the wall).

Figure 5-24 shows the measured *in situ* and post-installation total horizontal stresses at a distance of 1·275 m from the wall. The best-fit linear approximation to the *in situ* total horizontal stress is given by Equation 5-7. The best-fit linear approximation to the post-installation total horizontal stress measured by the instruments 1·275 m from the wall is:

$$\sigma_h \text{ (kPa)} = 7{\cdot}4 + 16{\cdot}7\, z \text{ (m)}. \qquad \textbf{Equation 5-11}$$

On the basis of the best-fit linear approximations, the reduction in total horizontal stress ranges from 10% at the top of the Atherfield Clay to 17% 15·3 m below ground level. However, this masks the true nature of the variation with depth of the change in effective horizontal stress, which is much greater (about 30%) at the mid-depth of the wall than at ground level or at the toe (approximately 4%) as shown in Figure 5-25. This is consistent with the transfer of lateral stress to the soil below the wall (sometimes referred to as vertical arching), which results in an increase in horizontal stress below the toe as shown by Ng *et al.* (1995). It also suggests that an attempt to quantify the effects of wall installation as a uniform with depth percentage reduction may be too much of an over simplification.

5-5-8 Effective stress changes due to wall installation

Figure 5-26 shows all the *in situ* effective horizontal stresses and the post installation effective horizontal stresses measured 1·275 m from the wall. The best-fit linear approximation to the *in situ* effective horizontal stress below the groundwater level of 1·2 m is given by Equation 5-12, and the best-fit linear approximation to the post-installation effective horizontal stress below groundwater level is given by Equation 5-13.

$$\sigma'_{ho}\ (\text{kPa}) = 15{\cdot}3\ (z - 1{\cdot}2) + 10.86 \qquad (\text{for } z \geq 1{\cdot}2\ \text{m}). \qquad \textbf{Equation 5-12}$$

$$\sigma'_{h}\ (\text{kPa}) = 11{\cdot}6\ (z - 1.2) + 5{\cdot}52\ z\ (\text{m}). \qquad (\text{for } z \geq 1{\cdot}2\ \text{m}). \qquad \textbf{Equation 5-13}$$

The change in effective horizontal stress calculated from the linear best-fit approximations to the measurements is 30% 3·3 m below ground level, falling to 25% 15·3 m below ground level (Figure 5-27). However, the linear approximations again mask the true pattern, and the actual measurements show a similar trend to the total stress changes (Figure 5-25) with the greatest reduction occurring at 8·3 m below ground level. The percentage changes in effective stress are greater than the percentage changes in total stress because there was no overall change in pore water pressures.

Current guidance given in CIRIA Report C580 (Gaba *et al.*, 2003) is that installation of a bored pile wall might be expected to reduce the *in situ* earth pressure coefficient by about 10%. This is largely based on work the work by Symons & Carder (1993) (see Section 2-2-5) who measured a reduction in lateral earth pressure coefficient K from 2·1 to 1·9 (~10%). At Ashford the lateral earth pressure coefficient reduced from approximately 1·1 to 0·8 (~25%), on the basis of the linear idealizations to the data indicated in Figure 5-26.

Although there appears to be a large discrepancy between these changes when expressed in percentage terms, they are consistent with a similar absolute reduction in total or effective horizontal stress of about 0·25 γz in each case (where γ is the unit weight of the soil). This suggests that the likely reduction in earth pressure due to *in situ* wall installation could be estimated in absolute terms. Given that the process might be expected to be controlled by the boundary stresses at the pile bore this is perhaps surprising, but may be more credible than an approach based on a reduction in K_o in percentage terms. However, it has already been noted that idealisation of the percentage stress change as uniform with depth may be inappropriate.

5-5-9 Total and effective horizontal stress changes after wall installation

Concern is sometimes expressed that the *in situ* horizontal stresses become re-established in the long-term. In this case, measured total horizontal stresses showed no tendency to change for a period of 10 months after wall installation (Figure 5-28), suggesting that the reductions in horizontal stress due to wall installation are permanent. This is consistent with long-term observations of horizontal pressures behind a number of in-service retaining walls, which show no significant change in total horizontal stress over periods of between 5 and 24 years after construction (Carder & Darley, 1998).

Although the *in situ* earth pressure coefficient of the Atherfield and Weald Clay at this site is low relative to other overconsolidated clay deposits, the reduction in total horizontal stress was similar to that for a clay with $K_o = 2$ excavated under bentonite, assuming a water table at ground level.

5-6 Effect of excavation in front of the wall on horizontal earth stresses

The total horizontal stresses and pore water pressures measured by the spade cells over the main cutting construction period are shown in Figures 5-29, 5-30 and 5-31 (for spade cells 1·275 m, 2·375 m and 3·475 m behind the wall respectively) and Figure 5-32 (in front of the wall).

The Figures show that excavation of the cutting caused reductions in total horizontal stress at all depths and distances behind the wall. Pore water pressures also reduced in all cases. In front of the wall much larger reductions in total horizontal stress were measured. Base

Slab Construction, however, caused an increase in horizontal stress, particularly in spade cells 11 and 13 which are located only 1·5 m below the base slab.

The compatibility of the total horizontal stress data, reinforced concrete prop loads and bending moment data was investigated by analysing the data collected on Day 517, just after Excavation Phase 1. Bending moments were calculated by taking moment up the wall from the toe by consideration of it as a free body diagram. A spreadsheet was used to find estimated values of total horizontal stress, within 10% of the spade cell measurements, which gave a wall bending moment profile which was a best-fit to the measured bending moment profile, using the least squares method (i.e. the sum of the difference between the calculated and average measured bending moment squared was minimised).

The measured and estimated horizontal stress profiles on Day 517 are shown in Table 5-2, Table 5-3 and Figure 5-34 and the measured and computed bending moments in Piles X and Y on Day 517 are shown in Table 5-4 and Figure 5-33.

Depth BGL, m	**Spade cell No.**	**Total horizontal stress, kPa**		**Estimated/ measured, %**
		Measured	**Estimated**	
0	ground level			
3.3	1	57	62	110
5.3	2	20	22	110
8.3	3	52	57	110
11.3	4	162	146	90
15.3	5	300	270	90
20.25	Wall toe		431.3	

Table 5-2: Measured and estimated total horizontal soil stress behind the wall

Depth BGL, m	Spade cell No.	Total horizontal stress, kPa		Estimated/ measured, %
		Measured	Estimated	
6.95	Exc level		0	
8.3			82	
11.6	11 (13)	101 (107)	111	110
15.3	(12) 17	(162) 331	329	99
20.25	Wall toe		386	

Table 5-3: Measured and estimated total horizontal soil stress in front of the wall

Pile gauges	Depth, m	Measured bending moments, kNm			Calculated bending moment, kNm
		Pile X	Pile Y	Average	
pile top	0.00	-	-	-	42.0
	0.50	-	-	-	58.1
25&26	2.24	102.1		102.1	114.4
	3.30	-	-	-	148.6
23&24	3.72	223.5	247.5	235.5	192.2
21&22	5.30	380.0	375.3	377.7	283.7
19&20	6.79	292.8	254.0	273.4	311.4
	6.95	-	-	-	298.7
17&18	8.30	222.4	199.8	211.1	254.8
15&16	9.76	306.3	214.6	260.5	225.7
13&14	11.30	149.5	130.0	139.8	181.2
	11.60	-	-	-	164.5
11&12	12.70	72.8	35.0	53.9	76.2
	15.30	-	-	-	-129.8
9&10	14.20		-49.2	-49.2	-63.0
7&8	15.70	-165.7	-98.2	-131.9	-138.8
5&6	17.20	-94.8	-83.7	-89.3	-111.5
3&4	18.70		-43.7	-43.7	-41.5
1&2	19.70	6.0	-30.8	-12.4	-6.3
pile toe	20.25	-	-	-	0.0

Table 5-4: Measured and calculated bending moments

The RC prop load that would occur under the estimated horizontal soil stress profile presented in Figure 5-33 can be found by analysis of the horizontal equilibrium, and yields

a load of 986 kN. The loads in the RC props indicated by the data presented in Section 4-4-3 are listed in Table 5-5, along with the loads measured directly before and after the period of 16 days during Excavation Phase 1 when no excavation was carried out in the instrumented section. During this time the RC props loads increased by between 168 and 512 kN, and the majority of this apparent increase in load is probably attributable to creep.

	Load after excavation phase 1A, kN	Load before excavation phase 1B, kN	Portion of load partially due to creep, kN	Load indicated after Excavation Phase 1, kN
Day	**489**	**503**	-	**517**
P1	857	1250	393	1226
P2	555	1076	512	1406
P4	129	297	168	594

Table 5-5: Increase in prop load over period where no construction activities were carried out during Excavation Phase 1

If the measured prop loads were reduced by the amount indicated by the increase in load over the period of no activity at the instruemented section, the loads in RC props P1 and P2 would compare favorably with those calculated in the simple equilibrium analysis carried out. The measurement of RC prop loads is not straightforward and although further refinements could possibly be made to these data, it is beyond the scope of this work.

5-7 Conclusions

Total stresses measured using push-in spade cells in Atherfield Clay may be corrected for installation effects by subtracting 0·35 × the undrained shear strength, c_u. This is generally less than corrections determined for spade cell installation effects in previous studies in London Clay.

Laboratory calibration of the spade cell indicated a very high stiffness in comparison with the surrounding soil, suggesting that errors due to over-compliance should not be significant even in a stiff clay. In the experiment reported in this paper, discrepancies between the measured vertical stress and the overburden could be accounted for by a combination of cell installation effects and the mobilization of shear stresses on the nadir sump chamber walls.

A comparison of total horizontal stresses measured in the self-boring pressuremeter tests with spade cell measurements adjusted by 0·35 c_u correction showed close agreement.

Measurement of the changes in total horizontal stress and pore water pressure during installation of a contiguous bored pile retaining wall forming part of the Channel Tunnel Rail Link at Ashford has shown that:

1. Pore water pressures fell during pile excavation and then increased during concreting. The magnitude of the changes decreased with increasing distance from the pile. In theory, the change in pore water pressure should be zero for a circular cylindrical cavity if the surrounding soil behaves elastically. However, different geometries would produce different theoretical results: e.g. in plane strain $\Delta u = 0{\cdot}5\ \Delta\sigma_h$, close to the trench.

2. Overall, wall installation had no effect on pore water pressures, which rapidly returned to their *in situ* values on completion of the process. This is in agreement with previous observations for both diaphragm and bored pile walls. In contrast, there was a very clear reduction in the effective horizontal stresses and lateral earth pressure coefficients.

3. The *in situ* total horizontal stresses did not re-establish during the 10 months that elapsed between wall installation and excavation in front of the wall.

4. Although the soil almost certainly yielded during installation, the size of the plastic zone was small. However, the measured changes in horizontal stress due to individual pile installation were generally greater than those calculated in a simple elastic analysis, even assuming zero pressure at the pile bore rather than the pressure of bentonite or wet concrete. This may have been due to shrinkage of the concrete due to thermal effects, and/or vertical arching not taken into account in the analysis.

5. The profiles of reduction in total and effective horizontal stress were not linear with depth, but greatest at the mid depth of the pile. This is consistent with the transfer of lateral stress to the soil below the wall (sometimes referred to as vertical arching). In this case study, wall installation caused a reduction in total horizontal stress varying from about 4% at the top and the bottom of the wall to approximately 30% at mid-depth. Attempting to quantify the effects of wall installation as a uniform with depth percentage reduction in total horizontal stress may be an over-simplification.

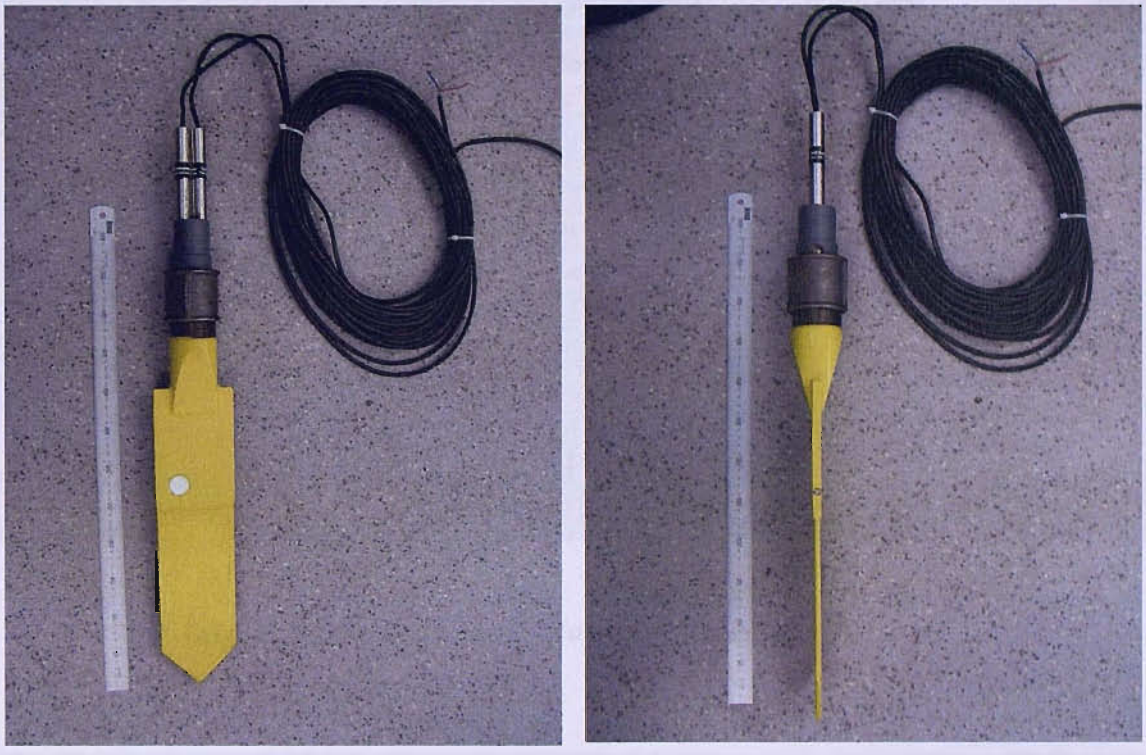

Figure 5-1: Spade cell

(a) Calibration equipment for total stress measurement

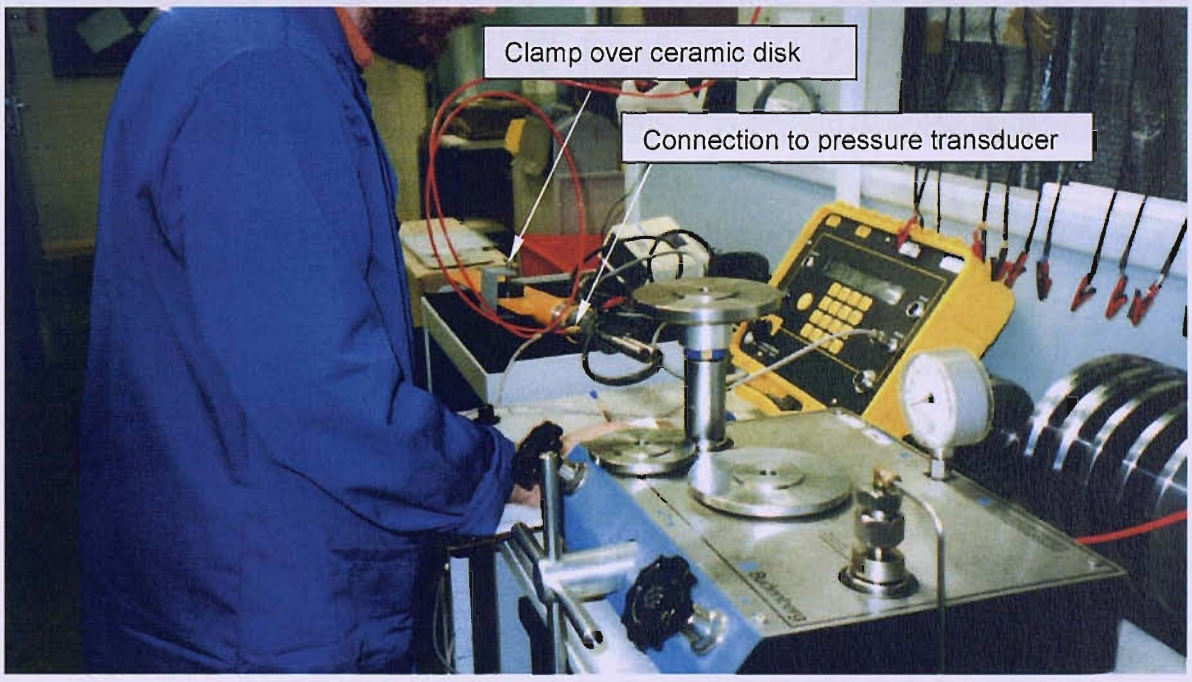

(b) Calibration equipment for pore water pressure measurement

Figure 5-2: Spade cell calibration equipment

Figure 5-3: Equipment for drilling horizontal borehole

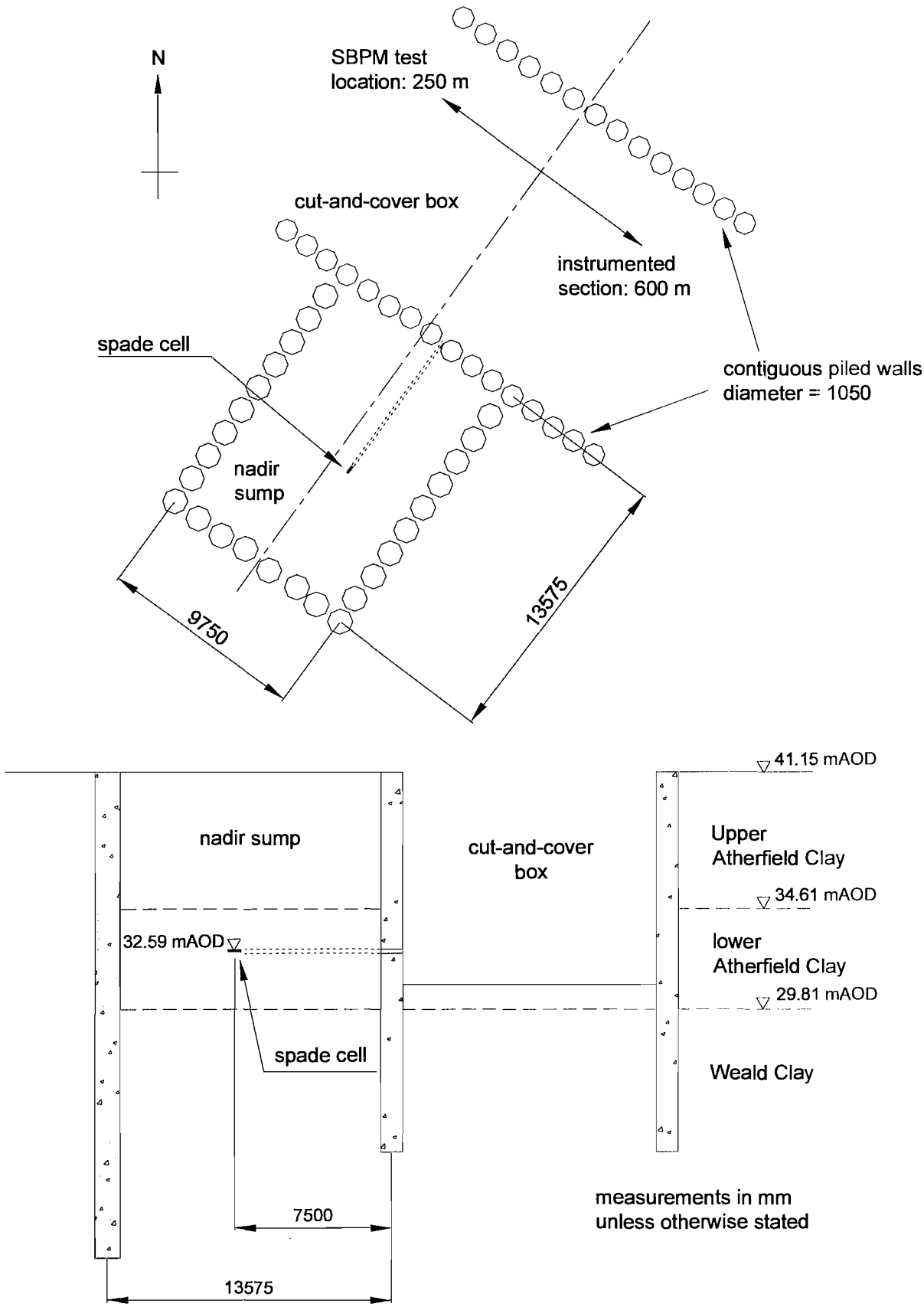

Figure 5-4: Nadir sump plan and elevation

Figure 5-5: Spade cell: uncovered in excavation

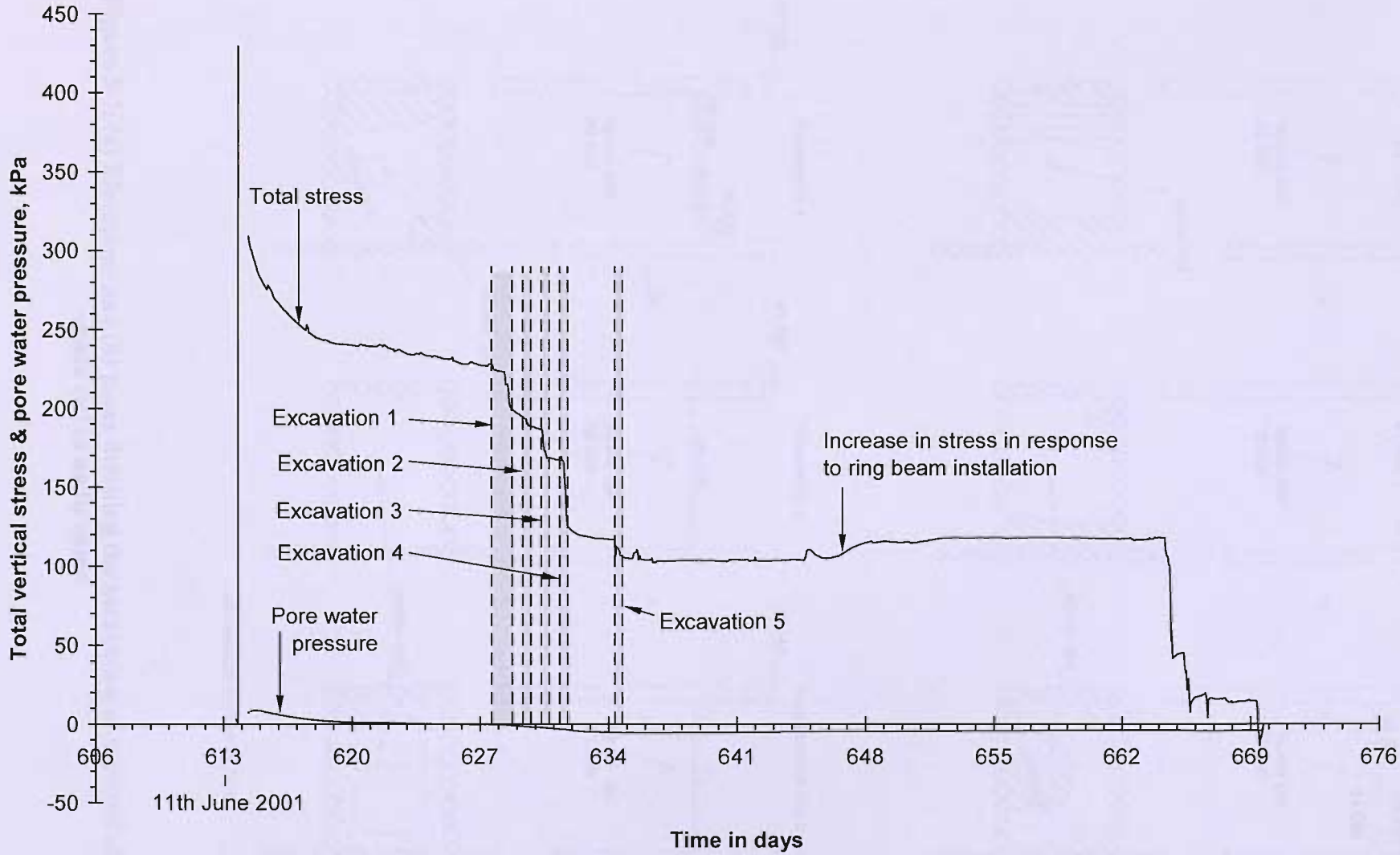

Figure 5-6: Total vertical stress measured by spade cell in nadir sump

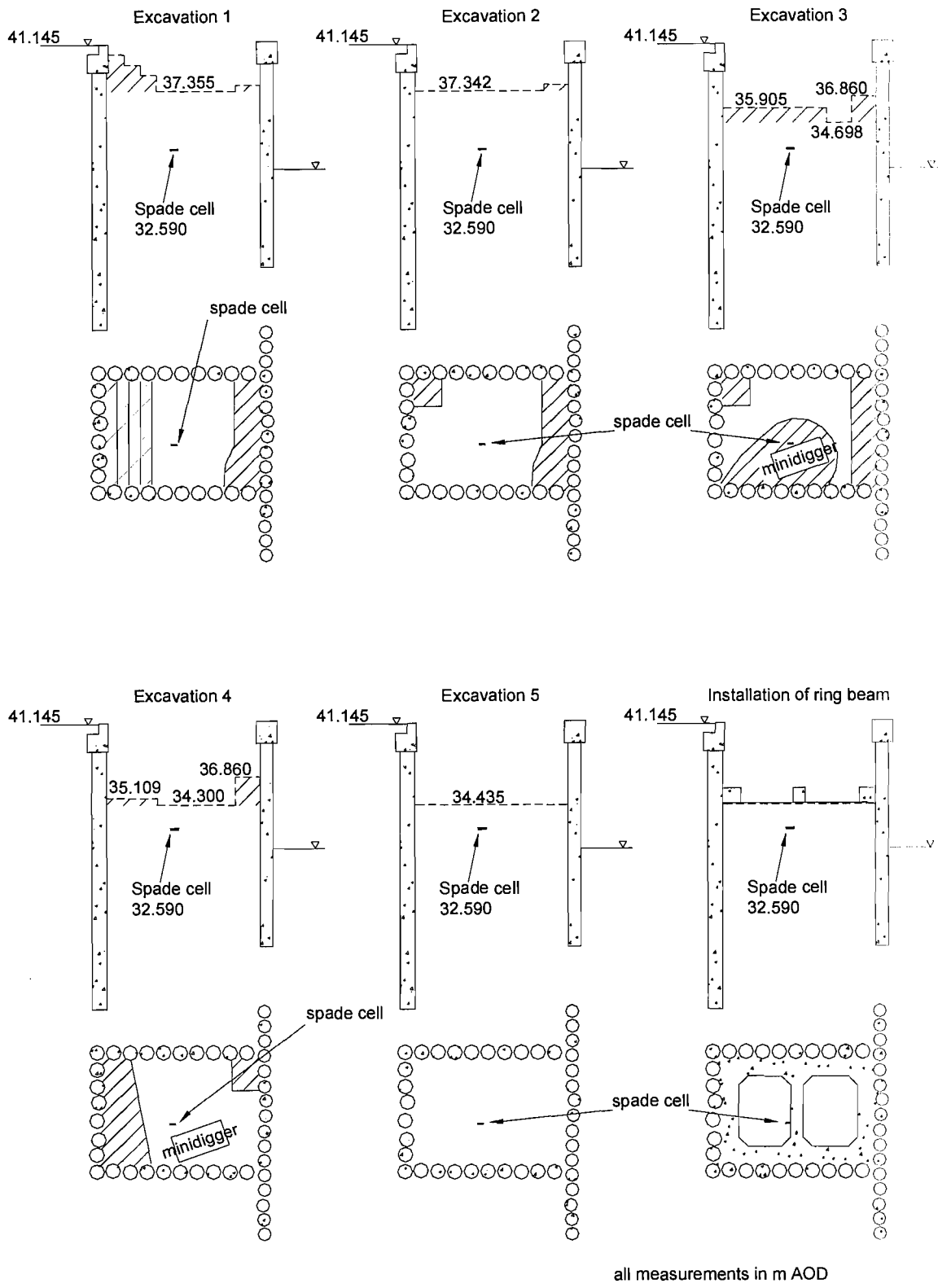

Figure 5-7: (a) Elevations and (b) plans detailing the excavation of material above spade cell in nadir sump

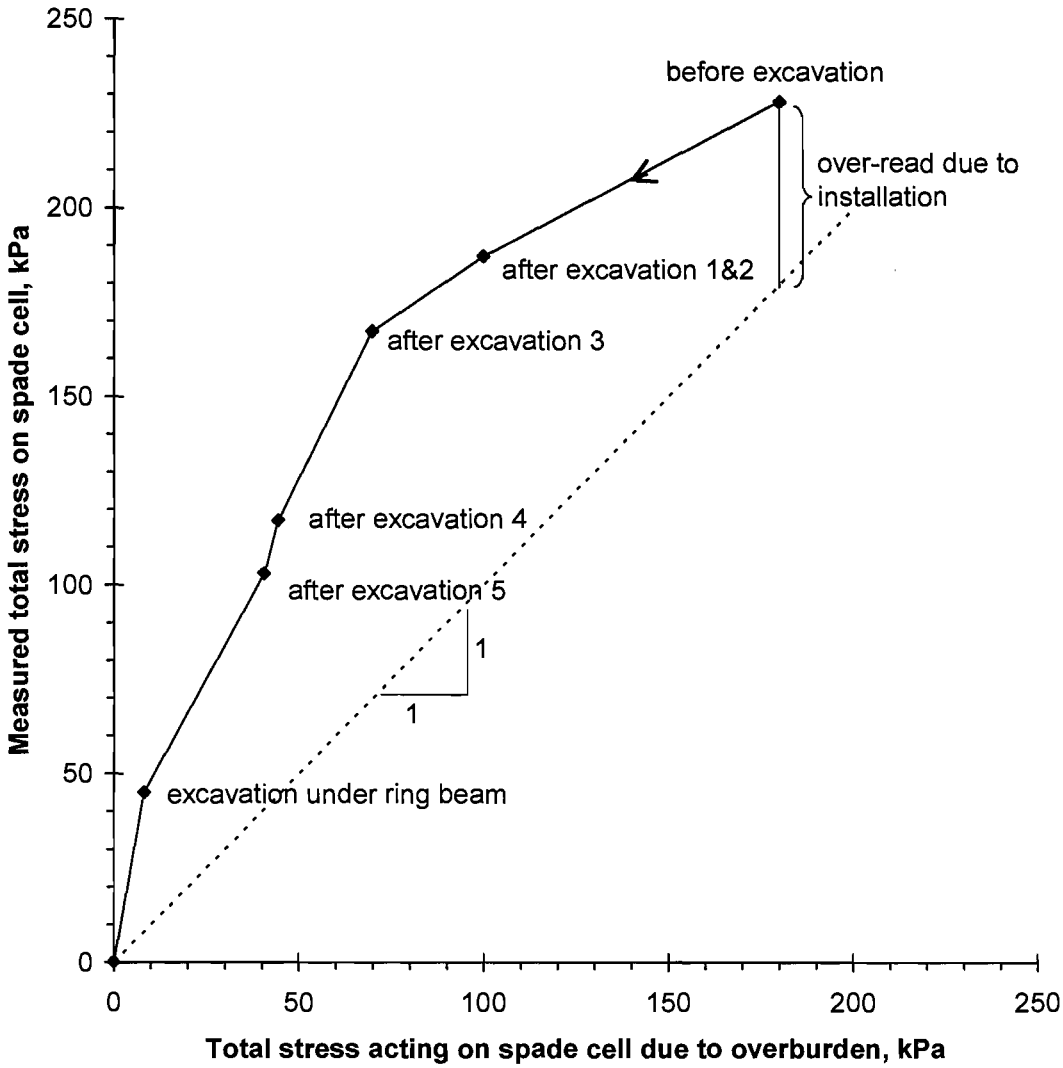

Figure 5-8: Measured total vertical stress versus overburden

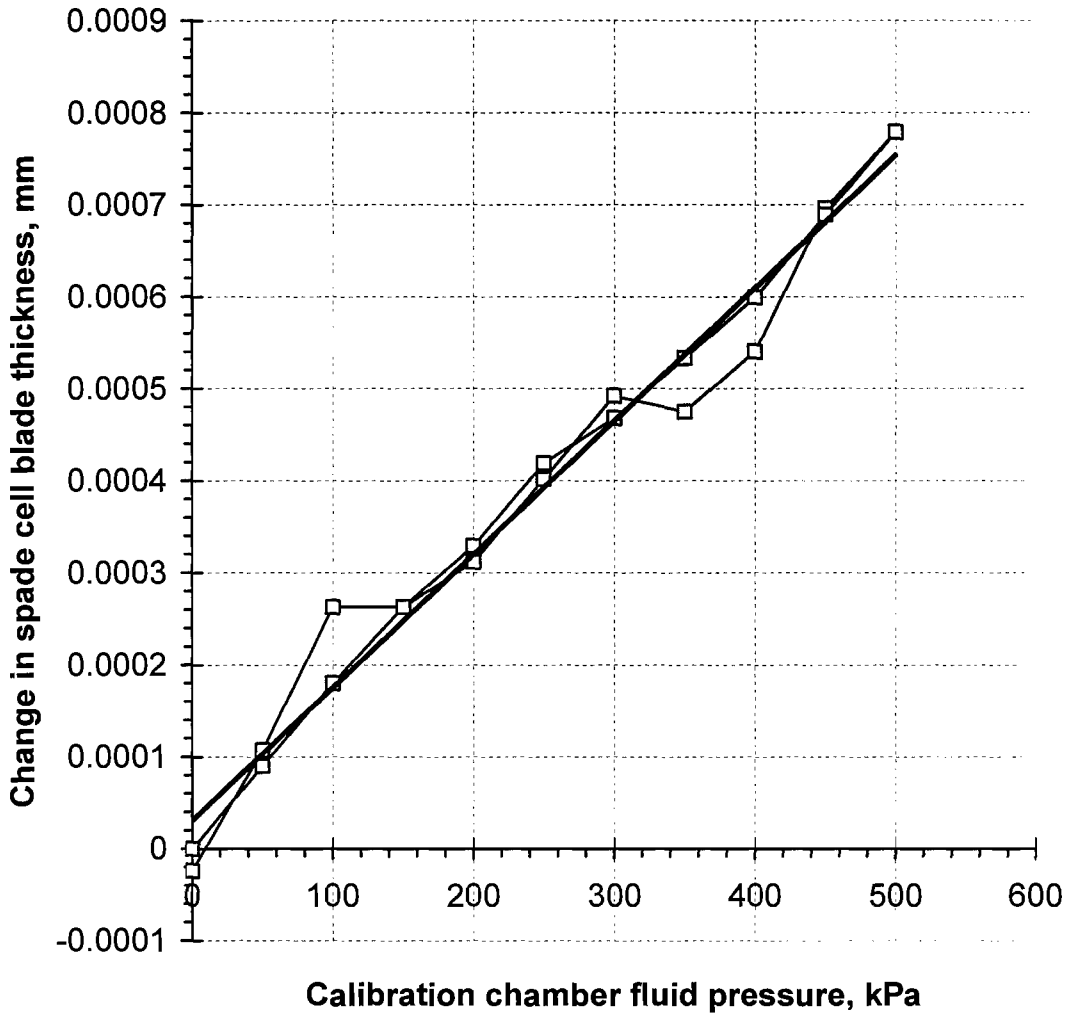

Figure 5-9: Nadir sump spade cell stiffness calibration

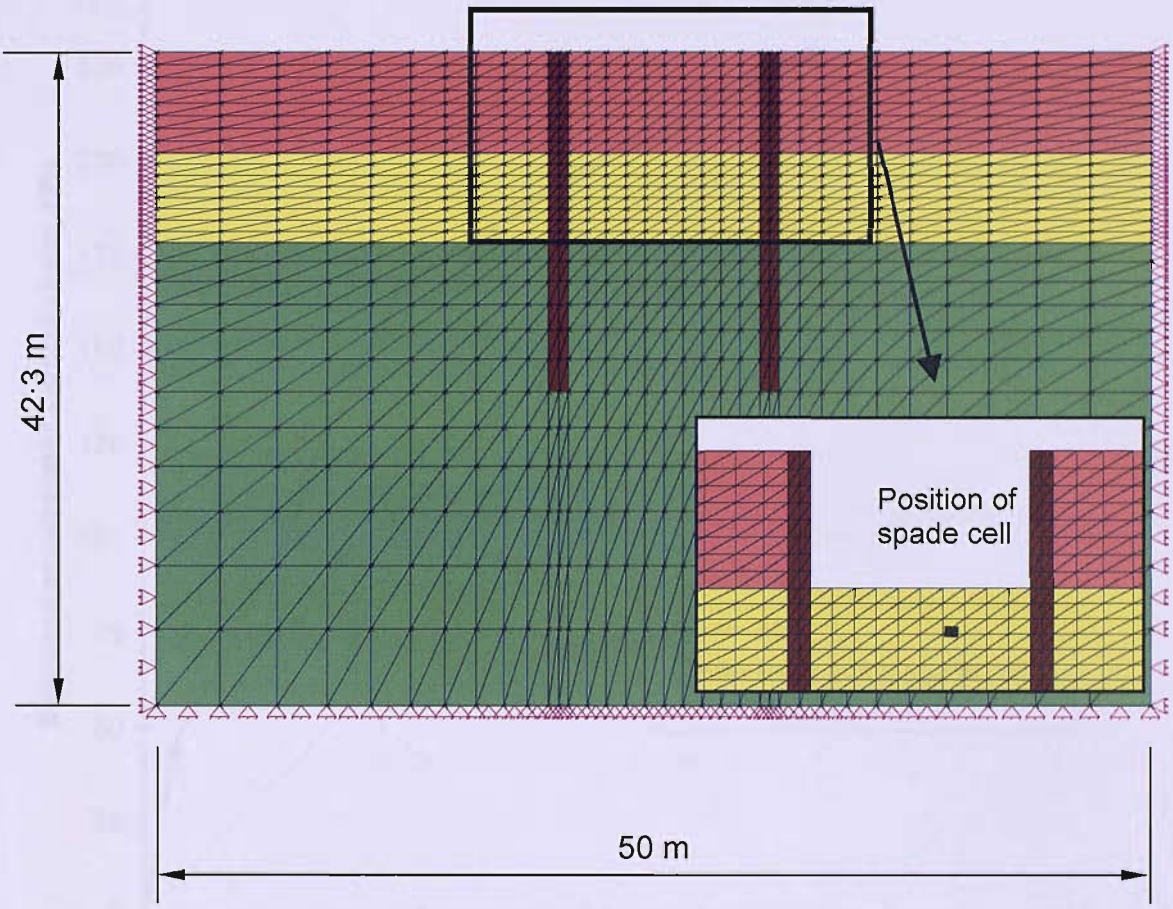

Figure 5-10: Finite element analysis mesh

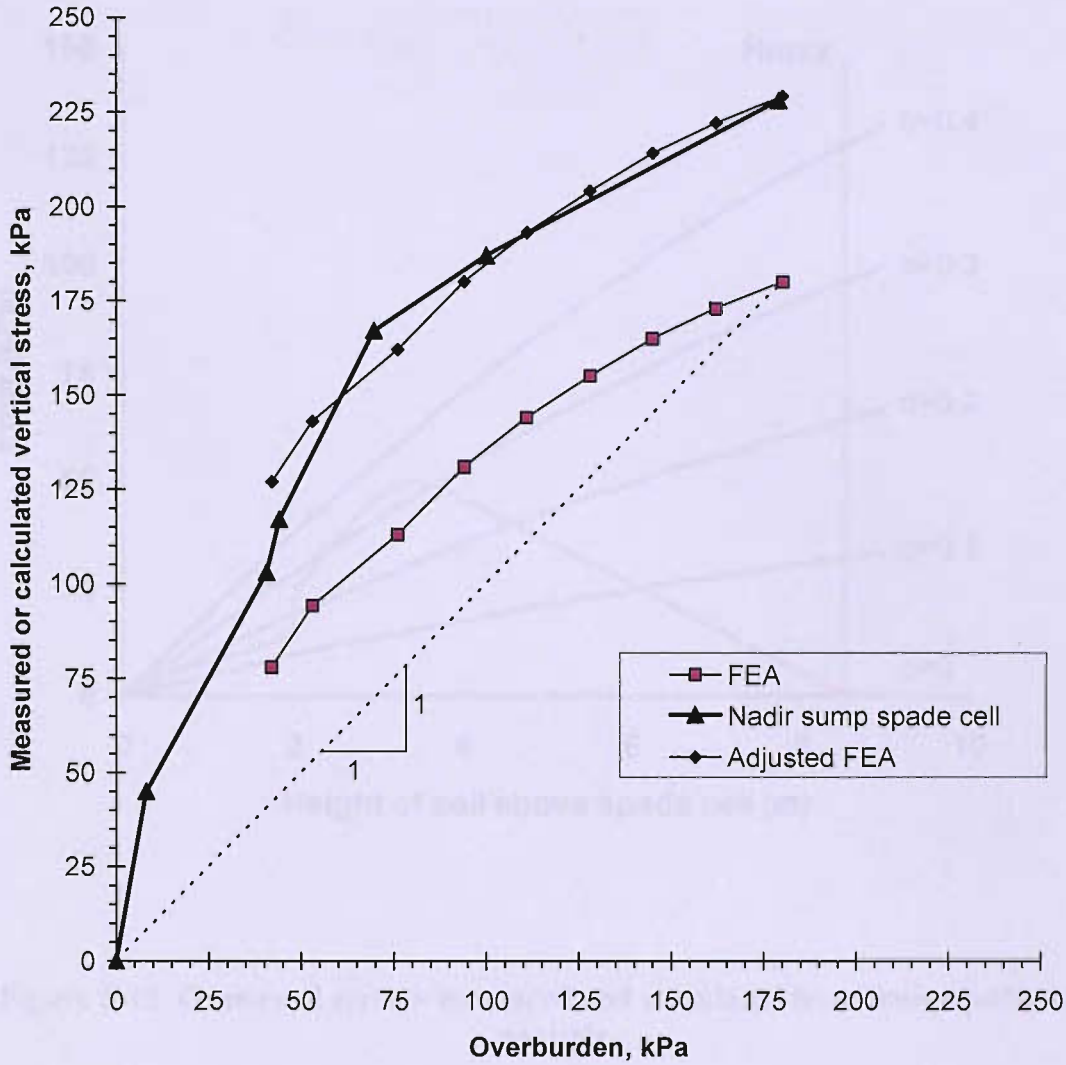

Figure 5-11: Measured and calculated vertical stresses against overburden

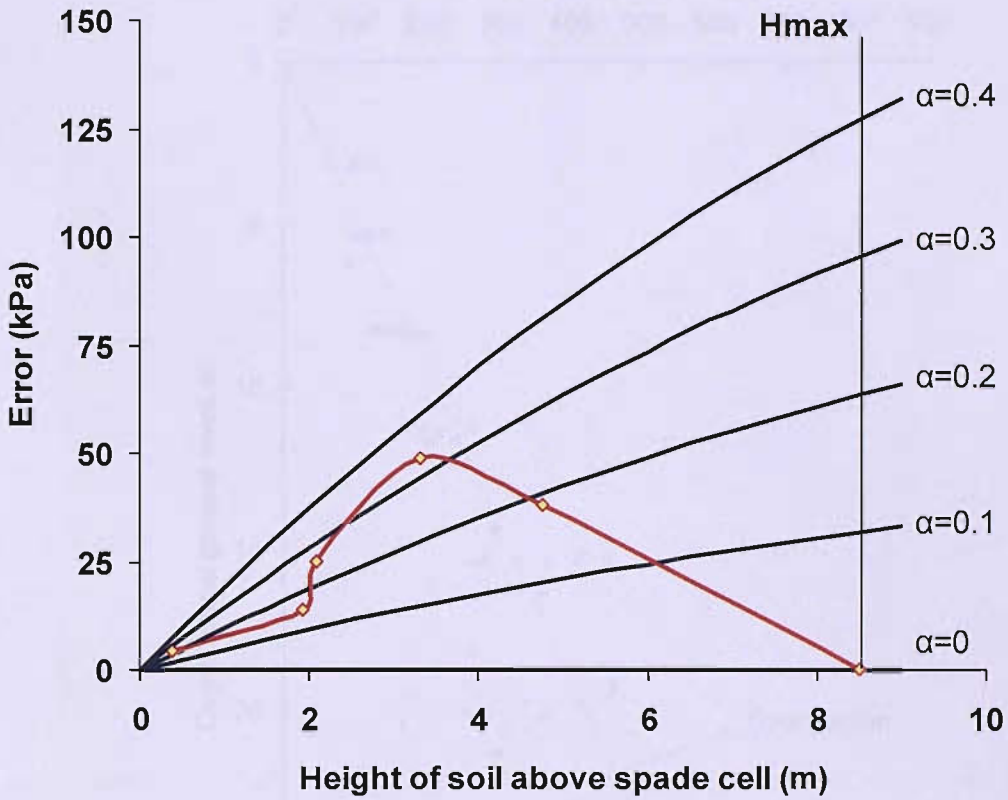

Figure 5-12: Over-read error – measured and calculated from limit equilibrium analysis

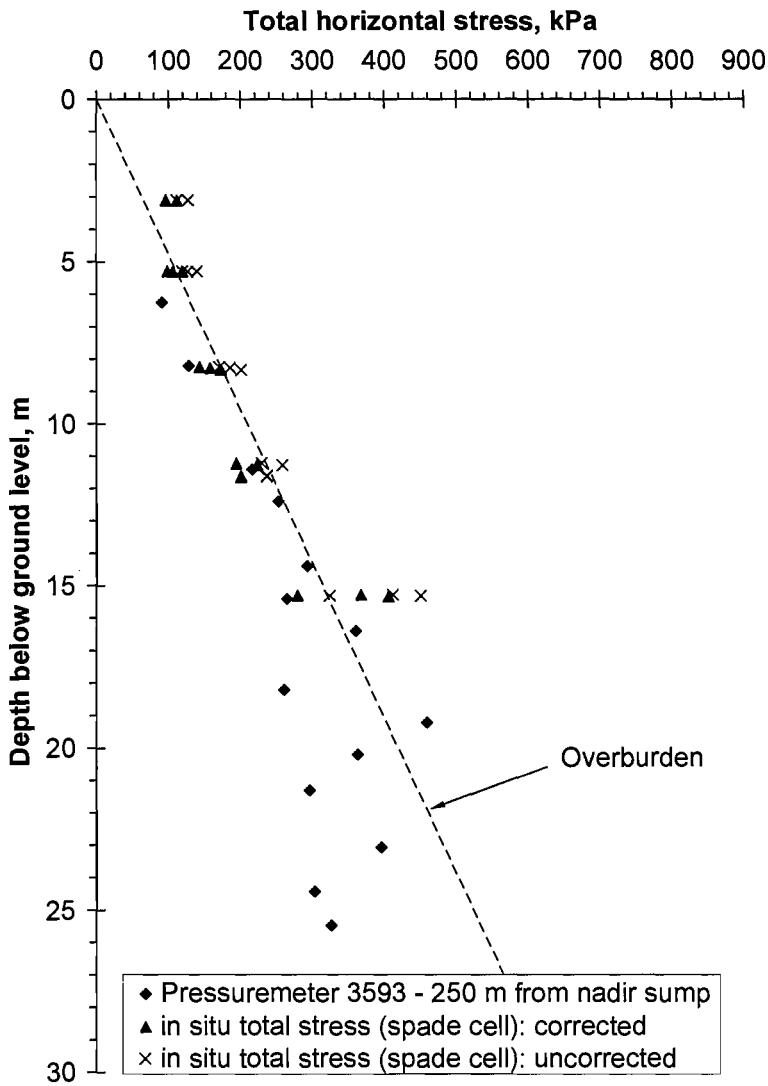

Figure 5-13: Comparison between spade cell readings corrected by 0·35 c_u and self-boring pressuremeter test results

Figure 5-14: Spade cell installation

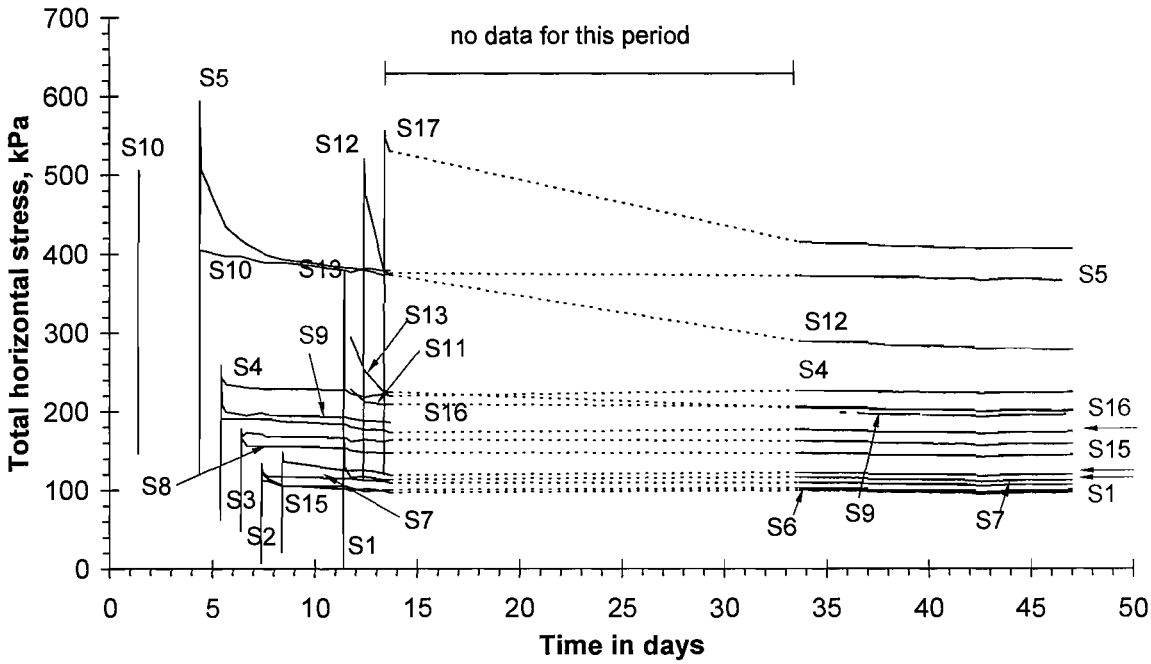

(a) Total horizontal stresses

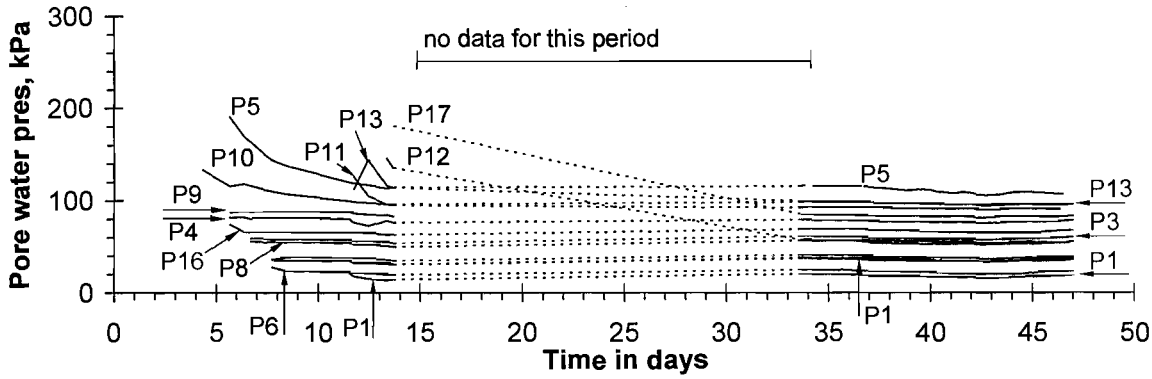

(b) Pore water pressures

Figure 5-15: Spade cell measurements taken between their installation and wall installation

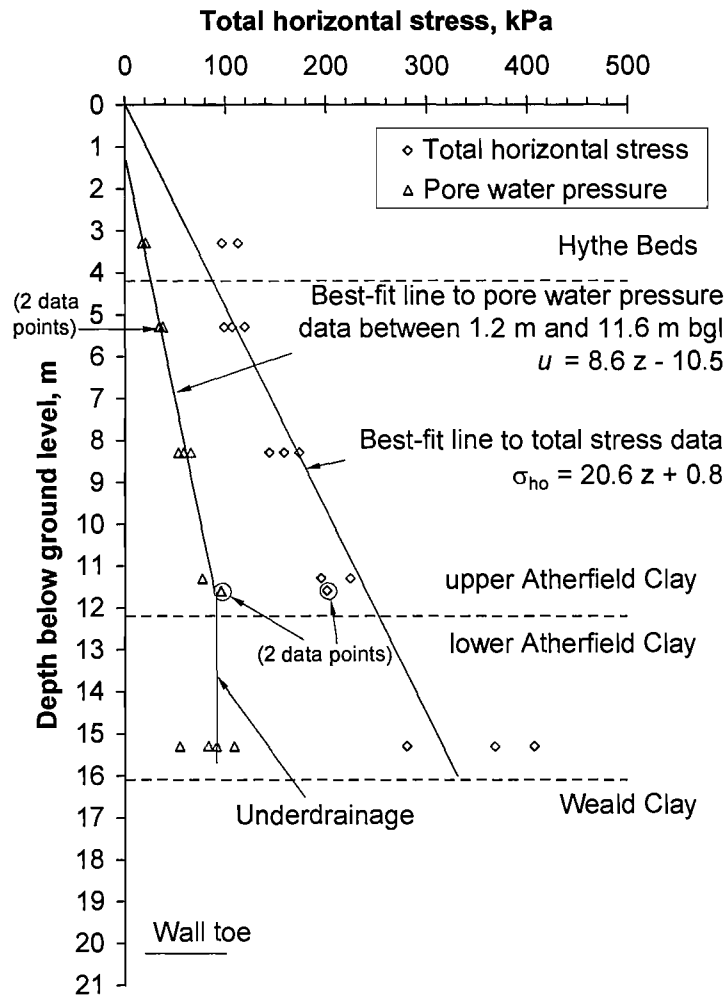

Figure 5-16: Stabilized readings of horizontal total stress and pore water pressure from all spade cells and piezometers, plotted against depth below original ground level (before wall installation)

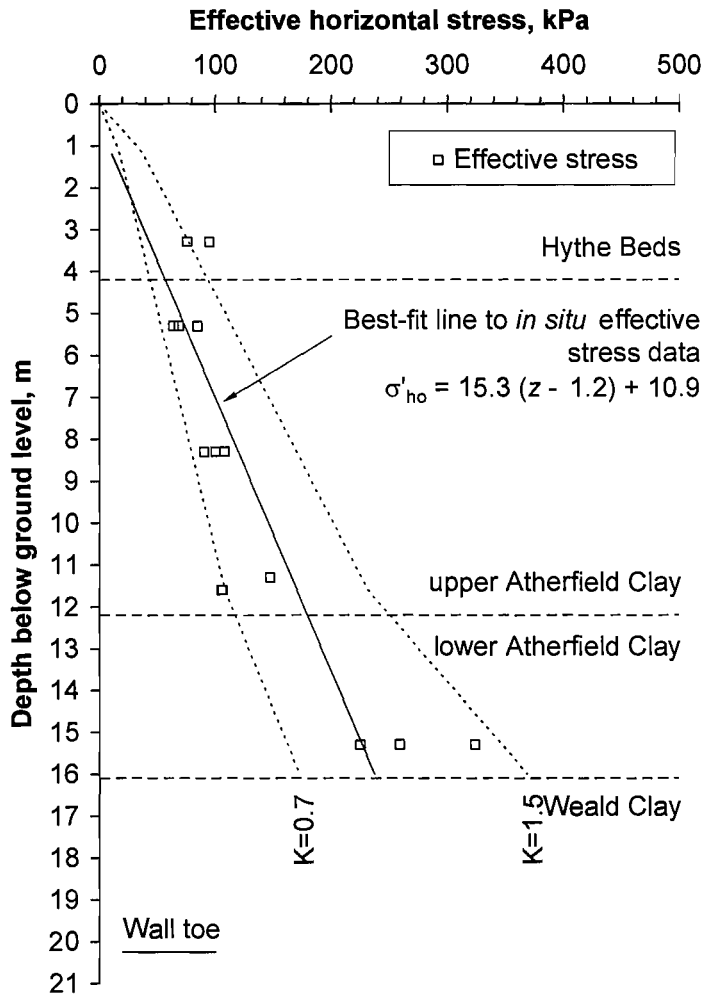

Figure 5-17: The profile of effective horizontal stress σ'_{ho} with depth (obtained by subtracting the measured pore pressure from the total horizontal stress at each location)

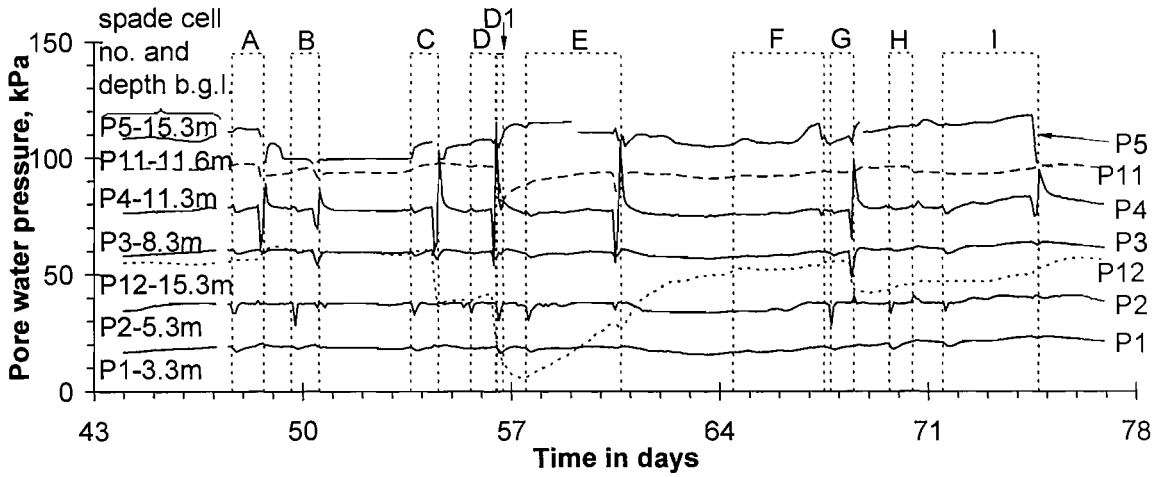

(a) 1·275 m from the wall

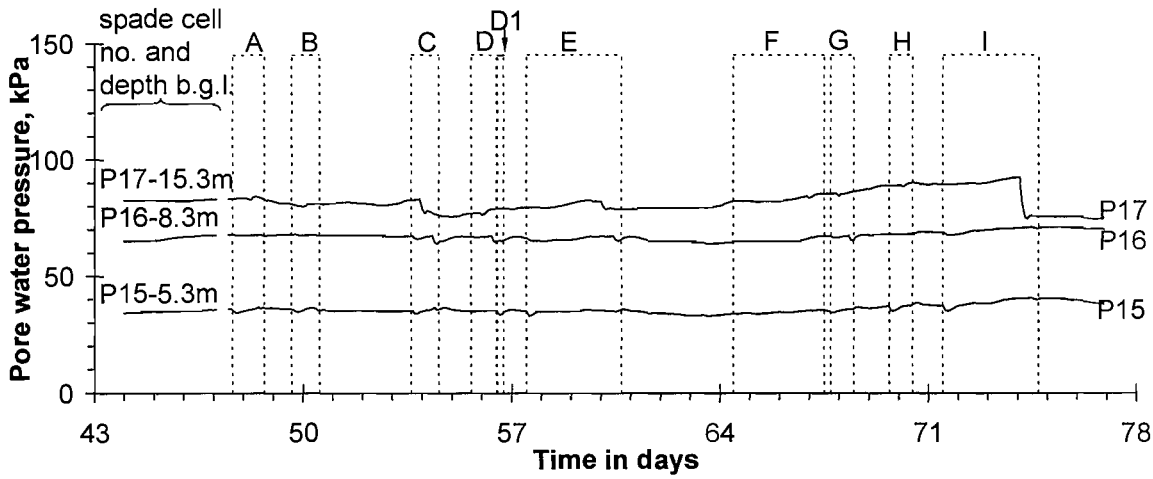

(b) 2·375 m from the wall

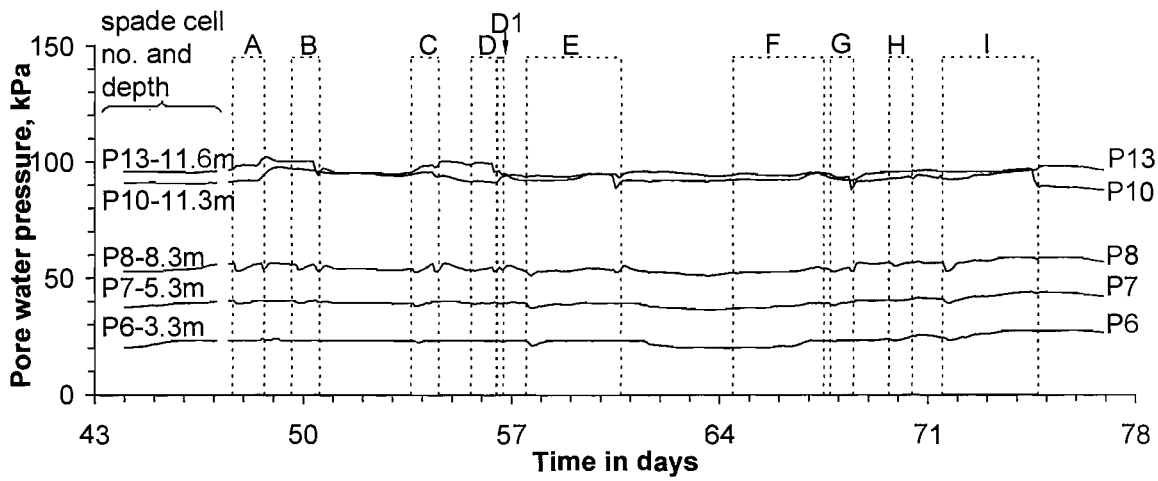

(c) 3·475 m from the wall

Figure 5-18: Piezometer readings over the period of wall installation

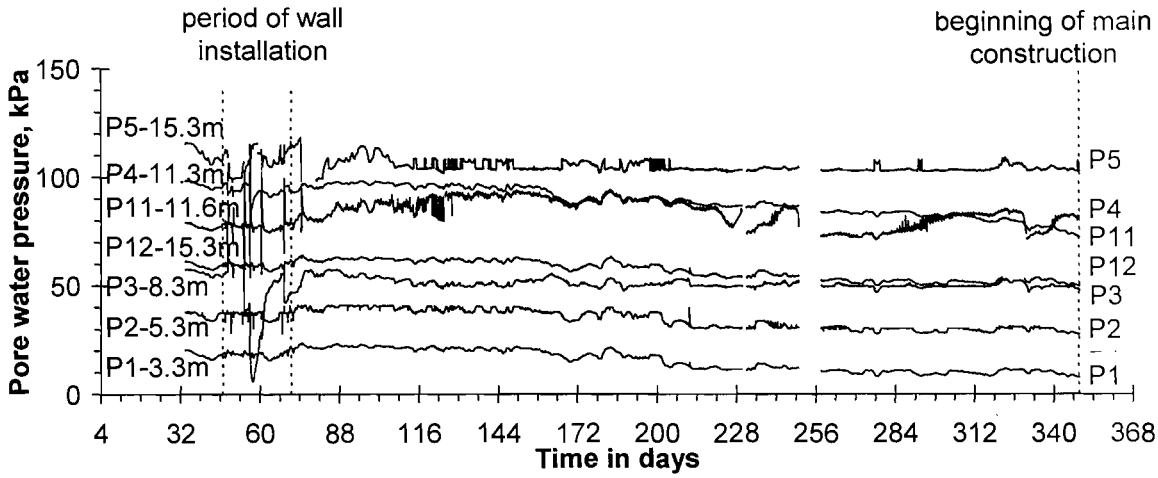

(a) 1·275 m from the wall

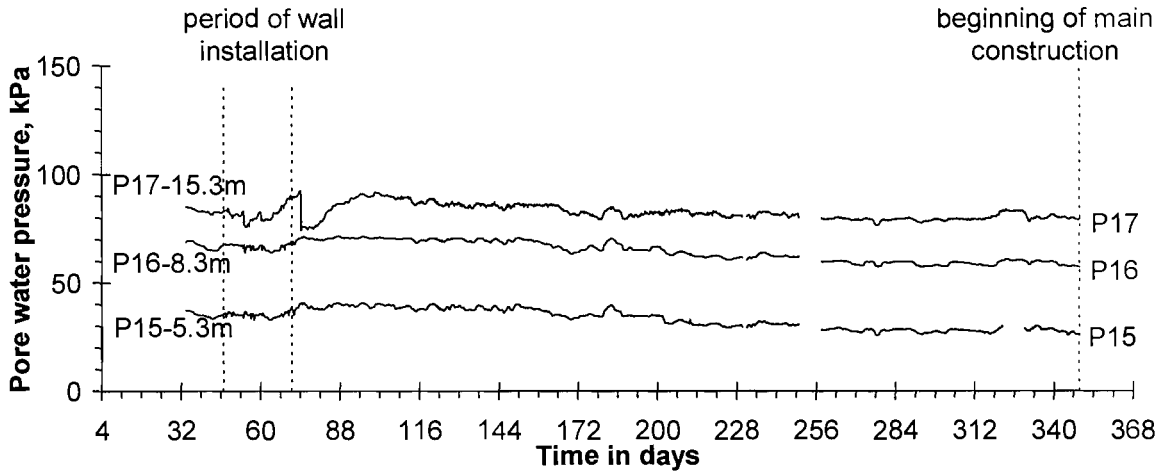

(b) 2·375 m from the wall

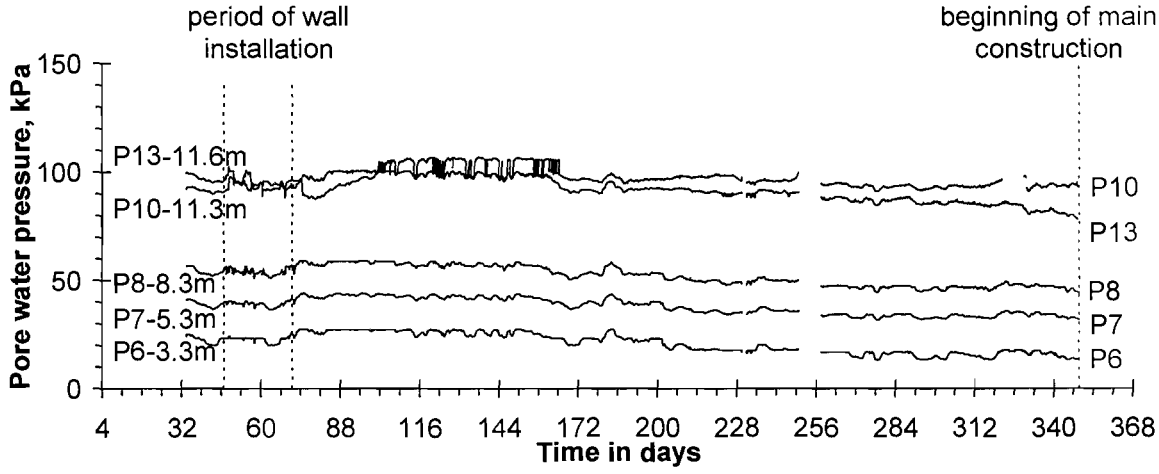

(c) 3·475 m from the wall

Figure 5-19: Pore water pressures measured before, during and 10 months wall installation

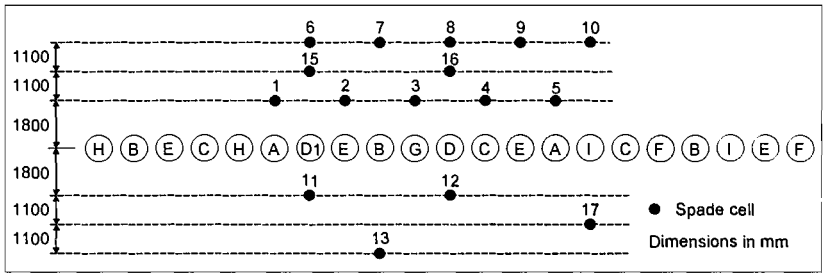

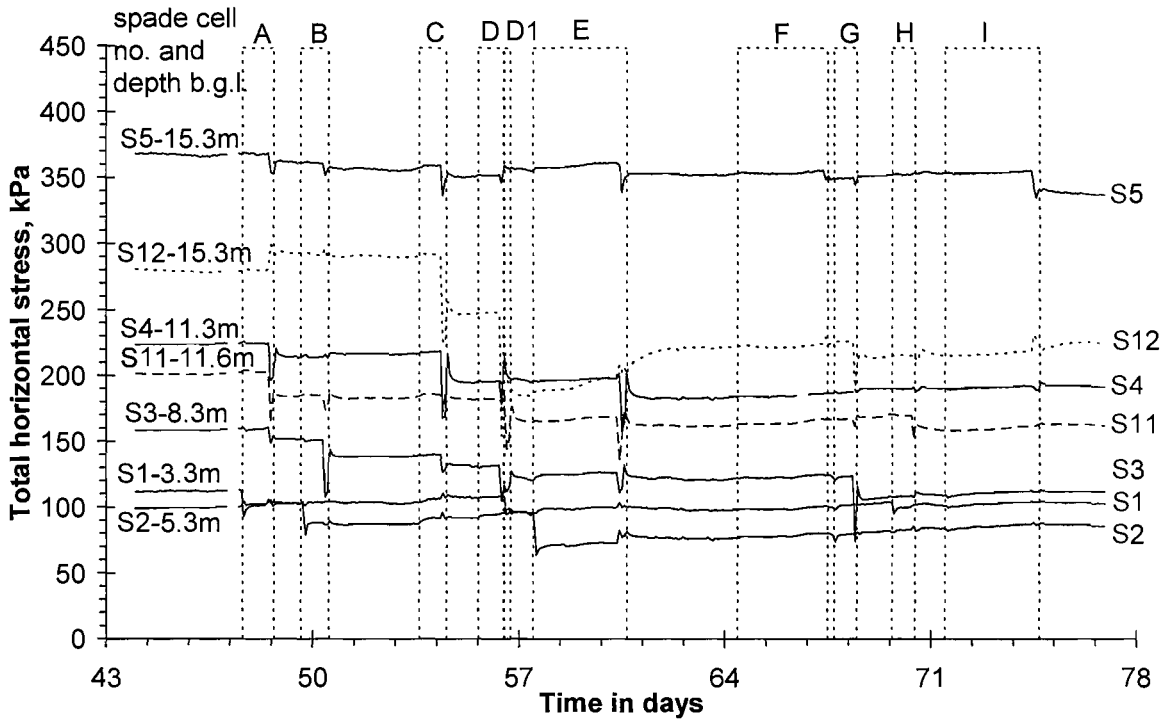

(a) 1·275 m from the wall

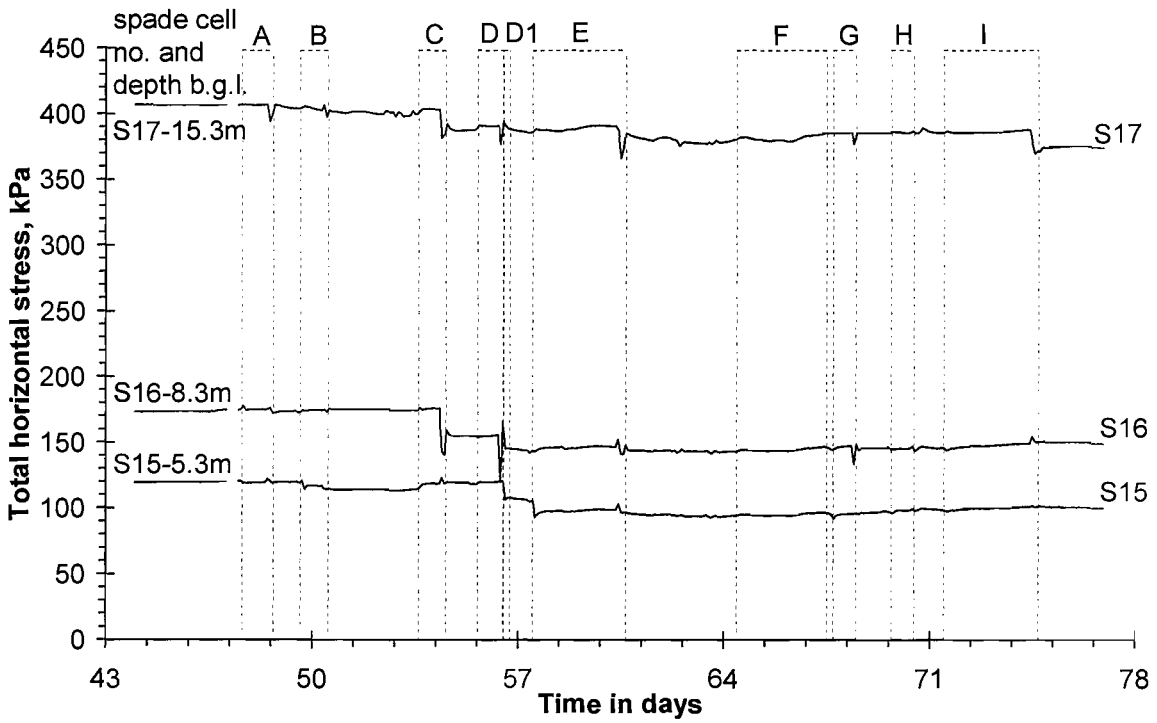

(b) 2·375 m from the wall

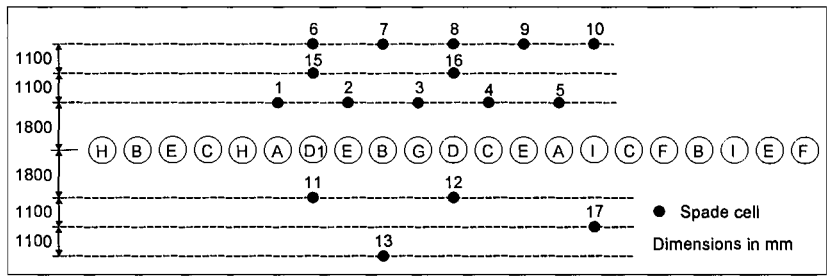

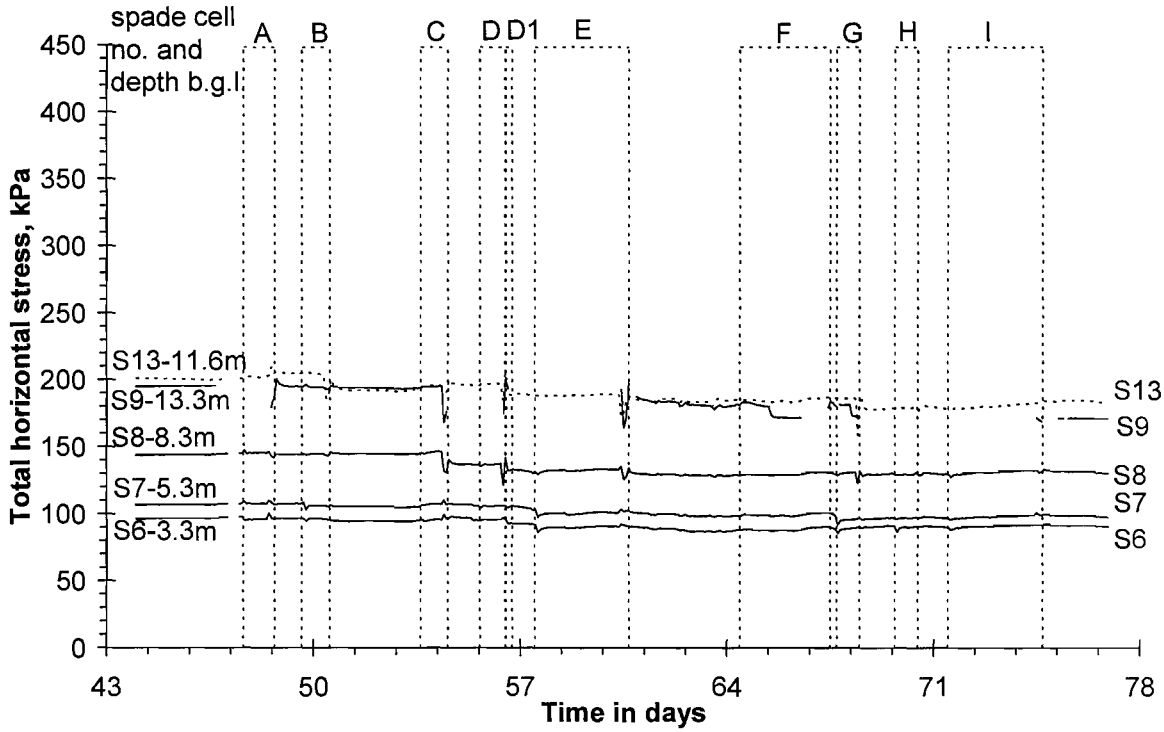

(c) 3·475 m from the wall

Figure 5-20: Total horizontal stress measurements taken during the period of wall installation

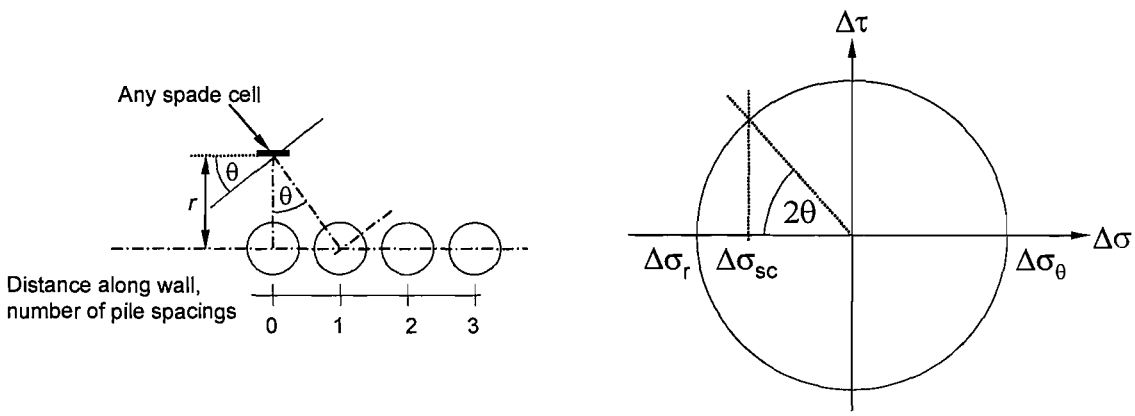

Figure 5-21: Pile installation sequence for the elastic analysis and Mohr circle showing calculation of correction for stress change measured on spade cell

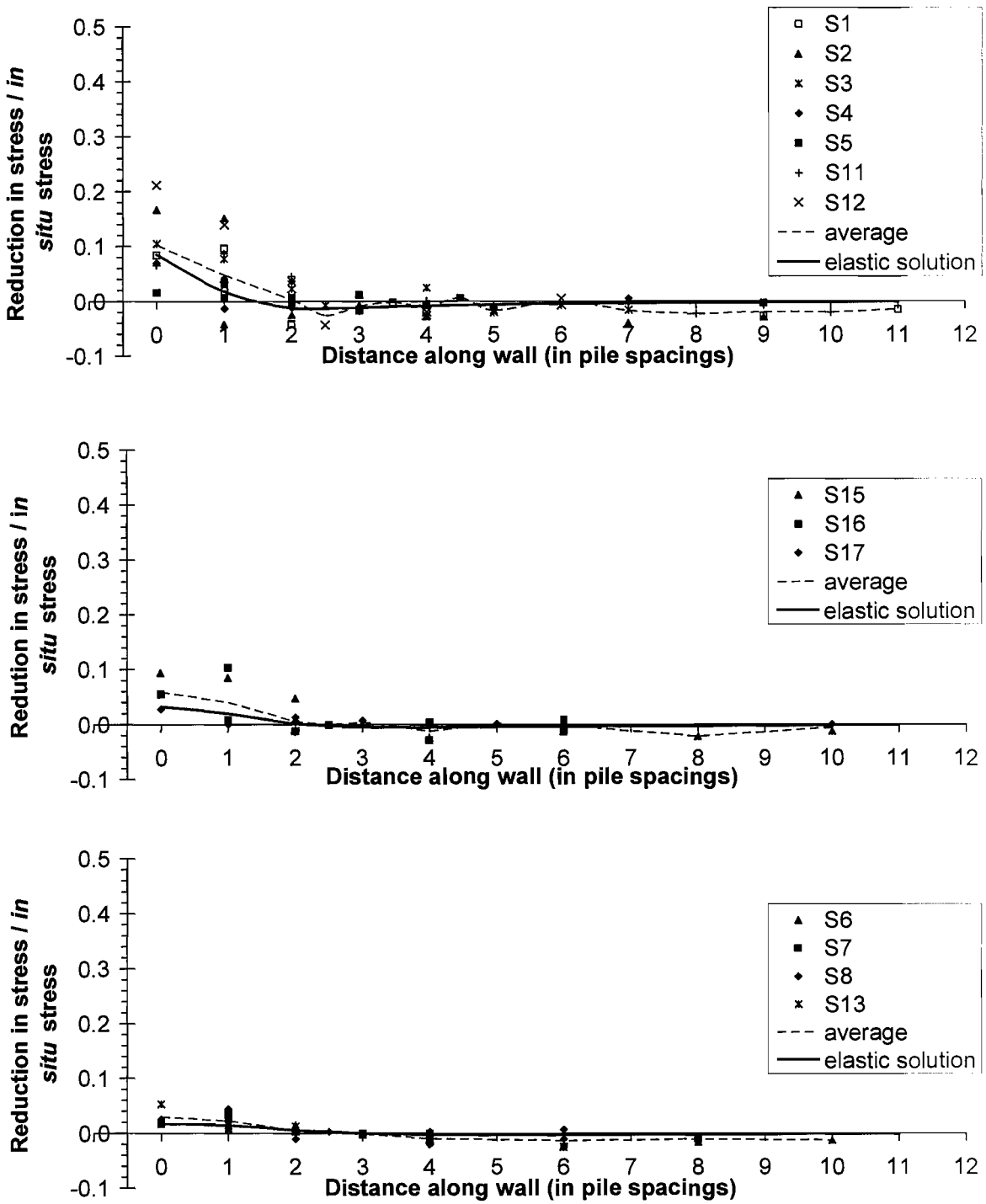

Figure 5-22: Measured reduction in total horizontal stress normalised with respect to the *in situ* total horizontal stress (showing prediction from elastic analysis)

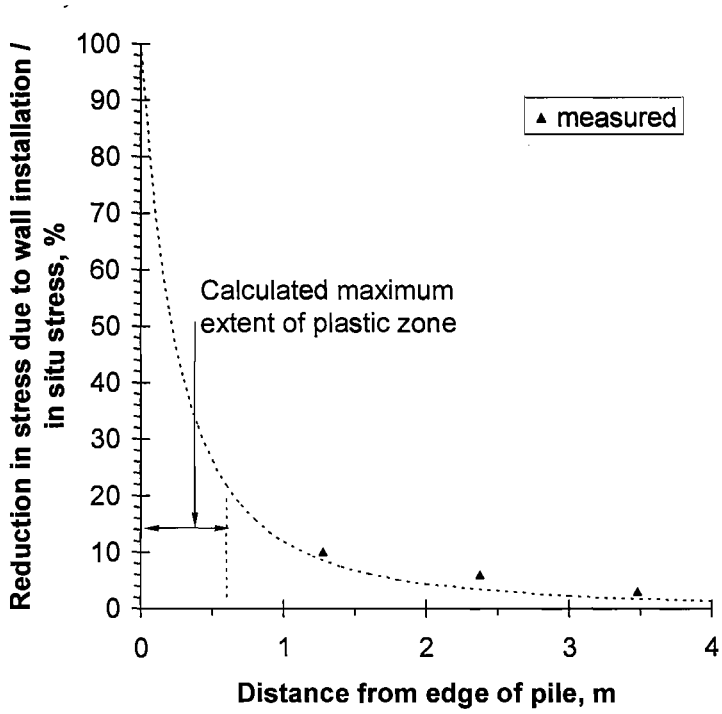

Figure 5-23: Reduction in total horizontal stress due to installation of pile nearest to spade cell only with distance from the wall compared with the elastic prediction

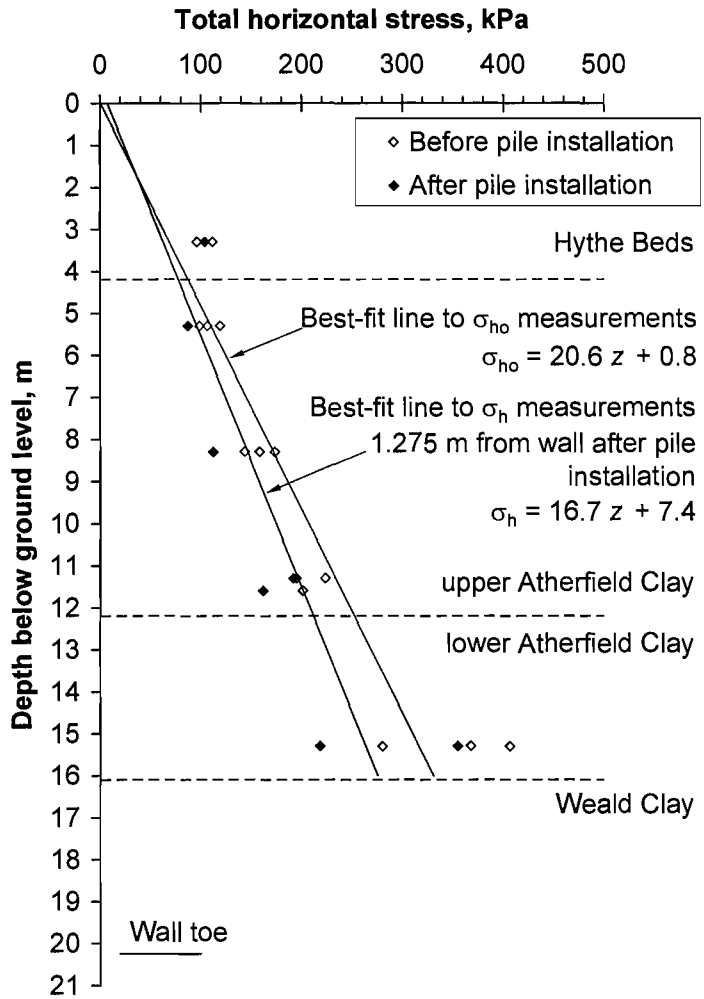

Figure 5-24: Total horizontal stresses measured by all spade cells before wall installation and by those 1.275 m from the edge of the wall after wall installation

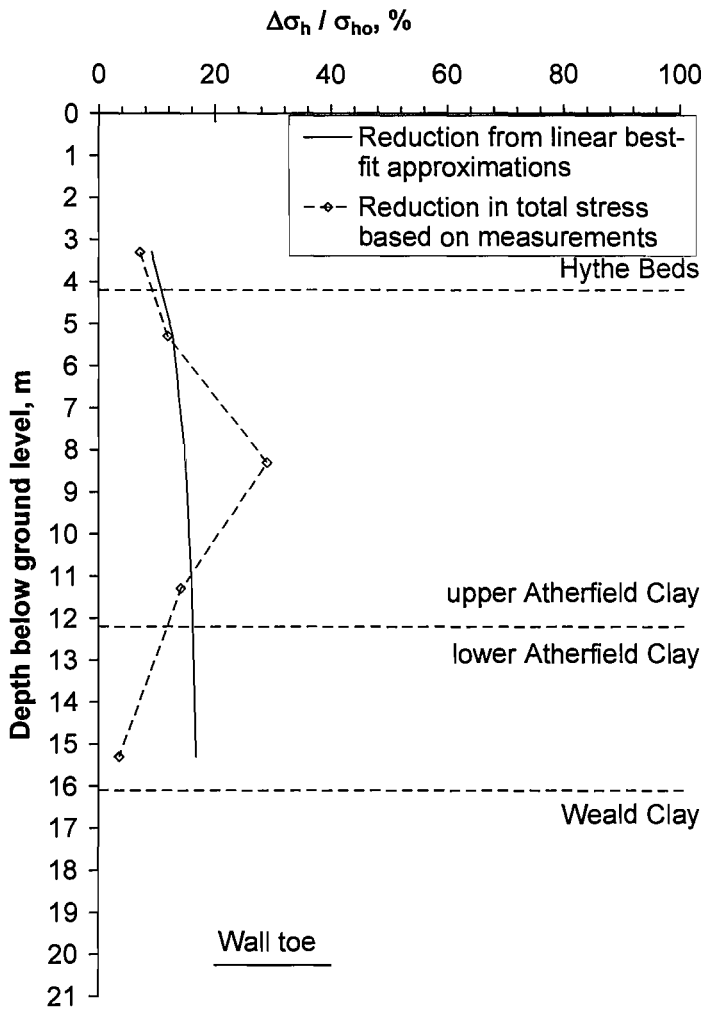

Figure 5-25: Change in total horizontal stress

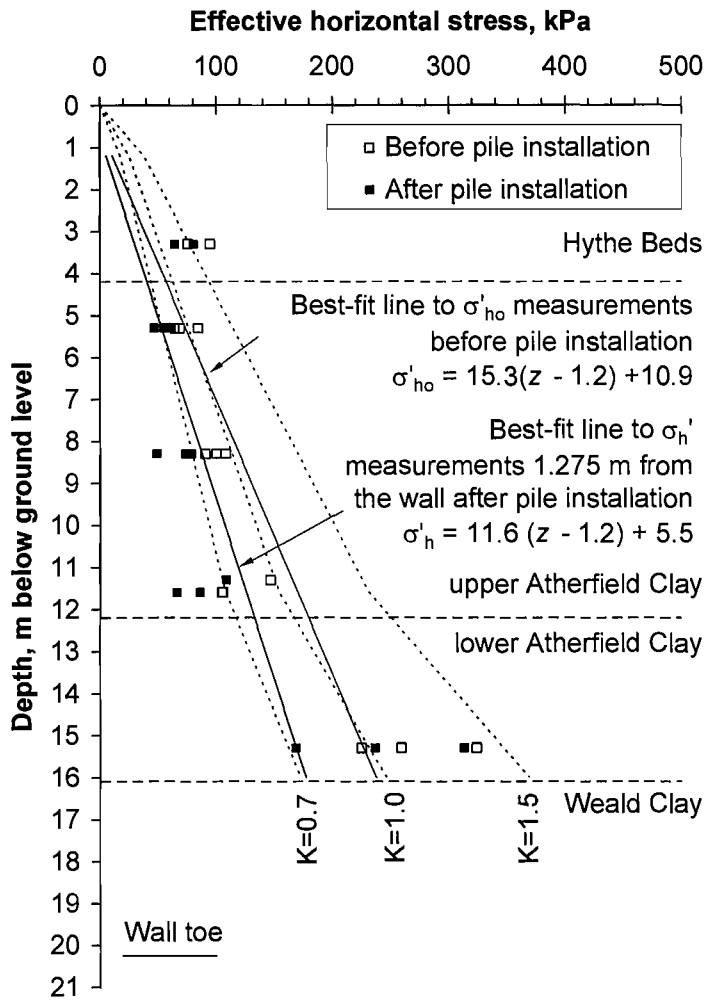

Figure 5-26: Effective horizontal stresses measured by all spade cells before wall installation and by those 1.275 m from the edge of the wall after wall installation

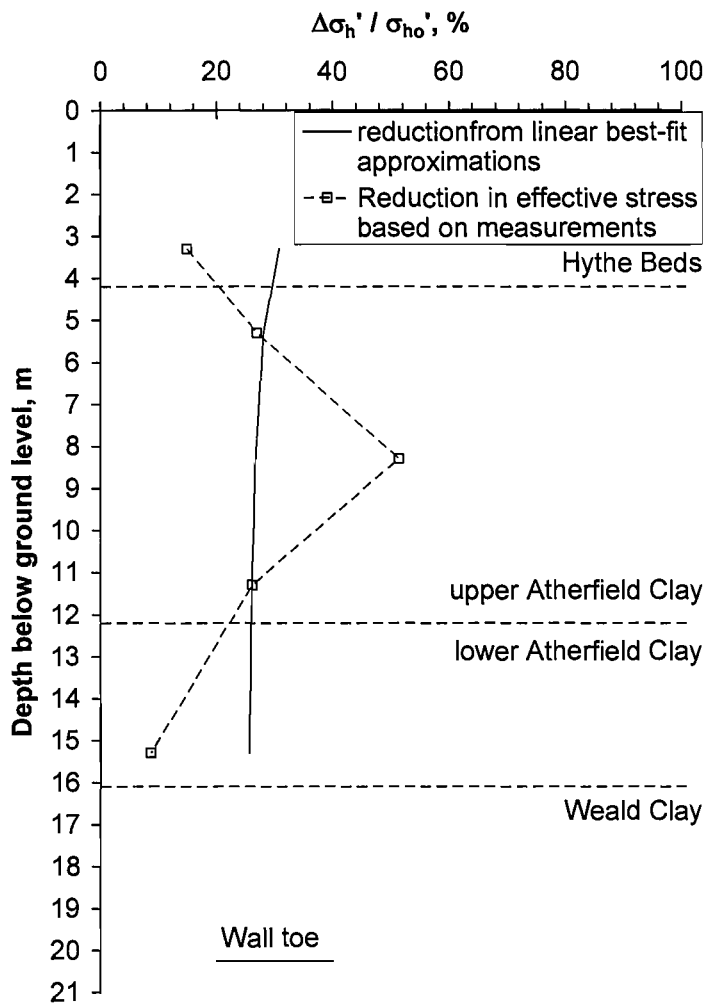

Figure 5-27: Change in effective horizontal stress

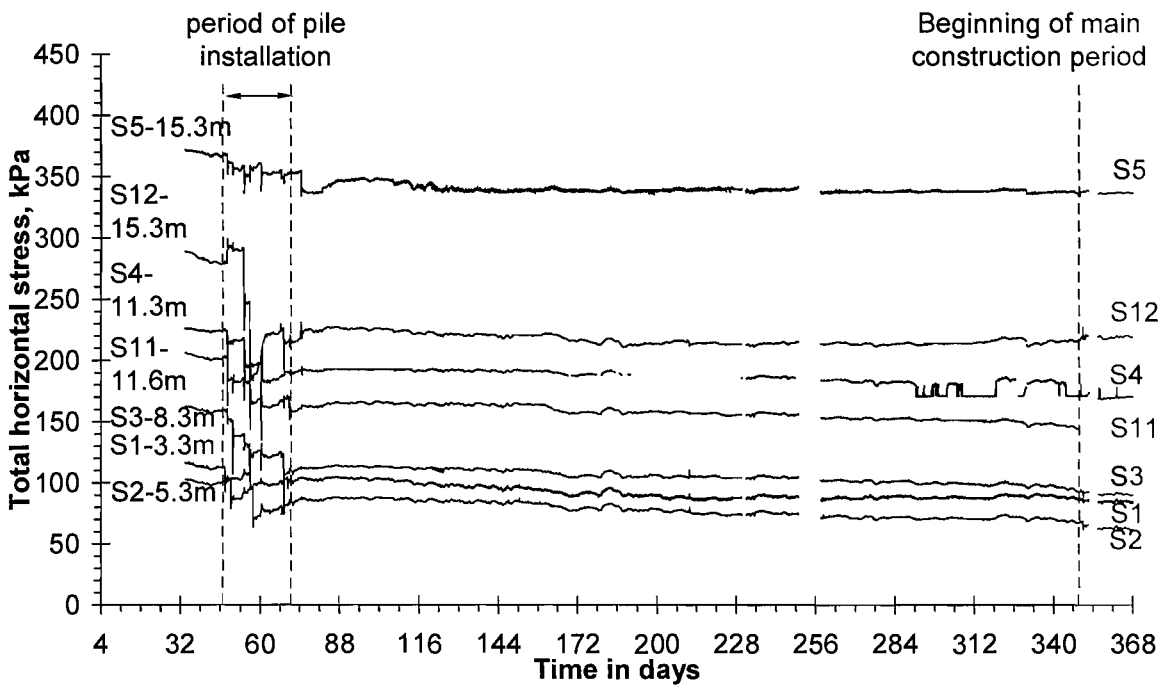

(a) 1·275 m from the wall

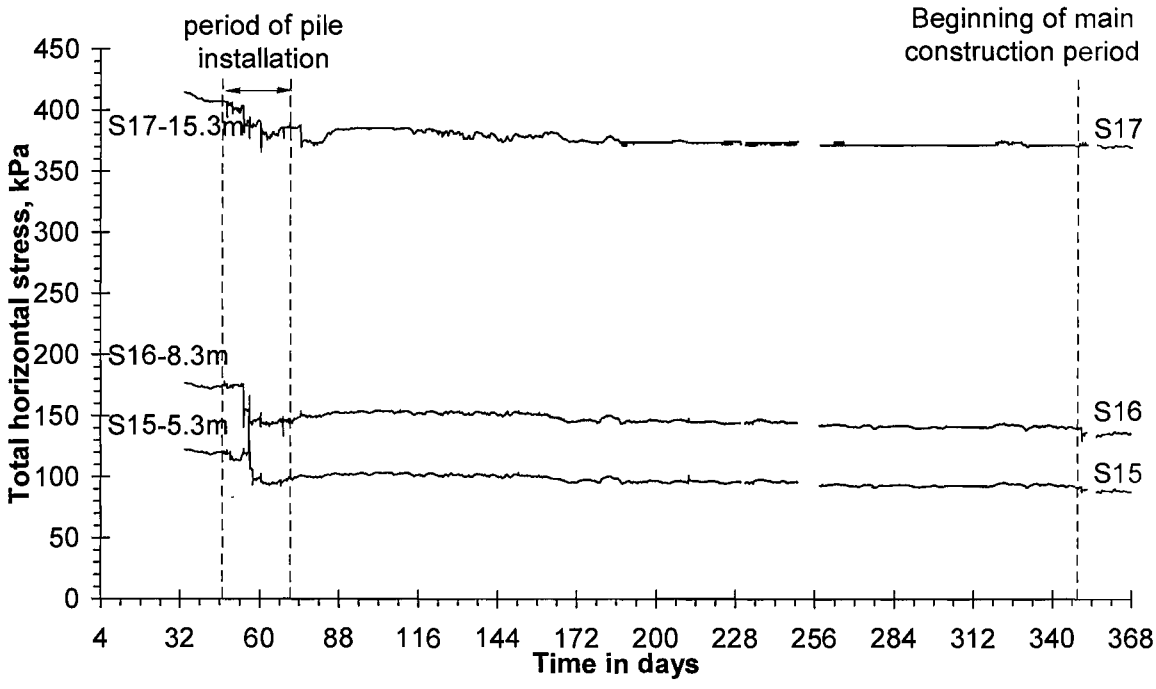

(b) 2·375 m from the wall

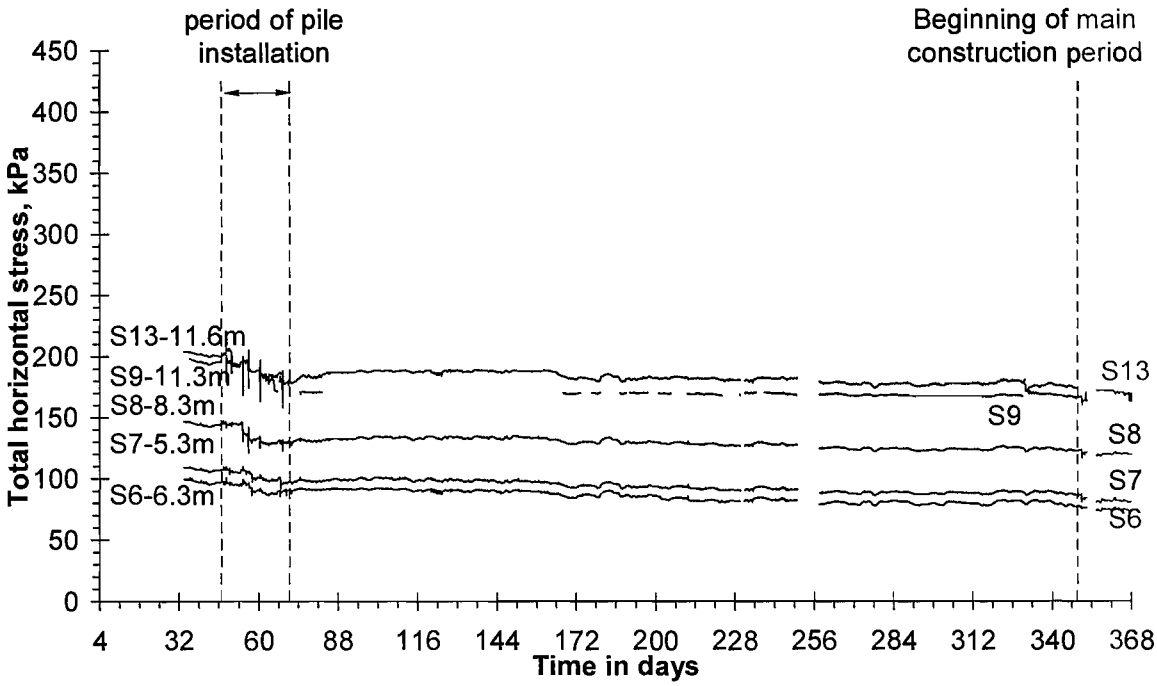

(c) 3·475 m from the wall

Figure 5-28: Total horizontal stress measured before, during and 10 months after wall installation

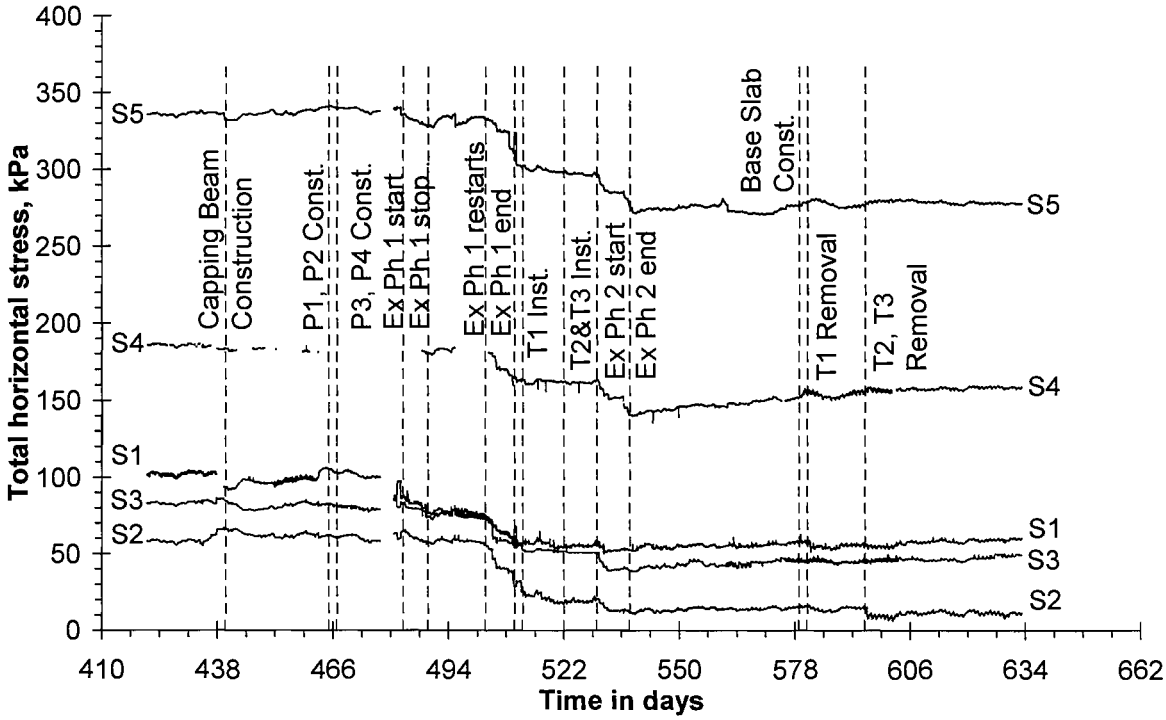

(a)

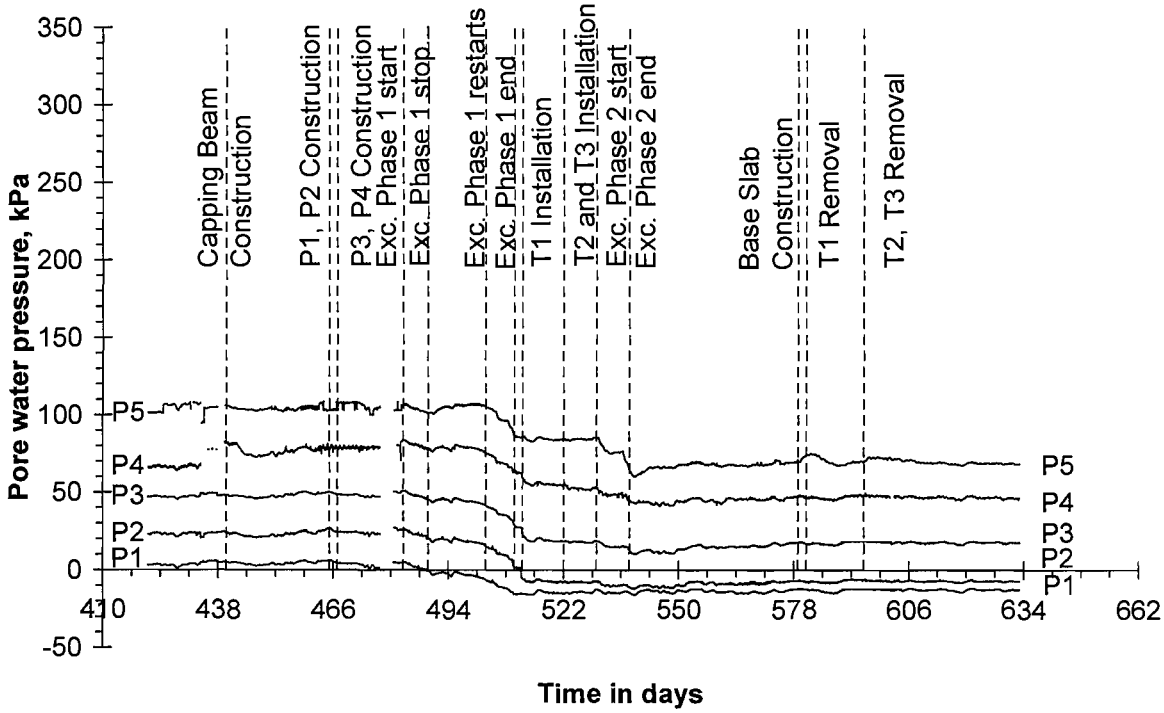

(b)

Figure 5-29: Total pressure and pore water pressure measured 1·275 m from the back of the wall during the construction period

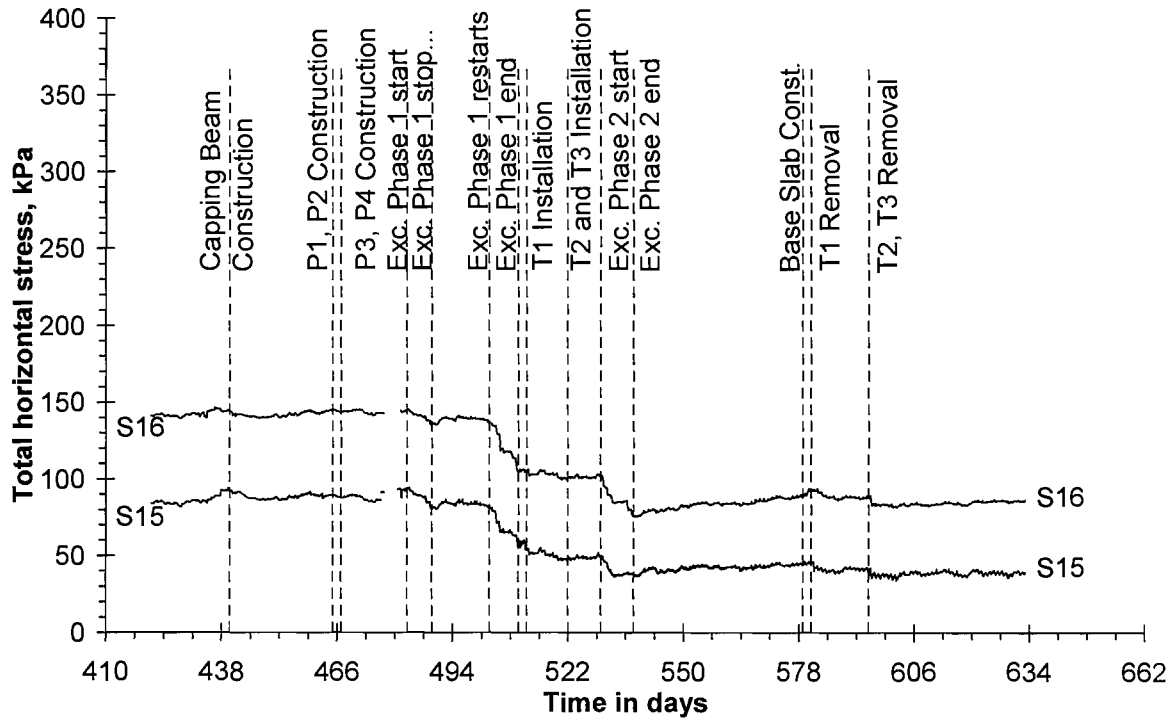

(a)

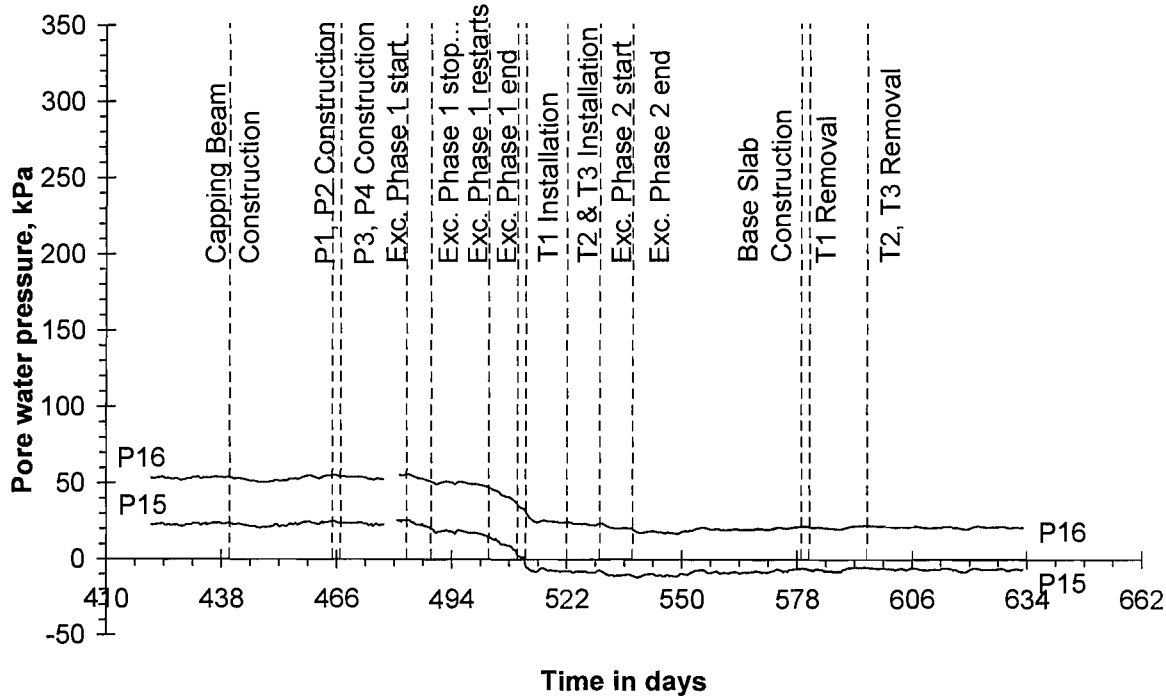

(b)

Figure 5-30: Total pressure and pore water pressure measured 2·375 m from the back of the wall during the construction period

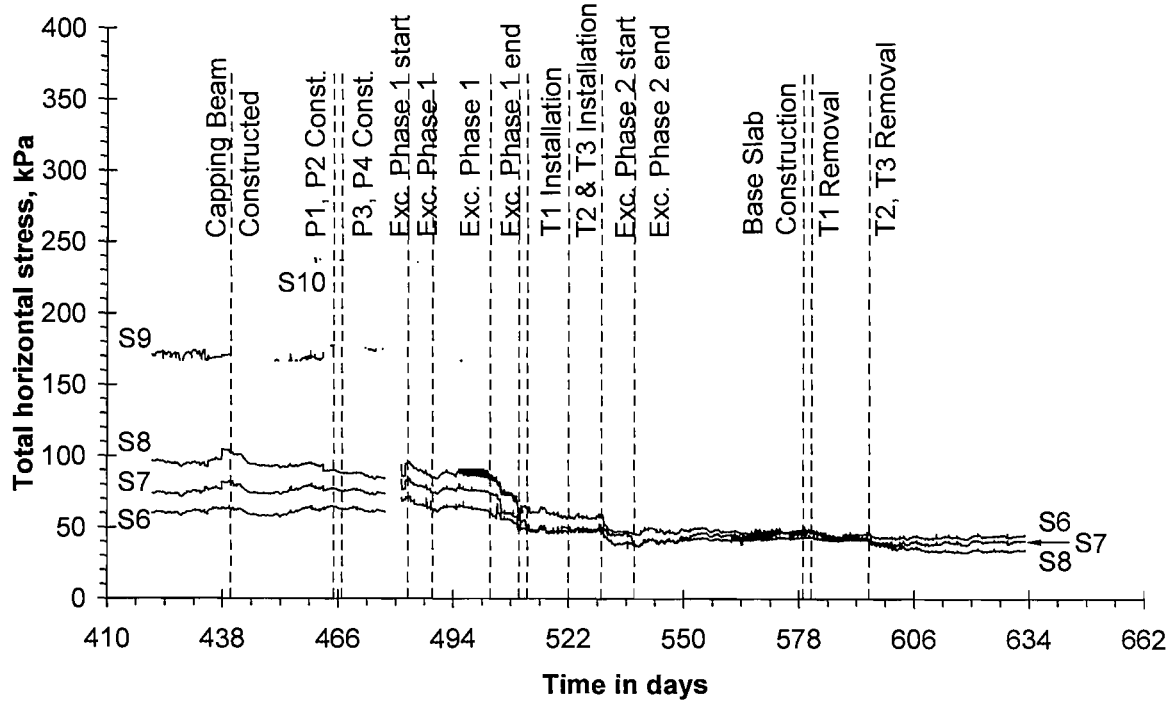

(a)

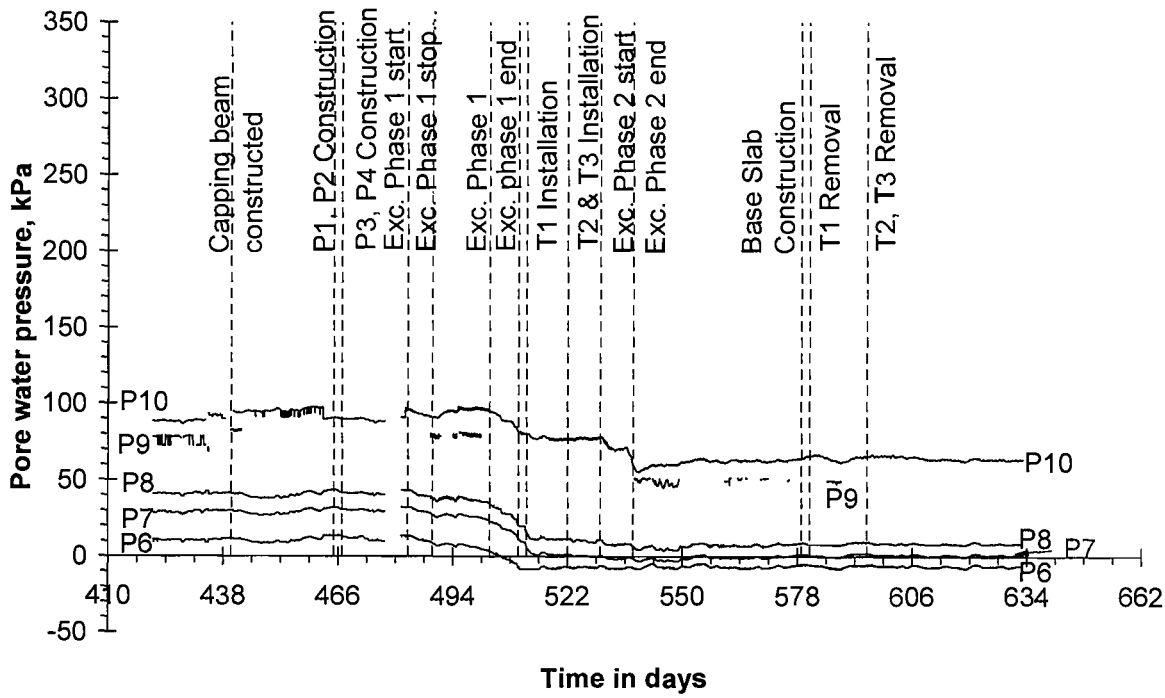

(b)

Figure 5-31: Total pressure and pore water pressure measured 3·475 m from the back of the wall during the construction period

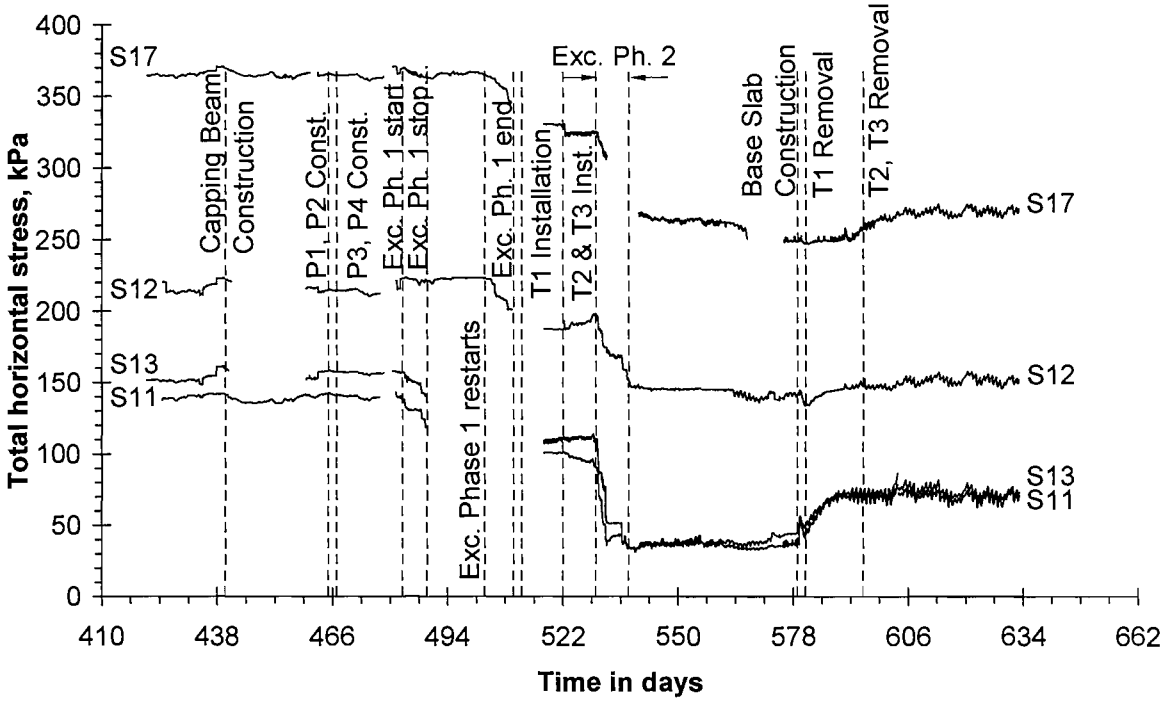

(a)

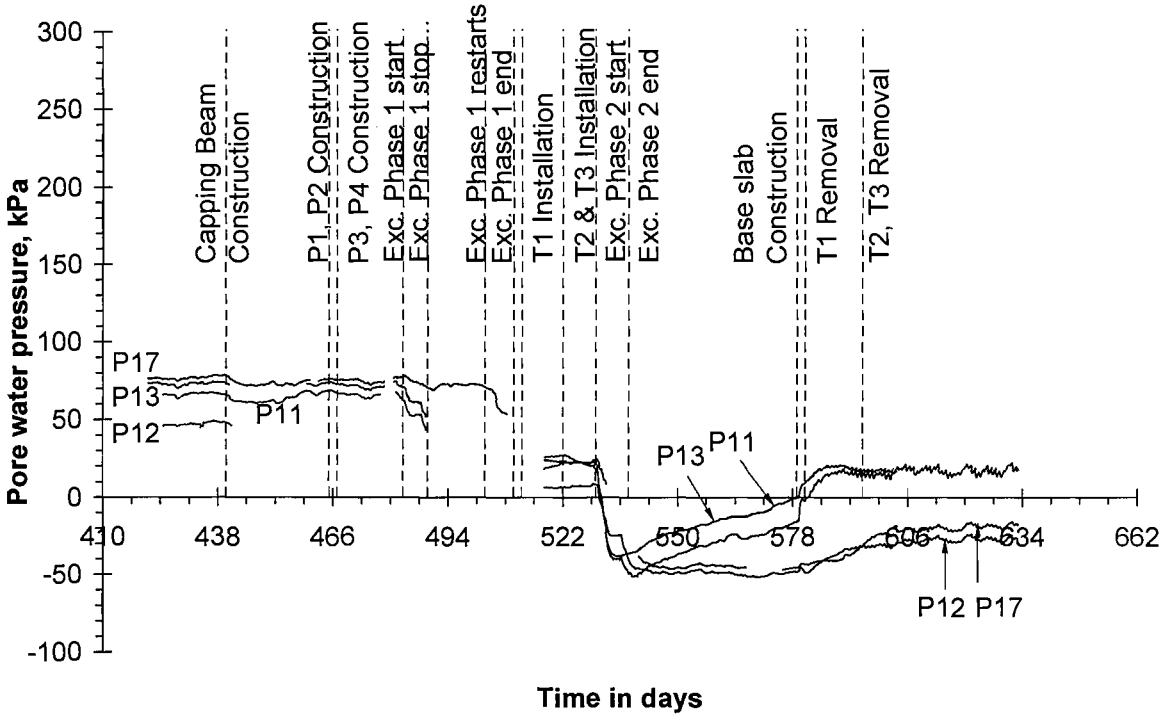

(b)

Figure 5-32: Total horizontal stress and pore water pressure measured in front of the wall during the construction period

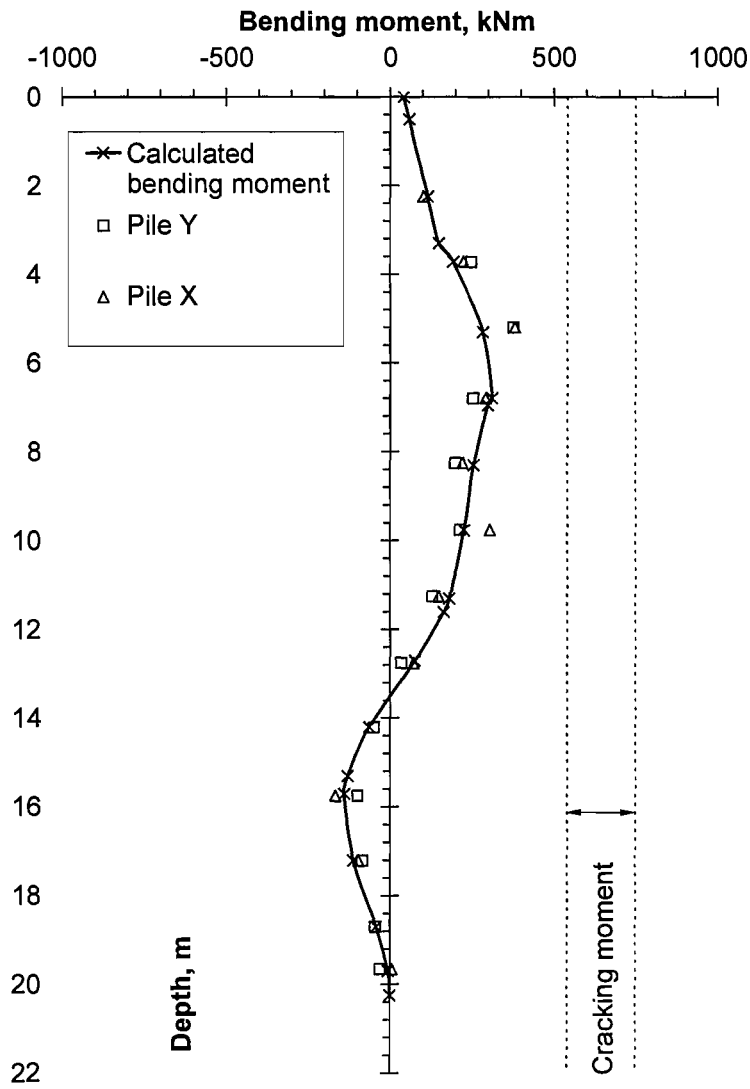

Figure 5-33: Measured bending moments and bending moment calculated from horizontal soil stresses within 10% of those measured

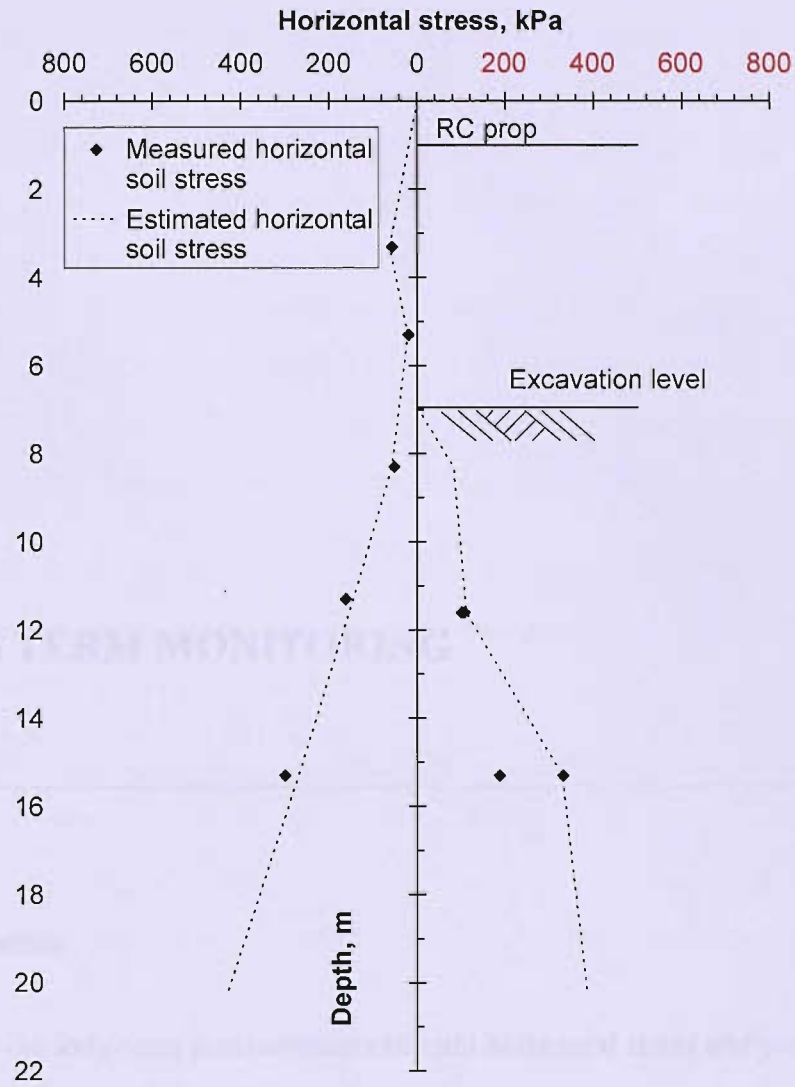

Figure 5-34: Measured and estimated total horizontal stresses

6 LONG TERM MONITORING

6-1 Introduction

In this chapter the long-term measurements of total horizontal stress and pore water pressure in the soil around the wall, and the reinforced concrete prop loads and pile bending moments in the structure, are presented and discussed.

6-2 Total horizontal stress and pore water pressure measurements

Figures 6-1 to 6-6 show the total horizontal stresses and pore water pressures measured over the period from before pile installation to late 2005 by the spade cells 1·275, 2·375 and 3·475 m behind the wall respectively. Figures 6-7 and 6-8 show the total horizontal stresses and pore water pressures measured in front of the retaining wall over the same period. These figures show that installation of the contiguous piled retaining wall and excavation of the cutting caused the main significant changes in total horizontal stress and pore water pressure. Since construction of the cutting was completed the total stress and

pore water pressure measurements have generally remained constant from year to year, although a few spade cells have recorded small overall reductions.

Figures 6-1 to 6-8 show that in the years following construction of the cutting the total stress measurements, and to a smaller extent the pore water pressure measurements, experience seasonal variation with temperature, particularly those close to ground level behind the wall and in front of the wall. The recorded loads are smallest in winter and higher in summer for the spade cells 1·275 m behind the wall, with the highest readings occurring between approximately July and October. The cells 2·375 m and 3·475 m behind the wall lag behind this slightly, with the highest readings occurring between approximately September and November. In front of the wall, the readings from the shallowest spade cells (S11 and S13) are highest between approximately September and November and from the deeper cells between October and February.

The total stress cells appear to suffer from noise, probably due to temperature effects (the deepest spade cells exhibit less noise). The pore water pressure transducers appear to be less affected than the total stress transducers.

There have been a number of other significant changes worth noting. The readings from total stress cell 4 appear to have shifted down by about 10 kPa over the period between approximately Days 1630 to 1966 (Figure 6-1). Total stress cell 8 appears to have malfunctioned (Figure 6-5) and total stress cell 12 performs unusually below about 160 kPa.

6-2-1 Installation of storm drain

Figures 6-1 to 6-6 show that before installation of the storm drain behind the instrumented wall (see Section 3-5-6 and Figure 3-48) the pore water pressures measured in gauges P1-P4, P15-16 and P6-8 increased. This was during late October and early November and was therefore probably due to seasonal rainfall. Installation of the storm drain generally caused a fall in pore water pressure. Ever since the storm drain was installed the pore water pressures have fluctuated very little by comparison. The total stress measurements in the same gauges also increased over the period before the storm drain was installed, although generally to a smaller degree, apart from the total horizontal stress measured in spade cell 1 which, if anything, dropped slightly over this period.

Over the period of storm drain installation, spade cell (SC) 1, 3·3 m below ground level and therefore above the bottom of the storm drain trench, recorded a reduction in total stress of about 15 kPa on excavation of the trench, and on backfilling the stress returned to its pre-trench excavation level. SC6, at the same depth as SC1 but much closer to the storm drain trench, recorded a reduction in total stress of approximately 50 kPa due to trench excavation, recovering to 20 kPa. These changes can be seen more closely in Figures 6-9, 6-10 and 6-11, and are essentially similar to the type of change exhibited as a result of pile excavation.

6-3 Reinforced concrete prop loads

Figure 6-12 shows the reinforced concrete (RC) prop loads, calculated assuming the Young's modulus of concrete is constant at 25 MPa, measured from before excavation within the cutting to late 2005. The average temperature measured in the gauges is also shown. The figure shows the load in the props increasing by between approximately 200 and 1000 kN each year.

Figure 6-13 shows the RC prop loads adjusted for the effects of creep (after Day 607) as described in Section 4-4-3. The minimum load recorded each year is constant (in approximately March to June), and the maximum load (recorded in October each year) is reducing, showing that the seasonal variation in load is reducing each year.

As more data is collected in the long-term it should be possible to improve the correction for the effects of creep.

6-4 Pile bending moments

Figures 6-14 to 6-17 show the pile bending moments measured over the period from before excavation within the cutting to late 2005 by the gauges in Pile Y and Pile X respectively. The buried gauges exhibit generally constant measurements with time but the others vary significantly with temperature. Similar bending moments are exhibited in gauges 15-24 in both piles, except in Pile Y gauges 21&22 and in Pile X 15&16 (and to some extent 17&18) are higher, because the section is cracked at these locations.

6-5 Conclusions

The long-term spade cell measurements are showing generally constant total horizontal stresses and pore water pressures over the years following construction of the cutting, and in a few cases overall reductions being recorded. There are some seasonal and daily variations in the readings, occurring more in the shallower spade cells than the deeper ones, which are probably due to temperature.

Correction for creep in the reinforced concrete props has produced prop loads which are generally constant from year to year. These loads vary seasonally like the spade cell data, and the seasonal variation is reducing from year to year.

The bending moment data are generally constant with time and the effect of cracking on the pile section is clear in the long-term data.

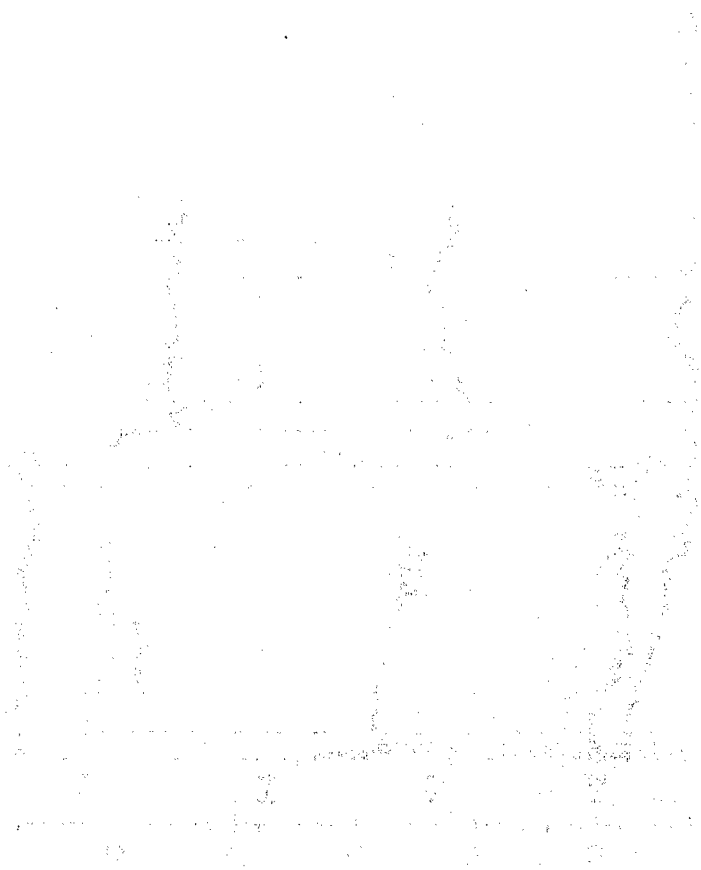

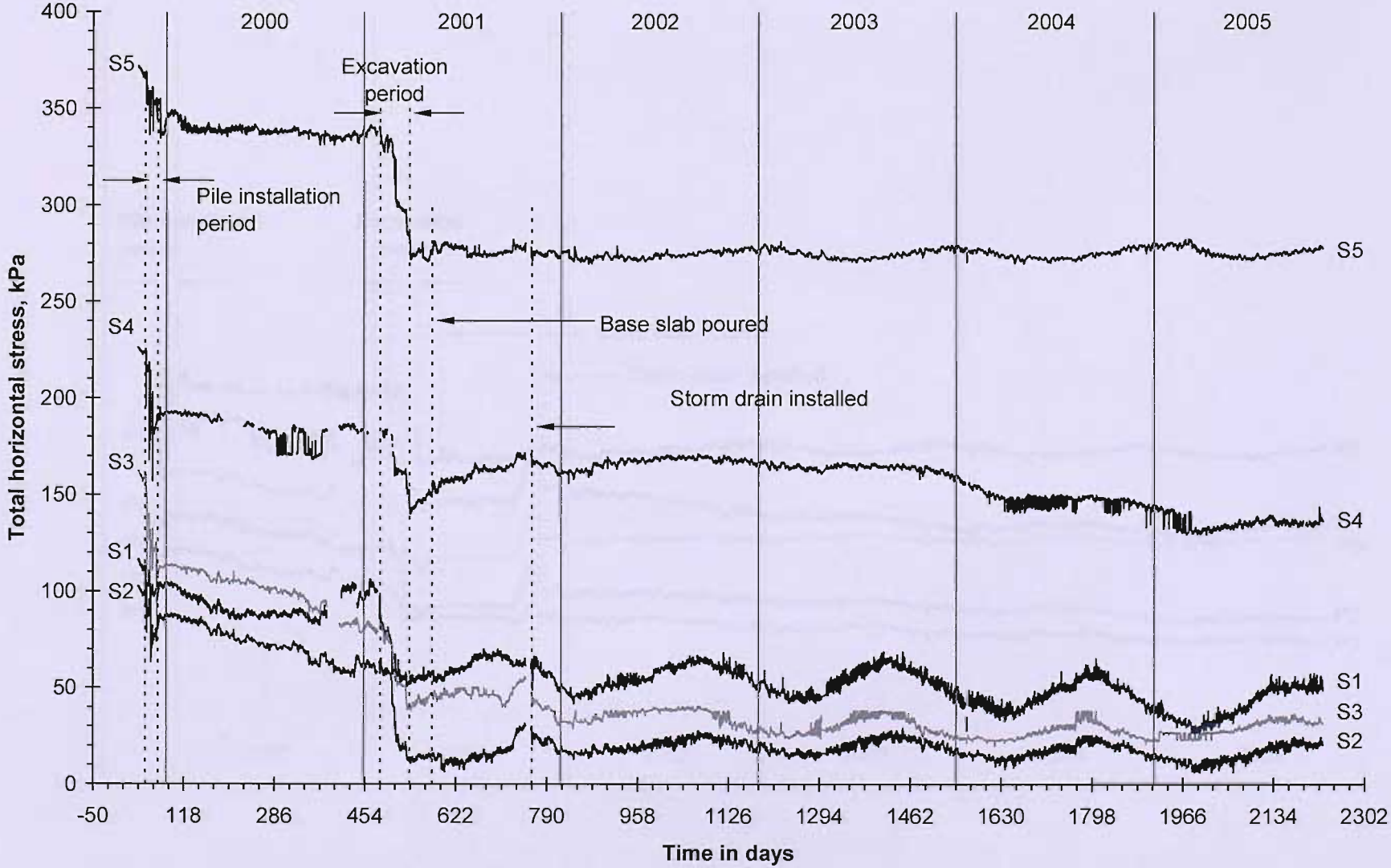

Figure 6-1: Long-term total horizontal stress measured in spade cells 1·275 m behind the wall

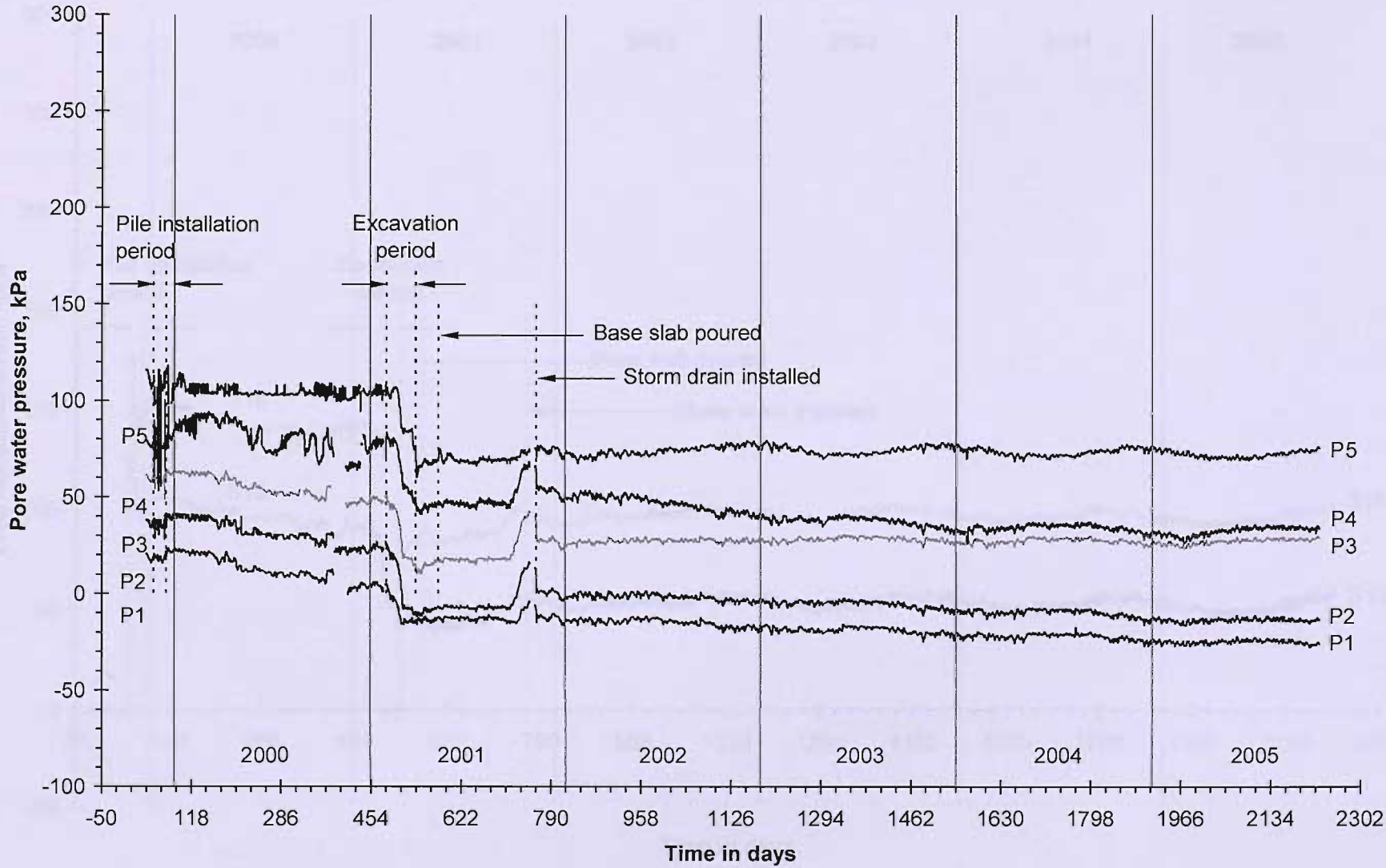

Figure 6-2: Long-term pore water pressure measured in spade cells 1·275 m behind the wall

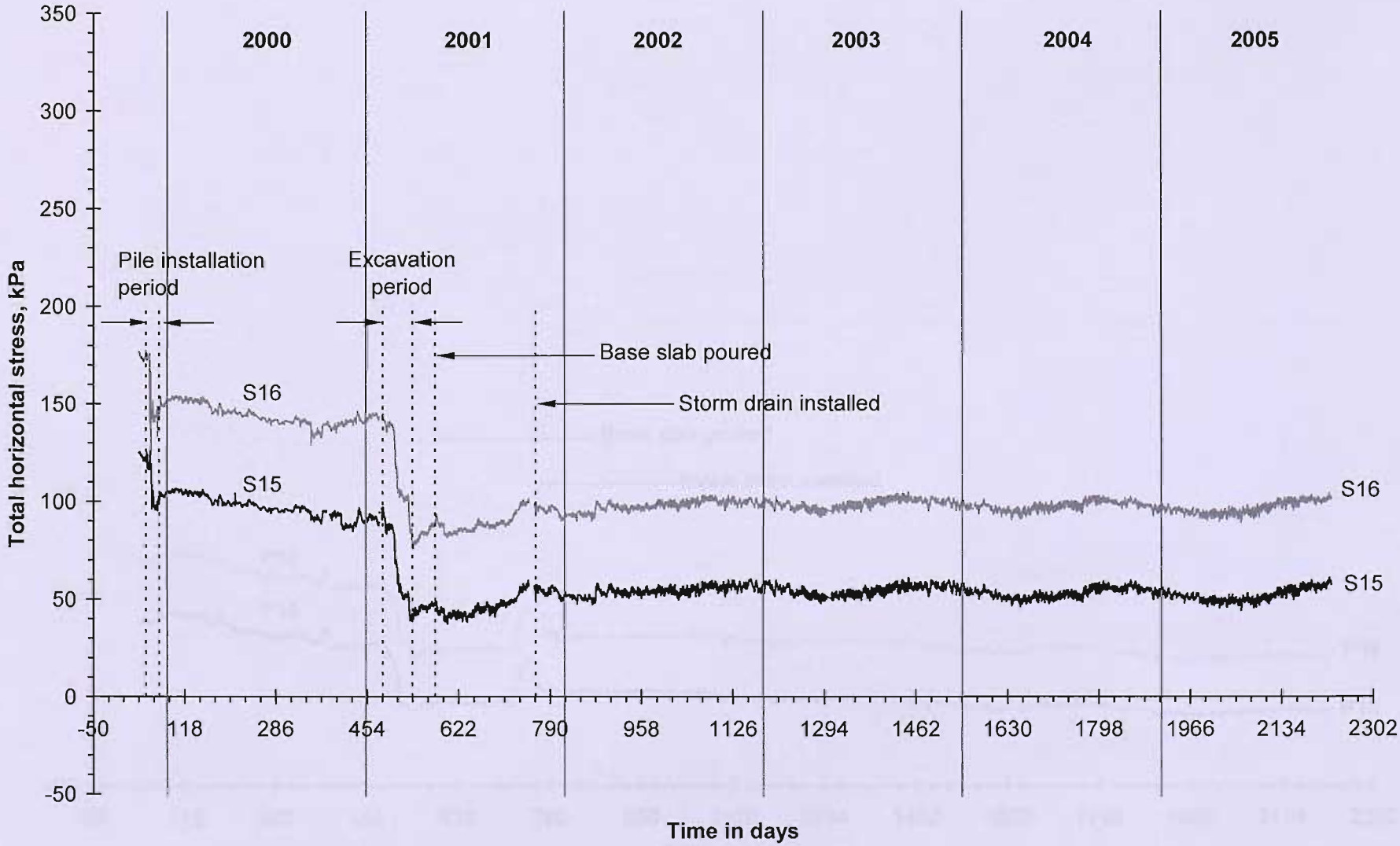

Figure 6-3: Long-term total horizontal stress measured in spade cells 2·375 m behind the wall

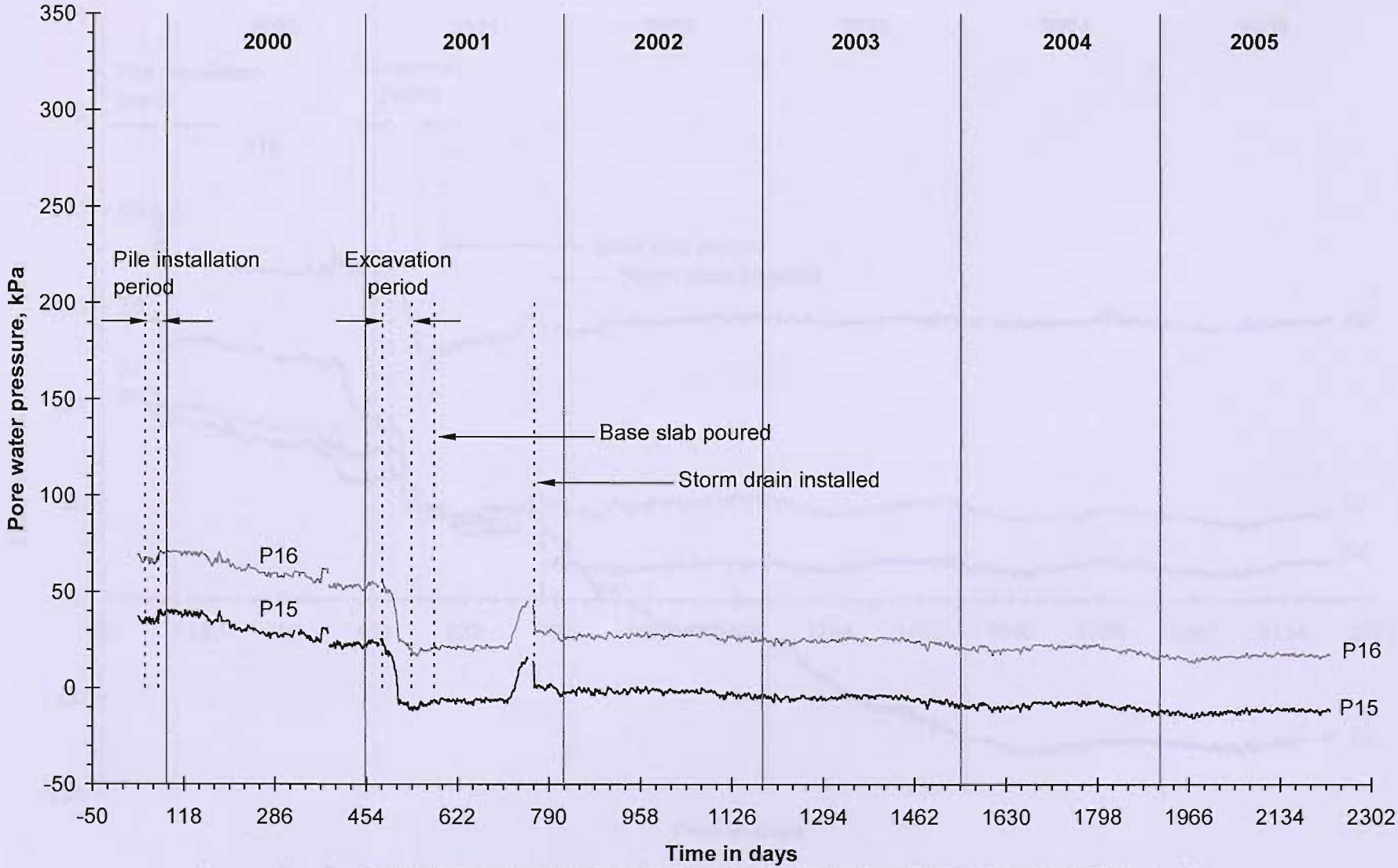

Figure 6-4: Long-term pore water pressures measured in spade cells 2·375 m behind the wall

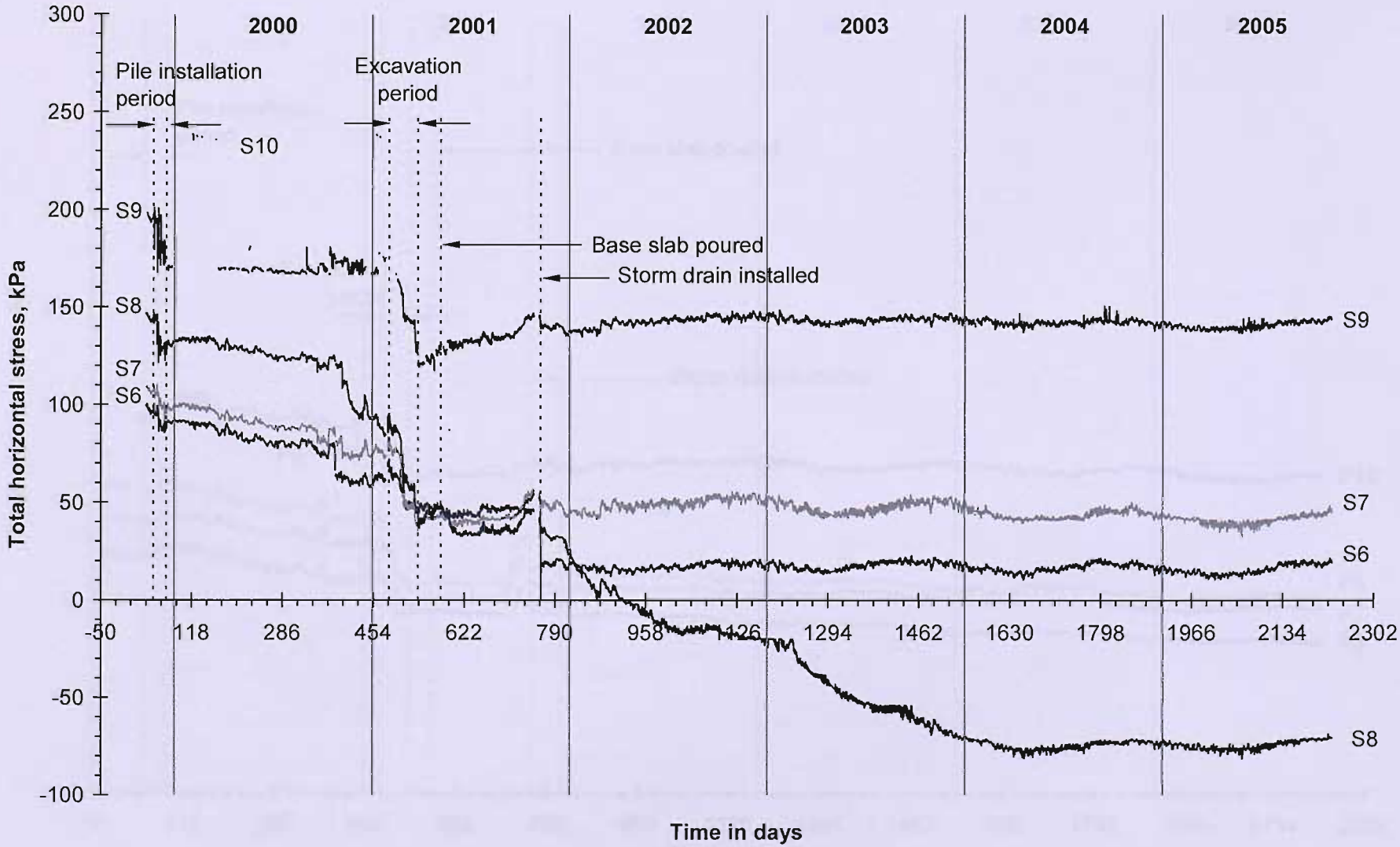

Figure 6-5: Long-term total horizontal stress measured in spade cells 3·475 m behind the wall

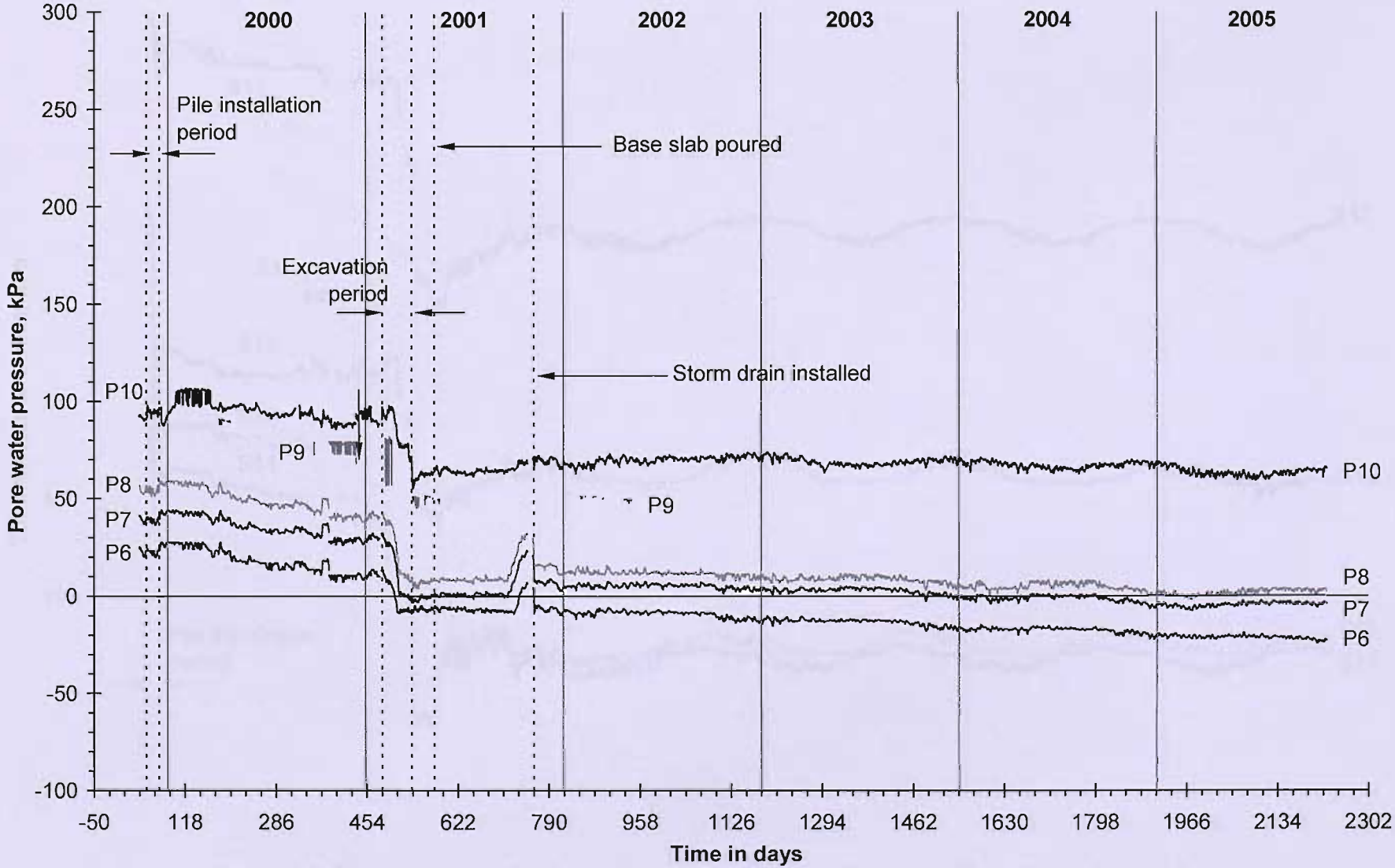

Figure 6-6: Long-term pore water pressures measured in spade cells 3·475 m behind the wall

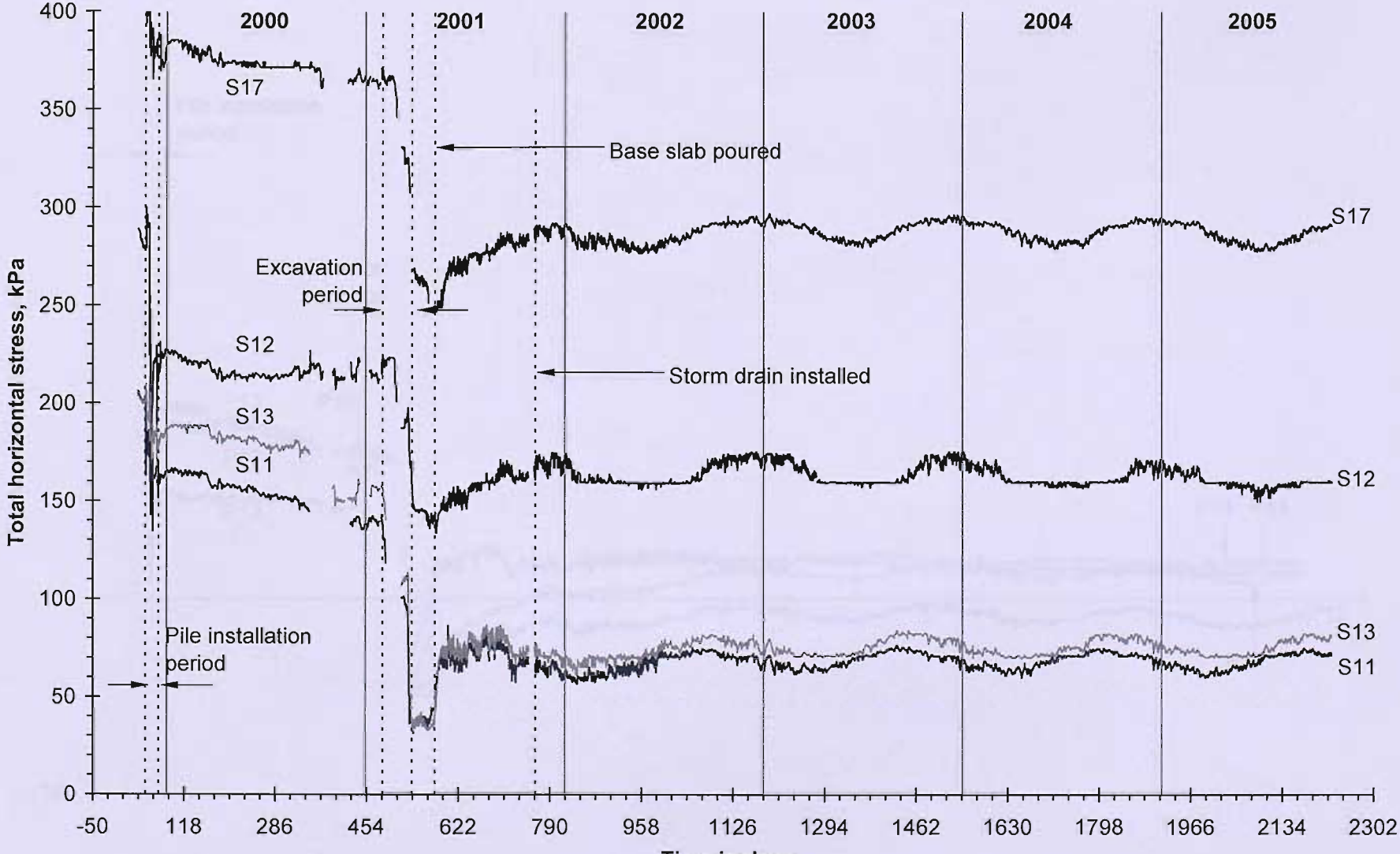

Figure 6-7: Long-term total horizontal stress measured in all spade cells in front of the wall

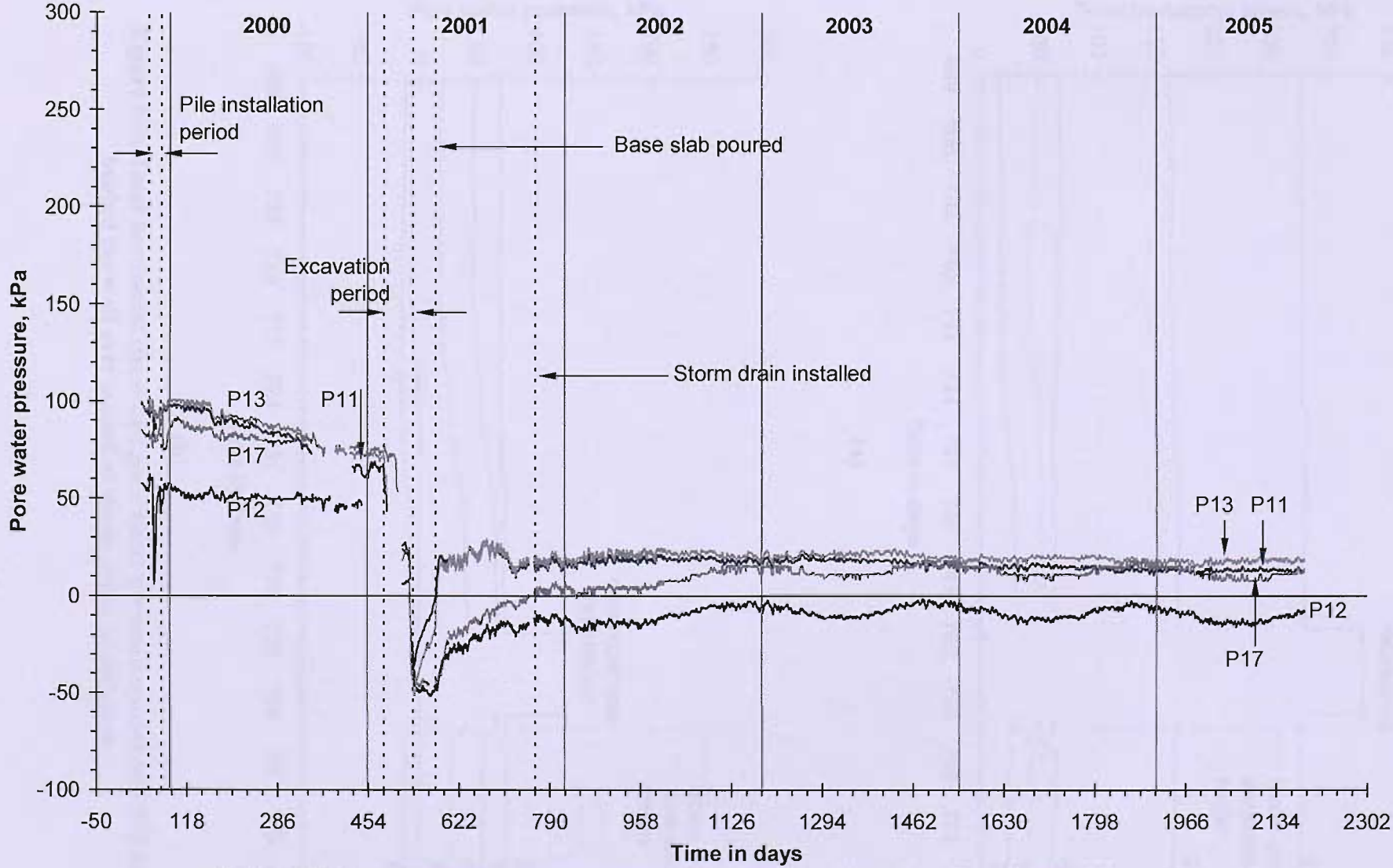

Figure 6-8: Long-term pore water pressure measured in all spade cells in front of the wall

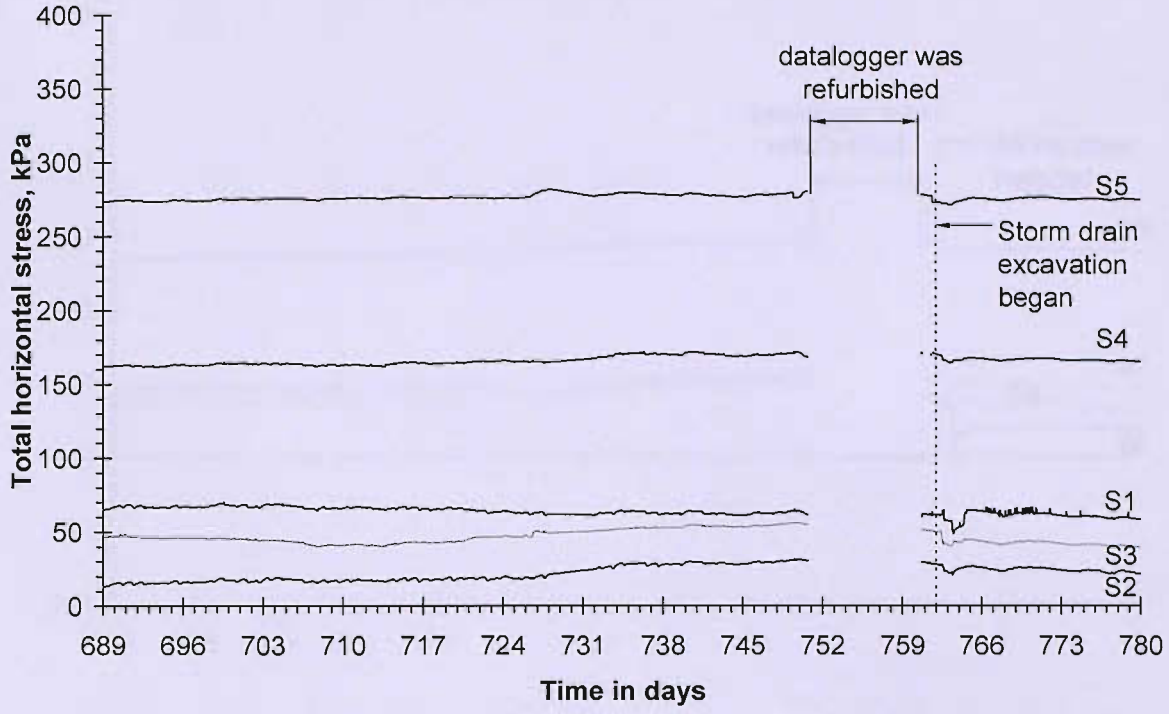

(a)

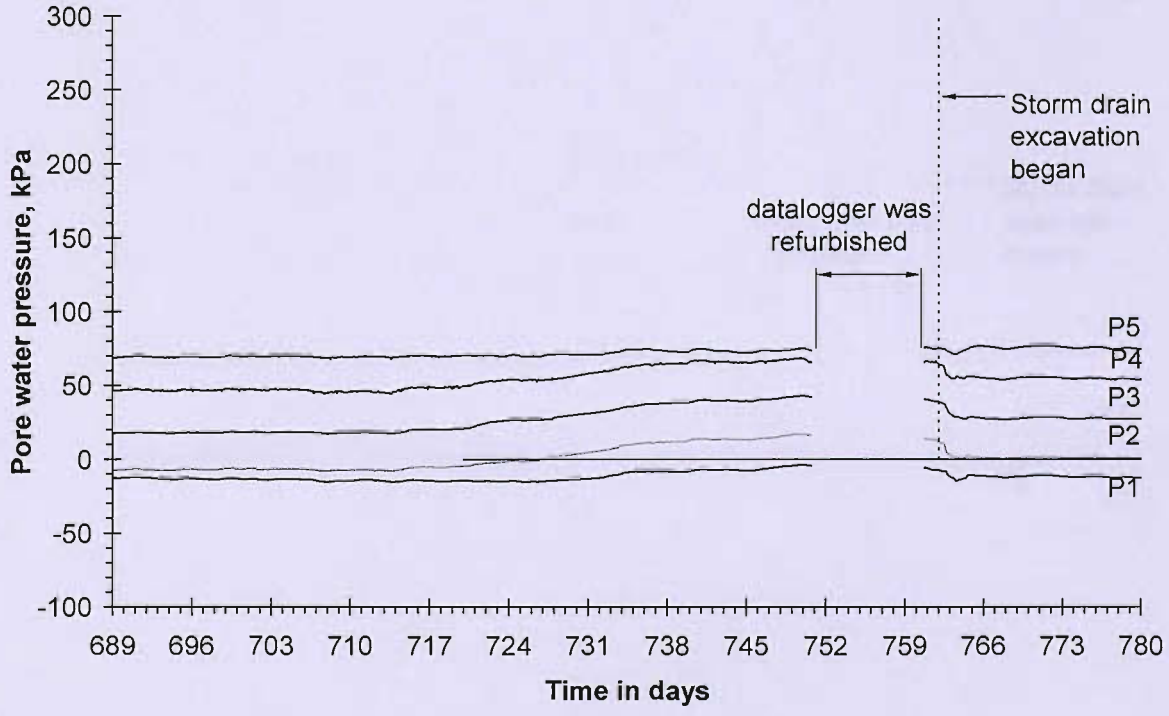

(b)

Figure 6-9: Total horizontal stress and pore water pressure measured 1·275 m behind the wall over period of storm drain installation

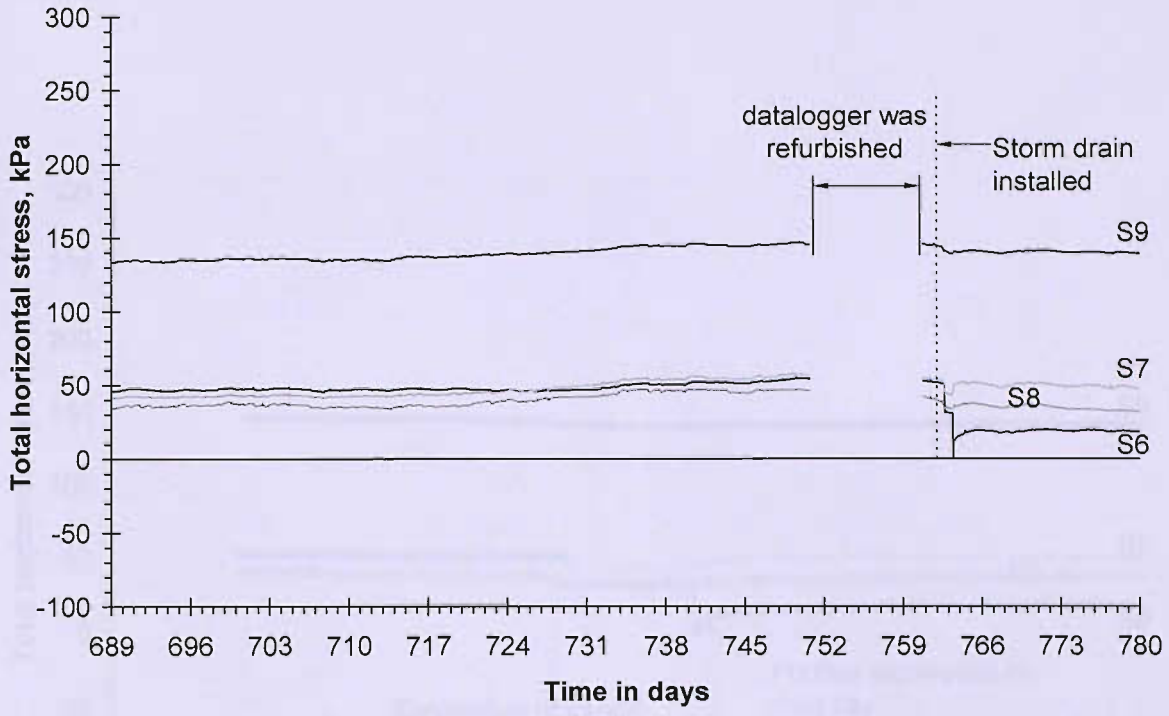

(a)

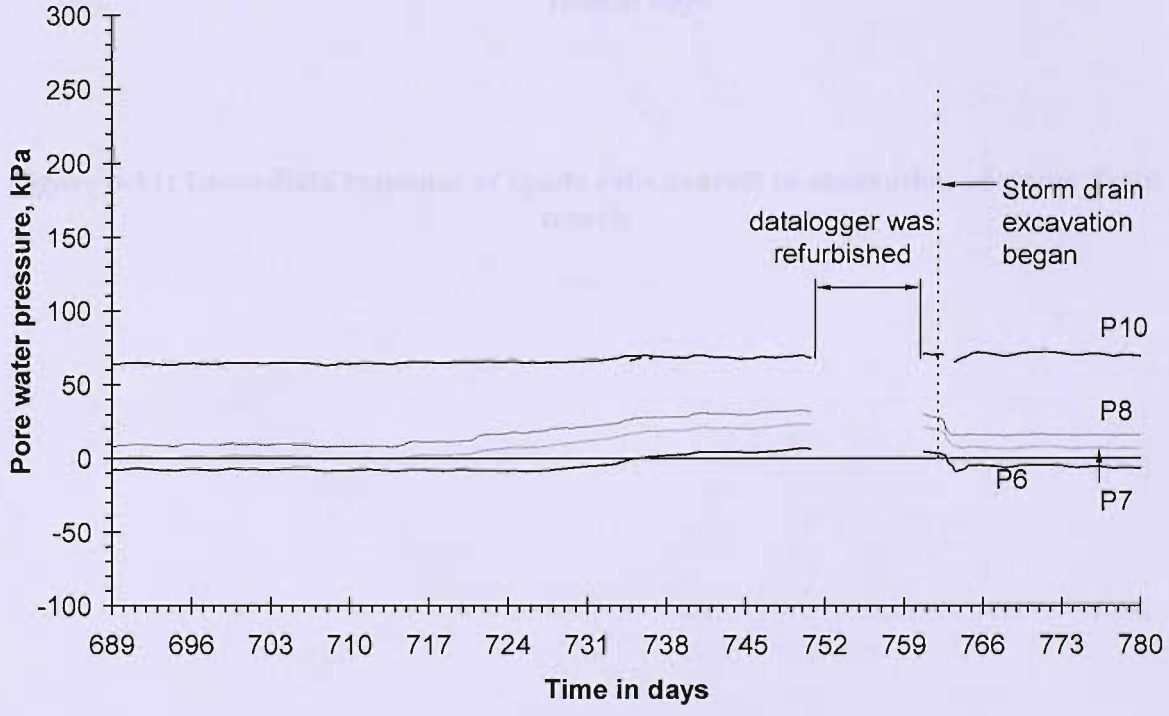

(b)

Figure 6-10: Total horizontal stress and pore water pressure measured 3·475 m behind the wall over period of storm drain installation

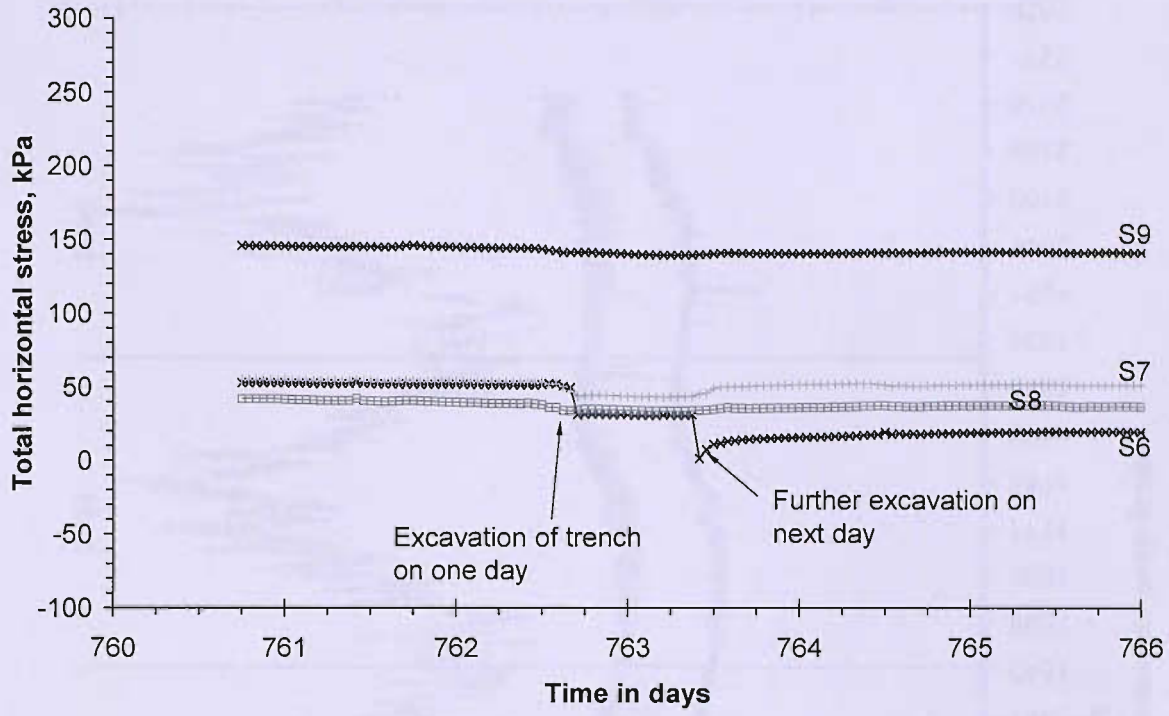

Figure 6-11: Immediate response of spade cells nearest to excavation of storm drain trench

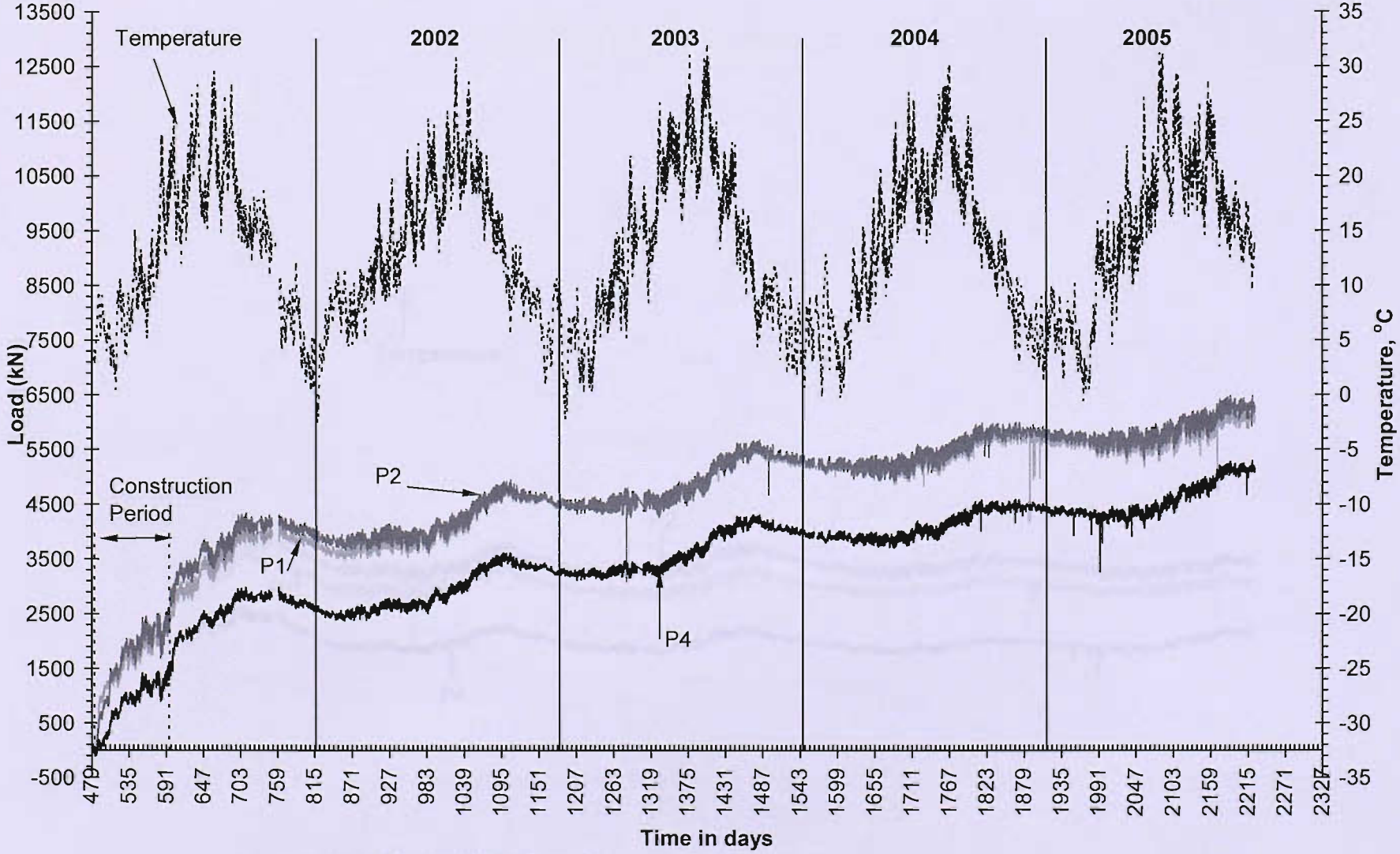

Figure 6-12: Long-term reinforced concrete prop loads

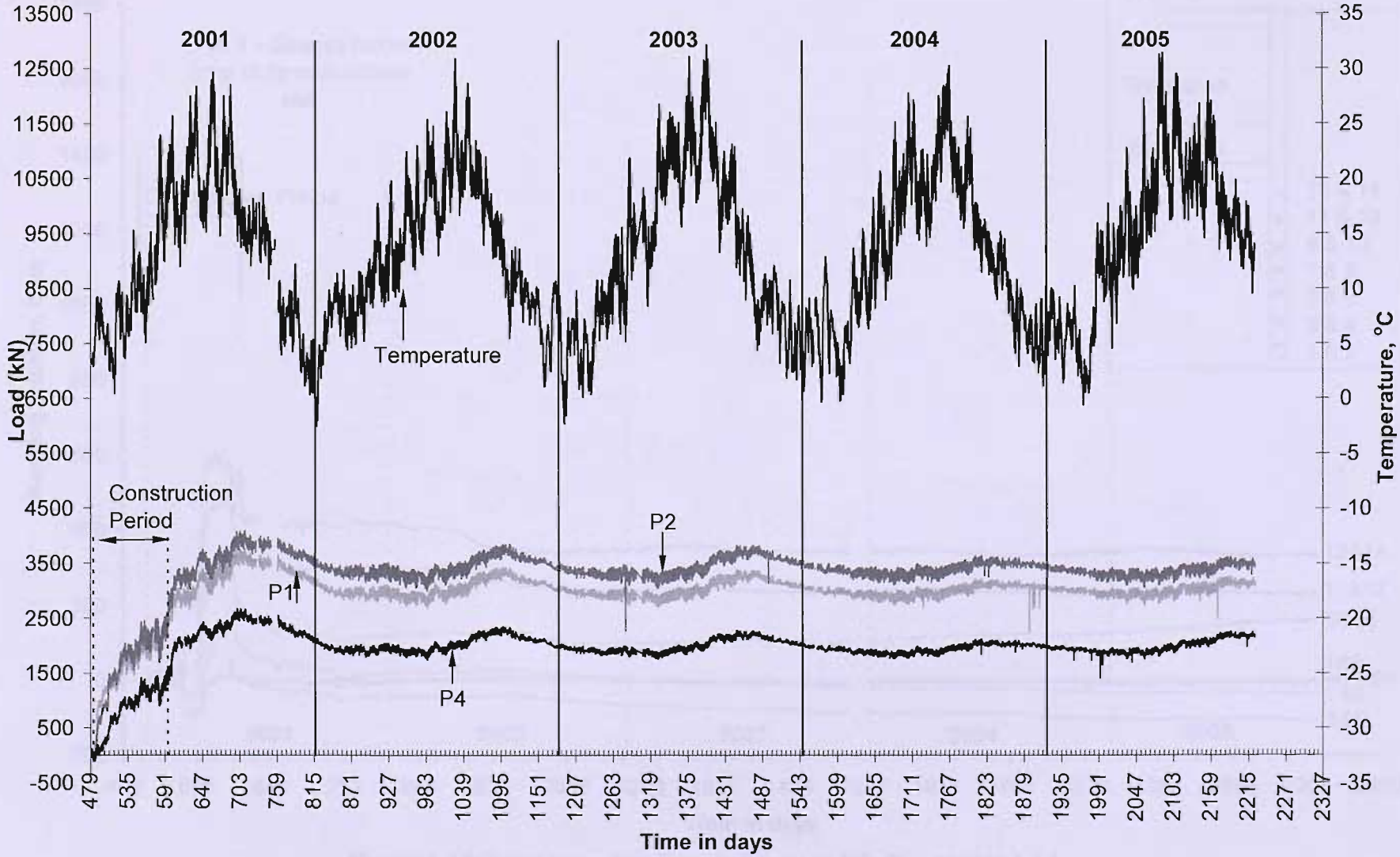

Figure 6-13: Long-term reinforced concrete prop loads corrected for the effects of creep

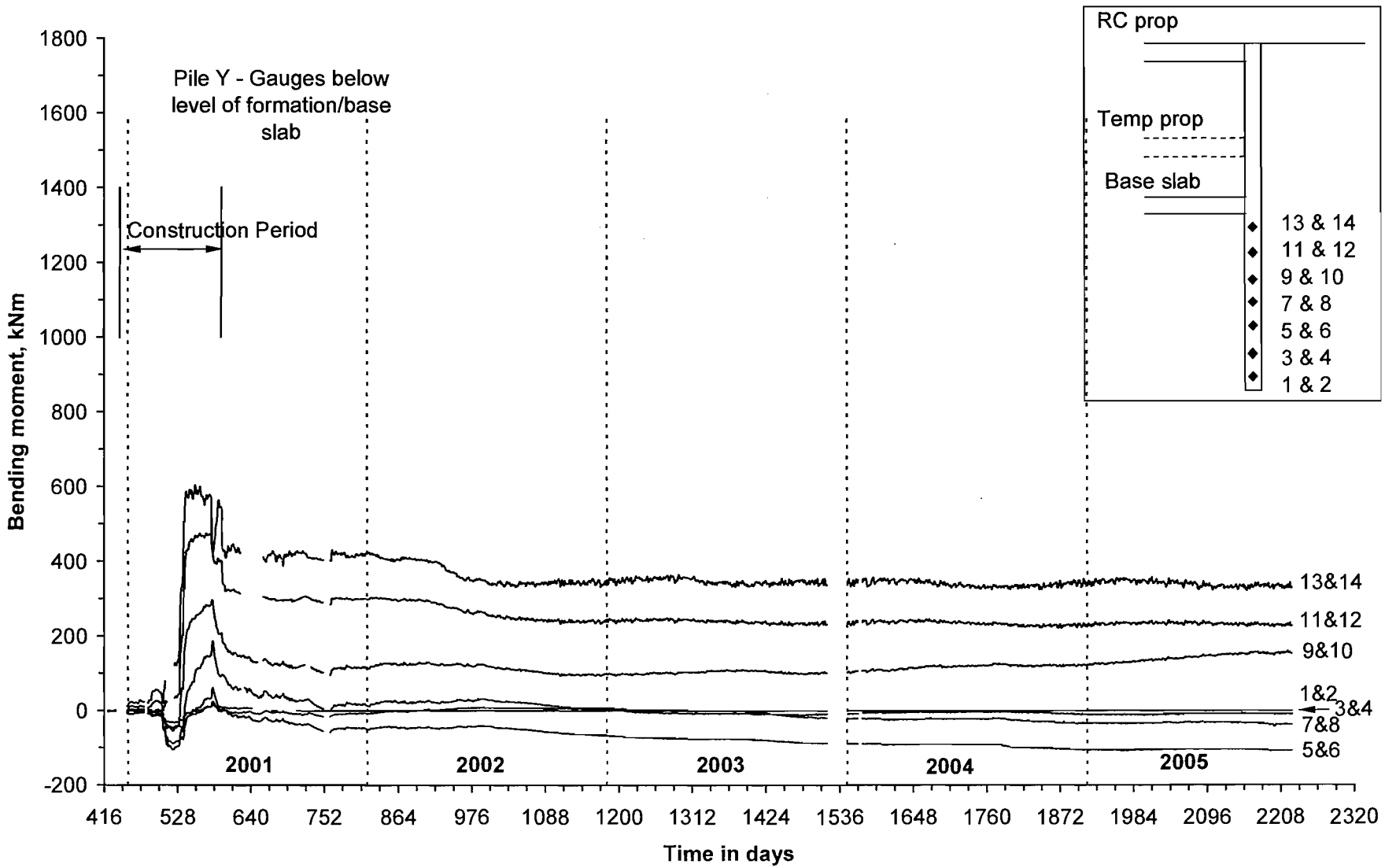

Figure 6-14: Long-term bending moments in Pile Y – gauges 1-14

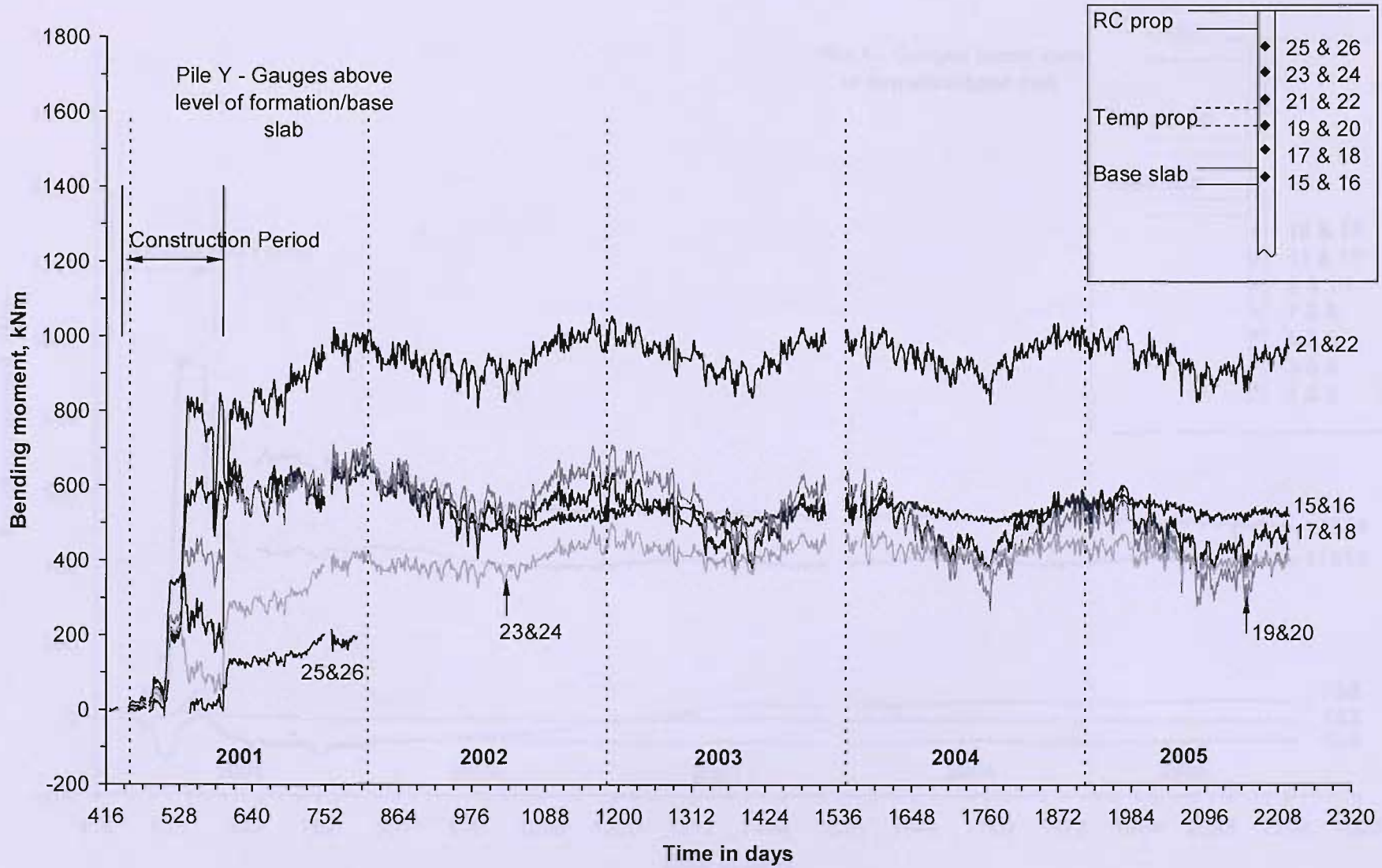

Figure 6-15: Long-term bending moments in Pile Y – gauges 15-26

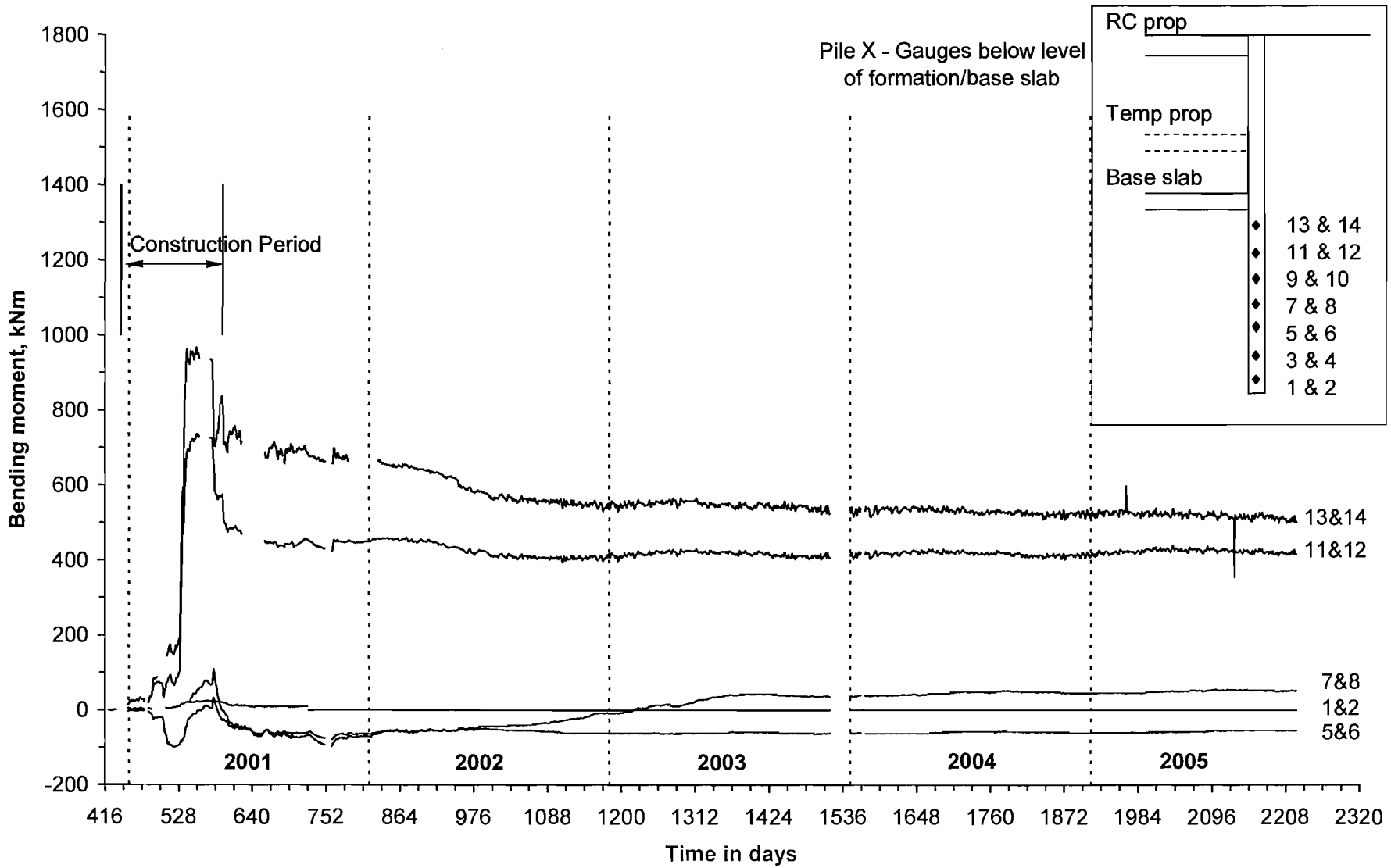

Figure 6-16: Long-term bending moments in Pile X – gauges 1-14

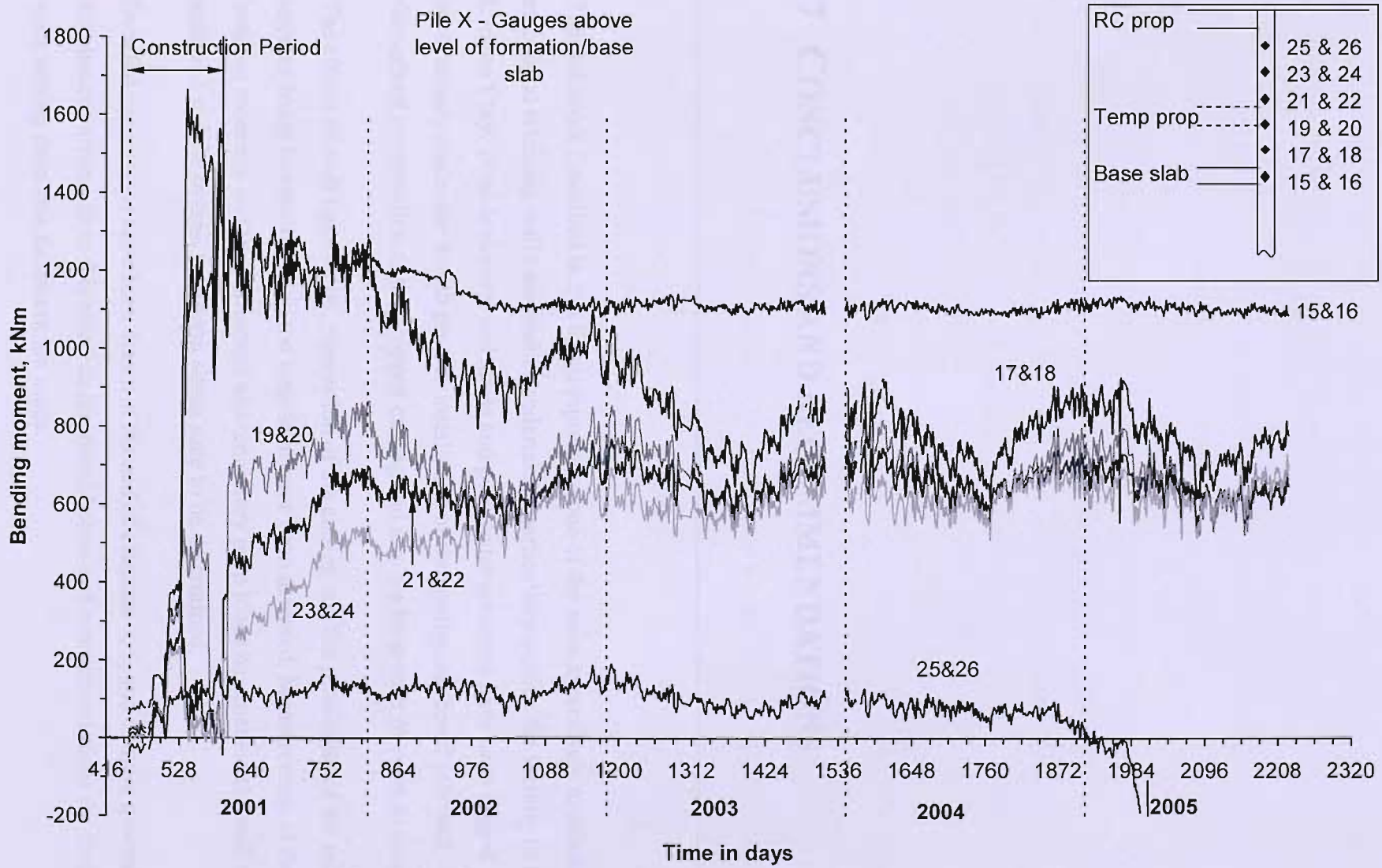

Figure 6-17: Long-term bending moments in Pile X – gauges 15-26

7 CONCLUSIONS AND RECOMMENDATIONS

The fieldwork described in this thesis represents one of the most extensively monitored embedded retaining wall case studies undertaken, particularly outside the vicinity of the London Clay. Total horizontal soil stress and pore water pressures have been logged continuously since one month prior to installation of the contiguous bored pile wall, throughout construction of the propped cutting and into the long-term (6 years to date).

The effects of wall installation, excavation of the cutting and the possibility of the *in situ* stresses being re-established in the long-term have been assessed. Measurement of the pile bending moments and the permanent and temporary prop loads has enabled the wall to be analysed and the overall long-term stress state to be determined.

Detailed conclusions have been drawn at the end of chapters 4, 5, and 6; more general conclusions arising from this research are stated below and recommendations for further work arising from this fieldwork are made.

7-1 Conclusions

- This study is a complete case record linking the wall behaviour to the change in horizontal stress in the soil, both behind and in front of the wall.

- There was no reinstatement of the total horizontal stress in the soil after either wall installation or excavation of the cutting.

- The work undertaken in order to evaluate the spade cell over-read due to installation in stiff overconsolidated clay adds significantly to the previous data as spade cells have not previously been used in the Atherfield and Weald clays, and the performance of a spade cell under a known changing load has not previously been measured.

- The process of installing an *in situ* embedded retaining wall in overconsolidated clay deposits produces a very clear reduction in the effective horizontal stresses and lateral earth pressure coefficients. The reductions between 15 and 50% were measured and the reduction was not linear with depth. This is a very significant result for walls embedded in overconsolidated clays as they are regularly designed to accommodate unnecessarily high horizontal stresses under working conditions.

- Identification of concreting cracking and analysis of the effect this has had on the bending moment profiles calculated from the inclinometer measurements has explained the differences in bending moment plots found by two different methods after cracking had occurred.

- Structural monitoring is regularly used in construction of large projects to minimise construction costs and maximise safety. Inclinometer measurements are regularly taken to monitor wall movements. The success of the calculation of bending moments and prop loads at the CTRL will provide confidence that structural monitoring can be used more extensively than at present.

- The work undertaken to separate the strain due to shrinkage, creep and applied load in the reinforced concrete props has allowed prop loads to be estimated which agree with the measured wall bending moments and total horizontal soil stresses by means of a simple equilibrium calculation.

- There has been no long term increase in the bending moments, reinforced concrete prop loads or horizontal soil stress.

- Although continuous monitoring is demanding, the benefits of collecting continuous data using vibrating-wire gauges connected to a datalogging system are numerous and must form the basis of any future fieldwork studies.

7-2 Recommendations for further work

This research has highlighted several areas of further work which will build on the important conclusions made above. Suggestions for this work are made in the following paragraphs.

- Development of a data management system format that assimilates construction events with the collected instrument responses would be highly desirable.

- The properties of the Atherfield Clay are not well understood. Further studies to help define its geotechnical parameters would be most welcome. In particular, the effect of the shear surfaces and fissuring on the permeability and the pore water pressure changes should be addressed.

- Concrete shrinkage and creep have been studied extensively in the past, however understanding the effect these factors have on the measurement of prop loads using embedded strain gauges is obviously crucial. Distinguishing the strain due to load from the shrinkage strain and creep strain proved difficult in this case, particularly because, due to the construction events, the props began to take up load very soon after the concrete was poured. Analysis of the data still being collected will allow a better understanding of the shrinkage due to creep to be attained.

- Further work should be undertaken to investigate the over-reading exhibited by spade cells installed in overconsolidated clays. The connection made between the over-read and the undrained shear strength could be improved upon.

- Measurement of the movement of the south wall would have been very valuable, helping to answer questions regarding the amount of load taken up by the props, the movement of the whole wall, issues surrounding the sway exhibited by the structure and the ground settlement behind the monitored wall.

- There is a general requirement for further fieldwork to improve our understanding of retaining wall behaviour.

- Finally, and possibly most importantly, the data collected in this field study should be used for input and comparison of results for finite element analyses, not least to study the overall performance of the wall; the three-dimensional nature of the bored pile installation process and to investigate the transfer of stress under the wall in the wall installation process which produced the non-linear stress reduction observed in this study.

Appendix A

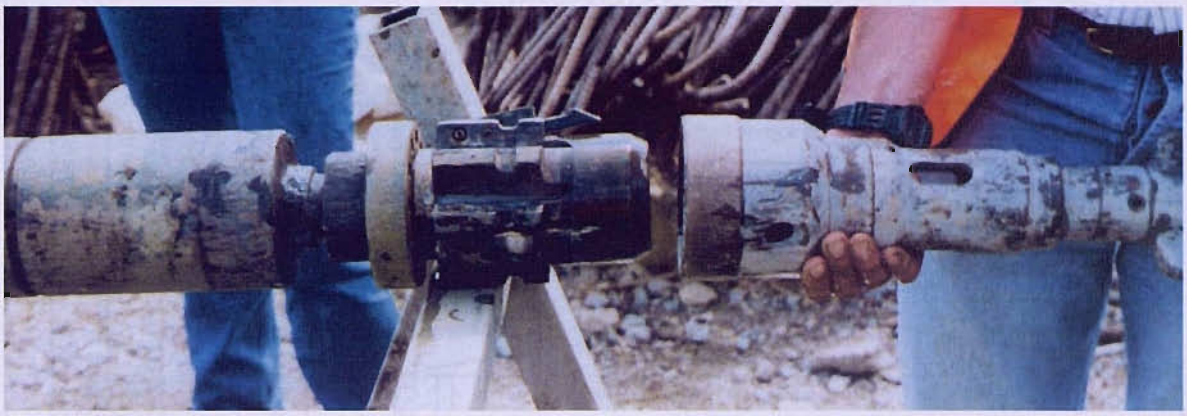

Figure A-1: Wireline borehole sample 'catch' mechanism

Figure A-2: Wireline borehole rig

Wireline borehole logs

borehole 1 page 1

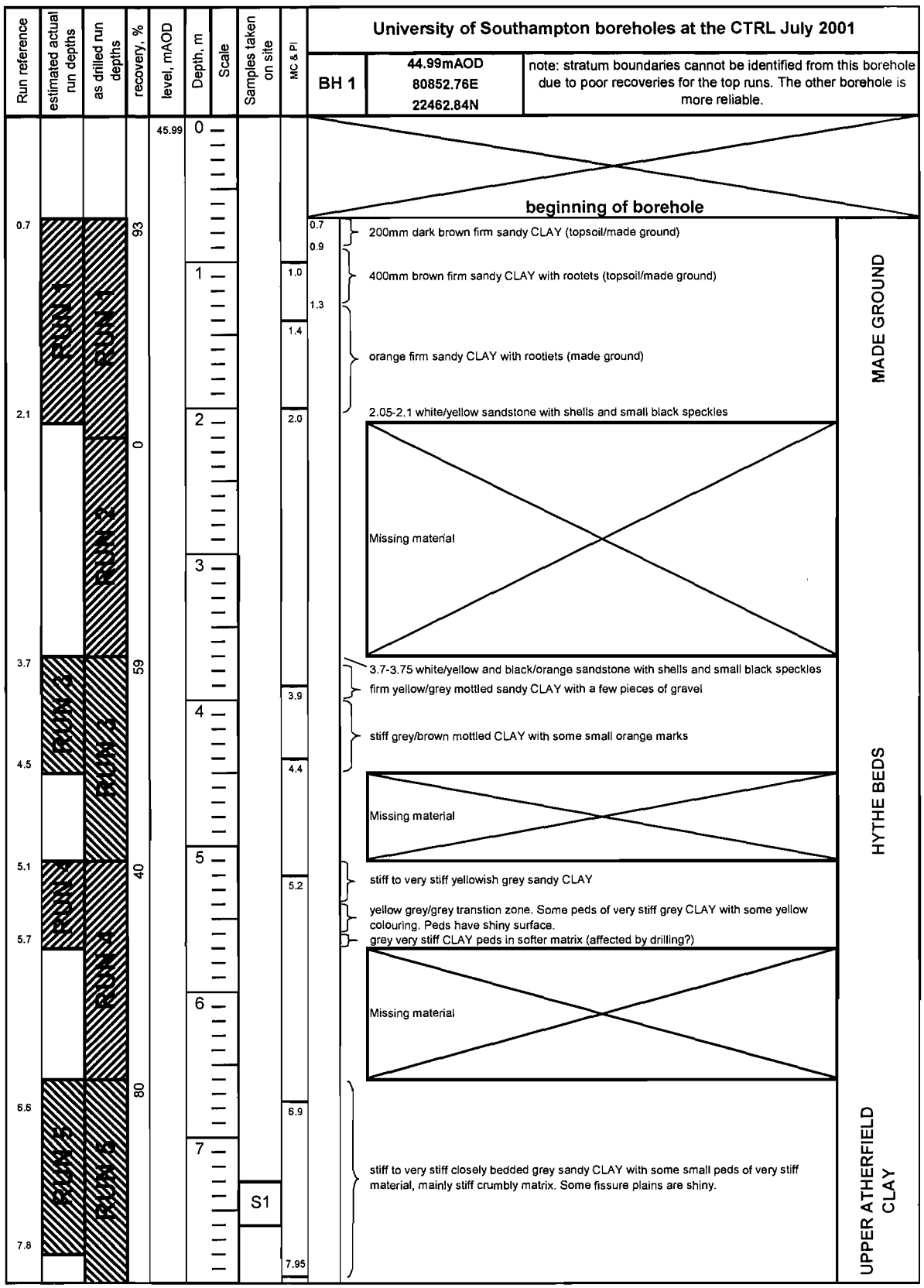

Appendix A – borehole 1 page 2

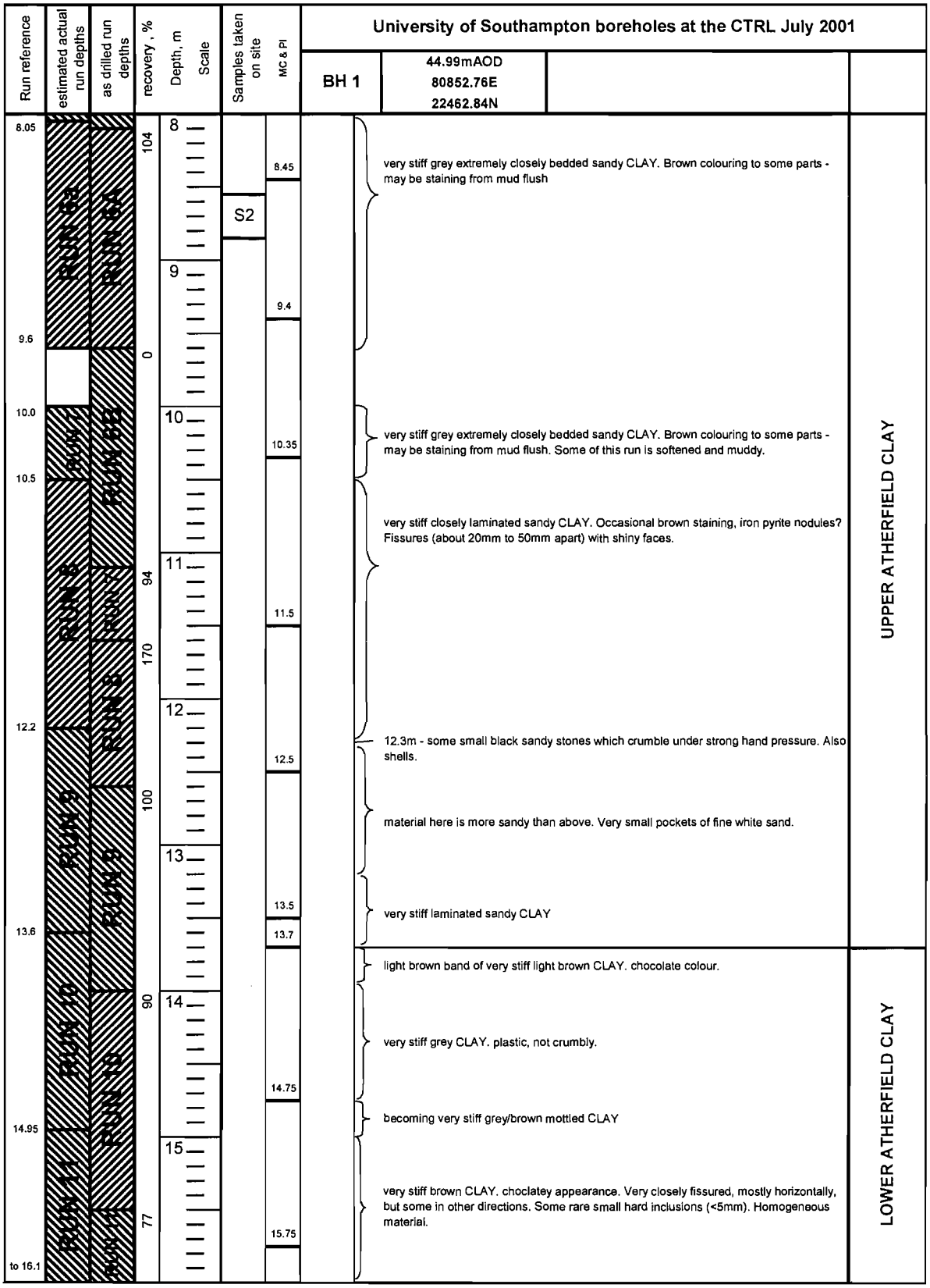

Appendix A – borehole 1 page 3

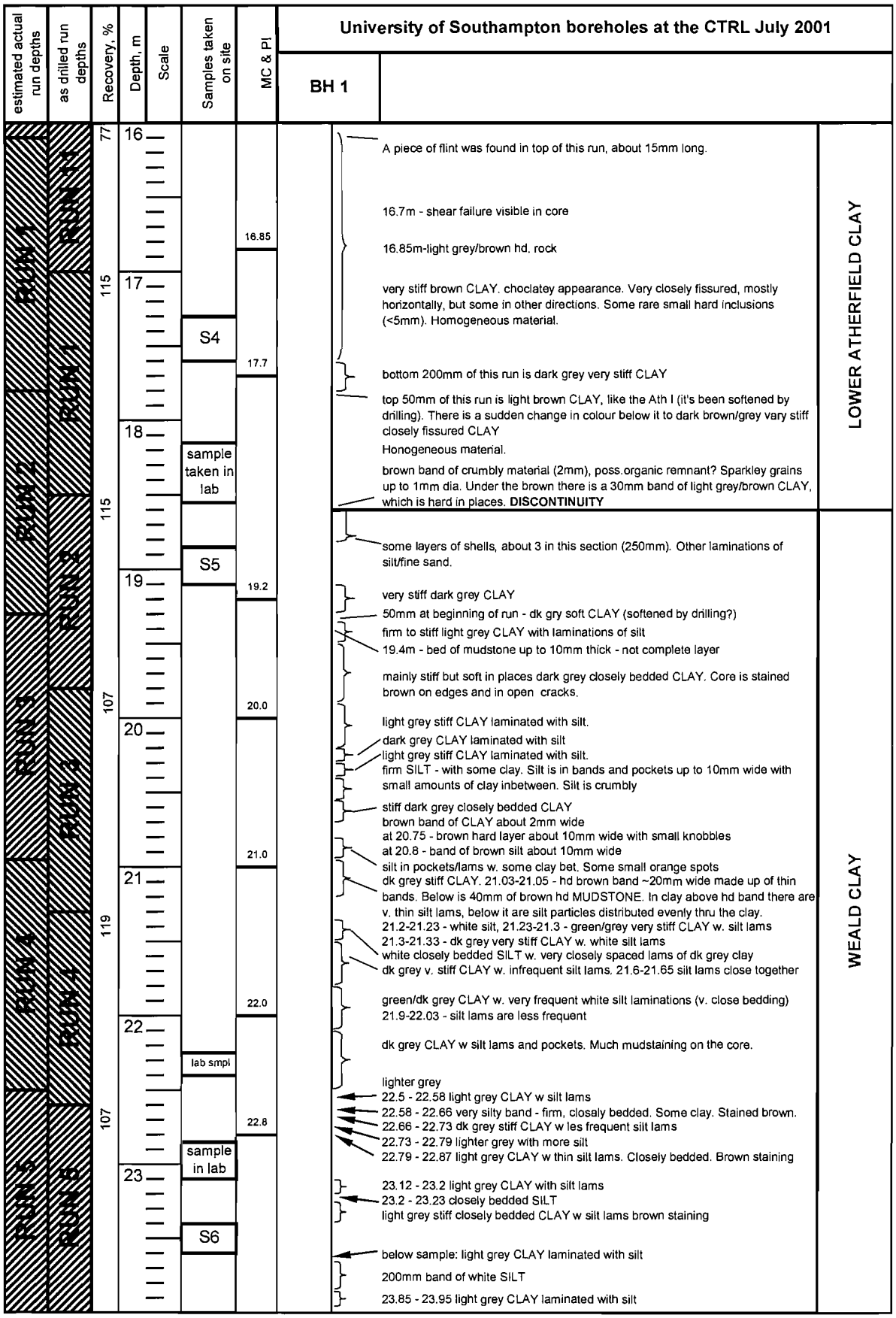

Appendix A – borehole 1 page 4

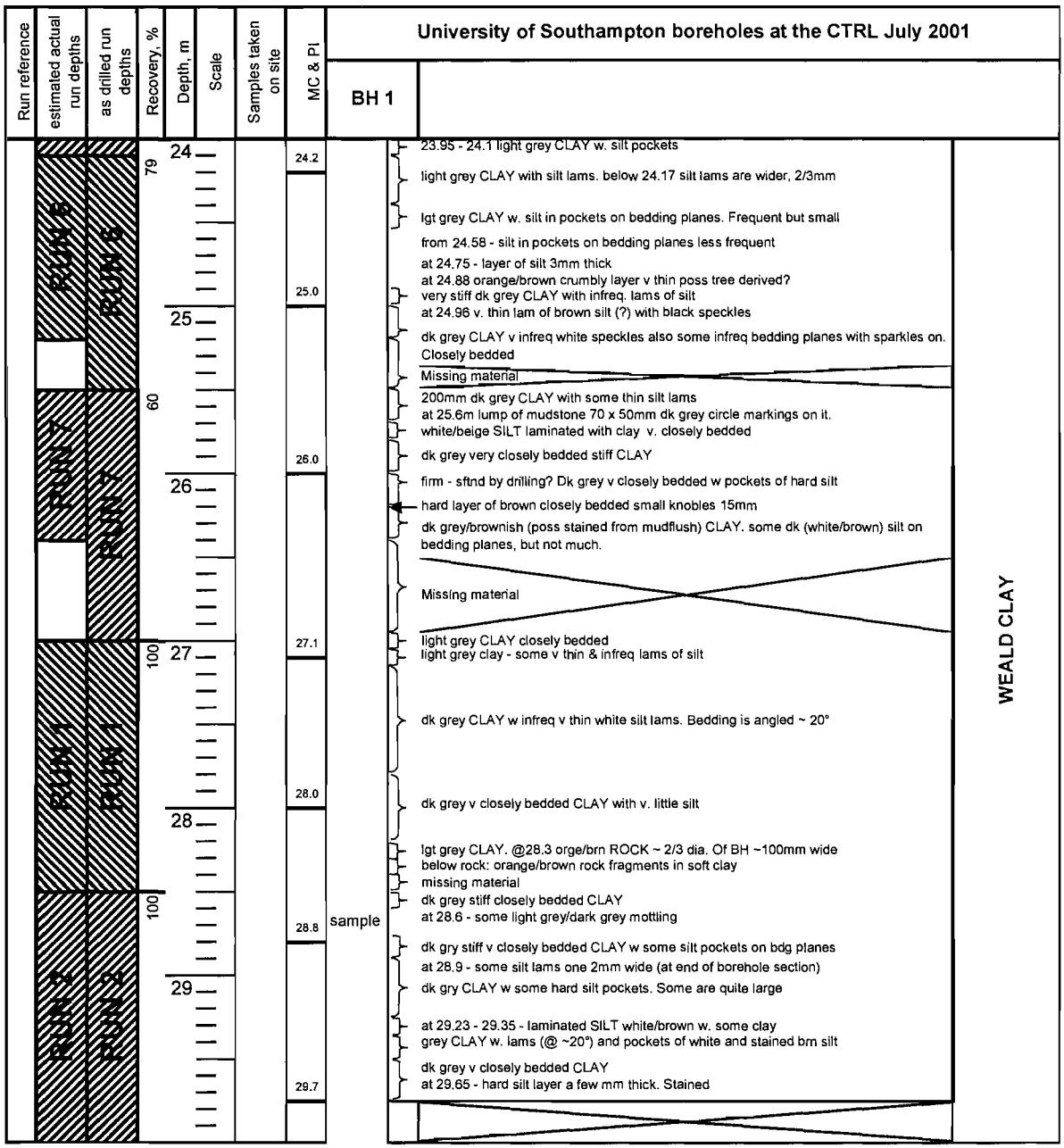

Appendix A – borehole 2 page 1

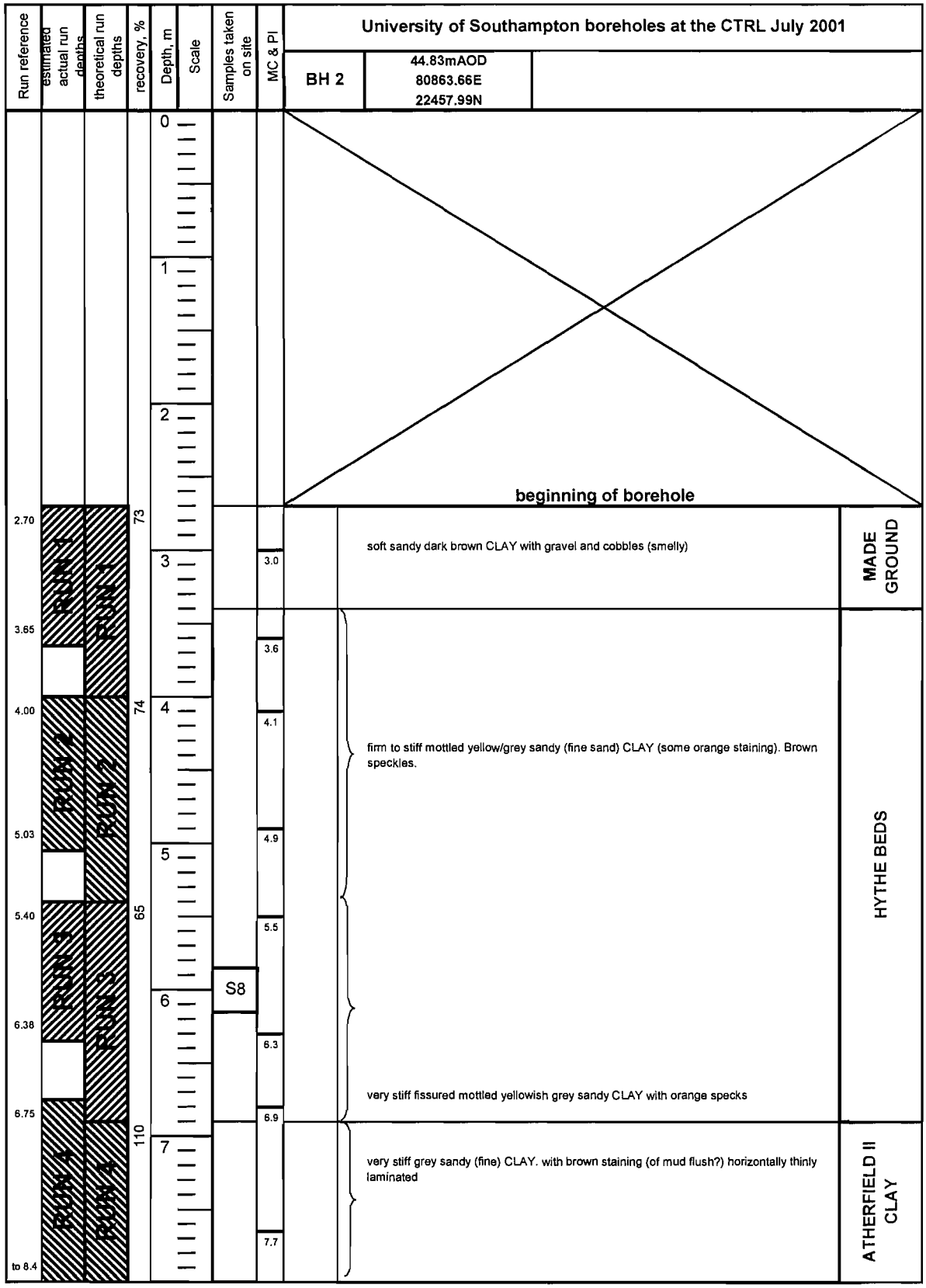

Appendix A – borehole 2 page 2

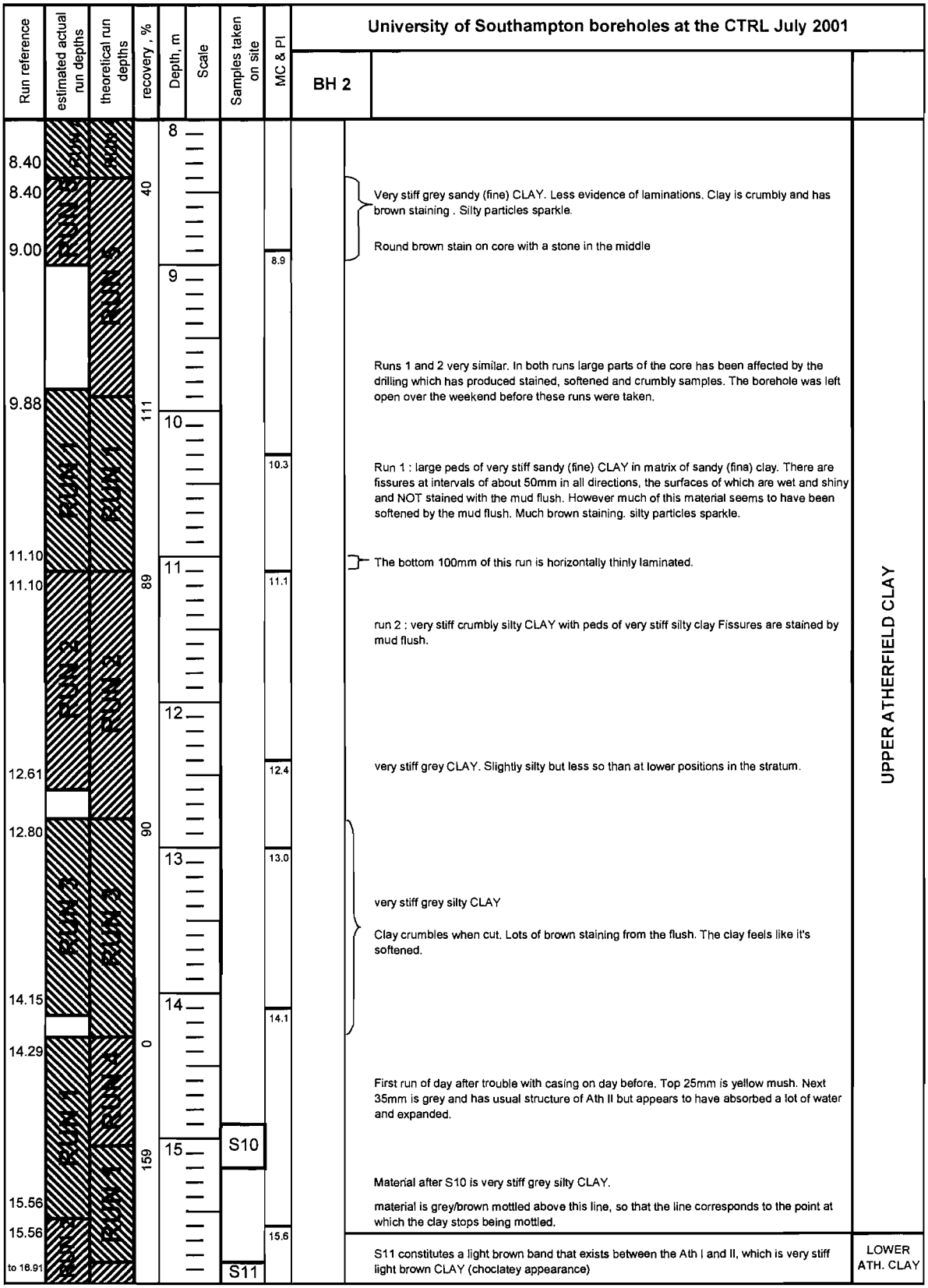

Appendix A – borehole 2 page 3

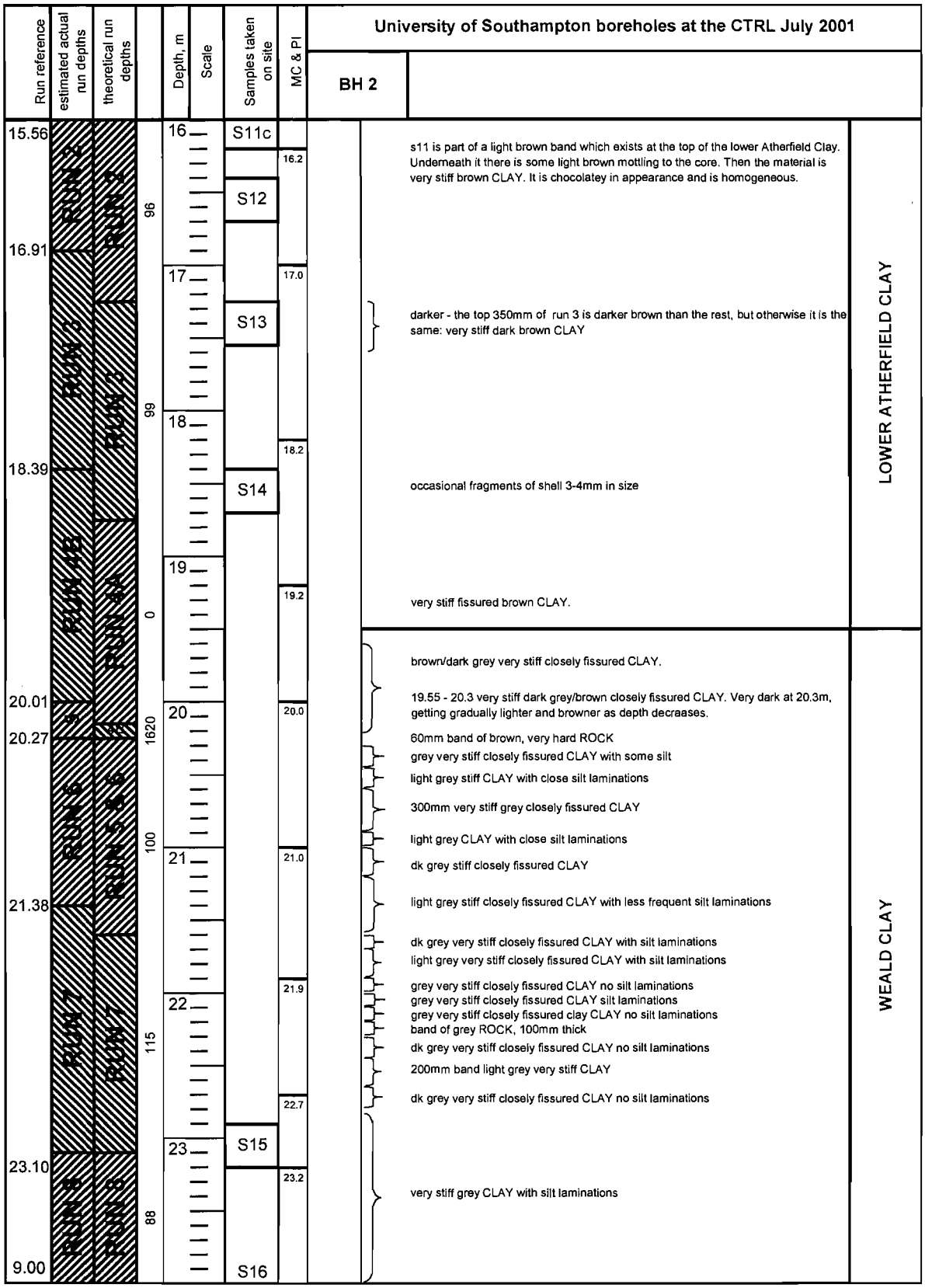

Appendix A – borehole 2 page 4

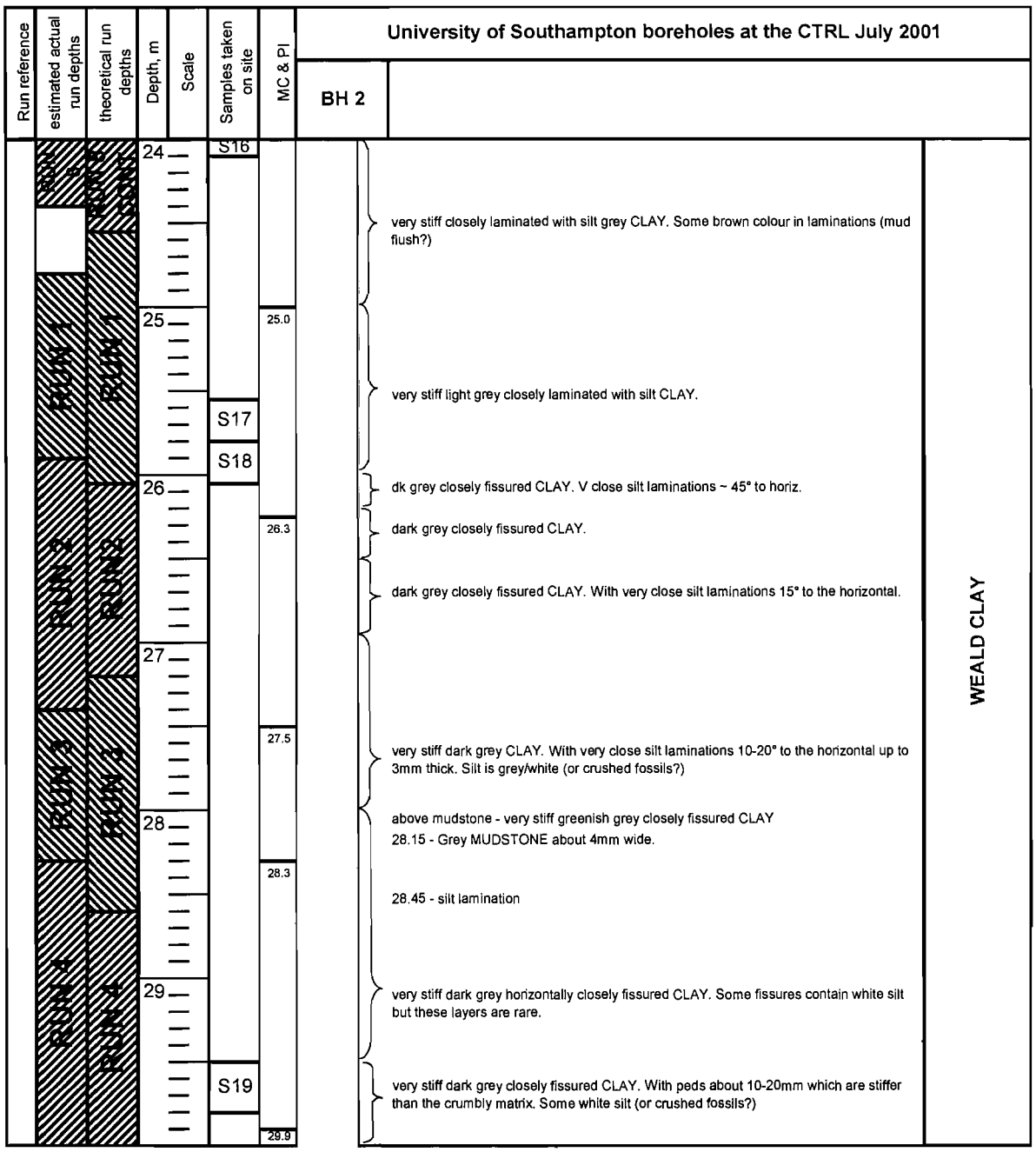

Appendix B – Piling diary

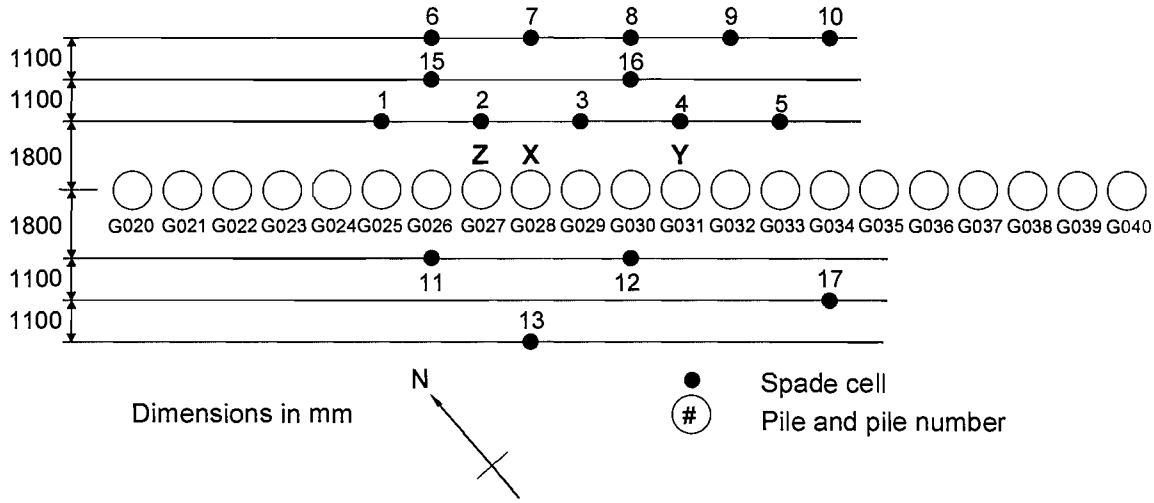

Figure B-1: Plan of piles showing pile reference numbers

Key – start and finish times for the following construction stages

ex.1 = 1st stage of excavation, 0 – 8 metres

ex.2 = 2nd stage of excavation, 8 – ~20 metres

Conc. = concrete pour

Date	Time interval	Pile no. and Procedure	Time
Tuesday 23/11/1999	14:00	G025 – ex.1	15:10 – 15:40
		G033 – ex.1	15:50 – 16:20
Wednesday 24/11/1999	10:00	G025 – ex.2	11:55 – 12:35
	12:00	G033 – ex.2	12:55 – 13:30
	14:00	G025 – Conc.	14:20 – 14:53
		G025 – Conc.	15:50 – 16:38
Thursday 25/11/1999	14:00	G021 – ex.1	14:40 – 16:00
	16:00	G037 – ex.1	16:50 – 17:10
		G028 – ex.1	17:20 – 17:40
Friday 26/11/1999	08:00	G021 – ex.2	08:05 – 08:45
		G028 – ex.2	0?:?? – 09:14
		G021 – Conc.	09:16 – 10:02
		G037 – ex.2	09:30 – 10:01
	10:00	G037 – Conc.	10:49 – 11:30
	12:00	G028 – Conc.	12:25 – 13:11
weekend			
Monday 29/11/1999	14:00	G035 – ex.1	14:59 – 15:20
		G031 – ex.1	15:55 – 16:15
	16:00	G023 – ex.1	16:25 – 16:46

Date	Time interval	Pile no. and Procedure	Time
Tuesday 30/11/1999	08:00	G035 – ex.2	08:00 – 08:35
		G031 – ex.2	08:35 – 09:07
		G023 – ex.2	09:34 – 10:00
		G035 – Conc.	09:55 – 10:32
	10:00	G023 – Conc.	11:08 – 11:46
	12:00	G031 – Conc.	12:27 – 13:15
Wednesday 01/12/1999	14:00	G030 – ex.1	15:18 – 15:42
Thursday 02/12/1999	08:00	G030 – ex.2	09:10 – 10:00
	10:00	G030 – Conc.	11:09 – 11:50
	12:00	G026 – ex.1&2	12:20 – 13:50
	14:00		
	16:00	G026 – Conc.	16:26 – 17:24
Friday 03/12/1999	10:00	G039 – ex.1	11:50 – 12:18
	12:00	G032 – ex.1	12:20 – 12:40
		G027 – ex.1	12:50 – 13:21
	14:00	G022 – ex.1	14:35 – 15:00
weekend			
Monday 06/12/1999	08:00	G022 – ex.2	09:06 – 09:41
		G027 – ex.2	09:44 – 10:14
	10:00	G032 – ex.2	11:04 – 11:40
		G022 – Conc.	11:12 – 11:56
	12:00	G027 – Conc.	12:30 – 13:15
		G039 – ex.2	13:10 – 13:35
	14:00	G032 – Conc.	14:20 – 15:15
		G039 – Conc.	15:40 – 16:27
Tuesday 07/12/1999			
Wednesday 08/12/1999			
Thursday 09/12/1999			
Friday 10/12/1999	10:00	G040 – ex.1	10:40 – 12:00
		G036 – ex.1	11:08 – 11:30
weekend			
Monday 13/12/1999	08:00	G036 – ex.2	08:10 – 08:42
		G040 – ex.2	08:42 – 09:05
		G036 – Conc.	09:50 – 10:36
	10:00	G040 – Conc.	11:14 – 12:01
	12:00		
	14:00		
	16:00	G029 – ex.1	17:15 – 17:46
Tuesday 14/12/1999	08:00	G029 – ex.2	08:48 – 09:08
	10:00	G029 – Conc.	10:58 – 11:45

Date	Time interval	Pile no. and Procedure	Time
Wednesday 15/12/1999	16:00	G020 – ex.1	16:31 – 16:57
		G024 – ex.1	16:59 – 17:21
Thursday	08:00	G020 – ex.2	08:10 – 08:40
		G024 – ex.2	08:41 – 09:05
		G020 – Conc.	09:33 – 10:06
	10:00	G024 – Conc.	10:40 – 11:17
Friday 17/12/1999	10:00	G038 – ex.1	11:35 – 12:00
	12:00	G034 – ex.1	12:03 – 12:25
weekend			
Monday 20/12/1999	10:00	G038 – ex.2	11:20 – 11:46
		G034 – ex.2	11:48 – 12:10
	12:00		
	14:00	G038 – Conc.	14:30 – 15:45
	16:00	G034 – Conc.	16:05 – 17:05

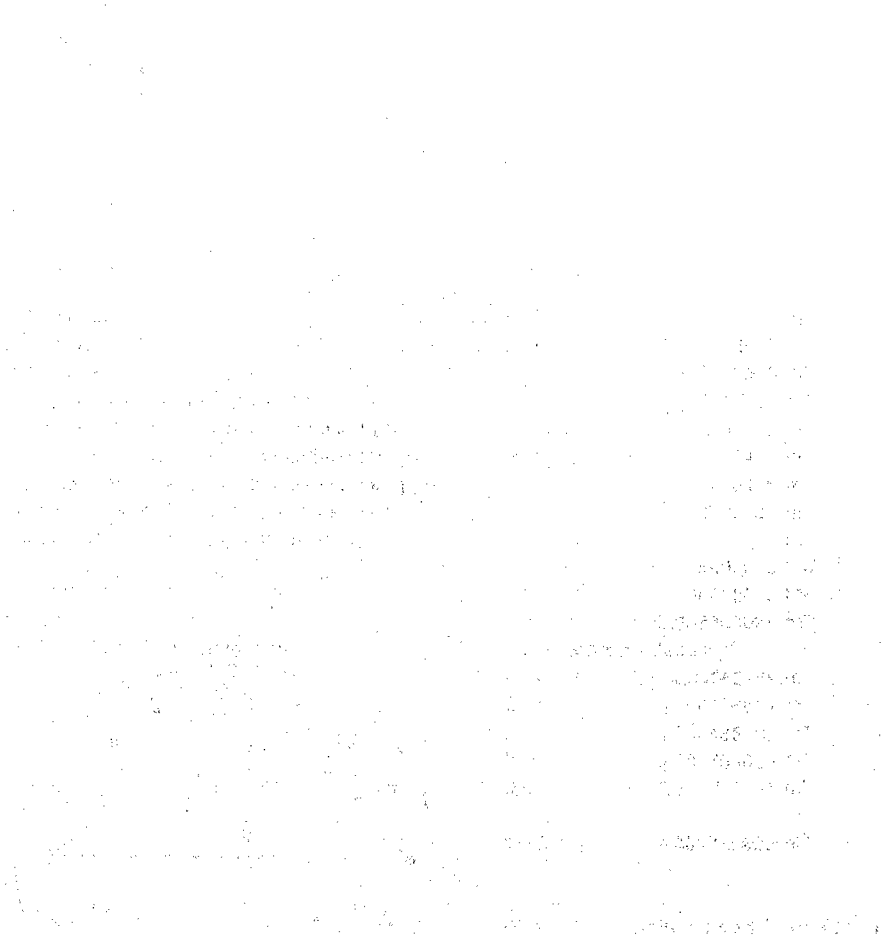

Appendix C - Calculation of flexural rigidity (*EI*) for pile

Upper part of pile (reinforcement bar diameter = 50 mm)

diameter of bar =	50	mm
Area of bar =	1963.5	mm^2
Area of bar =	0.0019635	m^2
second moment of area of bar, I =	3.0680E-07	m^4
distance to neutral axis of furthest bar, y_A =	0.43000	m
distance to neutral axis of 2nd furthest bar, y_B =	0.16455	m
distance to neutral axis of 2nd nearest bar, y_C =	0.30406	m
distance to neutral axis of nearest bar, y_D =	0.39727	m
distance to neutral axis of bar on NA, y_E =	0	m
E (concrete) =	25000000	kN/m^2
E (steel) =	205000000	kN/m^2
I pile =	**0.059666024**	**m^4**

assuming 70 mm cover to rebar

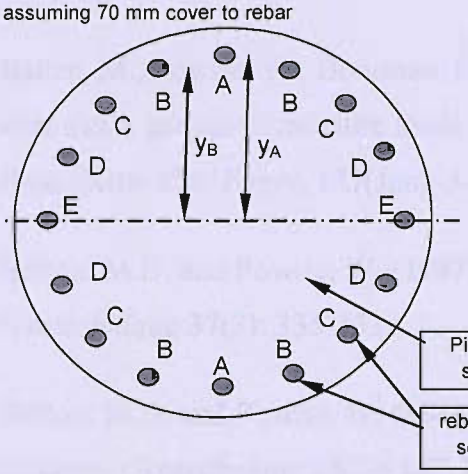

no of bars x (I + Area x y^2)

IA =	7.2671E-04	m^4
IB =	0.000213897	m^4
IC =	0.000727328	m^4
ID =	0.001240758	m^4
IE =	6.13592E-07	m^4
TOTAL =	**0.002909311**	**m^4**

IE = (Ipile x Econc) - (Isteel x Econc) + (Isteel x Esteel)

2015326.594 kNm^2

1492834.514 kNm^2/m run of wall

Lower part of pile (reinforcement bar diameter = 40 mm)

diameter of bar =	40	mm
Area of bar =	1256.6	mm^2
Area of bar =	0.0012566	m^2
second moment of area of bar, I =	1.2566E-07	m^4
distance to neutral axis of furthest bar, y_A =	0.43000	m
distance to neutral axis of 2nd furthest bar, y_B =	0.16455	m
distance to neutral axis of 2nd nearest bar, y_C =	0.30406	m
distance to neutral axis of nearest bar, y_D =	0.39727	m
distance to neutral axis of bar on NA, y_E =	0	m
E (concrete) =	25000000	kN/m^2
E (steel) =	205000000	kN/m^2
I pile =	**0.059666024**	**m^4**

assuming 70 mm cover to rebar

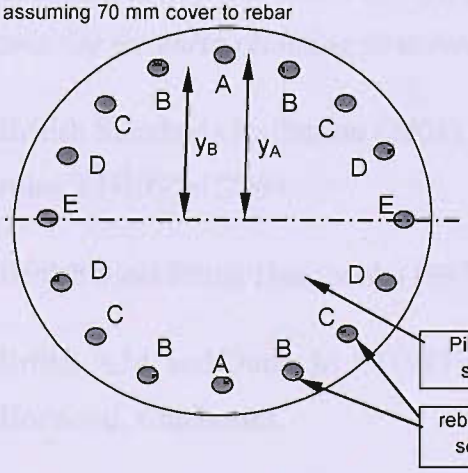

no of bars x (I + Area x y^2)

IA =	4.6496E-04	m^4
IB =	0.000136611	m^4
IC =	0.000465207	m^4
ID =	0.000793803	m^4
IE =	2.51327E-07	m^4
TOTAL =	**0.001860828**	**m^4**

IE = (Ipile x Econc) - (Isteel x Econc) + (Isteel x Esteel)

1826599.657 kNm^2

1353036.783 kNm^2/m run of wall

References

American Concrete Institute (ACI) (1992). *Causes, evaluations and repair of cracks in concrete structures* (ACI 318/318R-89) ACI, Detroit, Mich.

Atkinson, J.H., Richardson, D. and Stallebrass, S.E. (1990). Effect of recent on the stiffness of overconsolidated soils. *Geotechnique* **40**(4): 531-540.

Batten, M. and Powrie, W. (2000). Measurement and analysis of temporary prop loads at Canary Wharf underground station, east London *Proc. Inst. Civ. Engrs. Geotech. Engng* **143**(July): 151-163.

Batten, M., Powrie, W., Boorman, R., Yu, H.-T. and Leiper, Q. (1999). Use of vibrating wire strain gauges to measure loads in tubular steel props supporting deep retaining walls *Proc. Instn. Civ. Engrs*, **137**(Jan): 3-13.

Bolton. M.D. and Powrie, W. (1987). The collapse of diaphragm walls retaining clay. *Geotechnique* **37**(3): 335-353.

Bolton. M.D. and Powrie, W. (1988). Behaviour of diaphragm walls in clay prior to collapse. *Geotechnique* **38**(2): 167-189.

Branson, D.E. (1977). *Deformation of concrete structures*. McGraw-Hill, New York.

British Standard Institution (1951). *Code of Practice No. 2: Earth retaining structures*. London: BSI.

British Standard Institution (1986). BS 1881-206: *British Testing concrete – Part 206: Recommendations for determination of strain in concrete,* Milton Keynes: BSI.

British Standard Institution (1994). BS 8002: *British Standards Institution Code of practise for earth retaining structures,* Milton Keynes: BSI.

British Standards Institution (2004). Eurocode 7: Geotechnical design Part 1, General rules. EN1997-1:2004.

British Steel Piling Handbook (1997). British Steel Plc. 7th Edition.

Britto, A.M. and Gunn, M.J. (1987). *Critical state soil mechanics via finite elements*. Ellis Horwood, Chichester.

Burland, J.B., Potts , D.M. and Walsh, N.M. (1981). The overall stability of free and propped embedded cantilever walls, *Ground Engineering* **14**(5): 28-38.

Burland, J.B., Simpson, B. and St John, H.D. (1979). Movements around excavations in London Clay *Proc. 7th Eur. Conf. on Soil Mech. and Found. Engng*, Brighton. **1**: 13-29.

Carder, D.R. and Symons, I.F. (1989). Long-term performance of an embedded cantilever retaining wall in stiff clay. *Geotechnique* **39**(1):55-75.

Carder, D.R. and Darley, P. (1998). *The long term performance of embedded retaining walls.* TRL Report 381. Transport Research Laboratory, Crowthorne.

Carswell, I., Carder, D.R. and Gent, A.J.C (1993). Behaviour during construction of a propped contiguous bored pile wall in stiff clay at Walthamstow. *TRL Project Report 10.* Project Record E468A/BG.

Chandler, R.J. (2000). Clay Sediments in Depositional Basins: the Geotechnical Cycle. *Quarterly Journal of Engineering Geology and Hydrology*, **33**: 7-39.

Clayton, C.R.I. and Bica, A.V.D. (1993). The design of diaphragm-type boundary total stress cells *Geotechnique* **43**(4): 523-535.

Clayton, C.R.I. and Milititsky, J. (1983). Installation effects and the performance of bored piles in stiff clay. *Ground Engineering*, March.

Coulomb (1776). Essai ..., Paris **7**: 343-382.

De Moor, E.K. (1994). An analysis of bored pile/diaphragm wall installation effects. *Geotechinque* **44**(2): 341-347.

Department of Transport (2000). BD 42: *Design manual for roads and bridges*, Vol. 2 Section 1 Part 2: Design of embedded retaining walls and bridge abutments, Department of Transport, London: HMSO. Crown Copyright.

Dunnicliff, J. (1993). *Geotechnical instrumentation for monitoring field performance* (with the assistance of G.E. Green) Wiley, New York.

Eurocode 2 (1992) Design of concrete structures EN1992.

Fjaer, E., Holt, R.M., Horsrud, P., Raaer, R.M. and Risnes, R. (1992). *Petroleum related Rock mechanics,* Elsevier.

Fourie, A.B. and Potts, D.M. (1989). Comparison of finite element and limiting equilibrium analyses for an embedded cantilever retaining wall. *Geotechnique* **39**(2): 175-188.

Gaba, A.R. (2002). Presentation given at the ICE, London.

Gaba, A., Simpson, B., Powrie, W. and Beadman, D.R. (2003). *Embedded retaining walls: guidance for more economic design* Construction Industry Research and Information Association Report C580. CIRIA, London.

Garrett, C. and Barnes, S.J. (1984). The design and performance of the Dunton Green retaining wall. *Geotechnique* **34**(4):533-548.

Gibson, R.E. and Anderson, W.F. (1961). *In situ* measurement of soil properties with the pressuremeter. *Civil Engineering and Public Works Review* **56**(658): 615-618.

Glass and Powderham (1994). Application of the observational method at the limehouse Link. *Geotechnique* **44**(4):665-679.

Gourvenec, S.M. and Powrie, W. (1999). Three-dimensional finite-element analysis of diaphragm wall installation *Geotechnique* **49**(6): 801-823.

Gunn, M.J. and Clayton, C.R.I. (1992). Installation effects and their importance in the design of earth-retaining structures. *Geotechnique* **42**(1): 137-141.

Gunn, M.J., Satkunananthan, A. and Clayton, C.R.I. (1993). Finite Element modelling of installation effects. *Retaining structures*. Thomas Telford, London.

Hayward, T. (2000). *Field studies, analysis and numerical modelling of retaining walls embedded in weak rock.* Ph.D. thesis, University of Southampton, UK.

Heyman, G. and Clayton C.R.I., (1999) Block sampling of soil: Some practical considerations *Geotechnics for developing Africa* Wardle, Blight and Fourie, Balkema, Rotterdam.

Hight, D.W. and Leroueil, S. (2003). Characterisation of soils for engineering purposes. *Characterisation and Engineering Properties of Natural Soils.* Tan et al. (eds) A A Balkema ISBN 90 C5809 537 1: 255-360.

Hitchcock, A.R. (2003). Elimination of temporary propping using the observational method on the Heathrow airside road tunnel project *Ground Engineering*, May.

HMSO (1978) British Regional Geology – The Wealden District.

Humpage, A.J. and Booth K.A. (2000). *The Lower Greensand in the Mid-Kent and Ashford Contract Sectors of the Channel Tunnel Rail Link Construction Works.* British Geological Survey Commercial Report CR/00/19.

Jardine, R.J., Symes, M.J. and Burland, J.B. (1984). The measurement of soil stiffness in the triaxial apparatus. *Geotechnique* **34**(3): 323-340.

Jardine, R.J., Potts, D.M., Fourie, A.B. and Burland, J.B. (1986). Studies of the influence of non-linear stress-strain characteristics in soil-structure interaction, *Geotechnique* **36**(3): 377-396.

Loveridge, F. (2000). Evaluation of prop loads at CTRL contract 430 Ashford Tunnels. *Ground Engineering*

Mair, R.J. (1993). Developments in geotechnical engineering research, application to tunnels and deep excavations. *Proceedings of the Institution of Civil Engineers Civil Engineering*, **97**(1): 27-41.

Mair, R.J. and Wood, D.M. (1987). *In-situ Pressuremeter Testing: Methods, Testing and Interpretation.* Construction Industry Research and Information Association, Butterworths, London.

Mantell, G.A. (1833). *Geology of south-east England*, Longman, London.

Massarsch, K.R. (1975). New method for measurement of lateral earth pressure in cohesive soils. *Can. Geotech. J.* **12**:142-146.

Massarsch, K.R., Holtz, R.D., Holm, B.G. and Fredriksson, A. (1975). Measurement of horizontal *in situ* stresses. *Proc. of Speciality Conf. on in situ measurement of soil properties*, North Carolina, **1**:266-286. American Society of Civil Engineers.

Mikkelsen, P.E. (2003). Advances in inclinometer data analysis. *Symposium on Field Measurements in Geomechanics*, FMGM, Oslo Norway. September.

Mosley, W.H. and Bungey, J.H. (1976). *Reinforced Concrete Design* London, Macmillan.

Neville, A.M. (1970). *Creep of concrete: plain, reinforced, and prestressed.* North Holland publishing Company, Amsterdam.

Ng, C.W.W. (1992). *An Evaluation of Soil-structure Interaction Associated with a Multi-propped Excavation.* PhD thesis, University of Bristol.

Ng, C.W.W., Lings, M.L., Simpson, B. and Nash, D.F.T. (1995). An approximate analysis of the three-dimensional effects of diaphragm wall installation. *Geotechnique* **45**(3):497-507.

Ng, C.W.W. and Yan, R.W.M. (1999). Three-dimensional modelling of a diaphragm wall construction sequence. *Geotechnique,* **49**(6): 825-834.

Ooi, P.S.K. and Ramsey, T.L. (2003). Curvature and bending moments from inclinometer data, *ASCE International Journal of Geomechanics*, **3**(1):64-74.

Padfield, C.J. and Mair, R.J. (1984). *Design of retaining walls embedded in stiff clays.* Report 104. London: Construction Industry Research and Information Association.

Peattie, K.R. and Sparrow, R.W. (1954). The fundamental action of earth pressure cells *Journal of the mechanics and physics of solids,* **2**: 141-155.

Penman, A.D.M. and Charles, J.A. (1981). Assessing the risk of hydraulic fracture in dam cores. PRc. *10th Int. Conf. Soil Mech., Stockholm* **1**: 457-462.

Potts, D.M. and Bond, A.J. (1994). Calculation of Structural forces for propped retaining walls. *XIII ICSMFE*, New Delhi, India.

Potts, D.M. and Fourie, A.B. (1984). The behaviour of a propped retaining wall: results of a numerical experiment. *Geotechnique*, **34**(3): 383-404.

Potts, D.M. and Fourie, A.B. (1985). The effect of wall stiffness on the behaviour of a propped retaining wall. *Geotechnique* **35**(3): 347-352.

Potts D. M. and Zdravkovic, L. (1999). *Finite element analysis in geotechnical engineering*. Thomas Telford, London.

Powrie, W. (1985). Discussion on Performance in propped and cantilever rigid walls. *Geotechnique* **35**(4): 546-548.

Powrie, W. (2004). *Soil mechanics: concepts and applications* (2nd edition). London: Spon Press.

Powrie, W. and Kantartzi, C. (1996). Ground response during diaphragm wall installation in clay: centrifuge model tests. *Geotechnique* **46**(4): 725-739.

Powrie, W. and Li, E.S. (1991). Finite element analyses of an *in situ* wall propped at formation level. *Geotechnique* **41**(4): 499-514.

Powrie, W, Pantelidou H. and Stallebrass, S.E. (1998). Soil stiffness in stress paths relevant to diaphragm walls in clay. *Geotechnique* **48**(4): 483-494.

Raphael, J.M. (1984) Tensile strength of concrete *ACI Journal*, **81**(2): 158-165.

Rankine, W. J. M. (1857). On the stability of loose earth, *Phil. Trans. Royal Society* **147**(2): 9-27.

Richards, D.J. Chandler, R.J. and Lock, A.C. (2003) Electronic data transfer systems for field monitoring. *Proc. Inst. Civ. Engrs* **156**(1): 47-55.

Richards, D.J., Clark, J., Powrie, W. and Heyman, G. (2005) An evaluation of total horizontal stress measurements using push-in pressure cells in an overconsolidated clay deposit. *Proc. Inst. Civ. Engrs. Geotech. Engng accepted for publication.*

Richards, D.J., Holmes, G. and Beadman, D.R. (1999). Measurement of temporary prop loads at Mayfair car park. *Proc. Inst. Civ. Engrs. Geotech. Engng* **137**(July): 165-174.

Richards, D.J. and Powrie, W. (1994). Finite element analysis of construction sequences for propped retaining walls. *Proc. Inst. Civ. Engrs, Geotech. Engng.* **107**(1994): 207-216.

Richards, D.J. and Powrie, W. (1998). Centrifuge tests on doubly propped embedded retaining walls in overconsolidated kaolin clay, **48**(6): 833-846.

Roberts, M. (2003). *Private communication.*

Roberts, T.O.L., Roscoe, H., Powrie, W. and Butcher, D. (2005). *private communication.*

Roscoe, H. (2005). *Private communication.*

Roscoe, H. and Twine, D. (2001). Design collaboration speeds Ashford tunnels. *World Tunnelling*, **14**(5): 237-241.

Ross, A.D. (1937). Concrete Creep Data. *The Structural Engineer* **15**: 314-32.

Rowe, P.W. (1952). Anchored sheet-pile walls. *Proc. Inst. Civ. Engrs.* **1**(1): 27-70.

Rowe, P.W. (1955). A theoretical and experimental analysis of sheet piled walls. *Proc. Inst. Civ. Engrs.* **4**(1): 32-69.

Rowe, P. W. (1956). Sheet piled walls at failure. *Proc. Inst. Civ Engrs.* 276-315.

Ryley, M.D. and Carder D.R. (1995). The performance of push-in spade cells installed in stiff clay. *Geotechnique* **45**(3): 533-539.

Saxena, S.K. (1975). Measured performance of a rigid concrete wall at the World Trade Center, Proc. *Conf. on Diaphragm Walls and Anchorages* pp. 107-112.

Skempton, A.W. and Weeks, A.G. (1976) The Quaternary history of the Lower Greensand escarpment and Weald Clay vale near Sevenoaks, Kent. *Phil. Trans. R. Soc. Lond. A.* **283**: 493-526.

Simpson, B. (1992). Thirty-second Rankine lecture: Retaining structures: displacement and design. *Geotechnique* **42**(4): 541-576.

Simpson, B. and Powrie, W. (2000). Embedded retaining walls: theory, practise and understanding. *ISSMGE XVth International conference in Turkey.*

Smart J.G.O., Bisson G. and Worssam B.C. (1966). *Geology of the Country around Canterbury and Folkestone.* Her Majesty's Stationery Office, London.

Smethurst, J.A. 2003. *The use of discrete piles for infrastructure slope stabilisation.* PhD thesis, University of Southampton, UK.

Stroud, M.A. (1974). The standard penetration test in insensitive clays and soft rocks *Proc. Eur. Symp. on Penetration Testing* (ESOPTI) Volume 2:2, pp. 367-375, Swedish Geological Society, Stockholm.

Stroud, M.A. and Sweeney, D.J., (1977). Discussion appendix in: *A review of diaphragm walls*, pp. 142-148. London: Institution of Civil Engineers.

Symons, I.F. (1983). Assessing the stability of a propped, *in situ* retaining wall in overconsolidated clay *Proc. Inst. Civ. Engrs*, **75**(2): 617-633.

Symons, I.F. and Carder, D.R. (1990). Long term behaviour of embedded retaining walls in over-consolidated clay. *Geotechnical Instrumentation in Practice*, TTL, London.

Symons, I.F. and Carder, D.R. (1992). Field measurements on embedded retaining walls. *Geotechnique* **42**(1): 117-126.

Symons, I.F. and Carder, D.R. (1993). Stress changes in stiff clay caused by the installation of embedded retaining walls. *Retaining structures* Thomas Telford, London.

Symons, I.F. and Tedd, P. (1989). Behaviour of a propped embedded retaining wall at Bell Common Tunnel in the longer term. *Geotechnique* **34**(4): 701-710.

Tavenas, F.A., Blanchette, G., Leroueil, S., Roy, M. and La Rochelle, P. (1975). Difficulties in the *in situ* determination of K_o in soft sensitive clays *Proc. of speciality conference on in situ measurement of soil properties*, North Carolina, **1**:450-476. New York, American Society of Civil Engineers.

Tedd, P., Chard, B.M., Charles, J.A. and Symons, I.F. (1984). Behaviour of a propped embedded retaining wall in stiff clay at Bell Common. *Geotechnique* **34**(4): 513-532.

Tedd P. and Charles J.A. (1981). In-situ measurement of horizontal stress in overconsolidated clay using push-in spade-shaped pressure cells. *Geotechnique* **31**(4): 534 -538.

Tedd P. and Charles J.A. (1983). Evaluation of push-in pressure cell results in stiff clay. *Proceedings of the International Symposium on soil and rock investigation by in-situ testing.* Paris, Vol. 2, 579-584.

Tedd P., Powell J.A., Charles J.A. and Uglow I.M. (1990). In-situ measurement of earth pressures using push-in spade-shaped pressure cells – 10 years experience. *Geotechnical Instrumentation in practice*, Thomas Telford, London.

Terzaghi, K (1934). *Theoretical Soil Mechanics*, Wiley and Sons.

Terzaghi, K (1943). Large retaining wall tests, *Engineering News Record* **112**: 36-140.

Terzaghi, K (1954). Anchored Bulk Heads, *Trans. Am. Soc. Civ. Engrs* **119**: 1243-1280.

Tschebotarioff, G. (1951). *Soil mechanics, foundations and earth structures*, McGraw-Hill.

Union Railways Ltd (1997 A). Central Ashford – Geotechnical Design Basis Report chainage 87+842 to 92+042. Report number 440-RUP-LCEEH-00043-AA.

Union Railways Ltd (1997 B). Ashford Tunnel Design Criteria. Report number 430-RUG-RLEEZ-00120-AA.

Weiler, W.A. and Kulhawy, F.H. (1982). Factors affecting stress cell measurements in soil. *J. Geotechnical Engineering* ASCE, 108, No. GT12 (December): 1529-1548.

Wood, L.A. and Perrin, A.J. (1984). Observations of a strutted diaphragm wall in London clay: a preliminary assessment. *Geotechnique*, **34**(4): 563-579.

Xu (2005). *The behaviour of soil behind full-height integral abutments.* PhD thesis, University of Southampton.